Hybrid Radio Frequency/Free Space Optical Communications for Energy-Efficient Wireless Sensor Networks

Sashigaran Sivathasan
St Hugh's College

A thesis submitted for the degree of Doctor of Philosophy

Department of Engineering Science
University of Oxford

Hilary Term 2008

Hybrid Radio Frequency/Free Space Optical Communications for Energy-Efficient Wireless Sensor Networks

Sashigaran Sivathasan

St Hugh's College, University of Oxford

A thesis submitted for the degree of Doctor of Philosophy

Hilary Term, 2008

Abstract

A wireless sensor network (WSN) consists of a large number of networked sensor nodes deployed to sense and report a particular phenomenon to a base station. Currently, most WSNs use radio frequency (RF) communications, and this accounts for a significant amount of energy expended. Free space optical (FSO) communications using modulating retroreflectors is potentially attractive for WSNs, due to the lower communications energy required. However, for FSO communications, line of sight (LOS) is required between the transmitter and the receiver. In this thesis, a hybrid Radio Frequency/Free Space Optical (RF/FSO) WSN is proposed. FSO links are used for communications, with RF links providing backup in the absence of LOS. This network has the potential to lower the overall energy consumption of a traditional RF-only WSN.

Chapter 1 introduces the WSN and outlines the motivation for the RF/FSO WSN. Chapters 2 and 3 describe the RF and FSO link models used for the RF/FSO WSN. Chapter 4 describes how the WSN networks are configured. The energy model for the sensor node is discussed in Chapter 5. Chapter 6 discusses how network traffic and energy consumption are modelled. The results of the RF/FSO WSN simulations are presented in Chapter 7. Chapter 8 discusses the conclusions from the thesis and suggests areas for future work.

Simulations show that for the wide range of scenarios considered, the RF/FSO WSN consumes less energy and has a lifetime at least twice as long as the RF-only WSN. For low and average optical blocking conditions, the RF/FSO WSN is also able to offer at least the same level of network coverage as the RF-only WSN.

Acknowledgements

Aum Sri Ganeshaya Namaha. Firstly, I would like to thank Ganesha for giving me an opportunity to pursue my doctoral studies at the University of Oxford.

I also owe a very immense debt of gratitude to Amma, Papa, Aunty Thevi, Aunty Kili, Sudha, and Sudheer who have supported me throughout my studies, and for understanding how much this opportunity meant to me. Without their help, reading for a DPhil in Engineering Science at Oxford would have just remained a dream. This thesis and my doctoral work are lovingly dedicated to them. I also particularly want to thank Amma and Papa who sacrificed so much in educating me since young. Checking my schoolwork every day after school, helping me read with Peter and Jane, and marking my English and Malay essays, few parents would have sacrificed so much time to help their children with their studies. I am very grateful.

I would like to thank Dr. Dominic O'Brien, my supervisor, for supporting me in pursuing a programme of research which truly excited me. For encouraging me when my spirit flagged, and motivating me when I grew tired, I am thankful. I wish to also thank Grahame Faulkner for all his help and assistance.

I want to thank my college, St Hugh's, for the support they provided me as I completed my studies. I would also like to thank the friends I've made over the course of my studies for their company and friendship, especially Angela, Nick, Ahmed and Sasha.

List of Publications

[1] S. Sivathasan, D. C. O'Brien, "Lifetime comparison of RF-only and hybrid RF/FSO wireless sensor networks," in *Proc. International Conference on Computer and Communication Engineering*, 2008, pp. 328-331.

[2] S. Sivathasan, D. C. O'Brien, "Hybrid radio and optical communications for energy-efficient wireless sensor networks," submitted to *IEEE Transactions on Wireless Communications*.

[3] S. Sivathasan, D. C. O'Brien, "Wireless Sensor Networks: A Performance Study," submitted to *GLOBECOM 2008*.

Table of Contents

List of Symbols and Abbreviations

β	range ratio
γ	average E_b/N_0
γ_a	data aggregation ratio
δ	hotspot factor
ε_a	data aggregation factor
ε_p	data processing factor
ε_{sec}	data security factor
ε_L	RF transmission factor for the node to base station (LOS) channel
ε_{NL}	RF transmission factor for the node to base station (NLOS) channel
ε_{PP}	RF transmission factor for the peer-to-peer channel
θ_i	divergence half angle of the laser interrogation beam
λ	wavelength
μ	node density
a	length of each of the three CCR mirrors
A_c	light collection area
AWGN	additive white Gaussian noise
b_f	optical blocking factor
B	equivalent bandwidth of the radio receiver measuring device
BER	bit error rate
BPSK	binary phase shift keying
CCR	corner cube retroreflector
C_n^2	index of refraction structure parameter
C_r	average coverage ratio
d	transmission distance
d_0	free space reference distance

d_L	maximum radio range for node with line of sight to the base station
d_{NL}	maximum radio range for node without line of sight to the base station
d_{OPT}	maximum free space optical range
d_{PP}	maximum peer-to-peer radio range
D	diameter of the optical receiver collecting lens aperture
$E_{b,dp}$	energy per bit for data processing
$E_{b,opt}$	energy per bit for optical transmission
$E_{b,r}$	energy per bit for radio reception electronics
$E_{b,s}$	energy per bit for sensing
$E_{b,ta}$	range-dependent transmitted RF energy per bit
$E_{b,te}$	energy per bit for radio transmission electronics
E_R	mean energy ratio
E_{RF}	energy used by the RF-only network over the simulation period
$E_{RF/FSO}$	energy used by the RF/FSO network over the simulation period
f	carrier frequency in Hertz
F	noise figure
FSO	free space optics
G_r	receiver antenna gain
G_t	transmitter antenna gain
h	height of base station
I	irradiance
I_n	normalized irradiance
k_w	optical wave number
K_r	Ricean factor
L	radio system loss factor not related to propagation
L_r	lifetime ratio
LOS	line of sight
MRR	modulating retro-reflector
n	path loss exponent

N	number of nodes deployed
N_0	noise power density
NLOS	non line of sight
OOK	on-off keying (modulation)
P_e	probability of error
P_i	power of the interrogating laser
P_r	received power
P_t	transmitter power
P_L	power loss
QPSK	Quaternary Phase Shift Keying
$r_{h,opt}$	radius of base station optical hotspot
$r_{h,radio}$	radius of base station radio hotspot
r_m	mirror reflectivity
R	radius of deployment area
R_b	bitrate
R_p	photodetector responsivity
RF	radio frequency
T_0	ambient room temperature
WSN	wireless sensor network

Chapter 1

Introduction

A wireless sensor network (WSN) consists of a large number of networked sensors deployed to sense and report a particular phenomenon, such as temperature, movement or noise levels[1]. This chapter provides an introduction to WSNs and the architecture of sensors. Several of the key design factors associated with the WSN are discussed. This is followed by a survey on radio frequency/free space optical (RF/FSO) networks and an introduction to the proposed RF/FSO WSN.

1.1. The wireless sensor network (WSN)

The architecture of a typical WSN is shown in Figure 1.1.

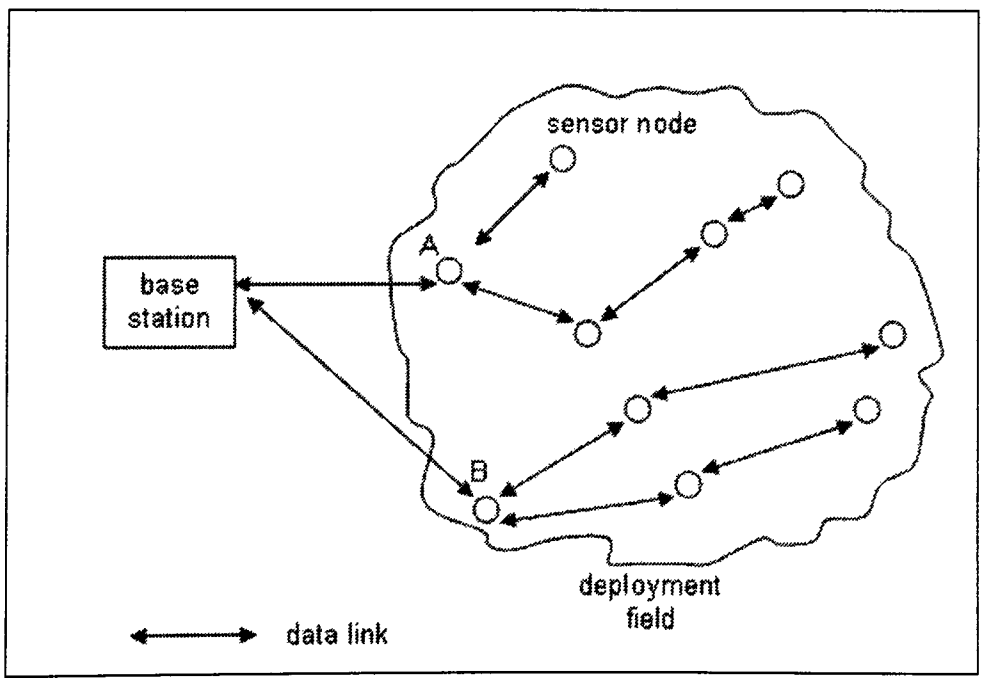

Figure 1.1: Sensor nodes in a deployment field

In a WSN, the base station connects the sensor nodes deployed in the field to an existing communications infrastructure, or to a remote station via the Internet[2].

Sensor nodes relay data relating to the phenomena they have sensed to the base station[3]. The base station processes this data before sending it to the intended recipient[4], possibly a user connected to the internet. The base station may perform complex data processing to manage the data harvested from the sensor field[4]. Figure 1.1 shows that there needs to be cooperative routing among the nodes forming the network[2]. Data from nodes without direct connection to the base station is relayed to the base station over multiple nodes (multihops) as shown in Figure 1.1[5, 6].

1.2. The sensor node

This section examines the architecture and energy source of a typical sensor node deployed in WSNs. A sensor node usually consists of a sensing unit, a processing unit, a transceiver and a power unit, as shown in Figure 1.2[7].

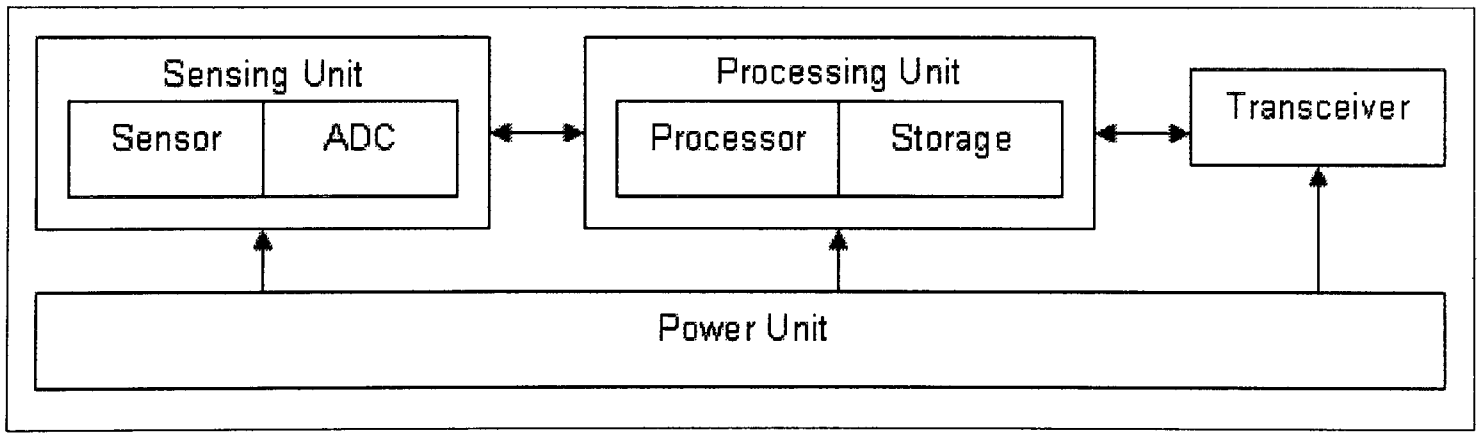

Figure 1.2: The components of a sensor node

The sensing unit is responsible for sensing a phenomenon, such as a change in temperature or noise levels. This signal, which is usually analogue, is converted to a digital signal by an analogue to digital converter (ADC)[8]. The processing unit then prepares this data to be transmitted by the transceiver[9]. The processing unit is

also responsible for determining the next node to transmit to and data aggregation (data aggregation is discussed in section 1.4.1.).

A sensor node is designed to be small, with some researchers suggesting that it needs to be matchbox-sized or smaller to operate successfully[10]. Due to node size restrictions, the power unit is usually a small battery with a limited life[11]. For example, wireless integrated network sensors (WINS) are powered by lithium cells 2.5cm in diameter and 1 cm thick[11].

Energy scavenging has been proposed as a way to increase the lifetime of sensors[12]. In energy scavenging, energy is extracted from the environment, for example by using solar cells[13]. In[14], piezoelectric converters, which convert low level vibrations to voltage, have been studied as a means of scavenging energy to power sensor nodes.

1.3. Medium of transmission

Currently, most wireless sensor networks use radio frequency (RF) channels for communications[7]. In designing a WSN, it is useful to choose a suitable radio band that is available globally and the unlicensed 2.4 GHz Industrial, Scientific and Medical (ISM) band is a popular choice. The μAMPS wireless sensor nodes and the Wireless Integrated Network Sensors (WINS) nodes are examples of sensor nodes that use RF for communication[15]. However, communication could also be achieved by using free space optics (FSO)[16]. The Smart Dust mote is an example of a sensor node which uses the optical medium for communication[17]. Optical

communication requires line of sight (LOS) between the transmitter and receiver. which may not always be possible. The absence of LOS is not as detrimental for RF-based communications[7], although the RF signal suffers a large degree of attenuation in the absence of LOS between the transmitter and receiver[18].

1.4. WSN design issues

Several factors need to be considered in the design of a WSN, and the three considered in this section are power consumption, node density and fault tolerance. Power consumption is important, as sensors need to sense for as long as possible. Node density and fault tolerance are also discussed in this section, as they influence the power consumption of a node.

1.4.1. Power consumption

Power consumption is an extremely important factor in the design of WSNs, as lower power consumption translates to longer node and network lifetime. Due to size restrictions, sensor nodes have a limited source of power. Smart dust sensors, for example, may have as little as 1 Joule of total energy available to them[19]. Sensing, communication and data processing contribute to the power consumption of a sensor node, with most power being consumed for communications[20]. Therefore, the lifetime of the network could be greatly extended by employing more energy-efficient communications.

Energy consumption can also be reduced by performing data aggregation, which can reduce the data communicated between nodes. Sensor nodes with

overlapping sensor ranges generate redundant data[21], and this can be aggregated using techniques like suppression, minima, maxima and averaging[2]. In Figure 1.1, nodes A and B can first perform data aggregation instead of sending all the data fed to them by their respective dependent nodes. This ensures that nodes A and B do not exhaust their energy resources too quickly, as data processing consumes less energy than data communication[20].

For RF communications, the minimum output power required to transmit data is proportional to d^n where d is the transmission distance and n is the path loss exponent[7]. The path loss exponent, n, is usually assumed to take values between 2 and 4[7]. Due to shadowing and path loss effects, the value of n is closer to 4 for near-ground channels and low-lying antenna [19] which is a typical characteristic of WSNs. Instead of transmitting over a large distance, sensor nodes employ RF multihop communications, i.e. transmitting data over several short distances[7]. Transmitting over shorter distances, therefore, reduces the overall power consumed by the network. RF multihop communication is possible as nodes are usually densely deployed and the distance from a node to its neighbour is usually small.

1.4.2. Node density

Node density is another important factor, as it has a bearing on the energy consumption of the sensor nodes of the WSN. This is especially true if the network employs multihop routing. For RF-based WSNs, more nodes mean a shorter average distance between nodes, which translates to lower levels of energy being transmitted for communications[7]. More nodes also provide for a greater degree of redundancy,

which can increase the reliability of the information relayed to the base station[22]. However, a larger number of nodes also increases the amount of data traversing network links. More data exhausts node energy resources quickly, although this can be alleviated to a certain extent by data aggregation[23]. It is therefore important to choose an appropriate node density for the network. The base station also needs to effectively manage the large number of nodes associated with WSNs and this could typically range from a few sensor nodes to a few hundred within an area with a radius of less than 5m[20]. In a domestic setting, up to two dozen home appliances could be equipped with their own sensor nodes[24]. For machine diagnosis applications, the node density could be as high as 300 sensors in a 25 m^2 area[20].

1.4.3. Fault tolerance

Fault tolerance is the ability of the network to function despite failures suffered by individual nodes[25-27]. An example of fault tolerance is the ability of the network to reconfigure itself as nodes begin to die. In the deployment phase, if nodes are dropped randomly over a sensor field from an aircraft for example[28], there is a high possibility that some nodes may be damaged. If optical links are used, there is a possibility that the nodes would not have line of sight (LOS) to the base station or neighbouring nodes[29]. This may be due to optical obstructions such as buildings or thick foliage. In a random outdoor deployment, there is also the possibility that the optical sensor node may be overturned, frustrating any communication between itself and the base station or other nodes. These are some of the possible node faults that the network needs to contend with.

1.5. WSN routing protocols

Section 1.4 identified several key design challenges associated with WSNs. In this section, WSN routing protocols are studied. Routing protocols determine how sensor nodes relay data to the base station and vice versa[2, 7]. A well-chosen routing protocol ensures fair distribution of network traffic among the nodes, ensuring that nodes do not fail prematurely for lack of power, thus jeopardizing the lifetime of the network. A comprehensive survey of WSN protocols is given in[2], in which the routing protocols are divided based on the network structure: flat network routing, hierarchical network routing or location-based routing.

In flat network routing, all the nodes are identical and perform the same functions[8]. In location-based routing, the deployment area is divided into geographical regions, and nodes become a member of a region[2]. Location-based routing enables the base station to communicate with specific regions of the network at a time[30]. The remainder of the discussion in this section focuses on hierarchical network routing, as the routing protocol proposed for the RF/FSO WSN in Section 1.11 is a hierarchical-based protocol. (The RF/FSO WSN is discussed further in Section 1.11.) The typical network topology of a hierarchical-based WSN is discussed next.

In hierarchical routing, nodes are divided based on their functions. The nomenclature used to describe the different classes of nodes in hierarchical-based WSNs may vary from protocol to protocol. However, hierarchical-based protocols typically identify two groups of nodes: cluster heads and non-cluster heads[31-36].

In some protocols, a cluster head which connects directly to the base station is labelled a gateway node. The Management Architecture for Wireless Sensor Networks (MANNA) protocol described in[37], for example, identifies three classes of nodes: common nodes, sink nodes (similar to cluster heads) and gateway nodes. The gateway nodes in [37] connect sink nodes to an *observer* (similar to the base station). The three types of nodes in hierarchical-based WSNs are shown in Figure 1.3.

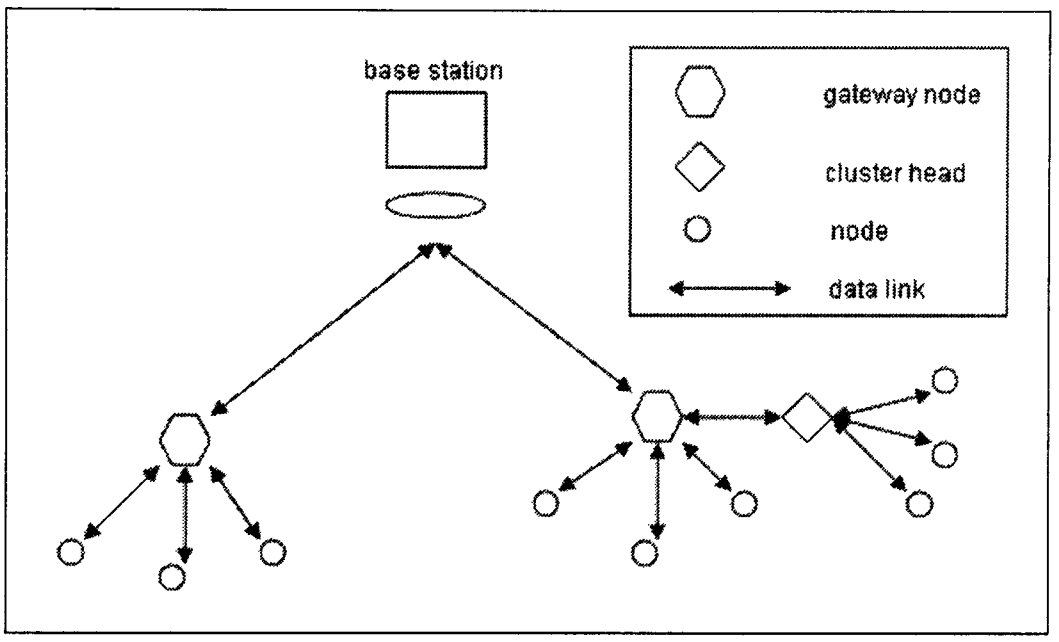

Figure 1.3: Nodes in hierarchical routing

(For the remainder of this section, cluster heads imply gateway nodes as well.) The function of each of the three classes of nodes shown in Figure 1.3 could vary between protocols. Non-cluster heads are usually only involved in sensing[2]. A cluster head can perform sensing duties as well, as in the network proposed in[38]. Some protocols, though, restrict the cluster head from performing sensing duties, an example being the Self-Organizing protocol proposed by Subramanian *et al.*[39]. For the Self-Organizing protocol, the process of data sensing and data routing are uniquely assigned to specialized sensors (such as camera, acoustic or temperature

sensors) and router sensors (which are analogous to cluster heads in Figure 1.3) respectively[39].

Cluster heads perform data routing, and this distinguishes them from other non cluster head nodes in the network[2]. Cluster heads are responsible for routing the data from nodes in their cluster to the base station, or even other cluster heads[31-36]. The cluster head serves as a control centre to co-ordinate the data transmissions in its cluster[22]. In the Low Energy Adaptive Clustering Hierarchy (LEACH) protocol described in[22], time division multiple access (TDMA) is used to schedule transmissions from nodes in the cluster. The cluster head prepares a TDMA schedule and transmits this schedule to the nodes in its cluster. Nodes could also transmit simultaneously by incorporating code division multiple access (CDMA) codes, as discussed in[40].

The cluster heads in some networks also perform data aggregation. Cluster heads in the Virtual Grid Architecture routing protocol [2, 41] and LEACH [22] WSNs perform data aggregation before transmitting data to reduce the energy consumption due to communications[22]. In LEACH, the authors assume that all of the signals from the nodes in a cluster, each of packet length L, can be aggregated by the cluster head into a single representative packet of length L[22]. In the Virtual Grid Architecture, data aggregation is performed at two levels: a local level by all cluster heads and a larger global level by a selection of cluster heads[2]. Cluster head selection is discussed next.

Cluster heads could be determined before node deployment, and they could continue performing this function until the network dies. This is known as static clustering[22]. As a cluster head expends considerable power managing data from all the nodes in its cluster[2], it may be equipped with a larger power source, such as Intel's XScale nodes[42]. The heterogeneous sensor network being researched at Intel consists of high-end Intel XScale nodes overlaid over a sensor field, each XScale node essentially serving as a cluster head[42]. The XScale nodes are equipped with a larger power source and route the traffic from the smaller battery-powered sensors to the base station. In the case of the XScale nodes, the cluster heads are pre-selected before node deployment, and continue functioning as cluster heads for the duration of the network's lifetime. The duty of serving as a cluster head can also be rotated among all nodes within a network. This ensures that the cluster head does not expire too early, especially in networks with homogenous nodes, as is the case for the LEACH WSN[22]. In the LEACH protocol, a group of cluster heads is elected randomly from the sensor nodes and this duty is rotated periodically[31].

1.6. Phases in the lifetime of the WSN

Section 1.5 looked at WSN routing protocols, with particular emphasis on hierarchical-based routing. In this section, the lifetime of the WSN is studied. There are typically three phases in the lifetime of the sensor network. The first phase is the deployment phase. Deployment can be random (e.g. dropping them from an aircraft) or deterministic (e.g. placing nodes at fixed co-ordinates on the ground) in nature[28]. This will typically depend on the deployment environment of the sensor network. When the sensor network is deployed indoors, it may be more

advantageous to determine the location of each node prior to deployment. This may not be practical if a large number of nodes need to be deployed over a large outdoor space. In an outdoor deployment, for example, it may be more practical to randomly drop nodes from an aircraft[20].

The next phase is the network configuration phase. This is the initial 'wake up phase' where nodes self-organize and establish a network to route traffic to the base station[43]. The network is not constant and will change with time. This is because nodes have a limited source of energy that will eventually expire. When nodes begin to expire, the network needs to reconfigure itself[7], entering the final phase of its lifetime.

For reconfiguring networks, the third and final phase of the WSN's lifetime is the reconfiguration phase [7] (reconfiguring networks are discussed in Section 7.3 of Chapter 7). As cluster heads die, nodes depending on them may route their traffic through other cluster heads. This could be accomplished by each node having a back-up cluster head ready in memory, in-case the current cluster head dies. When all the nodes in the network die or become isolated, the lifetime of the network comes to an end. (There are several definitions of network lifetime[44], and they are presented in Table 7.1 in Chapter 7.) An example of a WSN that uses network reconfiguration is the Localized Autonomic Configuration (LACON) sensor network. LACON networks perform reconfiguration to mitigate network impairments due to cluster head (called *parent nodes*) malfunctions[43].

1.7. WSN: Applications

Wireless sensor networks (WSNs) is a field of growing research interest. Sections 1.1-1.6 provided a background study on WSNs. This section discusses several possible applications of WSNs. WSNs can be used to monitor different conditions like vehicular movement, the levels of noise, temperature and humidity[1]. In[20], WSN applications are categorized into military, environmental, health, home and commercial applications. An example of an environmental application is the use of wireless sensor networks to detect forest fires and floods[20]. Sensor nodes monitor temperatures, periodically relaying information to a remote monitoring station. In addition to alerting forest rangers to possible forest fires, the information from the sensors also makes it easier for fire personnel to locate the origin of a fire[20]. The ALERT system [15] uses sensors to monitor rainfall and water levels to alert emergency centres of possible floods. Sensor networks are also used to detect and report car thefts, relaying information to security personnel via the Internet for further action[19].

Domestic-related solutions could potentially incorporate sensor nodes, with them being embedded in domestic appliances like microwave ovens, refrigerators and VCRs[24]. These appliances could communicate among themselves, creating an indoor sensor network, or with an external network through the internet. WSNs could also be used for medical-related applications. In[45], sensor networks are proposed to monitor elderly patients' movements at home. Each patient wears a miniaturized sensor. The sensor provides information which is monitored regularly by remotely-based healthcare workers who can attend to any emergencies like a serious fall.

To manage environmental control of office buildings [46], temperature sensors are deployed in different areas of the office. The temperature readings sent by these sensors are used to control the air conditioning or heating in the building. Another area of potential application is in managing inventory control, where a node is attached to each item in a warehouse[47]. Workers would be able to easily locate an item in the warehouse, and tally the number of items in the same category to prepare inventories.

Reducing network energy consumption was identified as one of the key design challenges in Section 1.4.1. This is the motivation behind the RF/FSO WSN proposal, which is discussed in the following section.

1.8. Radio Frequency/Free Space Optical (RF/FSO) WSN: Motivation

Energy consumption is a major consideration in designing a WSN. This is due to the limited and irreplaceable power source an individual sensor node is equipped with. The node's power source dictates the lifetime of the network. One solution would be to just increase the power supply of the individual nodes, but this could significantly increase the size of the node. Most of the energy consumed by the node is attributed to communications and current WSN research initiatives are aimed at reducing the communications in the network[20].

In[16], passive optical transmitters are proposed to provide free space optical (FSO) communication links using modulating retroreflectors for sensor networks. (Modulating retroreflectors are studied in more detail in Chapter 3.) The authors in

[16] were able to demonstrate an FSO link which could communicate up to 180m. with an average energy consumption of 19 pJ/bit. This is much lower than the communications energy demanded by current RF-based standards used for WSNs. such as Bluetooth. The average transmitted energy for the Bluetooth in [16] is 1nJ/bit over a few tens of metres. In[26], the transmitted RF energy per bit for WSN links is between 0.1 and 0.6 nJ/bit for a distance of 5m when there is no line of sight (LOS) between the transmitter and receiver. With line of sight, the transmitted energy over a distance of 10m in [31, 32] is 0.1 nJ/bit. Although FSO links promise lower communications energy, line of sight is required between the transmitter and receiver. This thesis investigates the hybrid radio frequency / free space optical wireless sensor network (RF/FSO WSN). For this network, FSO links are used for communications, with RF links providing backup in the absence of LOS. This hybrid RF/FSO WSN has the potential to reduce the energy consumption of WSNs.

1.9. RF/FSO networks: A survey

Currently, most WSN networks are RF-based[7].To the best of the author's knowledge, an RF/FSO WSN has not been previously researched. There is some interest in RF/FSO networks, but most of the work is devoted to wireless broadband networks[48-50].

FSO is a commercial technology, typically used in fixed configurations for high data rates. For broadband RF/FSO networks, the FSO link is established using modulated laser beams as shown in Figure 1.4[48]. Figure 1.4 shows a high speed gigabit building-to-building FSO link, with optical transceivers mounted to both

buildings. In the FSO link, both the receiver and transmitter have their own laser sources. A laser beam is modulated by the transmitter and this beam is collected using a telescope at the receiver.

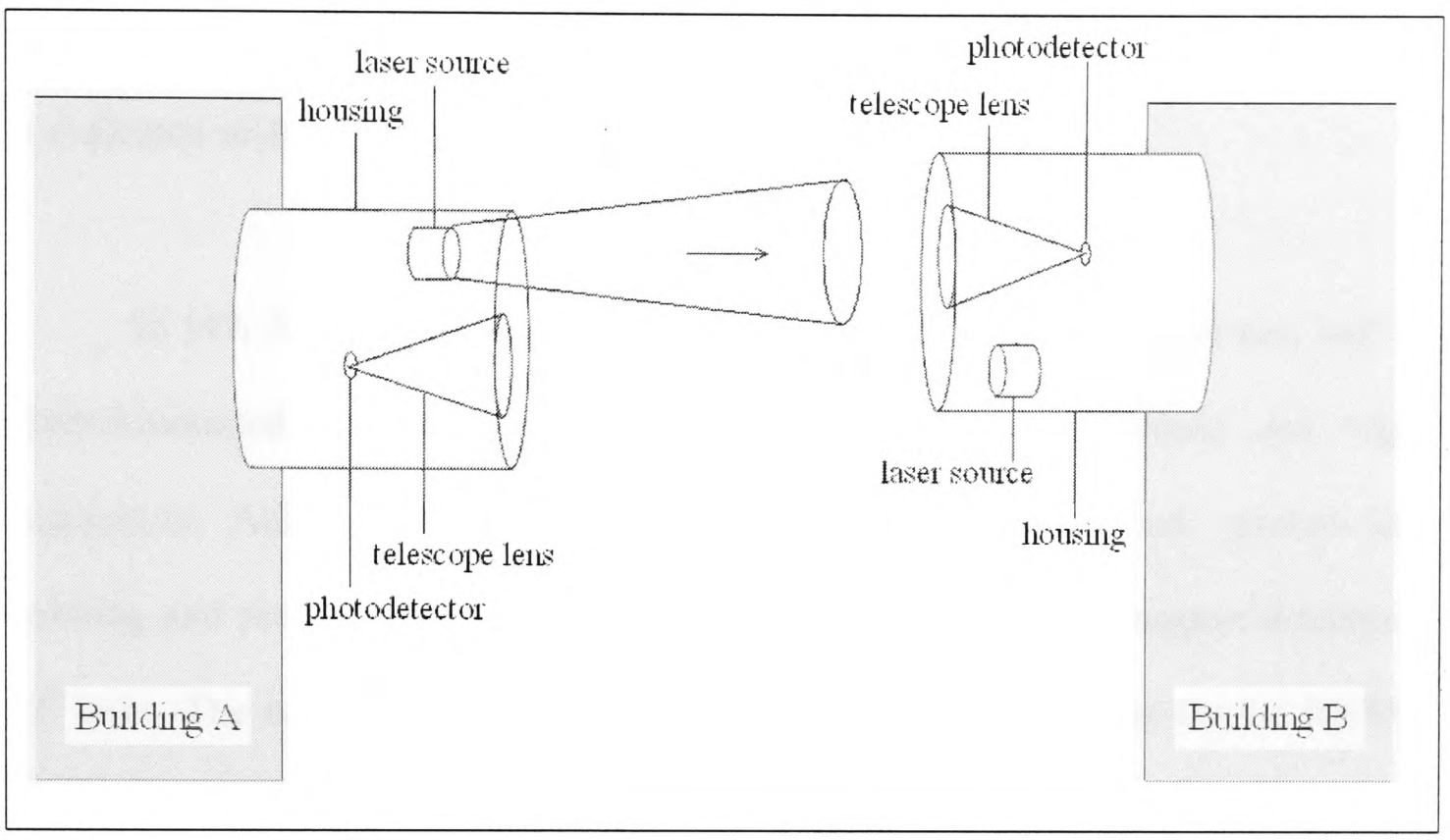

Figure 1.4: FSO broadband communications in an urban setting

However, FSO requires line of sight (LOS) between the transmitter and the receiver. In the absence of LOS, perhaps due to atmospheric obscuration, an RF broadband can be used as a backup[48-50]. Broadband RF/FSO networks use high speed narrow optical beam FSO links for point-to-point communications, and low speed directed RF links for backup [48-50]. In[50], the FSO and RF links are 1.25Gb/s and 100Mb/s respectively, and the overall RF/FSO broadband average data rate is 183Mb/s.

FSO links are affected by clouds, fog and snow[49], during which the RF links could serve as backup. RF links are prone to degradation from rain, which has little effect on FSO links[49]. The RF/FSO broadband network is highly robust, and there are almost no obscuration conditions which would cause both the RF and FSO links to fail simultaneously[48]. The performance of an RF/FSO broadband network is evaluated in[49, 50].

In [49, 50], transceivers are equipped with their own laser sources, and are gimbal-mounted with combined apertures for joint laser pointing and signal acquisition. Although a significant amount of energy is needed, gimbal-aided pointing and reception affords the apertures angular mobility to support directional RF links. The next section looks at the issue of link directionality for the RF/FSO WSN.

1.10. Communications energy and link directionality for RF/FSO WSN

In broadband RF/FSO networks, both the RF and FSO links are directional. An RF link is used as back-up to add robustness to the network, in the event of non line of sight. For RF systems, directional communications would consume less energy than omnidirectional or broadcast communications[51]. However, as providing RF directionality for a sensor node is difficult due to the small size of the node, RF transmissions of sensor nodes are typically broadcast-based[7].

Therefore, for the RF/FSO WSN, the ideal communications solution is a node capable of broadcast RF and directed FSO links. Directed optical links could be

established using modulating retroreflectors (MRRs). A retroreflector reflects the beam incident on it back in the opposite direction of incidence[52]. This beam is modulated to facilitate communications. (MRRs are discussed further in Section 3.1.)

Retroreflectors are passive optical transmitters, so the energy required for communications is lower than that of RF broadcast transmitters[16]. The energy expended for WSN FSO communications is further reduced as, unlike the broadband FSO link shown in Figure 1.4, optical pointing is only required at one end of the communications link. No pointing is done by the MRR, and the direction of the beam from the MRR depends on the direction of the incident beam.

Retroreflector-based FSO links are low speed, and in[16], a bit rate of 180bps was demonstrated. This speed is sufficient for sensor networks, which typically have data rates of several hundred bps per node[46]. The next section describes the proposed RF/FSO WSN in more detail.

1.11. The proposed RF/FSO WSN

The proposed RF/FSO WSN aims to combine the directionality of a low-energy FSO link with the robustness of a high-energy broadcast RF link. An overriding criterion in the design of wireless sensor networks is the issue of power conservation. The transceivers for RF/FSO broadband networks described in Section 1.9 require a significant amount of energy for gimbal-assisted transmission and reception. A large amount of energy is also expended by the transceiver's laser. Due to the sensor node's limited source of power, the transceiver and network

architecture proposed for the RF/FSO broadband networks in Section 1.9 is not suitable for RF/FSO WSNs. The proposed RF/FSO WSN is shown in Figure 1.5.

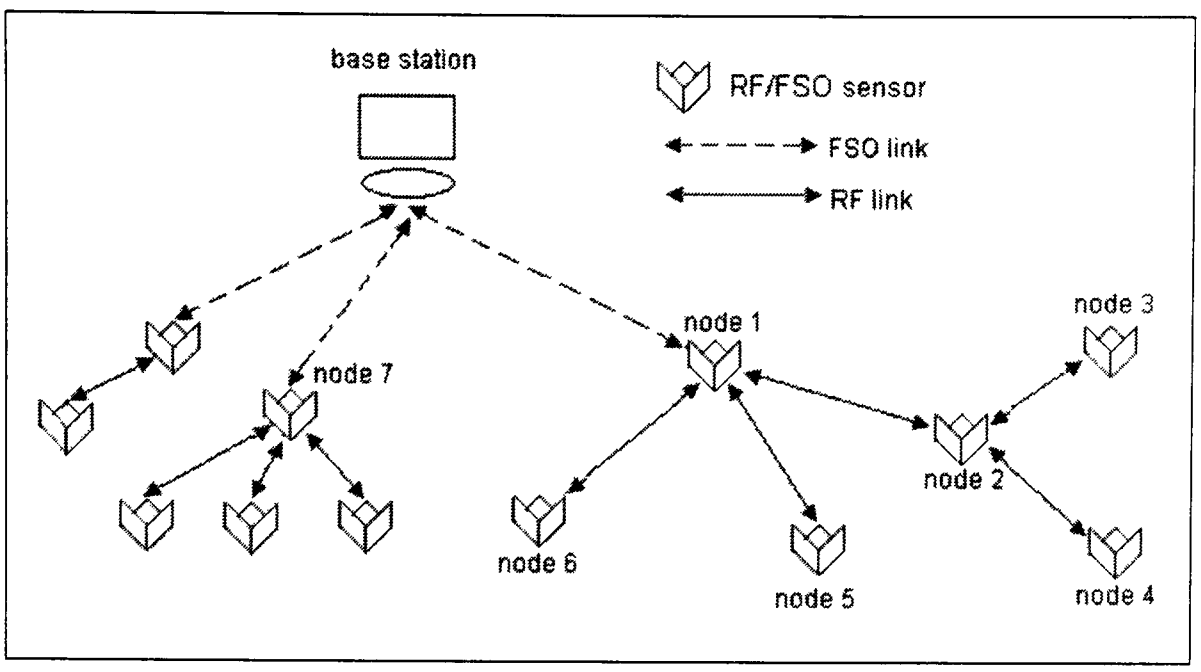

Figure 1.5: The proposed RF/FSO WSN

For the RF/FSO WSN in Figure 1.5, the base station is located directly above the middle of the deployment area. The base station, which has sight of a proportion of the sensor nodes, communicates with these nodes using Free Space Optical (FSO) links, as shown in Figure 1.5. Directional FSO communication is preferred as RF broadcast channels suffer high path loss. In addition to having line of sight to the base station, the sensor also needs to be sufficiently close to the base station to communicate optically, so link quality requirements can be satisfied.

Unlike the laser-equipped RF/FSO broadband network transceivers in[48-50, 53], the sensor nodes in the proposed RF/FSO WSN act as passive optical transmitters and do not have their own light sources, as shown in Figure 1.6.[16].

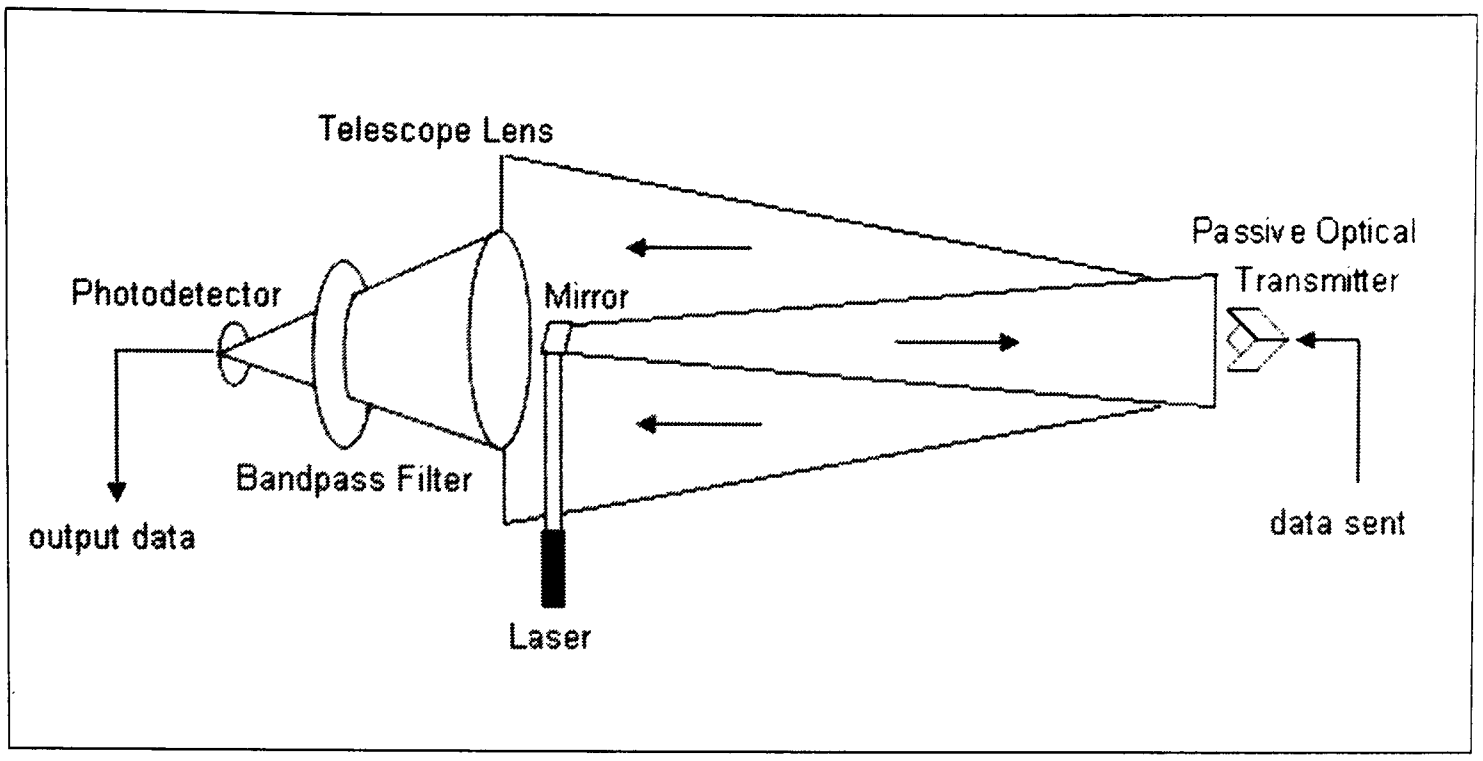

Figure 1.6: The RF/FSO WSN node as a passive optical transmitter [16]

The laser source and telescope lens are housed in the base station. The passive optical transmitter shown in Figure 1.6 is a modulating retroreflector [16] which reflects a laser beam to the telescope lens. (Modulating retroreflectors are studied in more detail in Section 3.1.) Communication is achieved by modulating this reflected beam. Passive optical transmission reduces the energy consumed by the sensor node, as the optical energy comes from the base station's laser. Passive optical transmission also consumes less energy than RF-based transmission, as the energy used for modulating the interrogation beam is relatively small (The FSO link is discussed in more detail in Chapter 3.)

In the proposed RF/FSO WSN model in Figure 1.5, the RF links function as backups to the FSO links. As the nodes are to be deployed randomly, some nodes may be overturned and these nodes will be unable to communicate optically with the base station. Overturned nodes could still communicate using RF communications. Nodes which do not have line of sight (LOS) to the base station, or which are too far

away to communicate optically with the base station, route their traffic to the base station through their closest neighbour using RF multihop links as shown in Figure 1.5. In the proposed model, the RF links are broadcast-based using omnidirectional antennas. Like the optical link, there is a maximum acceptable communication range for the RF link to ensure that the minimum quality of service is met. For RF multihop communications, a sensor node measures the relative signal strengths of its neighbouring nodes, and connects to the node with the strongest signal (which in most cases will be the closest neighbouring node).

The routing protocol suggested above is a hierarchical-based routing protocol, as the nodes in the RF/FSO WSN perform different functions depending on their proximity to and visibility of the base station. Gateway nodes and cluster heads are not predetermined, but elected from among the deployed nodes based on their relative distances and LOS with the base station. A specific example is shown in Figure 1.5. In Figure 1.5, nodes 1 and 7 act as cluster heads and gateway nodes whereas node 2 is a cluster head. The gateway nodes communicate optically with the base station. Nodes 1 and 7 are chosen as gateway nodes as they have LOS with the base station and are sufficiently close to the base station to communicate optically. Node 1 has five nodes in its cluster, imposing on it the additional duty of routing data from nodes 2-6 to the base station in addition to any of its own data.

To study the energy efficiency of the proposed RF/FSO WSN, the RF-only WSN in Figure 1.7 is used as a comparison. Nodes that are within the maximum

acceptable radio range connect directly to the base station. The other nodes route their traffic to the base station using radio multihop communications.

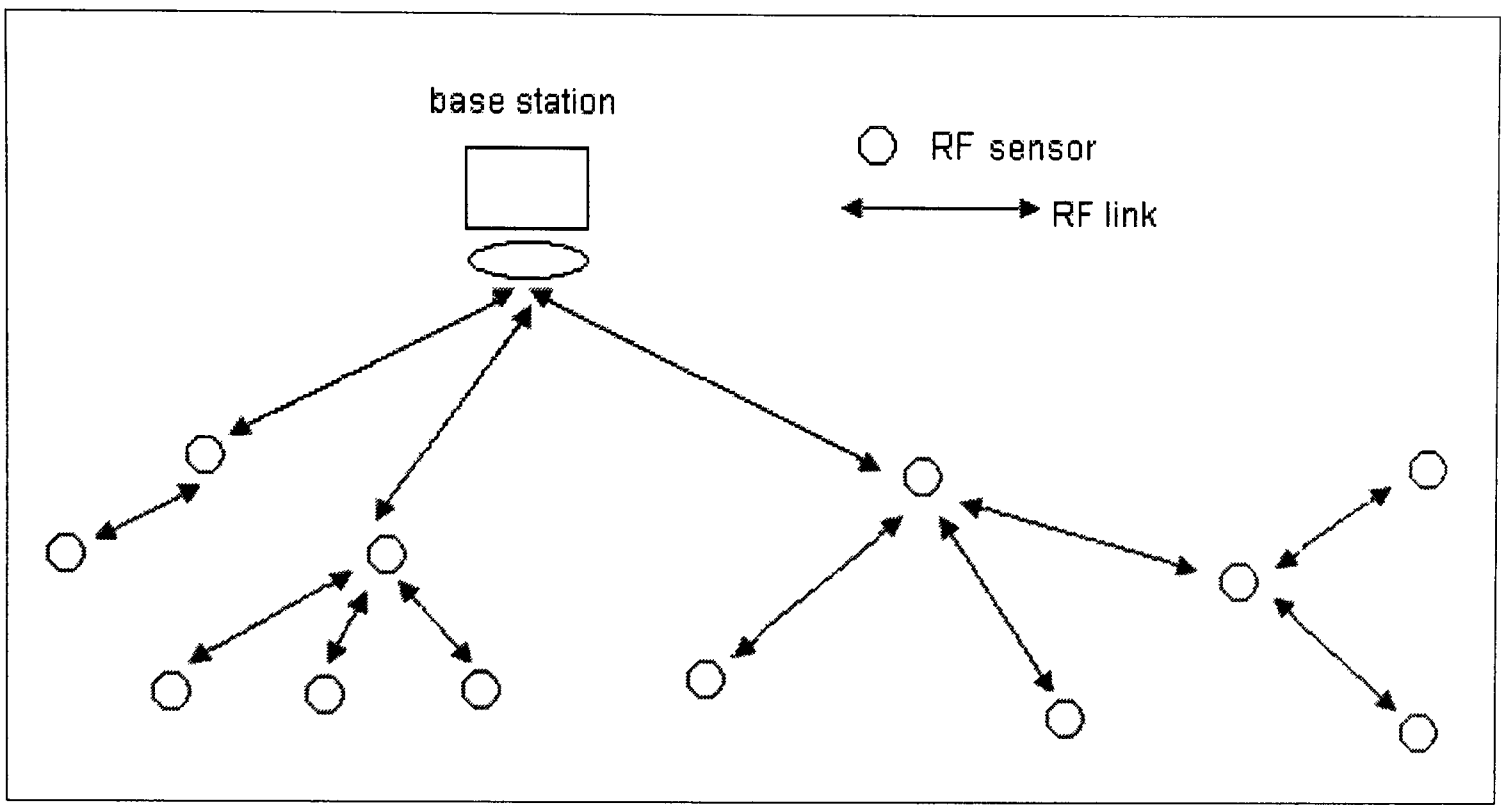

Figure 1.7: The RF-only WSN used for comparison

1.12. Thesis contributions

The contributions of this thesis are as follows:

- A novel RF/FSO WSN architecture that substantially reduces the energy consumption of a WSN. To the best of the author's knowledge, such an architecture has not been studied previously.
- A comparison study between the performance of the RF/FSO WSN and the RF-only WSN, in terms of average energy consumption, network lifetime and network coverage.
- A comparison with an existing network in the literature, showing the advantages of the proposed RF/FSO WSN.

- A performance study, comparing the RF/FSO reconfiguring and non-reconfiguring network performance.
- A guide to selecting suitable network parameters for optimum RF/FSO WSN network performance.

1.13. Conclusions and thesis outline

This chapter provided an introduction to the wireless sensor network (WSN) and some of the typical design issues associated with it. A key challenge in the design of WSNs is the issue of network energy consumption. To reduce the energy used by the WSN, the hybrid radio frequency/free space optical wireless sensor network (RF/FSO WSN) was proposed. The architecture and routing protocol for the RF/FSO WSN were introduced and discussed.

In Chapters 2 and 3, the RF and FSO link models used to support the hybrid RF/FSO WSN are investigated. Chapter 4 studies how the RF/FSO WSN configures itself. A model for the energy consumed by the sensor node is presented in Chapter 5. Chapter 6 discusses the simulation results of network traffic and network energy consumption. This is followed by a study on the relative network lifetimes for the RF/FSO and the RF-only networks in Chapter 7. Chapter 8 presents the conclusions from the research work, and proposes possible avenues for further work.

Chapter 2

The RF Link Model

In the previous chapter, the RF/FSO WSN was introduced as a possible approach to reduce the overall energy consumption of a WSN. In this chapter, the RF links supporting the hybrid network are studied in more detail. The modulation scheme for the RF link is discussed first. This is followed by a study on propagation models for the RF link. The noise figure and receiver structure are discussed next, followed by the RF link model adopted for the RF/FSO WSN simulations.

2.1. Modulation scheme for the RF link

Simple modulation schemes such as Quadrature Phase Shift Keying (QPSK) and Binary Phase Shift Keying (BPSK) are sufficient to support the low data rates characteristic of wireless sensor networks[54-58]. The energy consumption of a sensor node can be lowered if its transmit on-time is kept low[7], and M-ary modulation schemes (where M>2), like QPSK are able to reduce the transmit on-time of a sensor node. M-ary modulation supports the transmission of multiple bits per symbol, as opposed to binary modulation schemes which only transmit one bit per symbol. However, using M-ary modulation schemes increases power consumption and the complexity of the communication circuit, when compared to binary modulation schemes[59]. The BPSK modulation scheme is therefore adopted for the work in this thesis, due to its lower energy consumption.

For BPSK, the constant amplitude carrier's phase is switched between two values, usually π radians apart. The phase of the carrier signal is determined by the binary bit being transmitted, i.e. 1 or 0. The transmitted BPSK signals for logic levels '1'and '0' are given in Equations 2.1 and 2.2 respectively[60]. A is the amplitude of the sinusoidal carrier, f_c is the carrier frequency, θ_c is the carrier phase and T_b is the bit period.

$$s_{BPSK}(t) = A\ cos(2\pi f_c t + \theta_c),\ \ 0 \le t \le T_b\ \ (binary\ 1) \tag{2.1}$$

$$\begin{aligned} s_{BPSK}(t) &= A\ cos(2\pi f_c t + \pi + \theta_c) \\ &= -A\ cos(2\pi f_c t + \theta_c),\ 0 \le t \le T_b\ \ (binary\ 0) \end{aligned} \tag{2.2}$$

A transmitted signal will suffer from channel fading and noise. The noise is typically modelled as Additive White Gaussian Noise (AWGN). A model for a signal passed through a non-fading AWGN channel is given in Figure 2.1[61]. The probability of symbol error for a BPSK signal passed through a non-fading AWGN channel is given in Equations 2.3 and 2.4,

$$P_{e,AWGN} = \frac{1}{2} erfc\left(\sqrt{\frac{E_b}{N_0}}\right) \tag{2.3}$$

$$erfc(z) = \frac{2}{\sqrt{\pi}} \int_z^{\infty} e^{-x^2} dx \tag{2.4}$$

where E_b is the radio communications energy consumption per bit transmitted and N_0 is the noise power density[62].

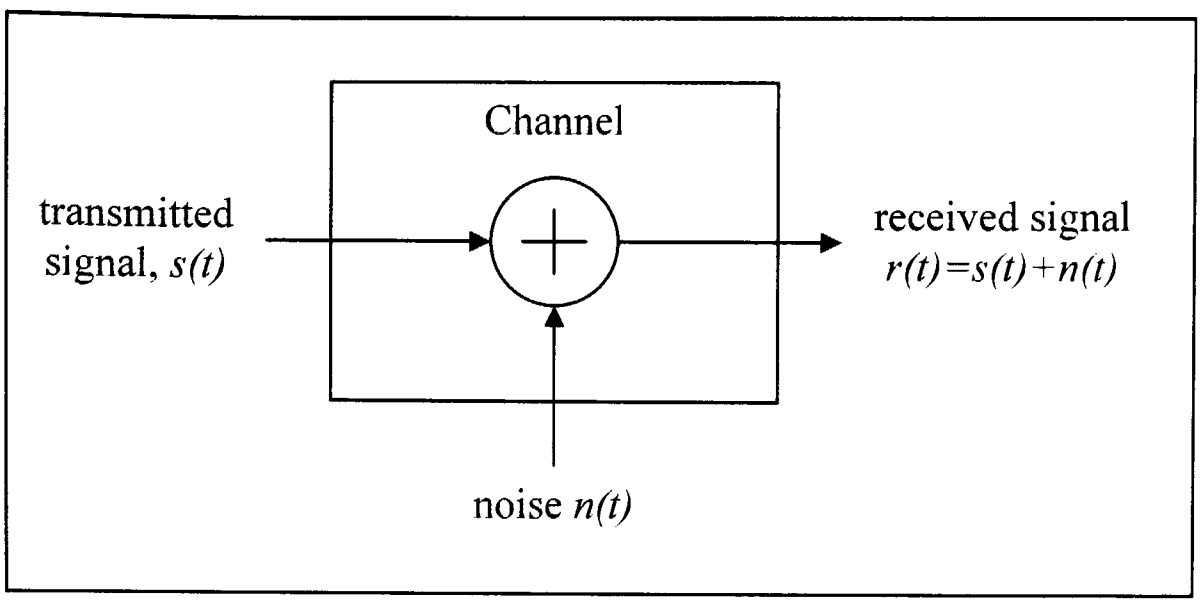

Figure 2.1: Received signal passed through a non-fading AWGN channel

In addition to AWGN, the transmitted signal also suffers from fading, which has a multiplicative rather than additive effect on the transmitted signal. (This is discussed in further detail in Section 2.2.2.)

2.2. RF propagation models

It is difficult to model radio signal propagation, due to the variability of the environment the signal propagates through. Two types of models are investigated in this section – large and small scale propagation models. Large scale propagation models, studied in Section 2.2.1, are used to determine the path loss suffered by an RF signal over large transmitter-receiver separation distances[60]. Small scale propagation models, investigated in Section 2.2.2, characterize the rapid fluctuations of the RF signal over very short distances[60].

2.2.1. Large scale propagation: Path loss model

The large scale propagation model is also known as the path loss model[60]. A number of empirical and analytical models have been proposed to model radio signal path loss[60]. The signal power at the receiver $P_r(d)$ is a function of the transmitter and receiver separation distance, d, and is given as:

$$P_r(d) = \frac{P_t}{P_L(d)} \tag{2.5}$$

where P_L is the power loss, P_t is the transmitted power and d is the transmitter and receiver separation distance. Some common path loss models are the free space path loss model and the log-distance path loss model[60]. The free space path loss model describes the path loss of the radio signal when there is a line of sight (LOS) path between the transmitter and receiver. The path loss for free space propagation, P_L, is given as[60]:

$$P_L(d) = \frac{(4\pi)^2 d^2 L}{G_t G_r \lambda^2} \tag{2.6}$$

where G_t is the transmitter antenna gain, G_r is the receiver antenna gain, and λ is the wavelength. L is the system loss factor not related to propagation and is usually due to filter losses, antenna losses and transmission line attenuation ($L \geq 1$)[60]. L=1 indicates zero loss in the system hardware. A more general model, applicable for either an LOS channel or a non-LOS (NLOS) channel between the transmitter and receiver, is the log-distance path loss model, given as:

$$\overline{P_L(d)}[dB] = \overline{P_L(d_0)}[dB] + 10n\log\left(\frac{d}{d_0}\right) \tag{2.7}$$

The path loss in Equation 2.7 is the average value of all the possible path loss values for a certain d, as indicated by the bar. The free-space reference distance, d_0, is determined from measurements close to the receiver[60]. The path loss exponent, n, is typically determined from field measurements and depends on the frequency of the radio signal and the propagation environment. Assuming average path losses, Equation 2.7 can be rewritten as:

$$P_L(d) = P_L(d_0) \cdot \left(\frac{d}{d_0}\right)^n \tag{2.8}$$

2.2.2. Small scale propagation: Channel fading model

In addition to AWGN, the radio channel also suffers from channel fading. Channel fading is incorporated into the RF models as, although the base station and nodes are static, the channel itself is not and could change due to environmental variations. The small scale propagation model is also known as the channel fading model[60]. Fading is caused by the interference of several versions of the same signal, travelling over different paths and arriving at the receiver at slightly different times. This could cause the received signal to vary rapidly over a small distance[60]. The distortion caused by fading is multiplicative, and therefore, the received signal which is distorted by AWGN and fading can be represented as[61]:

$$r(t) = a \cdot s(t) + n(t) \tag{2.9}$$

where a is the distortion caused by fading and $n(t)$ is the AWGN. The parameter a is randomly distributed and defines the type of channel fading suffered by the signal. For a non-fading channel, $a = 1$.

A number of channel fading models have been proposed, among them being the Rayleigh and Ricean models[60, 61, 63]. When there is a dominant line of sight (LOS) path between the transmitter and receiver, the channel fading fits a Ricean model[63]. In the absence of an LOS path, the Rayleigh model is used[63].

Figure 2.2 shows the various RF links considered for the WSN. WSNs typically have low transmission rates with symbol periods much higher than the root mean square (RMS) delay spread[64], so all three channels shown in Figure 2.2 can be assumed to be slow flat fading channels[64]. If the channel fading is slow enough for the receiver to estimate the signal's phase shift without error, the received signal can be coherently detected[61]. In the simulations in this thesis, the signals are assumed to be coherently-detected.

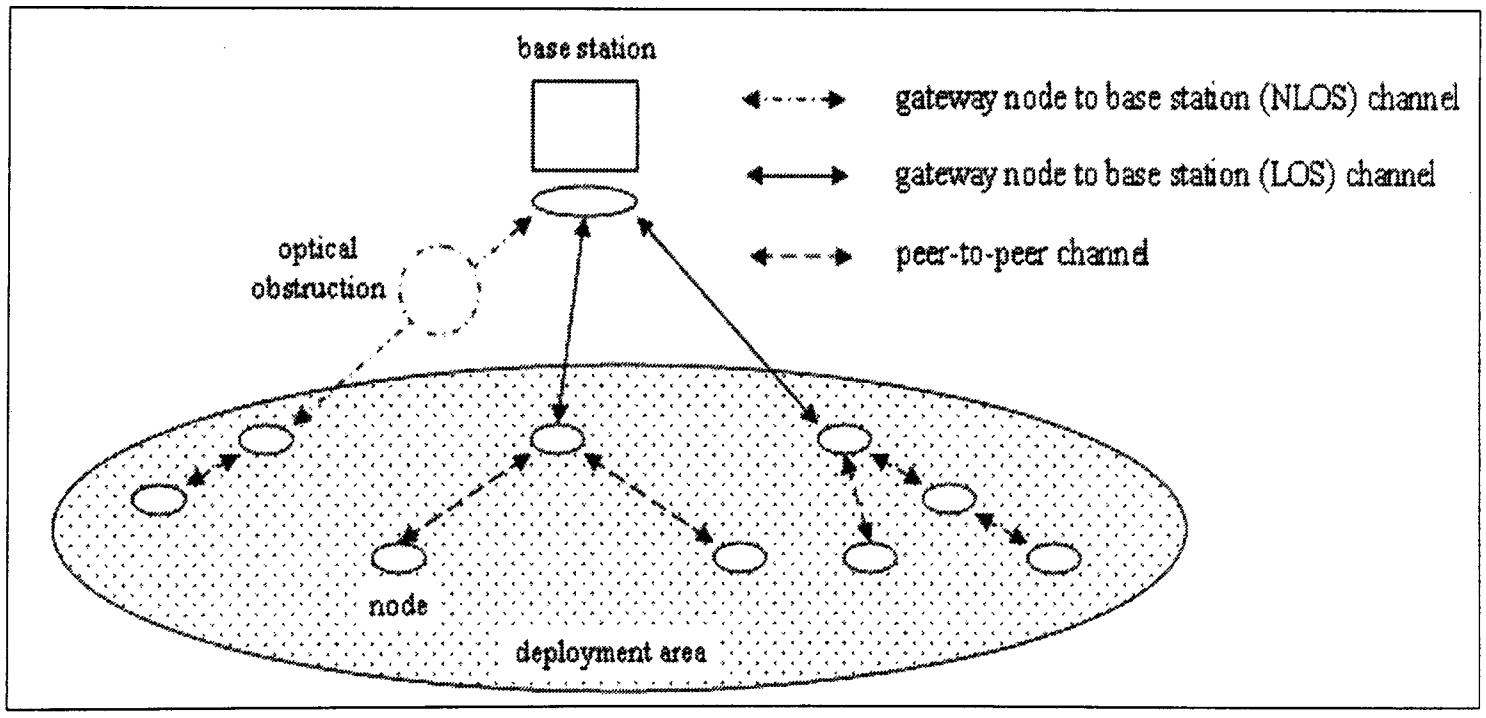

Figure 2.2: The RF links for the WSN

The probability of symbol error for a BPSK signal in a slow flat fading Rayleigh channel, $P_{e,Rayleigh,}$ is given as[63]:

$$P_{e,Rayleigh} = \frac{1}{\pi}\int_0^{\pi/2}\left(1+\frac{\gamma}{\sin^2 x}\right)^{-1} dx \qquad (2.10)$$

where γ is the average E_b/N_0:

$$\gamma = \frac{\overline{E_b}}{N_0} \tag{2.11}$$

A simplified form of Equation 2.10 is given in Equation 2.12[61].

$$P_{e,Rayleigh} = \frac{1}{2}\left(1 - \sqrt{\frac{\gamma}{1+\gamma}}\right) \tag{2.12}$$

The probability of symbol error for a BPSK signal in a slow flat fading Ricean channel, $P_{e,Ricean}$ is given as[63]:

$$P_{e,Ricean} = \frac{1}{\pi}\int_0^{\pi/2} \frac{(1+K_r)\cdot\sin^2 x}{(1+K_r)\cdot\sin^2 x+\gamma} \cdot \exp\left(-\frac{K_r\cdot\gamma}{(1+K_r)\cdot\sin^2 x+\gamma}\right) dx \tag{2.13}$$

where K_r is known as the Ricean factor and is defined as the ratio between the LOS signal power and the variance of the multipath[60]. As in the case of the path loss exponent, n, the Ricean factor, K_r, is dependent on the communications environment and is typically determined from field measurements[60].

Rayleigh fading is a special case of Ricean fading. In the absence of an LOS path, the Ricean fading model is the same as that of a Rayleigh channel. Substituting $K_r = 0$ (for a NLOS path) in Equation 2.13 gives:

$$P_e = \frac{1}{\pi}\int_0^{\pi/2} \frac{\sin^2 x}{\sin^2 x+\gamma} dx \tag{2.14}$$

which, with some rearrangement, is the same as Equation 2.10. For a channel with a single propagation path, K_r approaches infinity in Equation 2.13. As K_r approaches infinity, Equation 2.13 reduces to Equation 2.3, which is the probability of symbol error for a BPSK signal without fading. Table 2.1 summarizes the probability of error

formulae, P_e, for slow flat fading BPSK channels. Figure 2.3 shows the P_e curves for the different fading channels.

TABLE 2.1
Probability of error for slow flat fading BPSK channels

Channel fading	**Probability of symbol error, P_e**
AWGN (no fading, $K_r \to \infty$)	$P_{e,AWGN} = \frac{1}{\sqrt{\pi}} \int_{\sqrt{\gamma}}^{\infty} \exp(-x^2)dx$
Rayleigh (K_r=0)	$P_{e,Rayleigh} = \frac{1}{2}\left(1 - \sqrt{\frac{\gamma}{1+\gamma}}\right)$
Ricean	$P_{e,Ricean} = \frac{1}{\pi} \int_0^{\pi/2} \frac{(1+K_r)\cdot \sin^2 x}{(1+K_r)\cdot \sin^2 x + \gamma} \cdot \exp\left(-\frac{K_r \cdot \gamma}{(1+K_r)\cdot \sin^2 x + \gamma}\right) dx$

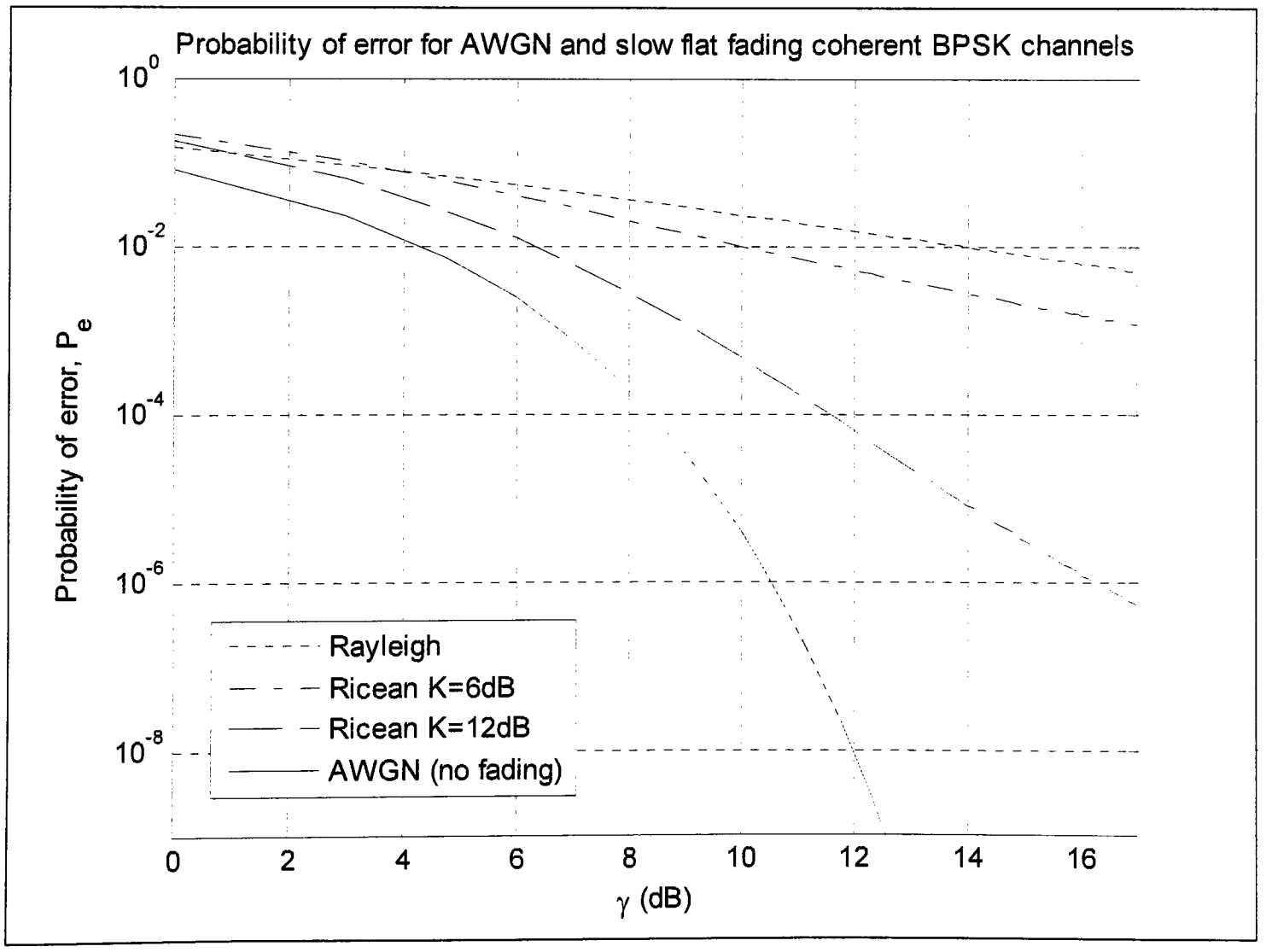

Figure 2.3: Probability of error, P_e, curves for the different fading channels

2.3. Radio receiver and noise figure

Power conservation is a crucial aspect of the sensor node's operation. Low power radio architectures proposed for sensors employ direct conversion receivers rather than the conventional superheterodyne receivers[55]. (The direct conversion receiver architecture is explained in detail in[65].) Superheterodyne receivers offer high selectivity and sensitivity. However, the complicated design and stringent design requirements associated with superheterodyne receivers result in high power dissipation[55]. Although a high level of sensitivity is necessary to support the long communication ranges typical of cellular systems, it is often sacrificed in favour of lower power dissipation for wireless sensor networks[66]. The advantages and disadvantages of both receiver architectures are discussed in[67].

The direct conversion receiver uses coherent detection, using a local oscillator operating at the carrier frequency to directly demodulate the received signal [65]. The noise figure, F, is the ratio of the input to output signal to noise ratios of the receiver[68]. The 2.4 GHz direct conversion receiver in [66] has a noise figure of 28dB. The receivers in [55] and[67], which operate in the 902-928 MHz and 868/915 MHz bands respectively, have a noise figure of 19dB. These noise figures would be too high for cellular systems, which need to support communication links several km in length[66]. Compared to cellular systems, wireless sensor networks support lower communication ranges due to the higher noise figures characteristic of sensor node receivers[66].

The signal to noise ratio at the receiver, SNR_r is given as[69]:

$$SNR_r = \frac{P_r}{kT_0BF} \tag{2.15}$$

where k is Boltzmann's constant and equal to 1.38 x 10^{-23} Joules / Kelvin, T_0 is the ambient room temperature (typically assumed to be 290K or 300K), B is the equivalent bandwidth of the receiver and F is the noise figure. Equation 2.15 will be used to derive the transmitted RF energy per bit, $E_{b,ta}$, which is discussed in the next section.

2.4. The transmitted RF energy per bit

This section derives the transmitted RF energy per bit, $E_{b,ta}$. A sensor node requires energy to perform data processing, sensing and communications (transmission and reception)[70], and Figure 2.4 shows a simplified energy consumption model of a node. (The sensor node energy model is studied in more detail in Chapter 5.) $E_{b,te}$ is the energy per bit required to drive the transmitter electronics (discussed in Chapter 5) and $E_{b,ta}$ is the transmitted RF energy per bit.

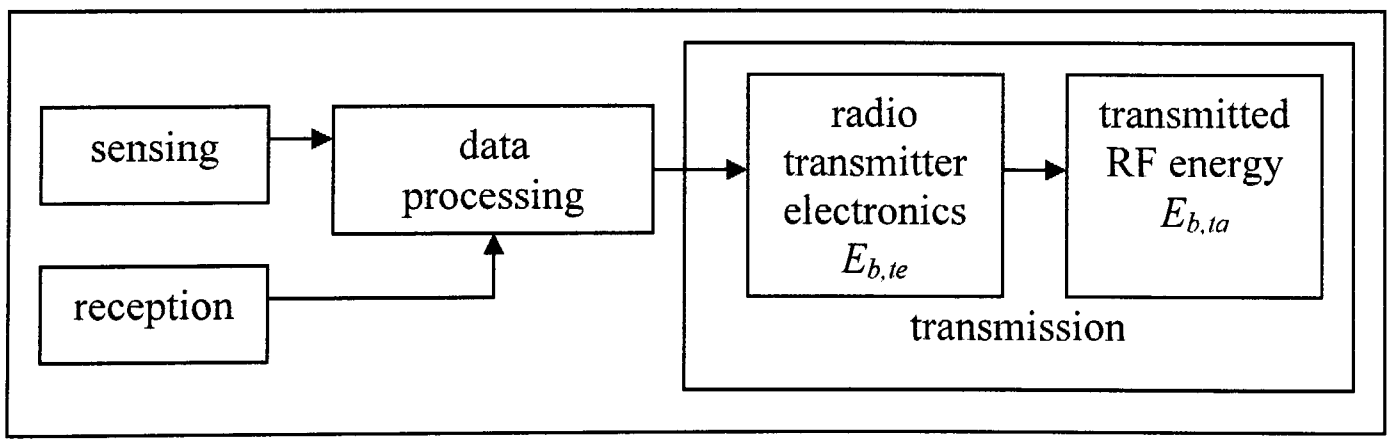

Figure 2.4: Energy consumption model of a node employing RF transmission

In this section, the RF path loss equation will be used to derive the transmitted RF energy per bit, $E_{b,ta}$. The path loss, $P_L(d)$, is given in Equation 2.8.

The free space path loss model is assumed between the transmitter and the free space reference distance, d_0. For $d>d_0$, Equation 2.8 can therefore be rewritten as:

$$P_L(d) = \frac{(4\pi)^2 \cdot {d_0}^2 \cdot L}{G_t \cdot G_r \cdot \lambda^2} \left(\frac{d}{d_0} \right)^n \tag{2.16}$$

from Equations 2.6 and 2.8. The SNR at the receiver is given in Equation 2.15. For a bitrate R_b, Equation 2.15 can be rewritten as[69]:

$$\frac{E_b \cdot R_b}{N_0} = \frac{P_r}{k \cdot T_0 \cdot F} \tag{2.17}$$

From Equations 2.5 and 2.16, Equation 2.17 can be rewritten as:

$$\gamma \cdot R_b = \frac{P_t}{kT_0F} \cdot \frac{G_t \cdot G_r \cdot \lambda^2 \cdot {d_0}^n}{(4\pi)^2 \cdot {d_0}^2 \cdot L \cdot d^n} \tag{2.18}$$

$$E_{b,ta} = \frac{\gamma \cdot k \cdot T_0 \cdot F \cdot (4\pi)^2 \cdot {d_0}^2 \cdot L \cdot d^n}{G_t \cdot G_r \cdot \lambda^2 \cdot {d_0}^n} \tag{2.19}$$

$$E_{b,ta} = \varepsilon \cdot d^n \tag{2.20}$$

where ε is the RF transmission factor. If the value of $E_{b,ta}$ is fixed, d is the maximum radio range which allows the transmission to adhere to signal to noise constraints (E_b/N_0) and is given as:

$$d = \left(\frac{E_{b,ta} \cdot G_t \cdot G_r \cdot \lambda^2 \cdot {d_0}^n}{\gamma \cdot k \cdot T_0 \cdot F \cdot (4\pi)^2 \cdot {d_0}^2 \cdot L} \right)^{1/n} \tag{2.21}$$

2.5. RF link model for RF/FSO WSN simulations

General models of the RF links were studied in Sections 2.1 to 2.4. In this section, specific values are assigned to the various RF parameters discussed, and these will be used for the simulations of the RF/FSO WSN in the following chapters.

The BSPK modulation scheme and a direct conversion receiver which performs BPSK detection is assumed for the simulations. Based on the noise figure values discussed in Section 2.3, F is set to 20dB. The carrier frequency is set to 2.4GHz, corresponding to the licence-free industrial, scientific and medical (ISM) RF band. The 2.4GHz ISM band is available worldwide, while the ISM 868MHz and ISM 915MHz bands are available in Europe and North America respectively[71]. The room temperature, T_0, is set to 27°C (300 K).

A microcell has a base station in the middle of the cell, with a radio range of between 100m and 1km[72], and this closely resembles the RF-only WSN shown in Figure 1.7. (Later discussions in this chapter will show that the RF-only WSN has a typical radio range of about 150m.) For microcellular systems, a suitable value for d_0 is 1m [60], and this is the value used for the simulations.

Due to the sizes of the node and its antenna relative to the wavelength used, it is difficult to produce high antenna gains[60]. Omnidirectional unity gain antennas are assumed for the work in this thesis, so G_t=G_r=1. Ignoring system loss not related to propagation (L=1), and with d_0 =1m in Equation 2.19, the transmitted RF energy per bit reduces to:

$$E_{b,ta} = \left(\frac{4\pi}{\lambda}\right)^2 \cdot \gamma \cdot k \cdot T_0 \cdot F \cdot d^n \tag{2.22}$$

The maximum radio range, d, in Equation 2.21 reduces to:

$$d = \left(E_{b,ta} \cdot \left(\frac{\lambda}{4\pi}\right)^2 \cdot \frac{1}{\gamma \cdot k \cdot T_0 \cdot F} \right)^{1/n}. \tag{2.23}$$

For the WSN considered in this work, the RF channels are categorized as node to base station channels with line of sight (LOS), node to base station channels with no LOS (NLOS) and peer-to-peer channels on the ground. All three channels are shown in Figure 2.2. For all three channels, the log-distance path loss model is assumed for $d \geq d_0$ and the free space model is used for $d<d_0$ (discussed in Section 2.2.1.).

The path loss exponent, n, is close to 4 for the low-lying antenna and near-ground channels that are typical of wireless sensor networks[7, 19]. Rayleigh fading conditions with $n = 4$ are therefore used to simulate the peer-to-peer channels on the ground for $d \geq d_0$ in Figure 2.2. If there is line of sight between the receiver and transmitter, the path loss exponent is close to 2[7, 19]. Therefore, for LOS channels to the base station in the simulations, Ricean fading with a Ricean factor, K_r, and $n =$ 2 are assumed for $d \geq d_0$. In most cases, the path loss exponent, n, has a range of $2 \leq n<4$[7, 19]. Therefore, to simulate the NLOS channels to the base station in Figure 2.2, a mid-value of 3 is chosen for n and Rayleigh fading is assumed for $d \geq d_0$.

A typical range for the value of K_r is 5-15 dB for WSNs[73-77]. The Ricean factor is set to 5 dB in [73, 74] and 9 dB in[75, 76]. The value for K_r ranges from 5-15 dB in[77]. For the simulations in this study, the Ricean factor is set to 10dB. A summary of the propagation models for the WSN RF links is given in Table 2.2. In the table, γ_{PP}, γ_L and γ_{NL} replace γ in Equations 2.12, 2.13 and 2.12 respectively.

TABLE 2.2
Summary of propagation models adopted for RF channels

RF channel	**Path Loss Model**		**Fading Model**	**Transmitted RF energy per bit, $E_{b,ta}$**
	$d < d_0$	$d \geq d_0$		
peer-to-peer	free space	log-distance, $n = 4$	Rayleigh	$E_{b,ta,PP} = \gamma_{PP} \cdot k \cdot T_0 \cdot F \cdot \left(\frac{4\pi}{\lambda}\right)^2 \cdot d^2, \quad d<d_0$ $E_{b,ta,PP} = \varepsilon_{PP} \cdot d^2, \quad d<d_0$ $E_{b,ta,PP} = \gamma_{PP} \cdot k \cdot T_0 \cdot F \cdot \left(\frac{4\pi}{\lambda}\right)^2 \cdot d^4, \quad d \geq d_0$ $E_{b,ta,PP} = \varepsilon_{PP} \cdot d^4, \quad d \geq d_0$
node to base station (LOS)	free space	log-distance, $n = 2$	Ricean, K_r=10 dB	$E_{b,ta,L} = \gamma_L \cdot k \cdot T_0 \cdot F \cdot \left(\frac{4\pi}{\lambda}\right)^2 \cdot d^2$ $E_{b,ta,L} = \varepsilon_L \cdot d^2$
node to base station (NLOS)	free space	log-distance, $n = 3$	Rayleigh	$E_{b,ta,NL} = \gamma_{NL} \cdot k \cdot T_0 \cdot F \cdot \left(\frac{4\pi}{\lambda}\right)^2 \cdot d^2, \quad d<d_0$ $E_{b,ta,NL} = \varepsilon_{NL} \cdot d^2, \quad d<d_0$ $E_{b,ta,NL} = \gamma_{NL} \cdot k \cdot T_0 \cdot F \cdot \left(\frac{4\pi}{\lambda}\right)^2 \cdot d^3, \quad d \geq d_0$ $E_{b,ta,NL} = \varepsilon_{NL} \cdot d^3, \quad d \geq d_0$

ε_{PP} : the RF transmission factor for the peer-to-peer channel

ε_L : the RF transmission factor for the node to base station (LOS) channel

ε_{NL} : the RF transmission factor for the node to base station (NLOS) channel

The tolerated probability of symbol error, P_e, will vary depending on the purpose of the sensor network. A lower probability of error can be achieved by increasing the transmit power of the signal. However, this is not always desirable, due to the limited power source of the nodes. Depending on the function of the WSN, a typical bit error rate can range from 10^{-2} to 10^{-11}[78]. WiseNET is a low-power platform used to implement WSNs, and operates at a bit error probability of 10^{-3}[79]. Therefore, the probability of error, P_e, is set to 10^{-3} for the work in this report.

The maximum amount of energy expended by the sensor node to transmit data is fixed, to avoid the node spending too much energy and dying prematurely. This could be done by capping the power transmitted by an individual node. (It is assumed that the node has the option of being able to choose an appropriate power level, depending on the communication distance[80]). Power control is a very useful method of improving wireless network performance and is described in detail in[81, 82]. To limit the amount of power used by the sensor node for communications, a maximum $E_{b,ta}$ is enforced. Limiting the $E_{b,ta}$ would encourage the node to route its data via a closer node. This consumes less energy, as $E_{b,ta}$ is proportional to d^n, where d is the communications range and n is the path loss exponent. Bluetooth is an industrial standard used for RF-based wireless personal area networks and WSNs. Work on WSNs based on Bluetooth is described in[83-85]. The average transmitted energy for the Bluetooth in [16] is 1nJ/bit over a few tens of metres. In[26], the transmitted RF energy per bit is between 0.1 and 0.6 nJ/bit for a distance of 5m when there is no line of sight between the transmitter and receiver. With line of sight, the transmitted energy over a distance of 10m in [31, 32] is 0.1 nJ/bit. Based on these

values, the maximum value of $E_{b,ta}$ is set to 1nJ/bit for the simulations in this work. Placing a limit on $E_{b,ta}$ means that there is a maximum radio range over which the sensor node can transmit to fulfil performance requirements. This maximum range, determined using Equation 2.23 and the specific values assigned earlier, is d_{PP}, d_L and d_{NL} for the peer-to-peer, node to base station (LOS), and node to base station (NLOS) channels respectively. A summary of the values which will be used for the simulations is given in Table 2.3.

TABLE 2.3
Summary of RF channel propagation values used for simulations ($P_e=10^{-3}$)

RF channel	**RF transmission factor**	**Average E_b/N_0**	**Maximum range**
peer-to-peer	$\varepsilon_{PP} = 10^{-12}$ J/bit/m^n	$\gamma_{PP} = 24.0$ dB	$d_{PP} = 5.6$ m
node to base station (LOS)	$\varepsilon_L = 4.7 \times 10^{-14}$ J/bit/m^n	$\gamma_L = 10.5$ dB	$d_L = 145.7$ m
node to base station (NLOS)	$\varepsilon_{NL} = 10^{-12}$ J/bit/m^n	$\gamma_{NL} = 24.0$ dB	$d_{NL} = 9.9$ m

2.6. Conclusions

This chapter investigated the RF link models which support the RF/FSO and RF-only WSNs. For the RF link, BPSK modulation and the log-distance path loss model are proposed. Ricean and Rayleigh fading models are adopted, depending on whether the channel is peer-to-peer or node to base station. The receiver used for the simulations is assumed to be a direct conversion receiver capable of BPSK demodulation. The next chapter will study the WSN's FSO link model.

Chapter 3

The FSO Link Model

In the previous chapter, the RF link model was studied. The free space optical (FSO) link supporting the hybrid RF/FSO network is studied in more detail in this chapter. FSO communications is based on light propagating through free space for point-to-point data transmission[86]. FSO communications is highly directional, but it requires line of sight (LOS) between the receiver and the transmitter. For transmission, a source of light – typically a laser, is required[87]. Communication is achieved by modulating the transmitted laser beam. On-off keying (OOK) modulation is typically employed for this purpose[20]. For the FSO links in the RF/FSO WSN, modulating retroreflectors (MMR) are considered as shown in Figure 3.1.

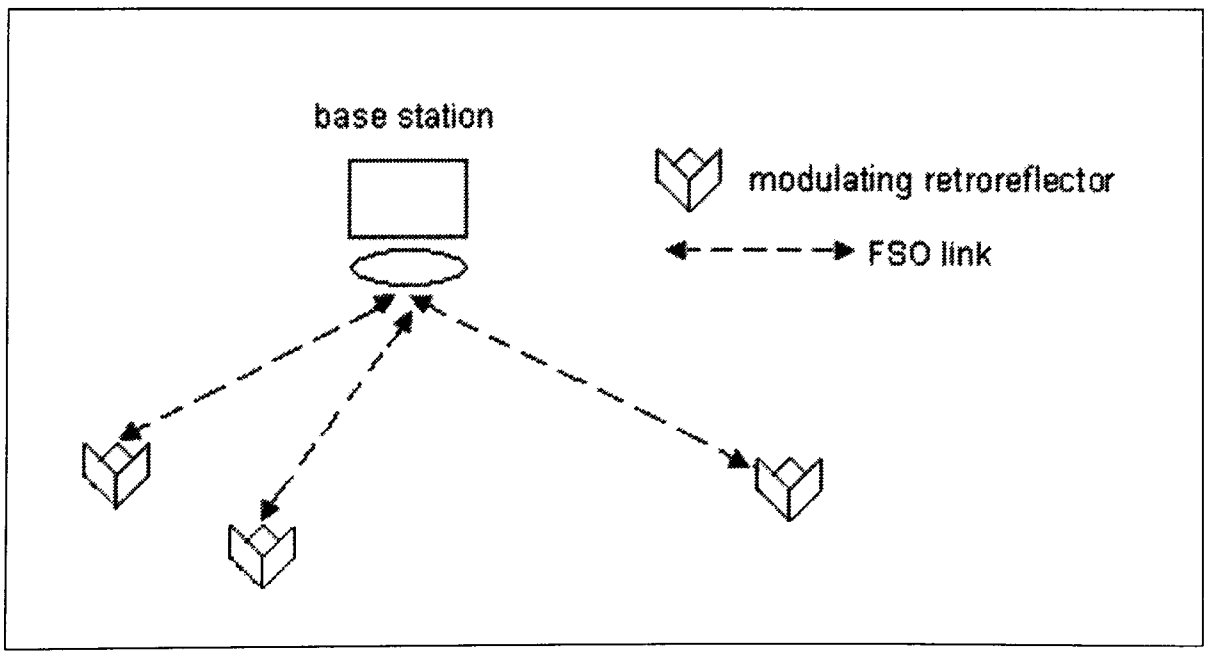

Figure 3.1: Base station and FSO links

3.1. The modulating retroreflector (MRR) as a passive optical transmitter

The modulating retroreflector (MRR) is an example of a passive optical transmitter, and it consists of an optical retroreflector and a modulation mechanism (see Figure 3.2). The optical retroreflector reflects the beam incident on it back in the opposite direction of incidence[52]. Sensor nodes have a limited source of energy, making the MRR a suitable choice for WSN communications.

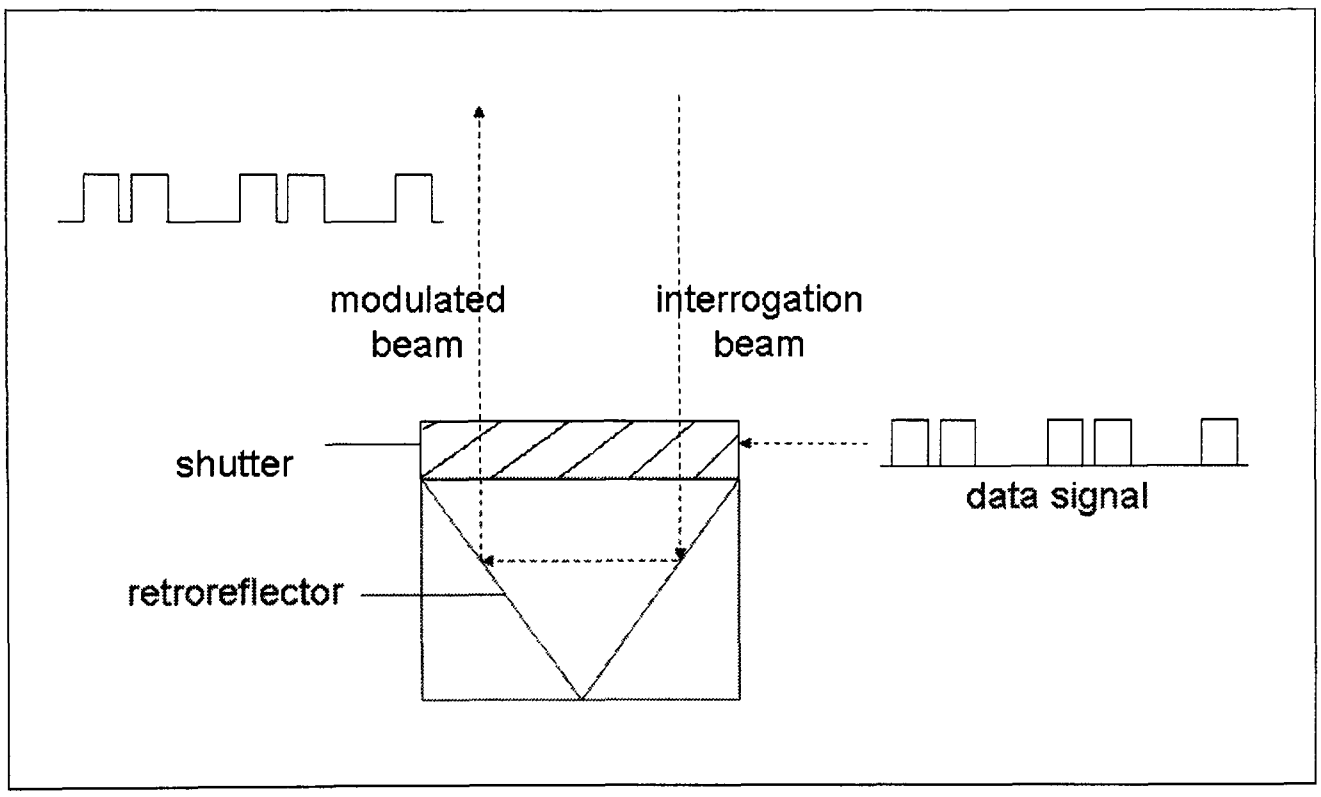

Figure 3.2: MRR with electro-optic shutter

Several retroreflector designs have been proposed, including spherical or ball-lens[88], the corner cube [89] and cat's eye[90]. The ray trace for the cat's eye retroreflector is shown in Figure 3.3[91]. Both hemispheres in the cat's eye retroreflector have the same refractive index, with one hemisphere having a larger radius than the other. The coating at the back of the larger hemisphere is highly-reflective. The incident ray focuses on the back surface of the larger hemisphere and is reflected in the opposite direction.

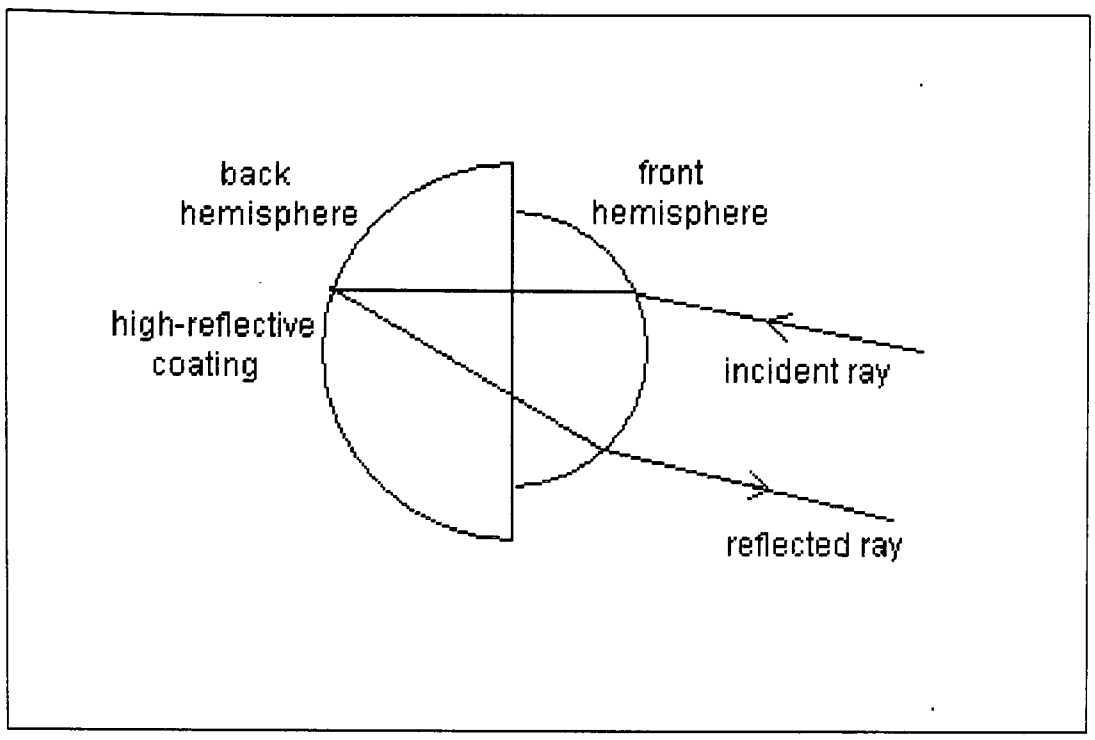

Figure 3.3: Ray trace of cat's eye retroreflector

The ray trace of the ball lens retroreflector is shown in Figure 3.4[92]. To function as a retroreflector, the ball-lens has a refractive index close to 2[93]. The incident ray focuses on the back of the ball lens and is reflected in the opposite direction. The high refractive index causes a significant amount of light to be reflected back towards the source[92]. The amount of reflected light could be increased by applying a light-reflective coating to the back of the ball-lens.

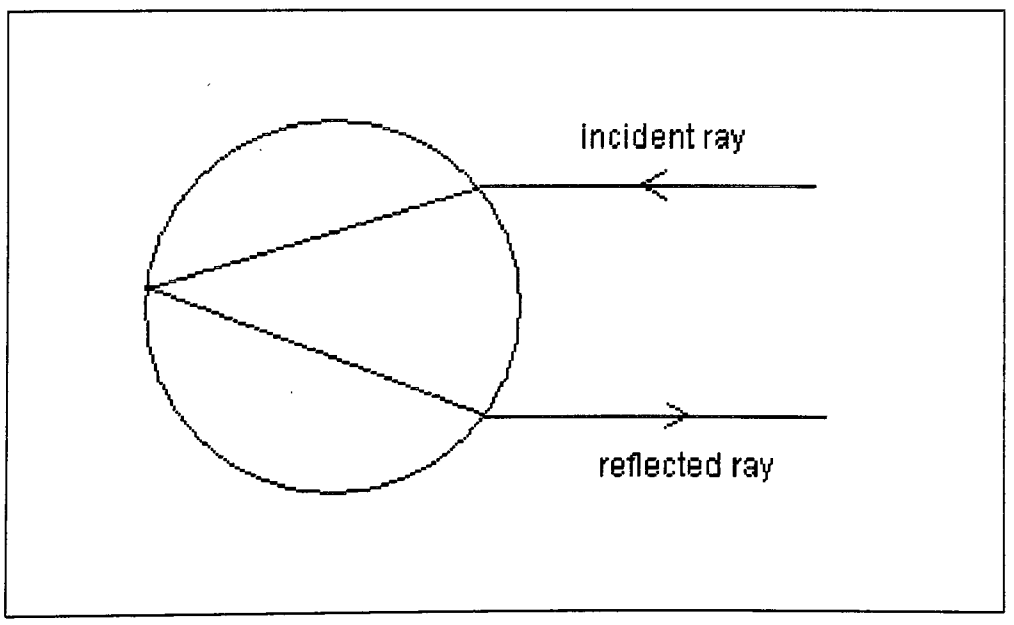

Figure 3.4: Ray trace of ball-lens retroreflector

The Smart Dust project uses corner cube retroreflectors (CCRs) for its sensor nodes[94]. The structure of a corner cube retroreflector is based on three mutually orthogonal mirrors forming a concave corner[94-97]. Figure 3.5 shows the ray trace of the CCR[97]. In an ideal CCR, the incident ray reflects off the orthogonal mirror surfaces of the CCR and returns to the source.

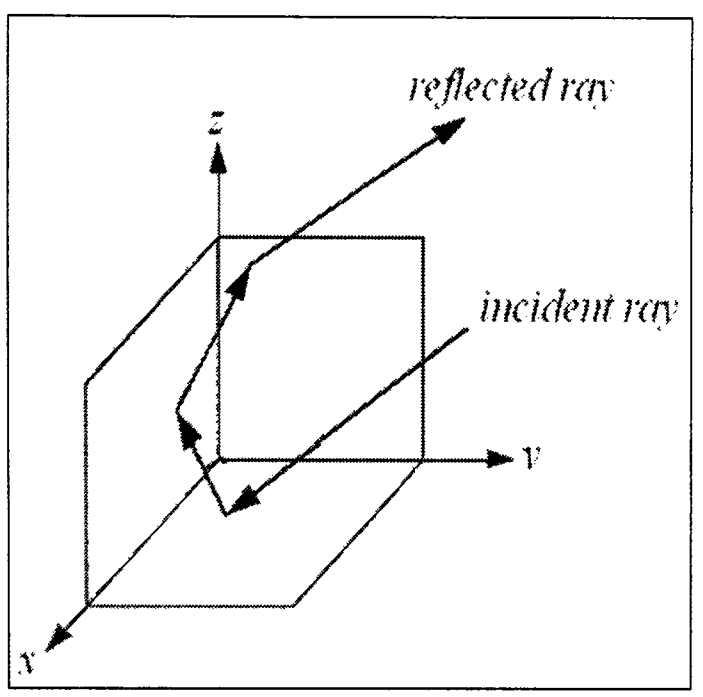

Figure 3.5: Ray trace of the corner cube retroreflector

A number of modulation mechanisms have been proposed for MRRs. The laser beam can be modulated by an active electro-optic shutter, such as a Multiple Quantum Well (MQW) [98]or liquid crystal [99] as shown in Figure 3.2. The shutter obstructs the return beam for a bit '0' and passes the return beam for a bit '1', or vice versa depending on the MRR's quiescent state. The MQW shutter operates by changing its absorption feature at the incident ray's wavelength[98]. In its quiescent state, the MQW obstructs incident light to the retroreflector. However, when a moderate voltage of 10 to 15V is applied across its shutter, its absorbance shifts and light is transmitted to and from the retroreflector.

For the liquid crystal shutter, the non-uniformity in the alignment of liquid crystal molecules in the quiescent state causes optical scattering[100]. When an electric field is applied across the shutter, the molecules align and the optical scattering effect is reduced. Light can therefore be transmitted to and from the retroreflector.

Liquid crystal shutters can also use crossed polarizers, with a liquid crystal cell placed between them [101]. Light passes through a polarizer, a liquid crystal cell, and an analyzer (the second polarizer). The liquid crystal cell alters the polarization state of the light depending on the voltage applied to it, and this polarization state is converted into an intensity modulation by the analyzer.

In[16], the authors propose to change the shape of the CCR by misaligning the bottom mirror of the CCR, to modulate the return beam. The transmitter passes the reflected beam to the receiver uninterrupted for a bit '1'. The transmitter obstructs or interrupts the return beam to the receiver to transmit a bit '0' by misaligning the bottom mirror of the CCR. Figure 3.6 shows a possible configuration for free space optical communication using the CCR with the actuating bottom mirror, as described in[16].

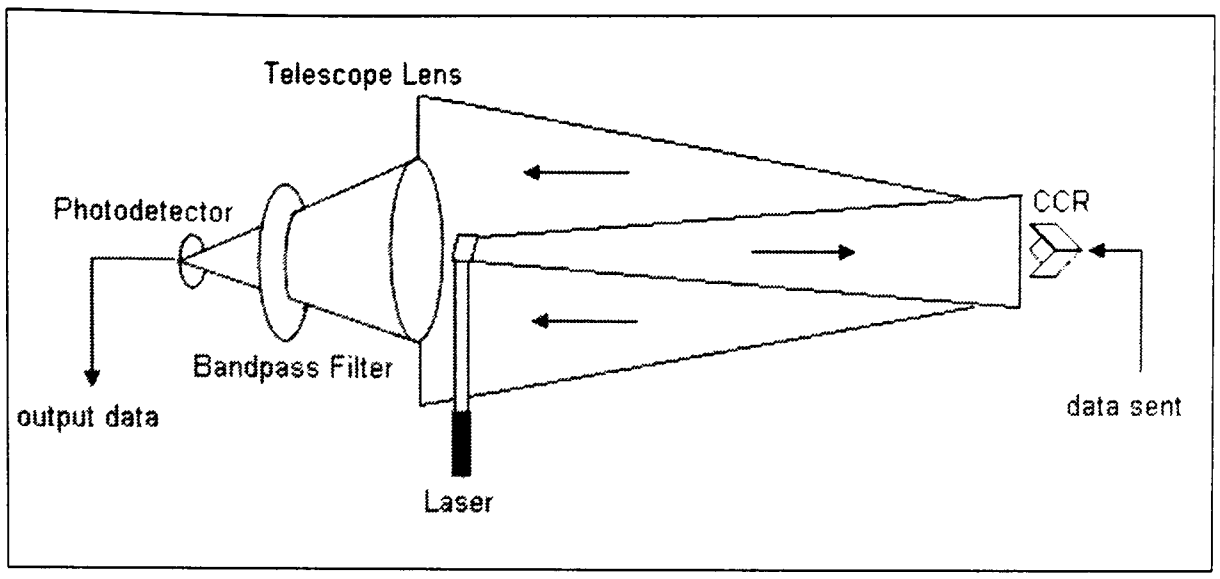

Figure 3.6: FSO communication using the CCR [16]

In Figure 3.6, a small mirror is placed in front of the telescope and it directs the laser beam to the CCR. If the CCR bottom mirror is not actuated, a return laser beam is reflected to the telescope lens with a small divergence angle (logical '1'). If the bottom mirror is actuated, the laser beam splits into two beams, both directed away from the central optical axis of the telescope lens and the telescope entrance aperture. The signal power collected by the telescope is, therefore, negligible if the bottom mirror is actuated (logical '0'). The centre wavelength of the bandpass filter is set to the wavelength of the laser. The mirror is comparatively smaller than the aperture of the telescope and the return optical signal it blocks is minimal compared to the overall amount of signal collected by the telescope. Figure 3.6 only shows the setup for communicating with one CCR. It is possible for the base station to be equipped with an imaging receiver incorporating multiple pixels so the return beams of multiples sensor nodes can be decoded simultaneously[16]. Energy is consumed by the sensor node to actuate the mirror for a bit '0' and no energy is consumed in the transmission of bit '1'. The average modulation energy per bit using the CCR is low, and is reported to be as low as 19pJ/bit in[16].

The switching energy required to modulate the return beam from the base station is related to CV^2, C being the capacitance of the modulating device and V being the switching voltage[16, 102]. The average energy per bit required for several modulation schemes is given in Table 3.1.

TABLE 3.1
Average modulation energy for different modulation schemes

Modulating scheme	**Average modulation energy**	**Reference**
Liquid crystal shutter	6 pJ/bit	[102]
Corner-cube retroreflector (CCR)	19 pJ/bit	[16]
Multiple Quantum Well (MQW) shutter	78 pJ/bit	[102]

3.2. The probability of error for non-turbulent channels

In this section, the error of probability for the non-turbulent FSO channel, $P_{e,FSO}$, is discussed. For the non-turbulent channel, assuming that noise sources are Gaussian-distributed, the $P_{e,FSO}$ is given as[16]:

$$P_{e,FSO} = Q\left(\frac{\sqrt{SNR}}{2}\right) \tag{3.1}$$

where SNR is the peak signal to noise ratio at the receiver and

$$Q(x) = \frac{1}{2} erfc\left(\frac{x}{\sqrt{2}}\right) \tag{3.2}$$

The error function, *erfc(x)*, is defined in Equation 2.4 in Chapter 2. The differential scattering cross section, ρ, can be used to describe the optical performance of the MRR, and is defined as[16]:

$$\rho = \frac{I_o \cdot d_{FSO}^2}{I_i} \tag{3.3}$$

where I_i is the irradiance (or intensity) incident on the MRR, I_o is the reflected irradiance at the base station and d_{FSO} is the range of communications. The MRR re-emits the reflected radiation into a range of solid angles. The base station telescope has a light collection area of A_c and captures the light from a solid angle of Ω. The solid angle $\Omega = A_c/d^2_{FSO}$ if d_{FSO} is sufficiently large and A_c is sufficiently small. If the incident and reflected light directions are along the same axis, and $\Omega = A_c/d^2_{FSO}$, Equation (3.3) can be rewritten as:

$$\rho = \frac{P_o}{I_i \cdot \Omega} \tag{3.4}$$

or

$$P_o = \frac{A_c}{d_{FSO}^2} \cdot I_i \cdot \rho \tag{3.5}$$

where P_o is the power collected by the base station's telescope. The irradiance incident on the CCR, I_i, is given as:

$$I_i = \frac{P_i}{\pi \cdot d_{FSO}^2 \cdot \tan^2 \theta_i} \tag{3.6}$$

where P_i is the power of the interrogating laser and θ_i is the divergence half angle of the laser beam, shown in Figure 3.7.

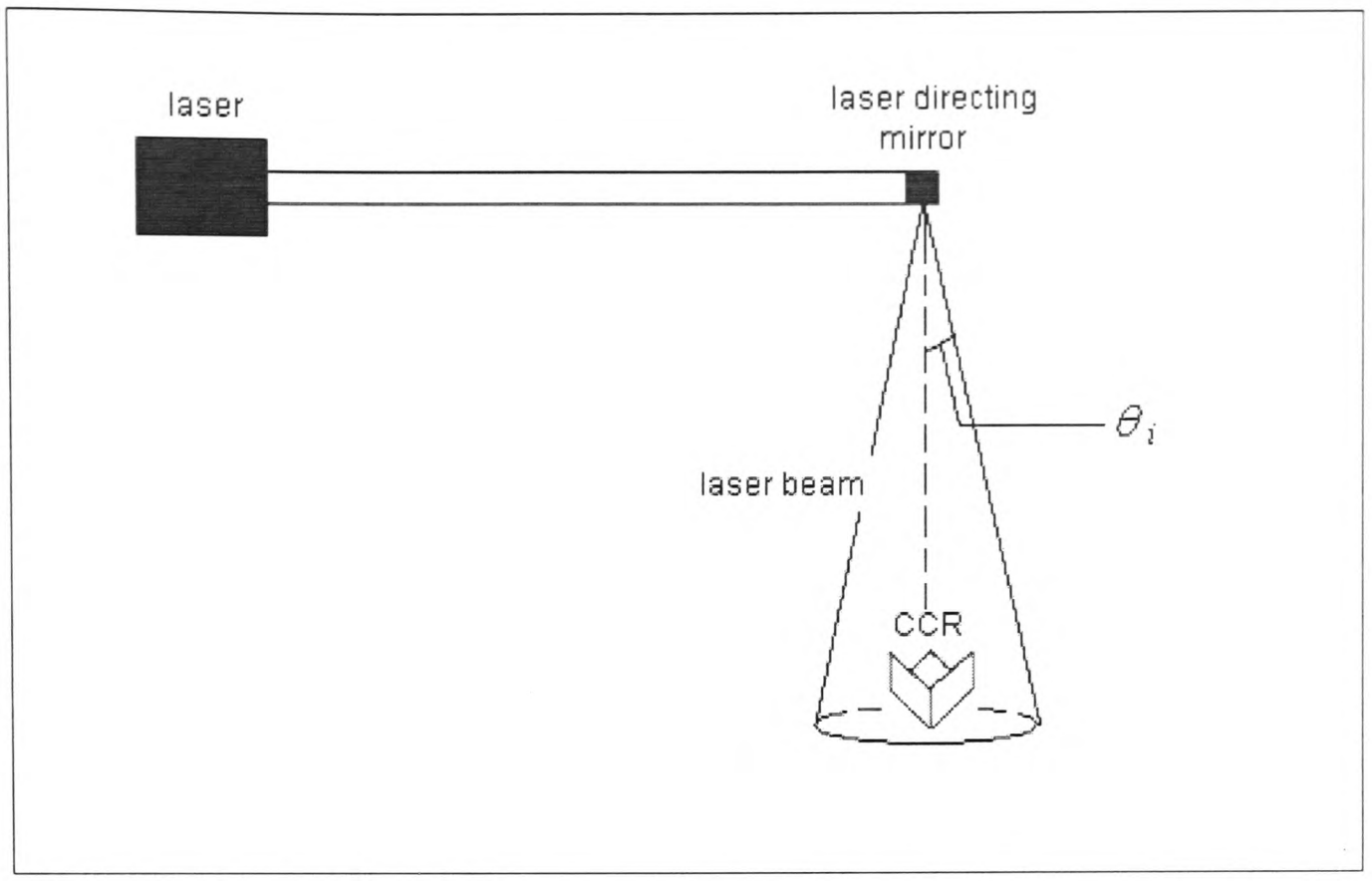

Figure 3.7: The divergence half angle, θ_i

If the CCR (described in Section 3.1), with three identical square mirrors of side lengths a and reflectivity r_m, is illuminated along the cube's diagonal by a light of wavelength λ_{FSO}, ρ is given as[16]:

$$\rho = \frac{3a^4 r_m^3}{\lambda_{FSO}^2} \tag{3.7}$$

From Equations 3.5-3.7, the power collected at the base station's receiver for the CCR is:

$$P_o = \frac{3A_c \cdot a^4 \cdot r_m^3 \cdot P_i}{\pi \cdot d_{FSO}^4 \cdot \lambda_{FSO}^2 \cdot \tan^2 \theta_i} \tag{3.8}$$

The modulation mechanism for the CCR was described in Section 3.1. If the photodetector responsivity is R_p, the signal photocurrent when the CCR is not actuated (corresponding to a logical '1') is given as:

$$i_{sig} = \frac{3A_c \cdot a^4 \cdot r_m^3 \cdot P_i \cdot R_p}{\pi \cdot d_{FSO}^4 \cdot \lambda_{FSO}^2 \cdot \tan^2 \theta_i} \tag{3.9}$$

Assuming that the beam is modulated by misaligning the bottom mirror of the CCR, as described in and shown in Figure 3.6, the peak SNR is given as[16].

$$SNR = \frac{i_{sig}^2}{\sigma_{tot}^2} \tag{3.10}$$

where σ_{tot}^2 is the total noise variance given as[16]:

$$\sigma_{tot}^2 = \frac{8Bk_BT}{R_F} \tag{3.11}$$

B is the noise bandwidth, k_B is Boltzmann's constant, T is the temperature in Kelvin and R_F is the load resistance.

3.3. Atmospheric turbulence

Free space optical signals can be degraded by atmospheric turbulence and atmospheric scattering[103-106]. Atmospheric scattering can be either Rayleigh or Mie scattering. Rayleigh scattering is caused by molecule-sized particles, but its effect on channel transmission is usually much smaller than Mie scattering[104]. Mie scattering is caused by larger particles, like smoke and fog. The effects of atmospheric scattering are not taken into account in the model. The model does, however, include blocking which is a consequence of fog.

Turbulence occurs as the temperature and pressure of the atmosphere is non-uniform. This results in random variation of the refractive index along the path of communication. The variation of the refractive index causes signal fading, which increases the link error probability[105, 107]. In retro-reflective channels, fading also

results in a spread of the interrogation and reflected beams, reducing the average received signal level[107]. Atmospheric turbulence has been widely studied, and a number of theoretical models have been proposed to describe the fading caused by atmospheric turbulence[108-114].

For the non-turbulent channel discussed in Section 3.2, the irradiance was fixed and given by Equation 3.6. The irradiance varies due to turbulence and a number of models have been proposed to describe this. Due to its simplicity, the log-normal distribution model is the most widely used to describe optical turbulence[115]. However, the model can only be applied to weak turbulence conditions[116]. Several other optical turbulence models proposed include the Rician/Log-normal model[117], the Nakagami/Gamma model [118] and the Negative Exponential/Gamma model[119].

Recently, the Gamma-gamma model has been proposed to describe turbulence. The advantage of this model is that it can be used to describe irradiance in both weak and strong turbulence[116]. In this model, the irradiance is assumed to have a Gamma-gamma probability density function (pdf), given in Equation 3.12[115]:

$$f(I_n) = \frac{2(\alpha_I \beta_I)^{\frac{\alpha_I+\beta_I}{2}}}{\Gamma(\alpha_I)\Gamma(\beta_I)} \cdot I_n^{\frac{\alpha_I+\beta_I}{2}-1} \cdot K_{\alpha_I-\beta_I}(2\sqrt{\alpha_I \beta_I I_n}), \quad I_n > 0 \qquad (3.12)$$

where I_n is the normalized irradiance such that the expected value of I_n, $E[I_n]$, is equal to 1:

$$E[I_n] = \int_0^{\infty} I_n . f(I_n) = 1 \tag{3.13}$$

and

$$\alpha_I = \left[\exp\left(\frac{0.49\chi^2}{(1+0.18d^2+0.56\chi^{12/5})^{7/6}} \right) - 1 \right]^{-1} \tag{3.14}$$

$$\beta_I = \left[\exp\left(\frac{0.51\chi^2(1+0.69\chi^{12/5})^{-5/6}}{(1+0.9d^2+0.62d^2\chi^{12/5})^{5/6}} \right) - 1 \right]^{-1} \tag{3.15}$$

$$\chi^2 = 0.5C_n^2 k_w^{\ 7/6} d_{FSO}^{\ 11/6} \tag{3.16}$$

$$d = \sqrt{\frac{kD^2}{4d_{FSO}}} \tag{3.17}$$

$$k_w = 2\pi / \lambda_{FSO} \tag{3.18}$$

The parameter k_w in Equations 3.16 and 3.18 is the optical wave number. D is the diameter of the receiver collecting lens aperture, d_{FSO} is the communications range in metres and λ_{FSO} is the wavelength of the laser. The turbulence is characterised by the index of refraction structure parameter, C_n^2 [107]. Generally, C_n^2 varies from 10^{-13} $m^{-2/3}$ for strong turbulence to 10^{-17} $m^{-2/3}$ for weak turbulence, with a typical value being 10^{-15} $m^{-2/3}$[115]. $\Gamma(\cdot)$ in Equation 3.12 is the gamma function and is defined as[61]:

$$\Gamma(x) = \int_0^{\infty} t^{x-1} e^{-t} dt,\ x > 0 \tag{3.19}$$

$K_\nu(\cdot)$ in Equation 3.12 is the modified Bessel function of the second kind of order ν, defined as[120]:

$$K_{\nu}(z) = \left(\frac{\pi}{2}\right) \cdot \frac{L_{-\nu}(z) - L_{\nu}(z)}{\sin(\nu\pi)} \tag{3.20}$$

where

$$L_{\nu}(z) = \left(\frac{z}{2}\right)^{\nu} \sum_{k=0}^{\infty} \frac{\left(z^2/4\right)^k}{k!\,\Gamma(\nu + k + 1)} \tag{3.21}$$

Figure 3.8 shows plots of $f(I_n)$ for different communication ranges with medium atmospheric turbulence ($C_n^2 = 10^{-15}$ m$^{-2/3}$). For the plots in Figure 3.8, λ_{FSO} and D were set to 632.8nm and 8cm respectively. Atmospheric turbulence becomes an important consideration for communication ranges over 1km[115], and the plots in Figure 3.8 suggest that turbulence can be ignored for communication ranges of several hundred metres. For d_{FSO} = 200m for example, the pdf for the normalized irradiance, $f(I_n)$ is centred about 1 with virtually zero spread. The authors in[16], who have demonstrated a 180m FSO link using retro-reflectors, ignored the effects of turbulence in their work, indicating that this is typically the case.

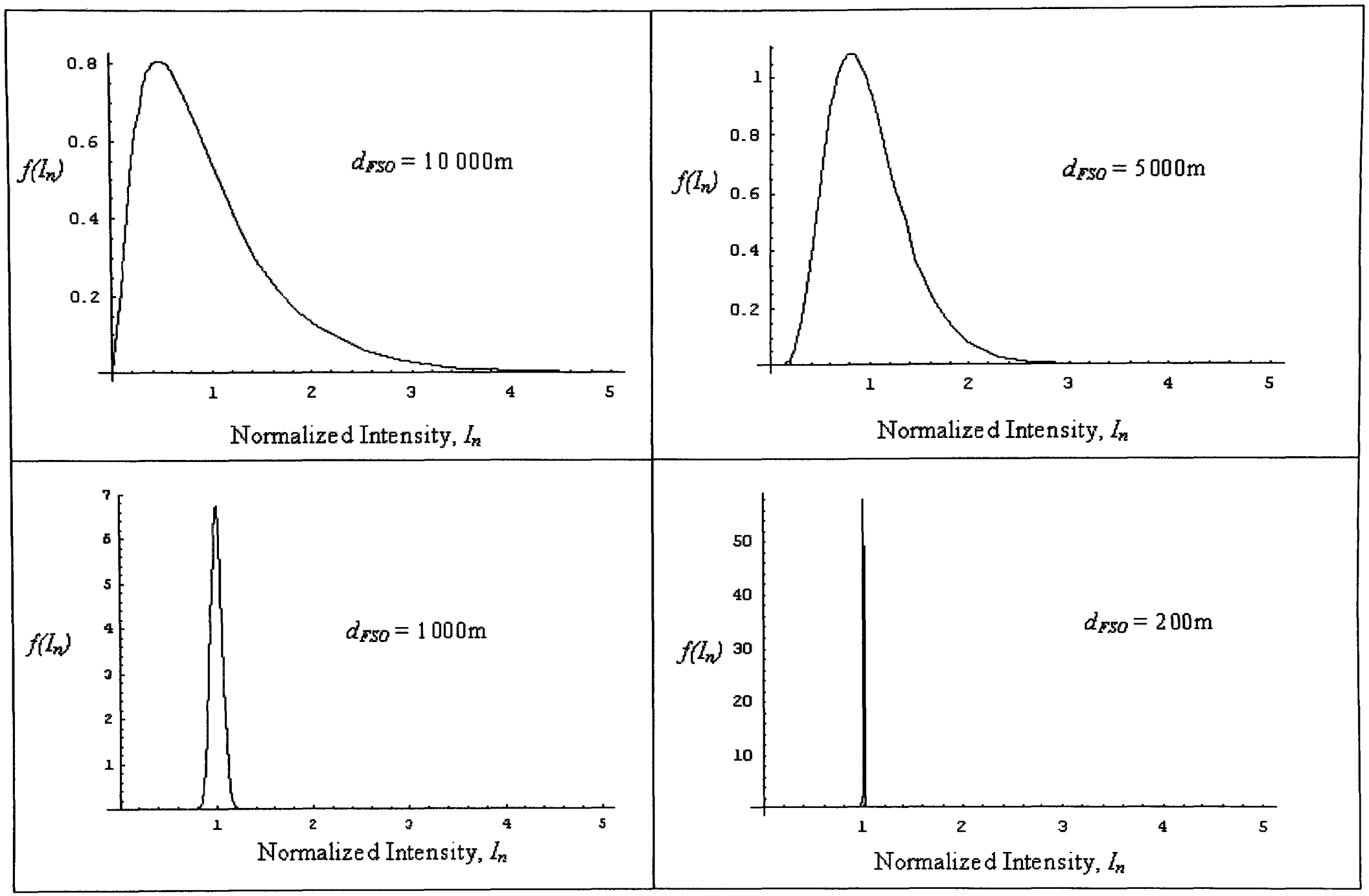

Figure 3.8: Normalised irradiance pdf, $f(I_n)$, for different communication ranges with medium turbulence ($C_n^2 = 10^{-15}$ $m^{-2/3}$)

The pdf for the non-normalized irradiance, I, is given as[121]:

$$f(I) = \frac{2(\alpha_I \beta_I)^{\frac{\alpha_I+\beta_I}{2}}}{\Gamma(\alpha_I)\Gamma(\beta_I) I_{av}} \cdot \left(\frac{I}{I_{av}}\right)^{\frac{\alpha_I+\beta_I}{2}-1} \cdot K_{\alpha_I-\beta_I}\left[2\sqrt{\alpha_I \beta_I \frac{I}{I_{av}}}\right], \; I > 0 \qquad (3.22)$$

where I_{av} denotes the average irradiance. α_I and β_I are defined in Equations 3.14 – 3.18. The probability of error for the non-turbulent FSO channel, $P_{e,FSO,}$ was given in Equation 3.1. For the turbulent channel, the average bit error probability, $P_{e,T}$ is given as:

$$P_{e,T} = \int_0^\infty Q\left(\frac{\sqrt{SNR}}{2}\right) \cdot f(I)\, dI \qquad (3.23)$$

where *f(I)* is the irradiance pdf given in Equation 3.22 and *SNR* is the peak signal to noise ratio. Assuming that the beam is modulated by misaligning the bottom mirror of the CCR, as described in [16] and shown in Figure 3.6, the *SNR* in Equation 3.23 is defined in Equations 3.9-3.11.

3.4. FSO link model for the proposed RF/FSO WSN

For the proposed RF/FSO WSN, it is assumed that the optical beam is modulated by the CCR as described in[16]. The parameters used for simulating the FSO channel are based on [16] and given in Table 3.2.

TABLE 3.2
Parameters for FSO link

Parameter	Description	Value
P_i	*laser power*	0.8 mW
a	*length of side mirror*	450 μm
r_m	*mirror reflectivity*	0.3
D	*diameter of aperture*	8 cm
A_c	*light collection area*	5×10^{-3} m^2
R	*photodetector responsivity*	0.012 A/W
λ_{FSO}	*wavelength*	632.8 nm
θ_i	*divergence half angle*	0.1 mrad
B	*noise bandwidth*	1 kHz
T	*absolute temperature*	300 K
R_F	*feedback resistance*	20 MΩ

Using these parameters, the plots of the probability of error for a non-turbulent FSO channel, $P_{e,FSO}$, are shown in Figures 3.9 and 3.10. From Figure 3.10, the communication range must be less than 180m to support a $P_{e,FSO}$ of 10^{-6}, consistent with values reported in[16]. For the RF links in Chapter 2, the probability of error was set to 10^{-3}. Assuming a similar probability of error for the FSO link, the corresponding d_{FSO} in Figure 3.10 is 200m. As the communications range is only several hundred metres, the effects of turbulence are ignored as previously stated. The maximum optical range, d_{OPT}, is therefore set to 200m for the simulations in the following chapters. The average energy per bit required to modulate the optical beam, $E_{b,opt}$, is range-independent, and is set to 19pJ/bit (see Table 3.1).

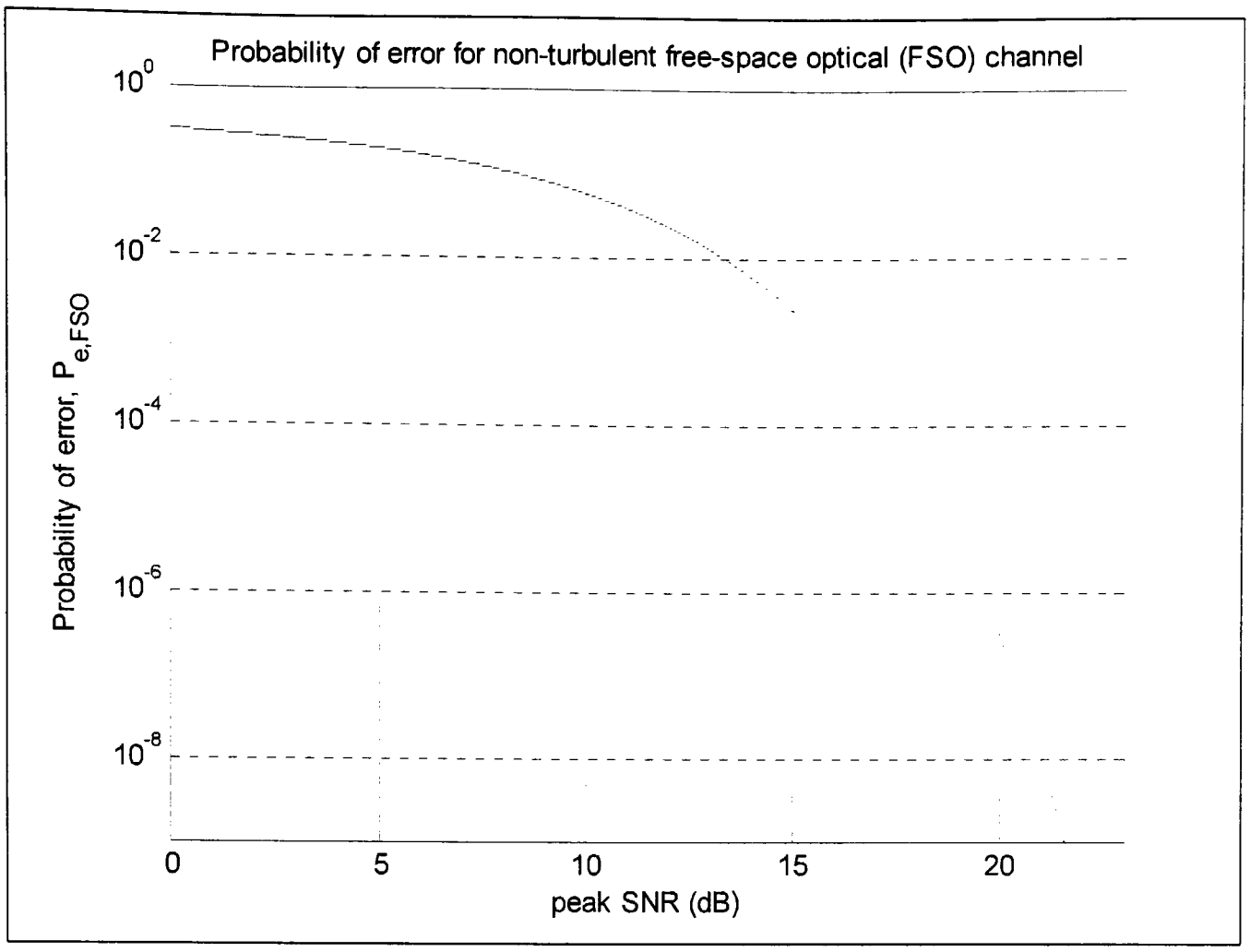

Figure 3.9: Plot of $P_{e,FSO}$ vs peak *SNR* for non-turbulent FSO channel

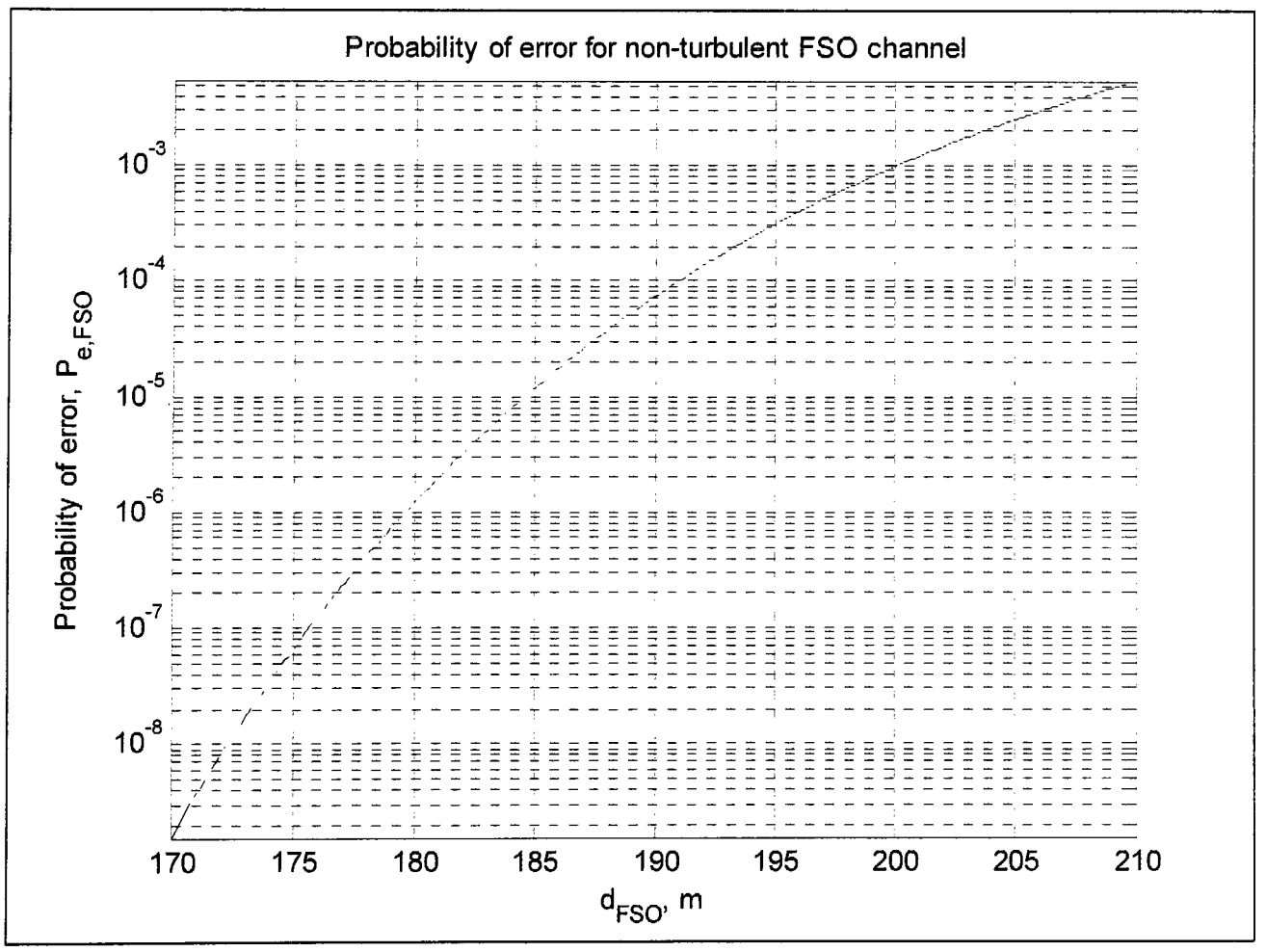

Figure 3.10: Plot of $P_{e.FSO}$ vs d_{FSO} for non-turbulent FSO channel

3.5. The base station: Optical interrogation

In this section, the RF/FSO WSN base station's optical interrogation is discussed. For the optical links, the RF/FSO WSN needs to be able to interrogate all the nodes deployed in the network. A broadcast-based optical base station that illuminates the entire deployment area has been proposed in[102]. However, due to its large divergence angle, this type of base station is not able to provide the levels of illumination intensity required for the RF/FSO WSN proposed in this work. For the highly directional FSO links in the RF/FSO WSN, a base station that is capable of beam steering is required. Such a base station is proposed in[101, 102], and shown in Figure 3.11[102].

In Figure 3.11, a laser source illuminates the liquid crystal on silicon (LCOS) spatial light modulator (SLM). The SLM can display a reconfigurable diffraction pattern or hologram, which causes the light incident on it to be deflected through an angle, depending on the pattern displayed [122]. Using these patterns, the SLM can steer the illuminating beam to address multiple nodes in the deployment field[101]. In Figure 3.11, the beam from the SLM is reflected by beam splitter A to the lens. The lens focuses the beam onto beam splitter B. The beam is transmitted through beam splitter B to reach the modulating retroreflector (MRR) of the node. The MRR reflects the incident beam to beam splitter B, which in turn reflects the beam to the image receiver. The image receiver is a detector array, capable of receiving signals from multiple retroreflectors.

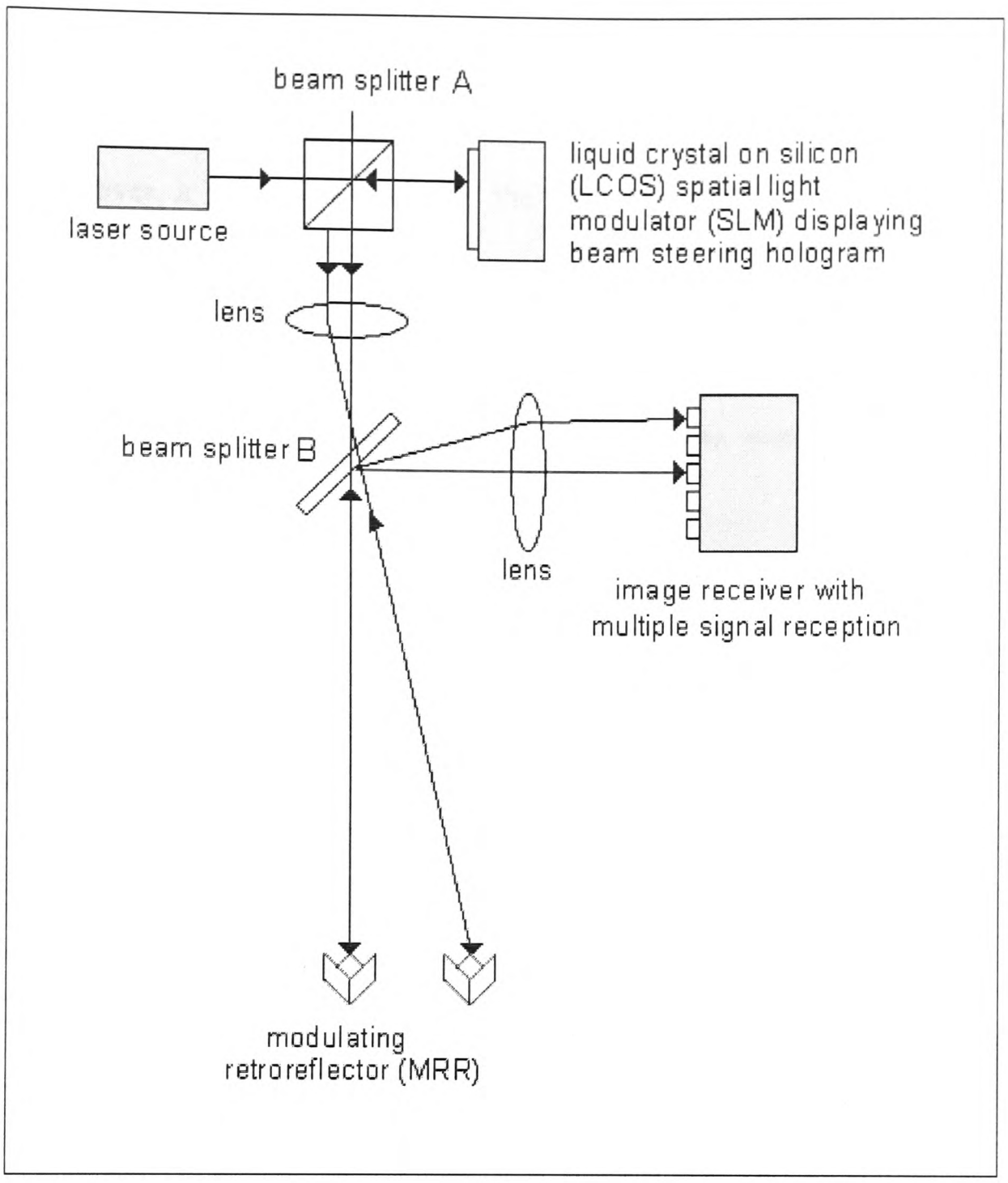

Figure 3.11: Optical beam steering for base station [102]

3.6. Conclusions

This chapter has investigated the FSO link model which will support the hybrid wireless sensor network. FSO communication is achieved using corner cube retroreflectors. The base station is equipped with its own laser source and the sensor node transmits information to the base station by OOK modulating the return beam to the base station. This chapter has also presented the gamma-gamma model to

describe optical turbulence. The model indicates that the effects of optical turbulence can be safely ignored if the FSO communications range is only a few hundred metres. However, a general formula for the probability of error for FSO links with turbulence was also presented in this chapter. The optical interrogation by the base station was also discussed. Chapters 2 and 3 have introduced and discussed the RF and FSO link models. The next chapter discusses the wireless sensor network configuration.

Chapter 4

Configuring the networks

In Chapters 2 and 3, the RF and FSO link models were studied. This chapter discusses the configuration of the RF/FSO and RF-only WSNs.

The RF/FSO WSN and RF-only WSN configuration is described in Figures 4.1 and 4.2 respectively. For the simulations, the base station is assumed to be directly above the centre of a circular deployment area. For the RF-only WSN, nodes communicate to the base station using radio links. Therefore, the base station height for the RF-only WSN needs to be lower than at least d_L or d_{NL}, depending on whether the node has line of sight to the base station (See Table 2.3 in Chapter 2). For the hybrid RF/FSO WSN, the base station's height needs to be sufficiently high so it can communicate optically with the nodes. A percentage of nodes in the RF/FSO WSN will not have line of sight (LOS) to the base station. This percentage is defined as the blocking factor, b_f.

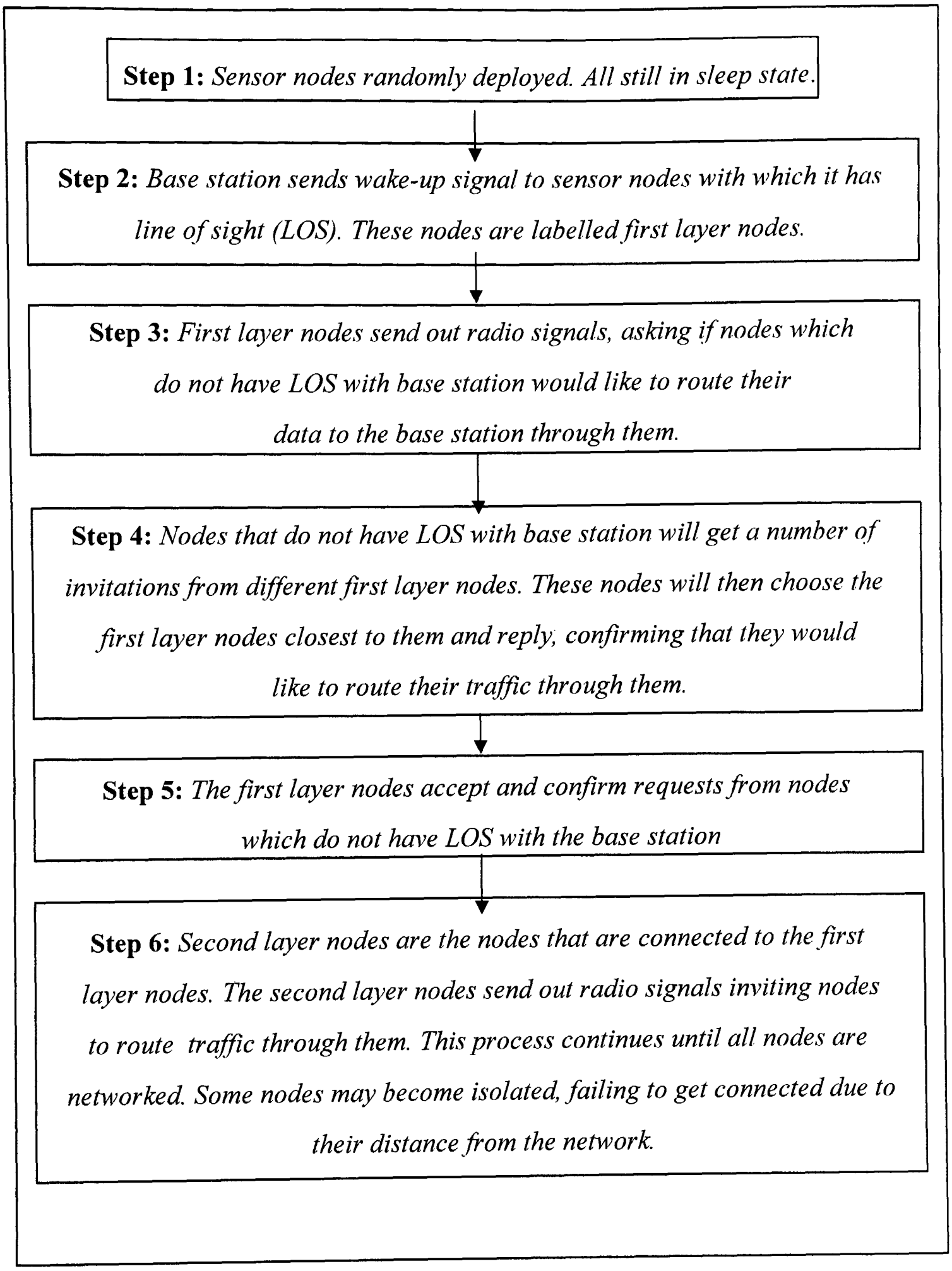

Figure 4.1: *RF/FSO network configuration for wireless sensors*

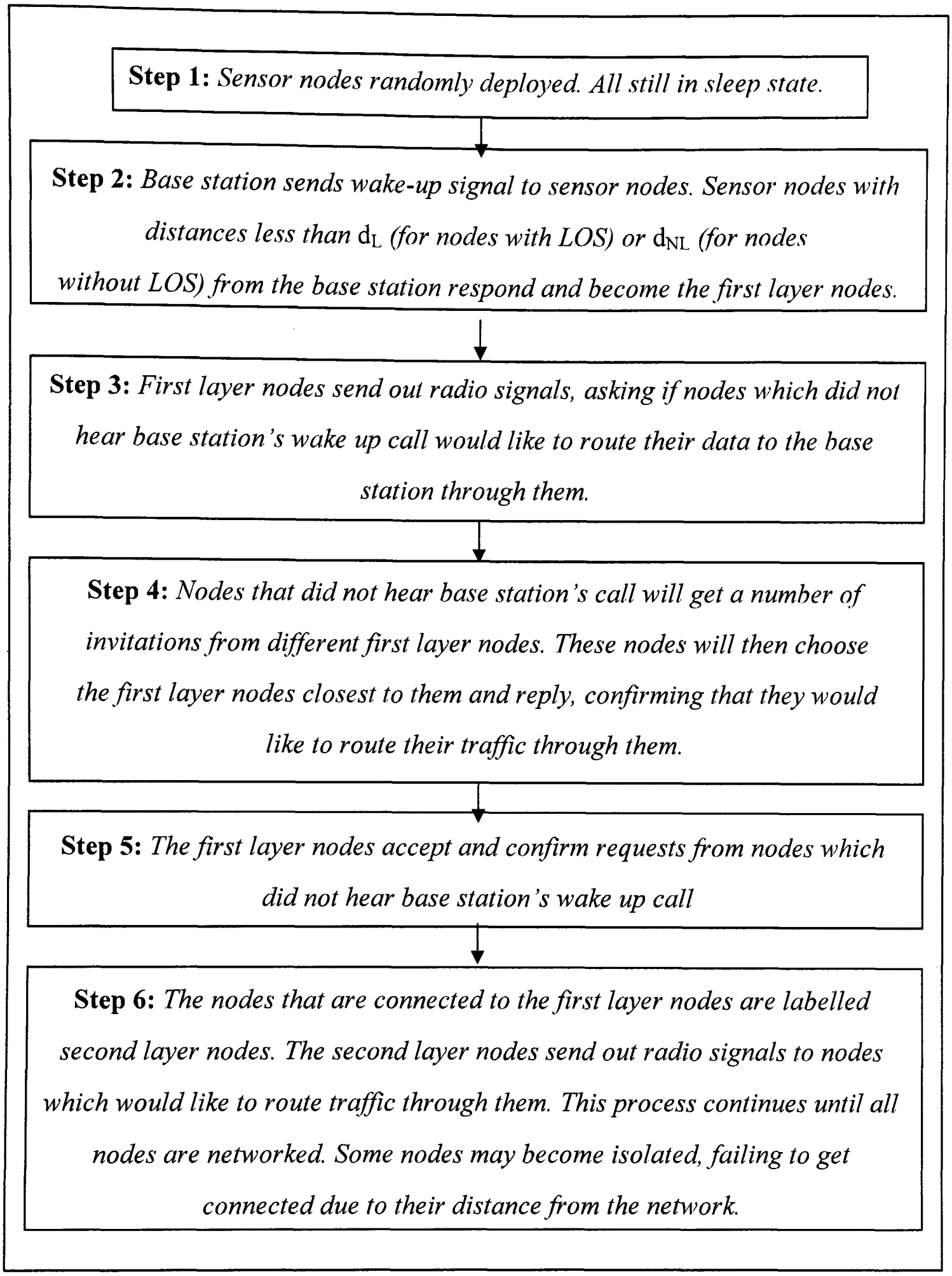

Figure 4.2: *RF-only network configuration for wireless sensors*

4.1. Example of network configuration

This section explains how the network configuration is simulated using MATLAB.

4.1.1. Simulating the RF/FSO network configuration

Step 1: Nodes randomly deployed over deployment area.

Step 2: The maximum peer-to-peer radio range, d_{PP}, is determined based on n, $E_{b,ta}$ and the maximum radio probability of error (discussed in Section 2.5)

Step 3: Based on the blocking factor, b_f, a number of nodes are randomly selected to have line of sight to the base station. For these nodes, the distance from the base station is calculated. If a node's distance to the base station is less than the maximum optical range, d_{OPT}, these nodes are connected to the base station.

Step 4: For each unconnected node, its shortest distance to an already connected node is determined. If this distance is $\leq d_{PP}$, the nodes are connected.

Step 5: The distances between an unconnected node to all nodes already connected are calculated. For each unconnected node, the shortest distance to an already connected node is determined.

Step 6: If this distance is shorter than d_{PP}, the nodes are connected. The distance of some nodes to the closest connected node may be greater than d_{PP}. These nodes are designated as isolated nodes. Step 6 is repeated until all nodes are connected or designated as being isolated. An array with all the nodes and the route they take to the base station is saved. Another array with the distances between connected nodes is also saved.

4.1.2. Simulating the RF-only network configuration

The RF-only network is simulated in a similar way to the RF/FSO network described in Section 4.1.1., varying only in Steps 2 and 3. In Step 2 in Section 4.1.1., the maximum radio range between the node and the base station in the presence and absence of line of sight (d_L and d_{NL} respectively) are determined, in addition to d_{PP}. The distance between each node and the base station is calculated. In Step 3 in Section 4.1.1., the distances between the nodes and the base station are calculated. A node with line of sight will connect directly to the base station if its distance to the base station is less than d_L. Similarly, a node without line of sight will connect directly to the base station if its distance is less than d_{NL}.

4.1.3. Verifying the network simulations

A simple network with ten nodes was simulated to check that the MATLAB code worked as expected. For this network, the distances between nodes were calculated by hand to check that they matched the results of the simulations. The expected network connections were determined from these calculations and verified by a three dimensional MATLAB plot of the simulated network. The calculated distances and network connections were compared against those saved in the two arrays described in Step 6 in Section 4.1.1. Verifications were performed for both the RF-only and the RF/FSO WSNs.

4.2. Network simulation results

Figures 4.3 and 4.4 show an RF/FSO and an RF-only WSN respectively, simulated using MATLAB. Figures 4.5 (a) and (b) show a much larger RF/FSO network deployment area, where the distance of a significant number of nodes from the base station is larger than d_{OPT}. These nodes, lying in the fringes of the deployment area, need to communicate using radio multihop despite having LOS with the base station. Node 10 in Figure 4.5(b) has three nodes in its cluster, imposing on it the additional duty of routing data from these nodes to the base station. Node 23 needs to transmit data from nodes 1, 12 and 5 in addition to its own data. In this network, some nodes are isolated because they are too far away for effective communication. For optimum operation, the distance of all the nodes in the RF/FSO WSN should be less than d_{OPT} from the base station, so only nodes without LOS need to depend on RF communication.

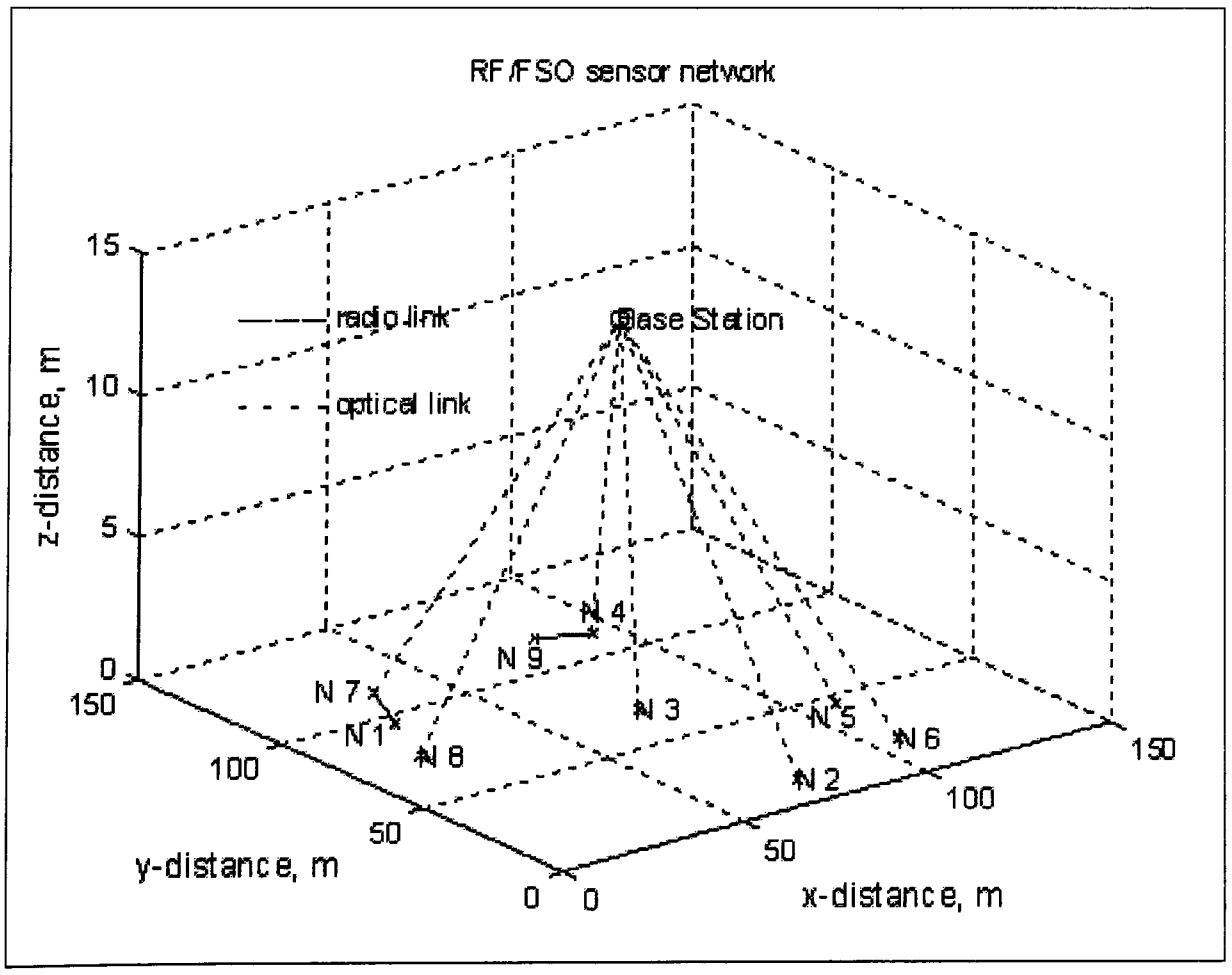

Figure 4.3: The RF/FSO WSN

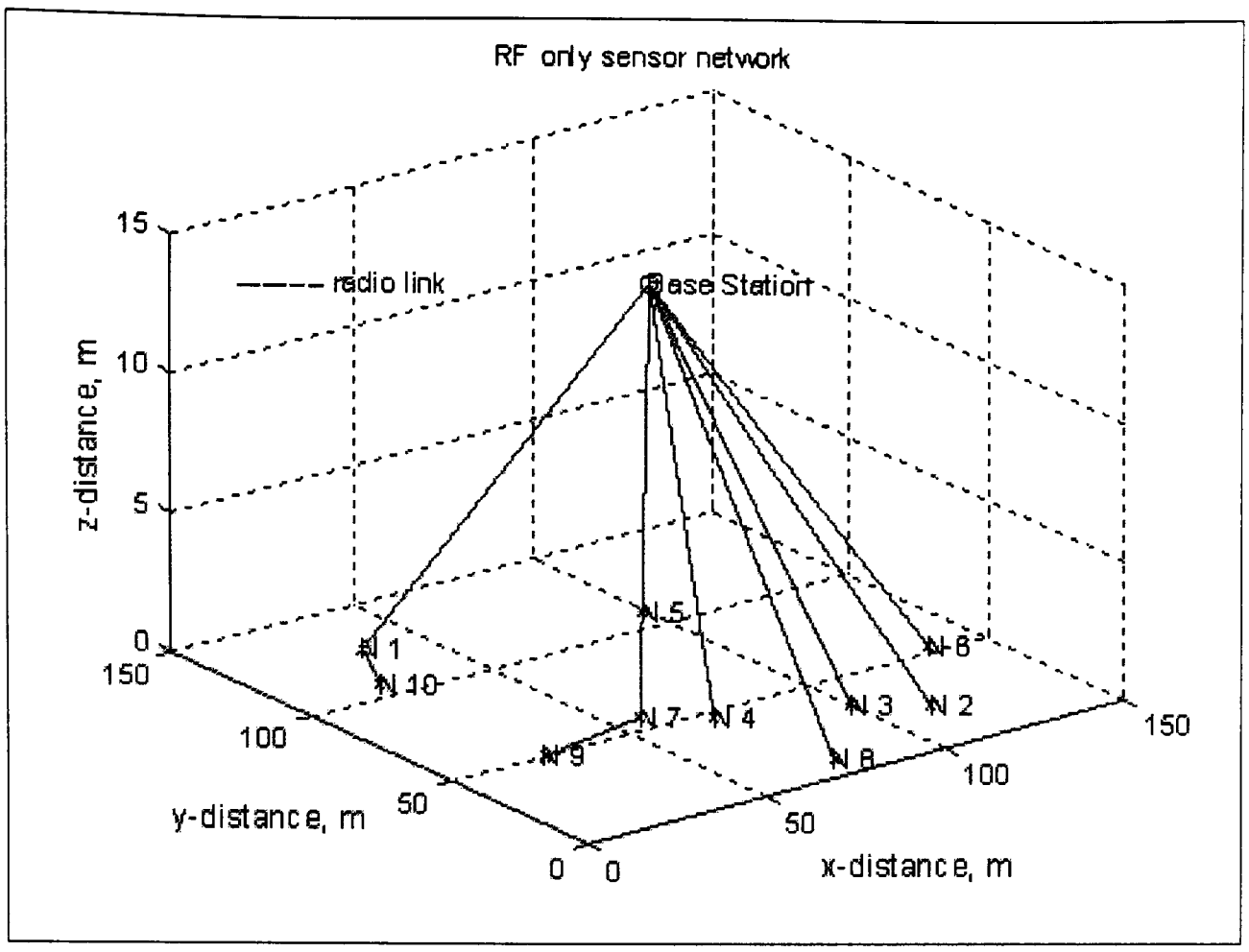

Figure 4.4: The RF-only WSN

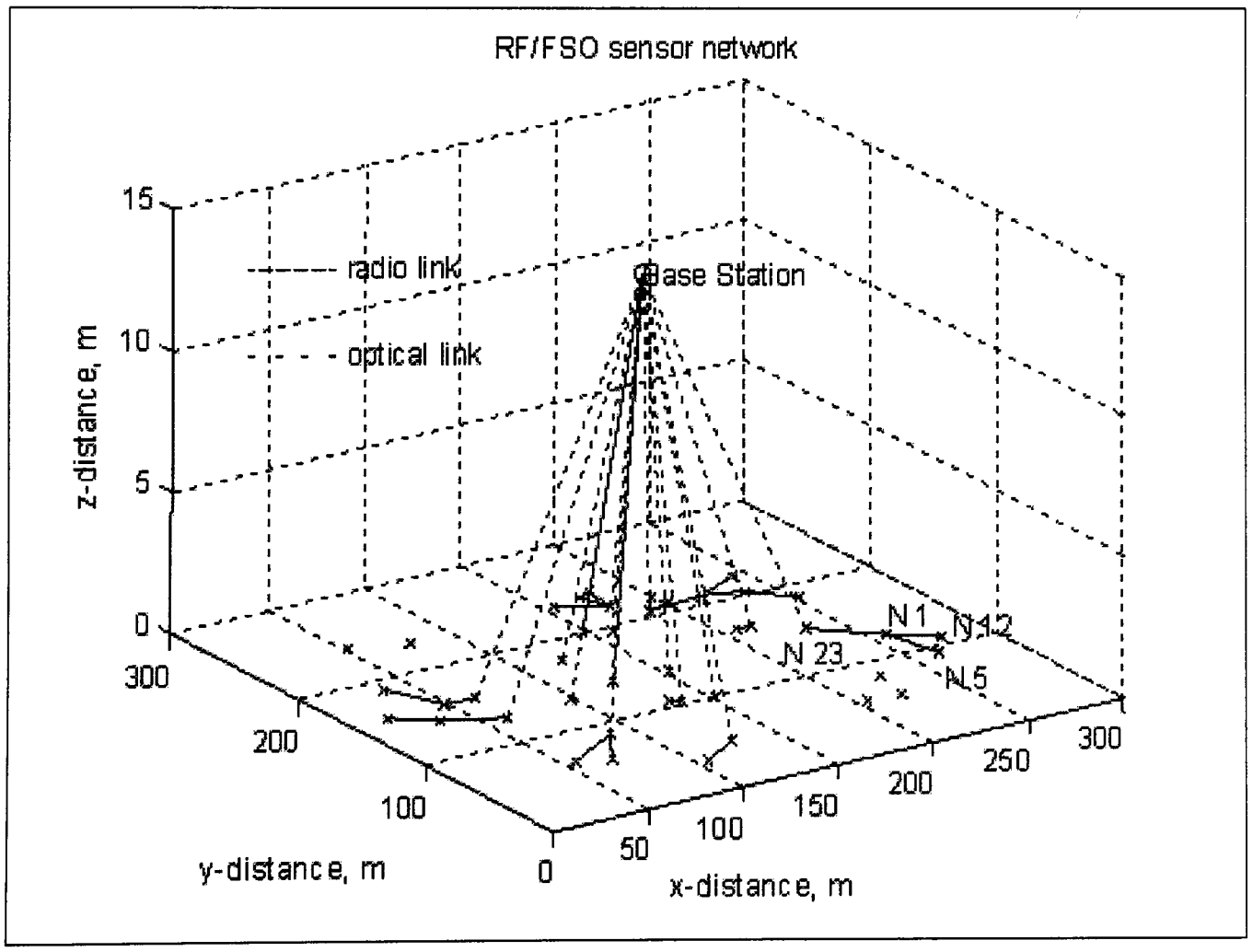

Figure 4.5(a): The RF/FSO WSN with larger deployment area

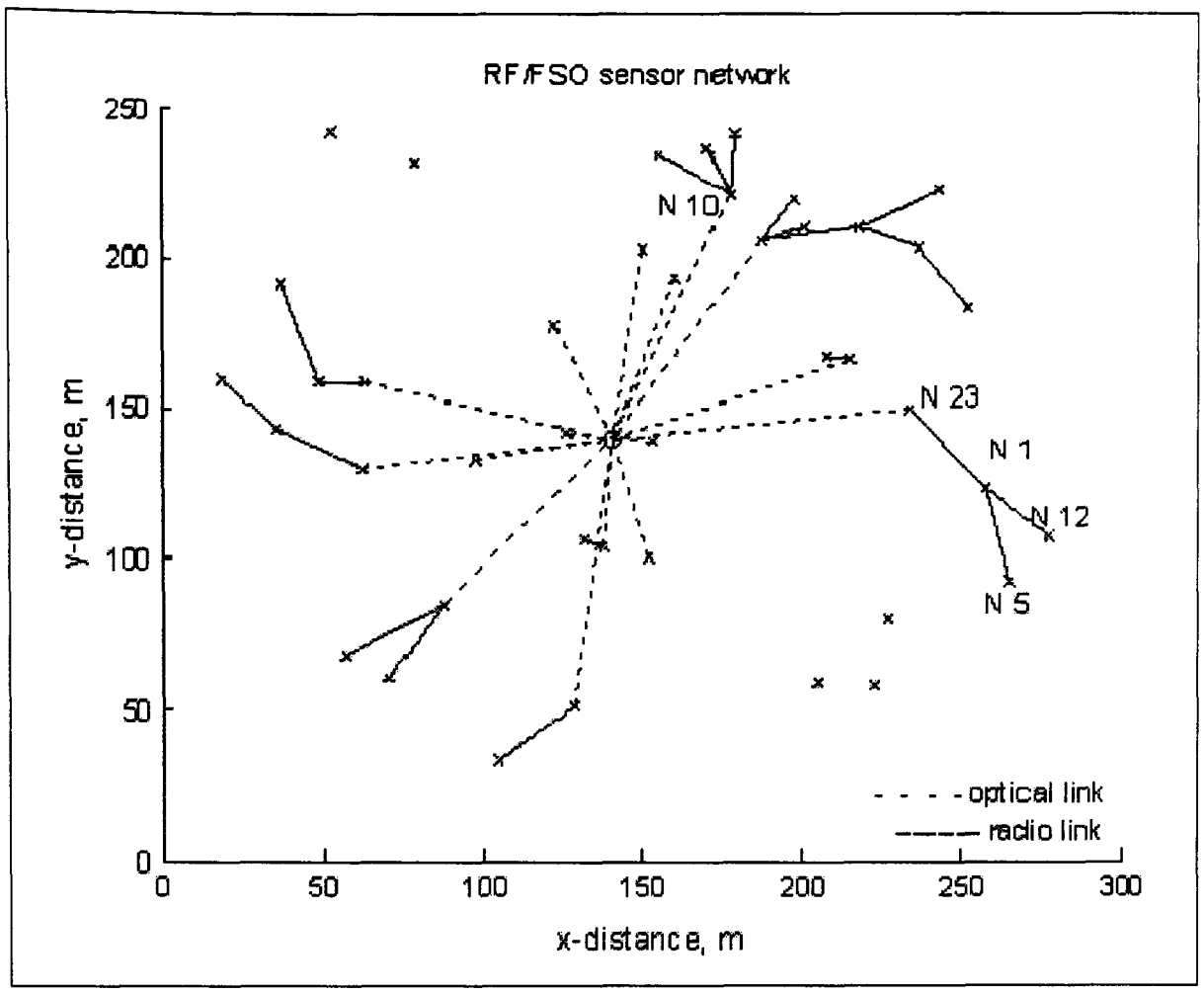

Figure 4.5(b): Aerial view of deployment area

4.3. Conclusions

In this chapter, the configuration of the RF/FSO hybrid WSN was discussed. The configuration of the RF-only WSN, which will be used for comparison, was also described and discussed. For the RF/FSO WSN, nodes which do not have LOS to the base station, or which are too far from the base station to communicate optically, rely on radio multihop. Simulations show that due to the maximum transmitted RF energy imposed (which translates to a maximum radio range of d_{PP}), some nodes may end up being isolated from the network. In the following chapter, the energy used by the sensor node for communications, data processing and sensing are studied.

Chapter 5

Sensor node energy model

In Chapters 2 and 3, the RF and FSO link models for the RF/FSO WSN and RF-only WSN (in Figures 5.1 and 5.2 respectively) were presented. This chapter discusses the sensors node's energy model. Nodes in the WSN typically perform the following roles – sensor, relay and aggregator[123]. To perform these roles, energy is expended by the three main components of the sensor node - the sensing unit, the data processing unit and the transceiver (described and discussed in Section 1.2, see Figure 5.3). To study the lifetime of the sensor network, which is discussed in Chapter 7, it is necessary to get a better understanding of the energy expended by the sensor node. Although current literature suggests that most energy consumption in WSNs can be attributed to communications[20], the energy expended due to data processing and sensing is also significant and needs to be considered[70]. This chapter investigates the energy expended for communications, sensing and data processing in more detail and introduces the energy models adopted for the work described in this thesis.

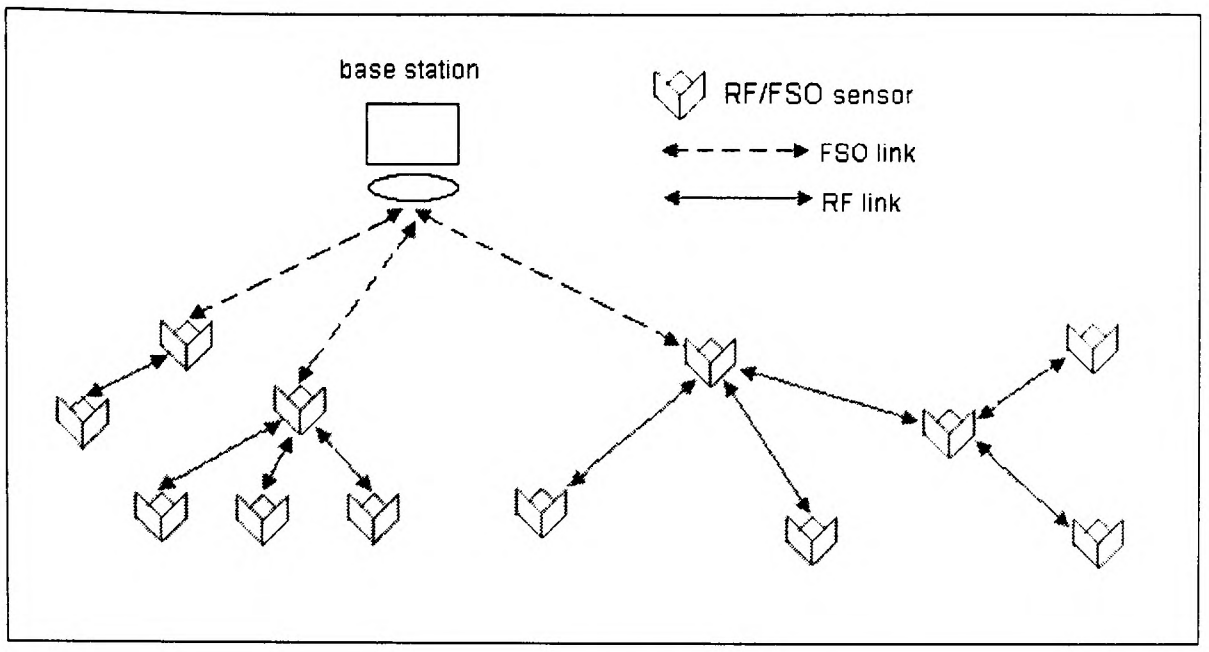

Figure 5.1: The RF/FSO WSN

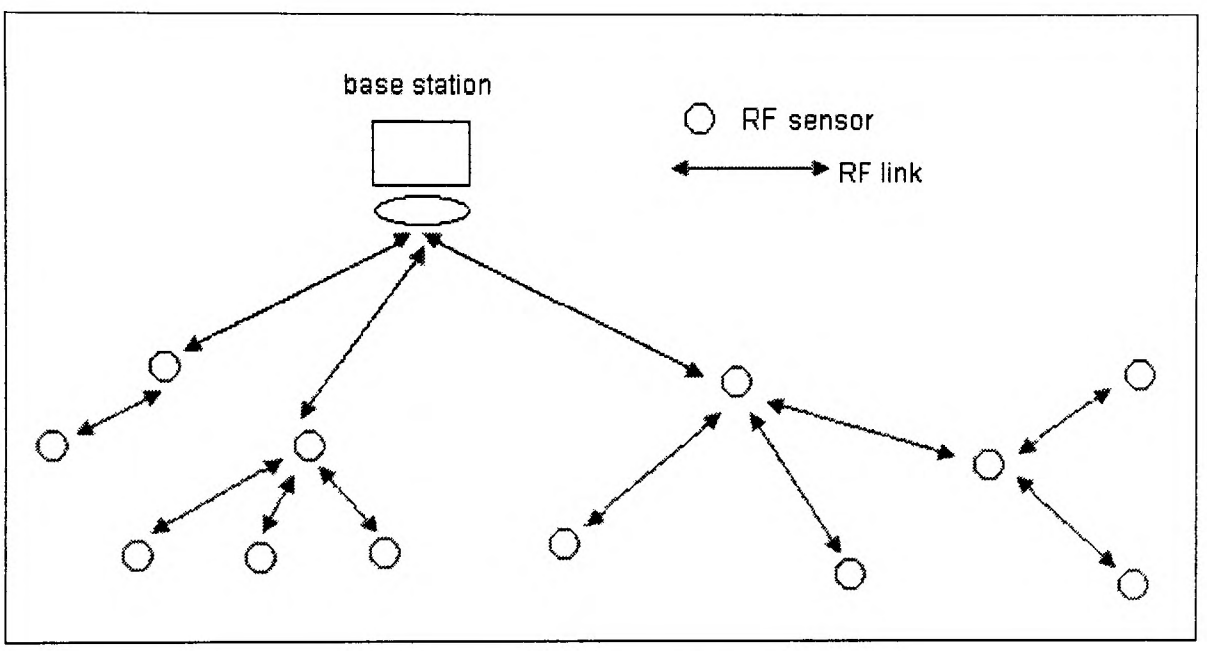

Figure 5.2: The RF-only WSN

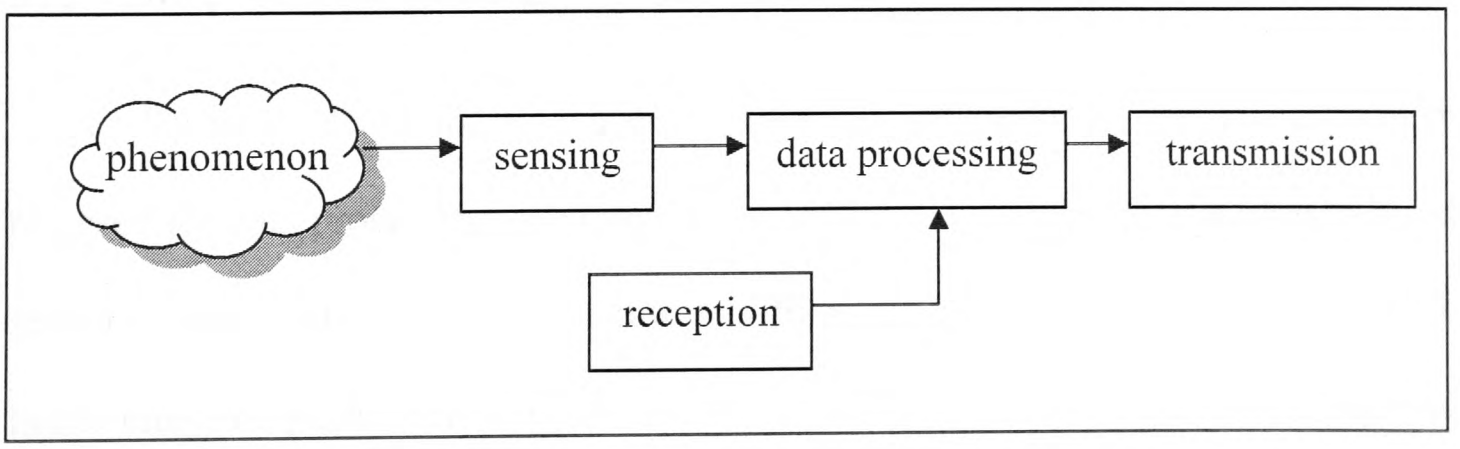

Figure 5.3: Roles performed by the sensor node

5.1. Sensing energy model

Various models have been proposed for the energy consumption of the sensor node[22, 124-130]. An energy model for the sensor node is required for the network simulations in Chapters 6 and 7. In this section, the energy model for sensing is developed. Energy is expended by the node to sense phenomena such as temperature, light intensity or motion. Energy is also required by the node's analogue to digital converter (ADC) to prepare the signal for subsequent data processing (see Figure 1.2 for sensor node architecture). The sensing energy is that required to support sensing tasks and the ADC. For both the RF/FSO and the RF-only WSNs, the energy per bit required for sensing, $E_{b,s}$ is assumed to be the same and constant, as is the case with most models of this type[22, 125]. $E_{b,s}$, will vary depending on factors such as the resolution of the digital signal required and the choice of the processor chip used. In[131] for example, the energy per bit required by the Ballistic audio sensor is 50nJ/bit. A typical value for $E_{b,s}$ is 20nJ/bit[125], and this is the value used for the simulations described in the following chapters.

5.2. Data processing energy model

Sensor nodes also expend energy for data processing. The energy per bit required for data processing can range from 1pJ/bit to several tens of nJ/bit[132]. All sensor nodes need to process the raw bits from the ADC for transmission. Cluster heads relay the packets from nodes in their cluster to other cluster heads or the base station. Therefore, in addition to the energy used for processing raw data from sensors, cluster heads also require energy for packet relaying. (This is in addition to the communications energy used for receiving and transmitting data, discussed in

Section 5.3.) A cluster head also requires energy for data aggregation, if data aggregation is employed[125]. To support higher levels of network security, additional energy is required for data encryption[127]. The energy per bit required for data processing is given as[125, 127]:

$$E_{b,dp} = \varepsilon_p + \varepsilon_a f(\gamma_a) + \varepsilon_{\text{sec}} \tag{5.1}$$

where γ_a is the data aggregation ratio, which is the size of original data divided by the size of the aggregated data[125]. The function $f(\gamma_a)$=0 when γ_a=1 (no data aggregation) [125]. When data aggregation is performed, $f(\gamma_a)$ depends on the data aggregation technique used, for example suppression, minima, maxima and averaging [2]. The parameters ε_p, ε_a and ε_{sec} are the data processing, data aggregation and data security factors respectively. The energy per bit expended to process raw sensor bits from the ADC, and the bits from packets in a cluster is represented by ε_p. A typical value for ε_p is 20nJ/bit[125]. Experimental results suggest that the energy expended by a cluster head to aggregate the data from the nodes in its cluster into a single representative signal can be as high as 5nJ/bit for every input signal to the cluster head [22].

Data encryption increases the energy expended by the nodes for data processing, and would only be beneficial if sensitive data traverses the network (possibly in military operations harvesting data from a battle field). Data aggregation reduces redundant data in the network, as discussed in Section 1.4.1, thus reducing the energy needed for communications. But, the energy expended for data processing increases if data aggregation is employed. However, as data processing consumes less energy than data communication[20], data aggregation could potentially reduce

the overall energy consumption of the sensor network significantly. For the work in this thesis, data aggregation and data encryption are not considered. $E_{b.dp}$ is therefore set to a typical value of 20nJ/bit. (Data aggregation is suggested as a possible avenue for further research in Chapter 8.)

5.3. Communications energy model

Most of the energy dissipated by the sensor node is due to communications[20]. Energy is required by the sensor node for the RF transmitted signal and to drive the transmitter and receiver electronics. To study the communications energy model, *peer-to-peer* and *gateway node-base station* communications (as shown in Figure 5.4) are studied separately in Sections 5.3.1 and 5.3.2 respectively.

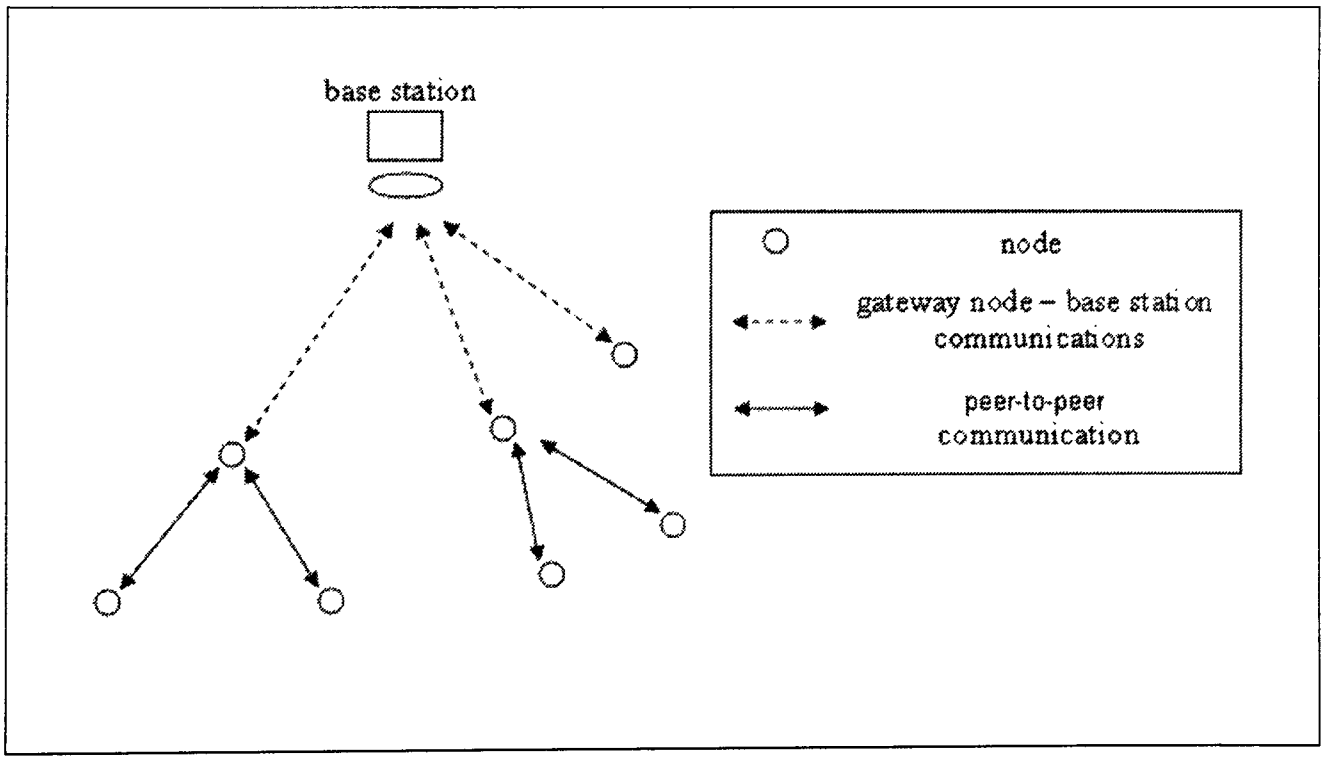

Figure 5.4: Communication links in wireless sensor network

5.3.1. Peer-to-peer communications energy model

Both the RF/FSO and RF-only WSN use radio links for peer-to-peer communications, and energy is required for data transmission and reception. The energy per bit required for radio transmission, $E_{b,tx}$, and reception, $E_{b,rx}$, are given in Equations 5.2 and 5.3 respectively;

$$E_{b,tx} = E_{b,te} + E_{b,ta} \tag{5.2}$$

$$E_{b,rx} = E_{b,r} \tag{5.3}$$

$E_{b,te}$ and $E_{b,r}$ are the energy per bit required for the radio transmitter and receiver electronics respectively. $E_{b,ta}$ is the transmitted RF energy per bit. The value of $E_{b,tx}$ is typically higher than $E_{b,rx}$, due to the range-dependent transmitted RF energy per bit[129]. The energy per bit required for transmitter and receiver electronics are assumed to be constant and equal as in[22, 127]. A typical value for $E_{b,te}$ and $E_{b,r}$ is 50nJ/bit[22, 125, 126, 130], and this is the value used for the simulations. Figure 5.5 shows the energy consumption modules of a non-cluster head WSN node.

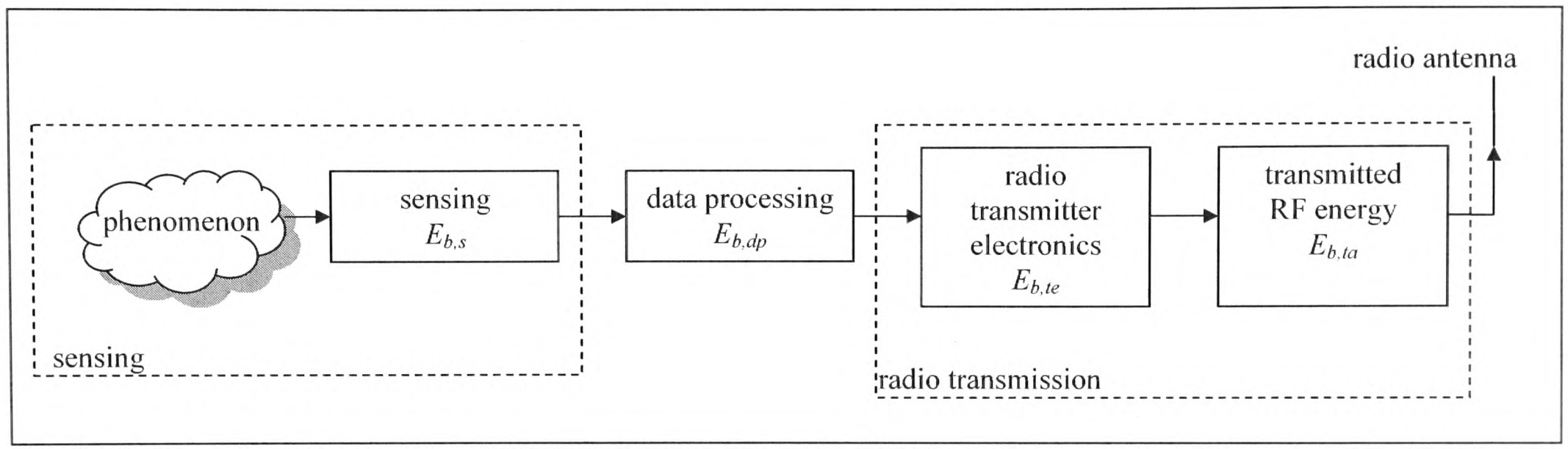

Figure 5.5: Energy consumption modules of a non-cluster head WSN node

The transmitted RF energy per bit expended by the node, $E_{b,ta}$, is dependent on the communication distance and the environment in which it operates. For high path loss environments, the node will need to increase its transmitting power, so quality of service commitments can be satisfied. As discussed in Section 2.5, it is assumed that the node has the option of being able to choose an appropriate power level, depending on the communication distance. The transmitted RF energy per bit, $E_{b,ta}$, was discussed in detail in Chapter 2. $E_{b,ta}$ for the peer-to-peer channel is given in Tables 2.2 and 2.3. Figure 5.6 shows the radio path loss model adopted for peer-to-peer communications. The value of d_0 is set to 1m, as discussed in Section 2.5.

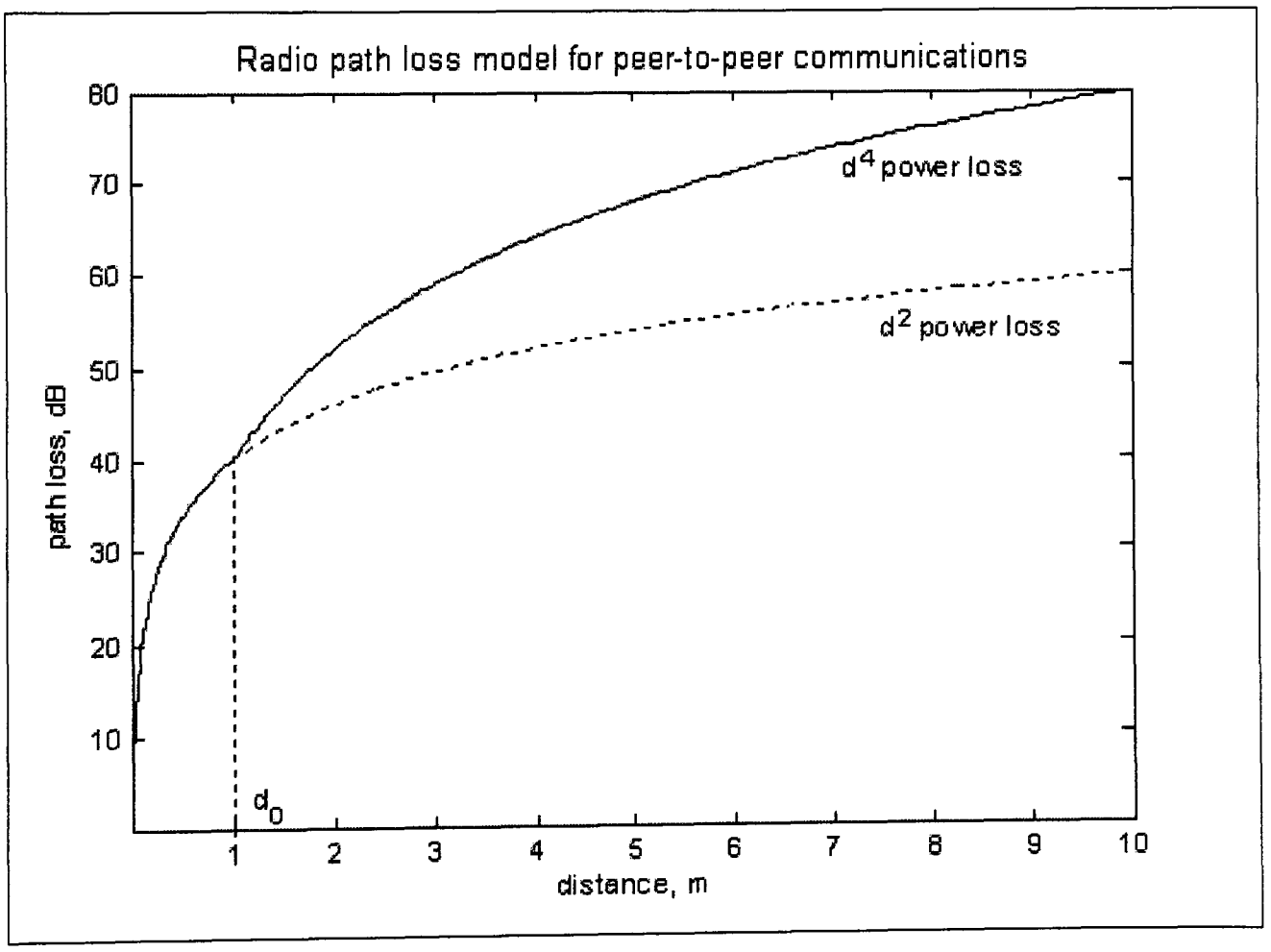

Figure 5.6: Radio path loss model adopted for peer-to-peer communications

5.3.2. Gateway node-base station communications energy model

The base station is assumed to be elevated in both the RF/FSO and the RF-only WSN. For the RF/FSO WSN, modulating retroreflectors (MMRs) communicate data to the base station. The energy consumption modules of an RF/FSO WSN gateway node are shown in Figure 5.7. $E_{b,opt}$ in Figure 5.7 is the switching energy required to modulate the return beam from the base station. Several different modulation schemes for the FSO link were discussed in Section 3.1. The average energy per bit required for several modulating schemes was given in Table 3.1. For the work reported in this paper, the average energy per bit required to modulate the optical beam, $E_{b,opt}$, is set to 19pJ/bit, as was decided in Section 3.4.

Figure 5.8 shows the energy consumption modules of an RF-only WSN cluster head/gateway node. To transmit data to the base station, the node expends energy to drive the transmitter electronics ($E_{b,te}$) and to transmit RF data ($E_{b,ta}$). $E_{b,te}$ is set to 50nJ/bit, as discussed in Section 5.3.1. The transmitted RF energy per bit depends on whether the node has line of sight to the base station. $E_{b,ta}$ was discussed in Chapter 2, and presented in Tables 2.2 and 2.3. A summary of the energy consumption model adopted for the work presented in this thesis is summarized in Table 5.1.

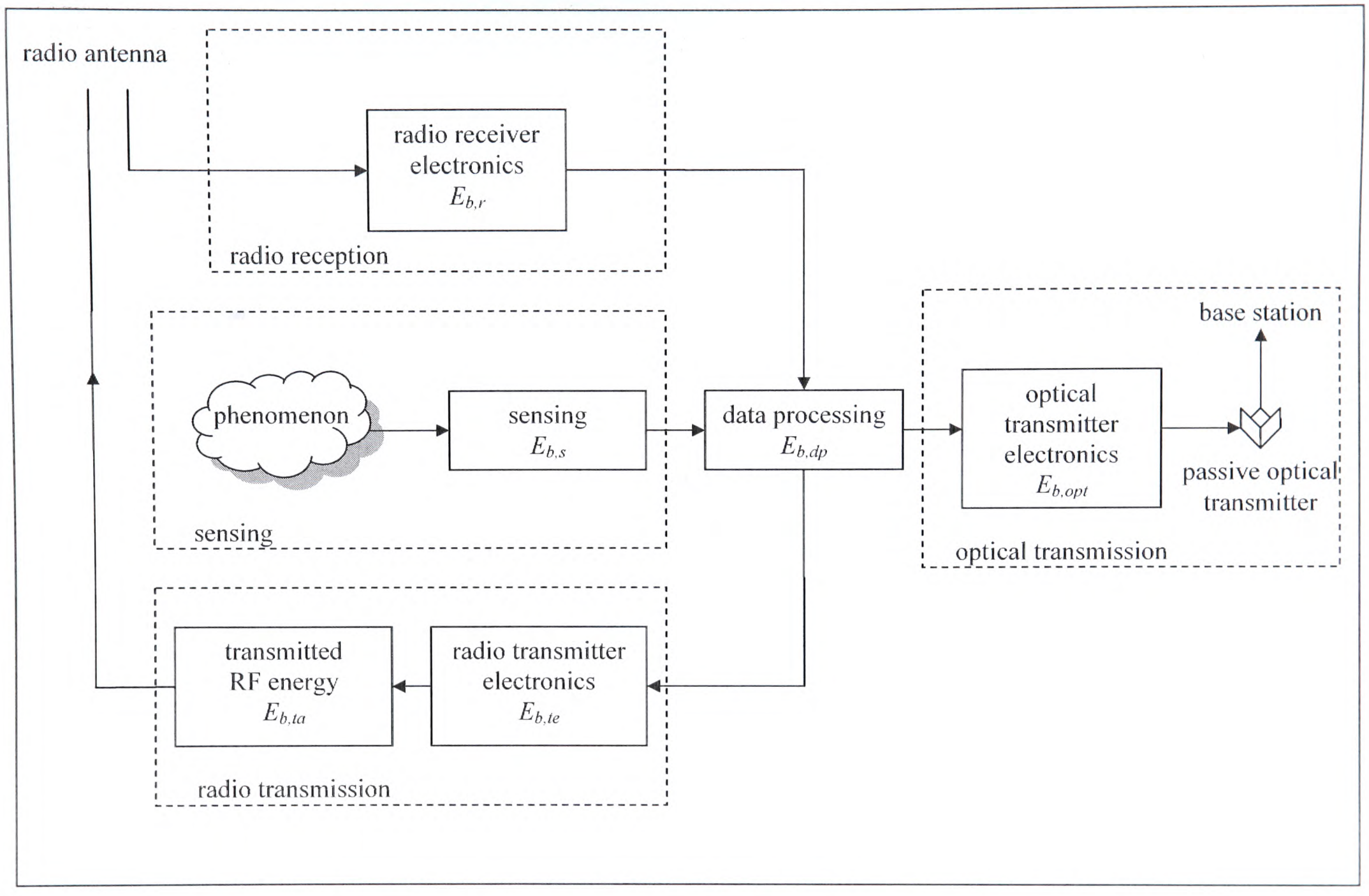

Figure 5.7: Energy consumption modules of an RF/FSO WSN gateway node

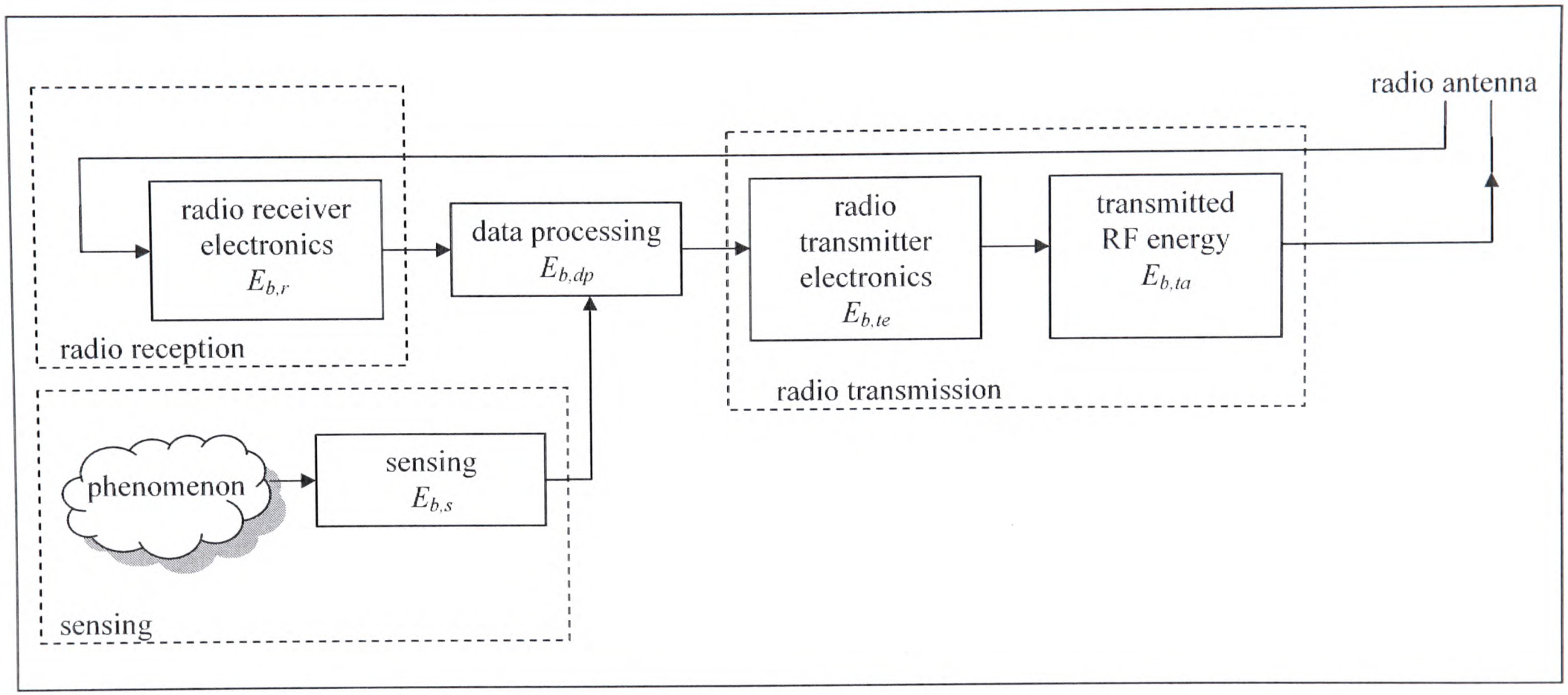

Figure 5.8: Energy consumption modules of an RF-only WSN cluster head/gateway node

TABLE 5.1
Summary of energy consumption model adopted

Energy parameter		**Description**			**Value** (nJ/bit)
$E_{b,s}$		energy per bit for sensing			20
$E_{b,dp}$		energy per bit for data processing			20
radio transmission	$E_{b,te}$	energy per bit for radio transmission electronics			50
	$E_{b,ta}$	transmitted RF energy per bit	peer-to-peer	$d < d_0$	$\varepsilon_{PP} \cdot d^2$
				$d \geq d_0$	$\varepsilon_{PP} \cdot d^4$
			node-base station (LOS)		$\varepsilon_L \cdot d^2$
			node-base station (NLOS)	$d < d_0$	$\varepsilon_{NL} \cdot d^2$
				$d \geq d_0$	$\varepsilon_{NL} \cdot d^3$
		$\varepsilon_{PP} = 1\ pJ/bit/m^n$, $\varepsilon_L = 0.047\ pJ/bit/m^2$, $\varepsilon_{NL} = 1\ pJ/bit/m^n$			
	$E_{b,r}$	energy per bit for radio reception electronics			50
(passive) optical transmission	$E_{b,opt}$	energy per bit for optical transmission			0.019

ε_{PP}: the RF transmission factor for the peer-to-peer channel
ε_L: the RF transmission factor for the node to base station (LOS) channel
ε_{NL}: the RF transmission factor for the node to base station (NLOS) channel

5.4. Conclusions

In this chapter, the sensor node energy model was presented. The node's energy consumption is due to sensing, data processing and communications. Although most of the energy expended by the node is due to communications, the energy expended for tasks related to sensing and data processing also account for a significant portion of energy used by the sensor node. The next chapter discusses the network traffic and energy consumption of the wireless sensor network.

Chapter 6

Simulating network traffic and energy consumption

In Chapter 4, the network configurations of the RF/FSO and RF-only WSNs were discussed. In Chapter 5, the sensor node energy model was presented. In this chapter, the network traffic and the energy consumption for the RF/FSO and the RF-only WSNs are simulated and discussed. In Chapter 1, power consumption was identified as one of the key challenges in the operation of WSNs. The simulations in this chapter aim to investigate if the energy expended by the RF/FSO WSN is lower than that of the RF-only WSN. This is investigated for a selection of network deployment scenarios.

6.1. Data reporting techniques

Sensor nodes need to report data to the base station and several reporting techniques have been proposed[2]. Data reporting techniques could be categorized as time-driven, event-driven, query-driven or a combination of any of these three methods[2]. For time-driven reporting, nodes periodically send data to the base station. This would be particularly suitable for sensor networks which send periodic reports to the base station, such as a sensor network monitoring environmental variables. In event-driven reporting, the sensor node sends data in response to a certain event. For query-driven reporting, sensor nodes send data in response to a

query from the base station.

6.2. Simulation of network traffic: Assumptions and methodology

For the simulations, the time-driven data reporting method is adopted and only routing to the base station is considered. A sample signal is periodically sent by a selection of nodes in each network. These signals' bits propagate through the network until they reach the base station. As the signal propagates through the network, the energy expended by each node in the network is recorded. At the end of the simulation period, the average energy expended by the nodes in the RF/FSO WSN is determined and compared against the average energy expended by the nodes in the RF-only WSN.

Power consumption of the sensor nodes is attributed to sensing activities, communications and data processing[20]. For the simulations, it is assumed that the cluster head does not perform data aggregation. (Data aggregation was discussed in Section 1.4.1. of Chapter 1.) In the simulations, a cluster head is merely responsible for routing the data of the nodes in its cluster to the base station (if they are gateway nodes) or other cluster heads.

In the Low Energy Adaptive Clustering Hierarchy (LEACH) WSN proposed by Heinzelman, *et al* [31, 32], the lifetime of the network is divided into two phases – the network wakeup (or setup) phase and the steady state phase. Sensing and data transfer to the base station occurs during the steady state phase[2]. The duration of the network wakeup phase is kept very much shorter than the setup phase to

minimize overhead. The networks considered in this report also have the same two phases. The nodes will expend some energy during the network wakeup phase. However, this energy is ignored as wakeup only occurs at the beginning of the network's lifetime. In some WSNs, the network enters a dormant state during periods of inactivity[133, 134]. In these cases, the energy expended for network wakeup constitutes a significant overhead, as nodes need to be roused from sleep when required. The WSNs considered in this report are assumed to be awake throughout the course of its lifetime.

For the simulations in this report (except the reconfiguring networks discussed in Chapter 7), the network topology is assumed to remain the same over the entire period of the simulation. The optical conditions are also assumed to be the same throughout the network's lifetime. None of the simulation time has been used for network wakeup, as it is assumed that the network is already configured and operational.

The RF/FSO WSN used for simulations in this report is located within the base station's optical hotspot. The base station optical hotspot is a circle of radius $r_{h,opt}$, where the nodes at the edge of the circle are exactly d_{OPT} from the base station as shown in Figure 6.1.

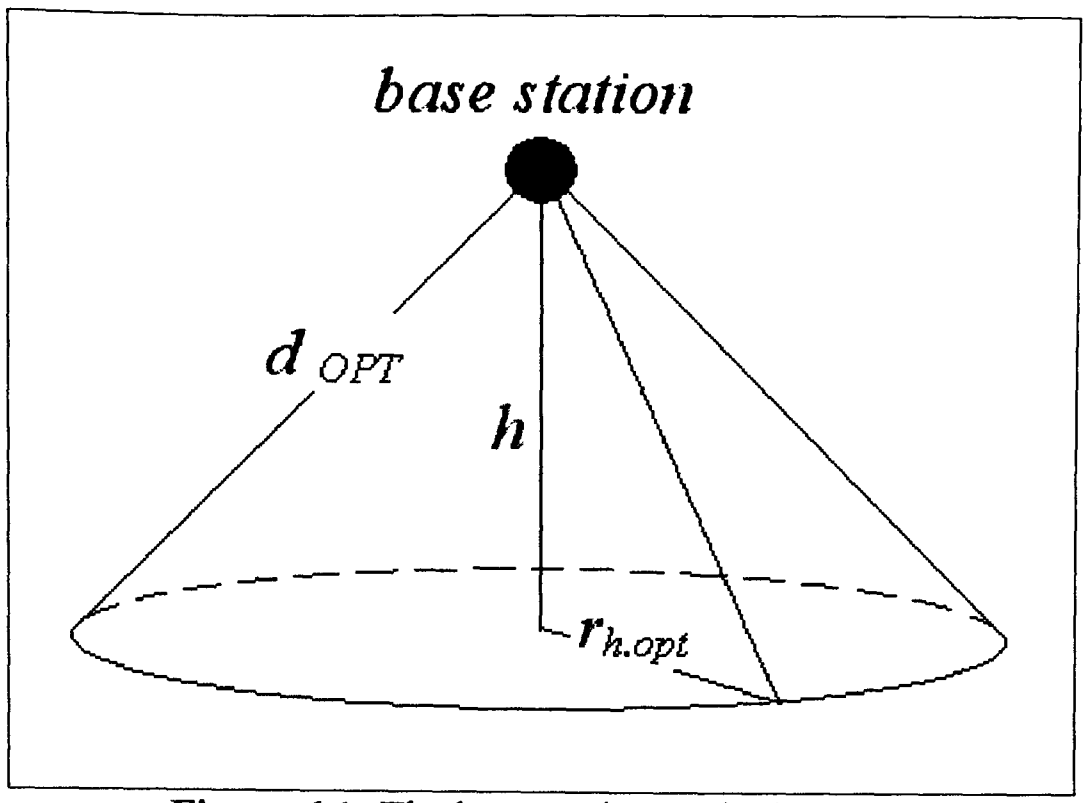

Figure 6.1: The base station optical hotspot

Nodes are within the base station optical hotspot if the maximum range of the nodes to the base station is d_{OPT}. In the optical hotspot, all RF/FSO WSN nodes are connected to the base station if their line of sight to the base station is not obstructed. If a node's line of sight (LOS) to the base station is obstructed, the node relays its data via RF links to a gateway node (which does have LOS to the base station).

6.3. RF medium access control (MAC) protocol

In this section, the MAC protocol assumed for the sensor networks is discussed. A suitable MAC protocol will fairly and efficiently share communications resources between sensor nodes[7]. Fixed allocation and random access MAC protocols have been proposed for wireless sensor networks[135, 136]. Time division multiple access (TDMA) is an example of a fixed allocation MAC protocol for WSNs[6]. In TDMA, nodes are given a specific time slot to transmit data[6]. This MAC protocol can be wasteful, if time slots are frequently allocated to nodes with

nothing to transmit during their allocated slots. In this respect, a random access MAC protocol like Carrier Sense Multiple Access (CSMA) may be more suitable for WSNs[2]. For CSMA, the node listens to the communications channel to ensure that it is idle before it transmits its own packets[2]. In the simulations presented in this thesis, it is assumed that more than one node may transmit simultaneously at any time. Therefore, a fixed allocation MAC protocol is unsuitable.

It is assumed that code division multiple access (CDMA) is used for RF resource management in the sensor networks, as proposed in[40]. The use of CDMA enables multiple nodes to transmit simultaneously. Each node is assigned a unique code, so the cluster head and base station are able to distinguish between the packets from different nodes[40]. Cluster heads will store the codes of the nodes in its cluster, thus ignoring transmissions from other nodes which will have different codes. However, the number of codes available for the network is an important consideration. If there are more nodes than there are codes, some nodes will have to reuse the same codes, and this might cause data collisions if the nodes are too close to each other[22]. Code assignment is expected to be done by the base station, which would have knowledge of the locations of the individual nodes. Code reuse is possible for sufficiently separated nodes[40]. The base station is expected to calculate the best code assignment possible at the beginning of the network's lifetime, based on individual node locations. This will ensure that multiple access interference (MAI) is kept to a minimum. For the simulations, it is assumed that each node is able to transmit successfully without MAI. In the modelling in Chapter 5, $E_{b,te}$ and $E_{b,r}$ are assumed to include any processing energy required by CDMA

nodes.

The data rate in sensor networks is quite low – several hundred bits per second per node[46]. In Chapter 7, the largest number of nodes simulated for a single network is 2135. Assuming each node transmits 200 bits per second, the channel needs to be able to support up to 0.5Mbps. WSNs based on Bluetooth, which operates in the 2.4 GHz ISM band, are able to support data rates of up to 1Mbps[137].

6.4. Comparison of energy consumption

The mean energy ratio E_R is used to study the relative energy-saving benefits of the RF/FSO WSN compared to the RF-only WSN. E_R is defined as:

$$E_R = \left(\frac{mean(E_{RF})}{mean(E_{RF/FSO})} \right) \tag{6.1}$$

where E_{RF} is the energy used by the RF-only network over the simulation period, and similarly $E_{RF/FSO}$ for the RF/FSO network. The energy expended is given in terms of simulation time units, each time unit being the amount of time taken to successfully transmit one packet from the source node to the destination node (or base station).

6.5. Simulating RF/FSO network traffic

Step 1: At the beginning of every simulation time unit, half of the total nodes are randomly selected to transmit 100 bits (simulating low data rate sensor signals).

Step 2: The number of bits transmitted by each node during subsequent time units is updated. Supposing node 10, connects only to node 15, which in turn is only

connected to the base station. Assuming that during the first time unit, node 10 transmits 100 bits. Then during the second time unit, node 15 will need to transmit the 100 bits of node 10 to the base station, in addition to any of its own bits.

Step 3: Step 2 is repeated for the entire period of the simulation.

Step 4: The energy used by each node during for each time unit is calculated. Energy is expended for sensing, processing and data transmission. Table 6.1 gives a summary of the parameters and values used in determining the energy consumption of each node. (This was discussed in Chapter 5, see Table 5.1.)

TABLE 6.1
Summary of energy consumption model adopted

<table>
<tr><th colspan="2">Energy parameter</th><th colspan="3">Description</th><th>Value (nJ/bit)</th></tr>
<tr><td colspan="2">$E_{b,s}$</td><td colspan="3">energy per bit for sensing</td><td>20</td></tr>
<tr><td colspan="2">$E_{b,dp}$</td><td colspan="3">energy per bit for data processing</td><td>20</td></tr>
<tr><td rowspan="8">radio transmission</td><td>$E_{b,te}$</td><td colspan="3">energy per bit for radio transmission electronics</td><td>50</td></tr>
<tr><td rowspan="6">$E_{b,ta}$</td><td rowspan="5">transmitted RF energy per bit</td><td rowspan="2">peer-to-peer</td><td>$d < d_0$</td><td>$\varepsilon_{PP} \cdot d^2$</td></tr>
<tr><td>$d \geq d_0$</td><td>$\varepsilon_{PP} \cdot d^4$</td></tr>
<tr><td colspan="2">node-base station (LOS)</td><td>$\varepsilon_L \cdot d^2$</td></tr>
<tr><td rowspan="2">node-base station (NLOS)</td><td>$d < d_0$</td><td>$\varepsilon_{NL} \cdot d^2$</td></tr>
<tr><td>$d \geq d_0$</td><td>$\varepsilon_{NL} \cdot d^3$</td></tr>
<tr><td colspan="4">$\varepsilon_{PP} = 1\ pJ/bit/m^n$, $\varepsilon_L = 0.047\ pJ/bit/m^2$, $\varepsilon_{NL} = 1\ pJ/bit/m^n$</td></tr>
<tr><td>$E_{b,r}$</td><td colspan="3">energy per bit for radio reception electronics</td><td>50</td></tr>
<tr><td>(passive) optical transmission</td><td>$E_{b,opt}$</td><td colspan="3">energy per bit for optical transmission</td><td>0.019</td></tr>
</table>

ε_{PP}: the RF transmission factor for the peer-to-peer channel
ε_L: the RF transmission factor for the node to base station (LOS) channel
ε_{NL}: the RF transmission factor for the node to base station (NLOS) channel

6.6. Simulation results and discussion

Table 6.2 and Figures 6.2-6.5 show the parameters and results of the simulations for several different deployment scenarios. For all the simulations, the base station is located directly above the midpoint of the deployment area. The base station's height is set to 140m for the simulations. It needs to be lower than d_L=145.7m at least, so nodes with LOS in the RF-only WSN are close enough to communicate with the base station and form a network. The results of Figures 6.2, 6.3 and 6.5 in Table 6.2, show that increasing the blocking factor causes E_R to decrease, suggesting the RF/FSO WSN operates best in environments where the blocking factors are low. The RF/FSO WSN is also able to support a larger deployment area (with fewer isolated nodes) compared to the RF-only WSN. This is shown by comparing the results of Figures 6.2 and 6.4 in Table 6.2.

TABLE 6.2
Simulation parameters and results for various deployment scenarios

Figure	Number of nodes deployed, N	Radius of deployment area, R	Base station height, h	Blocking factor, b_f	E_R	Number of isolated nodes	
						RF only	RF/ FSO
Figure 6.2	230	40m	140m	10%	1.84	1	1
Figure 6.3	230	40m	140m	30%	1.52	1	1
Figure 6.4	230	80m	140m	10%	N/A*	173	7
Figure 6.5	230	40m	140m	0%	2.27	0	0

* ignored due to large number of isolated nodes in RF-only WSN

For the RF/FSO WSN, a node connects directly to the base station if it has LOS to the base station and its distance to the base station is less than d_{OPT}=200m. For the RF-only WSN, a node connects directly to the base station if it has LOS to

the base station and its distance to the base station is less than d_L=146m. In the absence of LOS, nodes in the RF-only WSN can also connect directly to the base station if its distance to the base station is less than d_{NL}=9.9m. In Figure 6.4, fewer nodes are able to connect directly to the base station for the RF-only WSN, compared to the RF/FSO WSN. This is due to the longer distance d_{OPT} of 200m, compared to the d_L distance of 146m. The optical range d_{OPT} will generally always be longer than d_L, as the optical link is narrow and highly directional, and the RF link is broadcast-based and omnidirectional. In Figure 6.4, many nodes in the RF-only WSN need to rely on multihop radio links to communicate with the base station, but this is difficult due to the short peer-to-peer radio range, d_{PP}. If the deployment area is large, the RF-only WSN requires high node density to ensure that nodes are not too distant from each other (thus causing them to become isolated). The effect of low node density on the number of isolated nodes is more pronounced in Figure 6.4. Due to its longer free space optical distance, the RF/FSO WSN is able to support larger deployment areas.

6.7. Conclusions

This chapter discussed the simulation of the network traffic for both the RF-only and the RF/FSO WSN. One of the key aims of the simulations was to show that the average energy expended by the RF/FSO WSN was lower than its RF-only counterpart. To show this, a number of different deployment scenarios was considered. Simulations showed that the average energy expended by the RF/FSO WSN is substantially less than the RF-only WSN for the deployment scenarios considered. The RF/FSO WSN works best when the blocking factor is low, but it still provides some benefit when 30% of the nodes are blocked. The RF/FSO WSN is also

shown to be able to support larger deployment areas. The lower overall energy expended by the RF/FSO WSN should translate into longer network lifetime, which is studied in the following chapter.

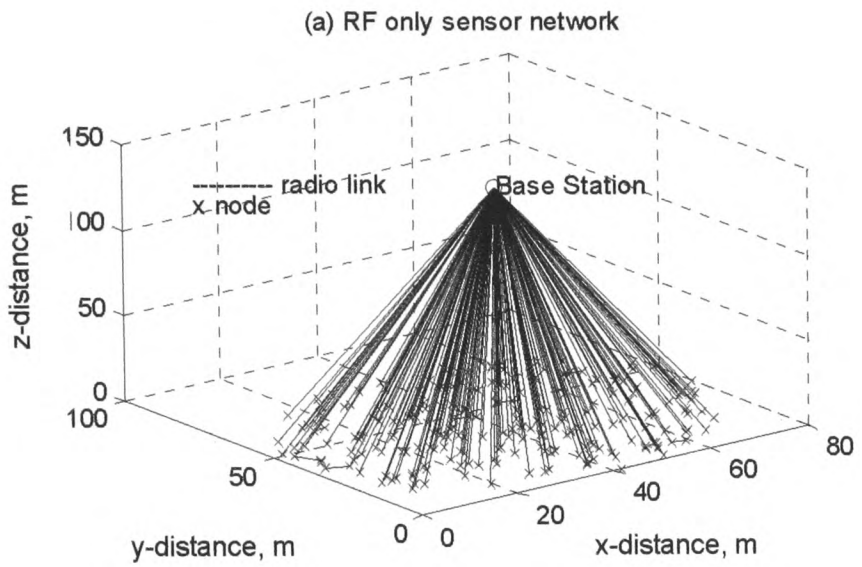

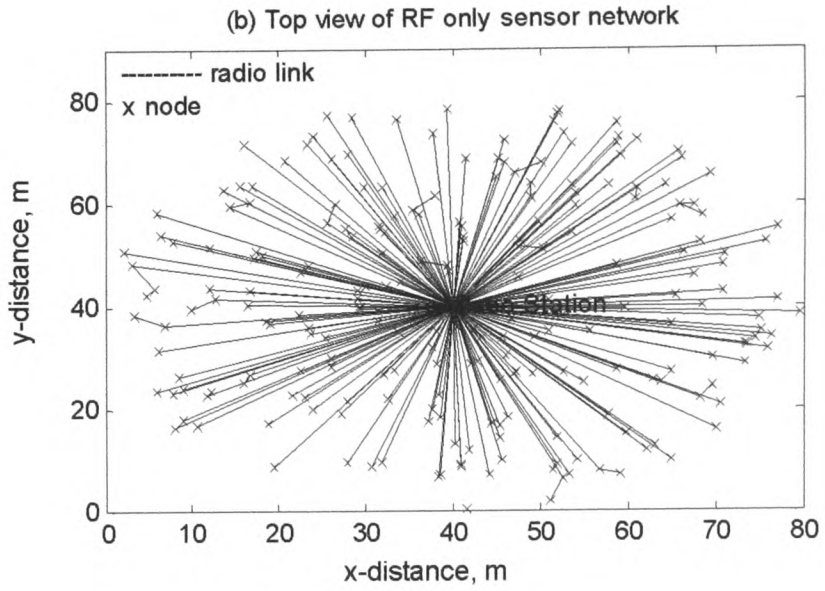

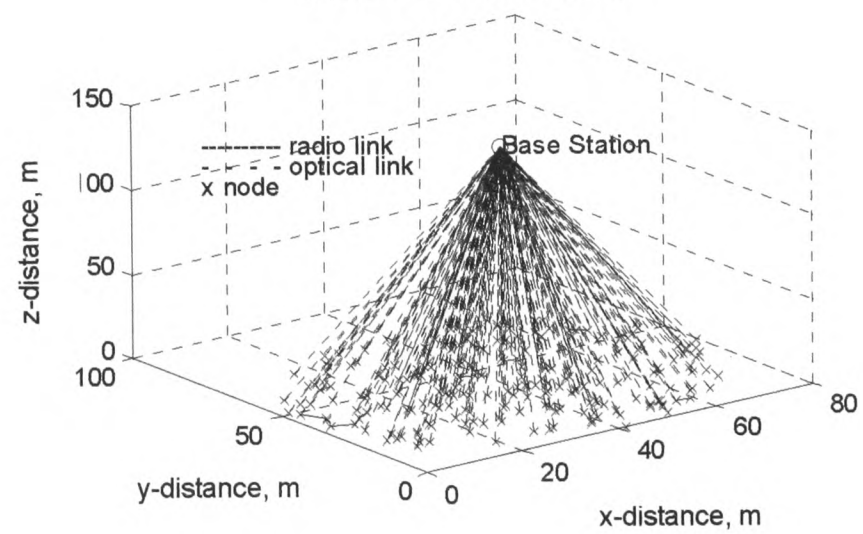

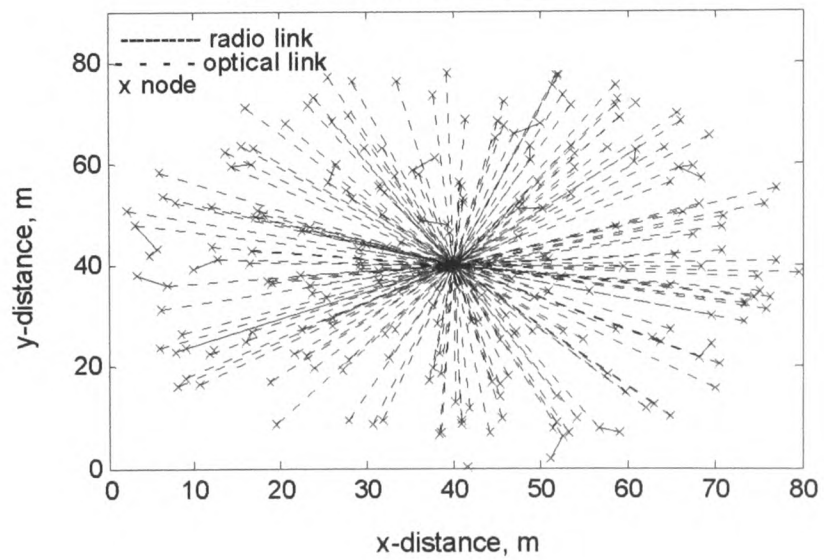

Figure 6.2: The WSNs for N=230, R=40m, h=140m, blocking factor=10%

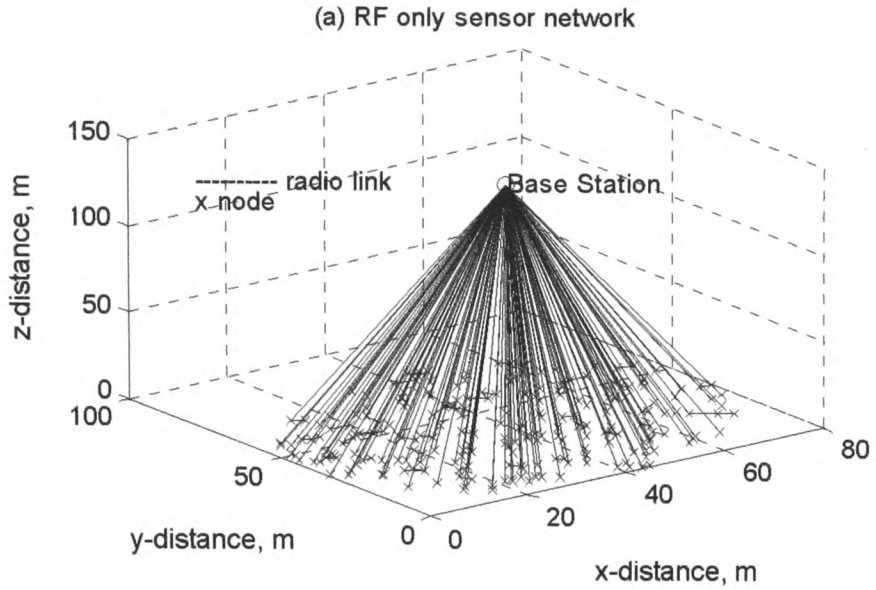

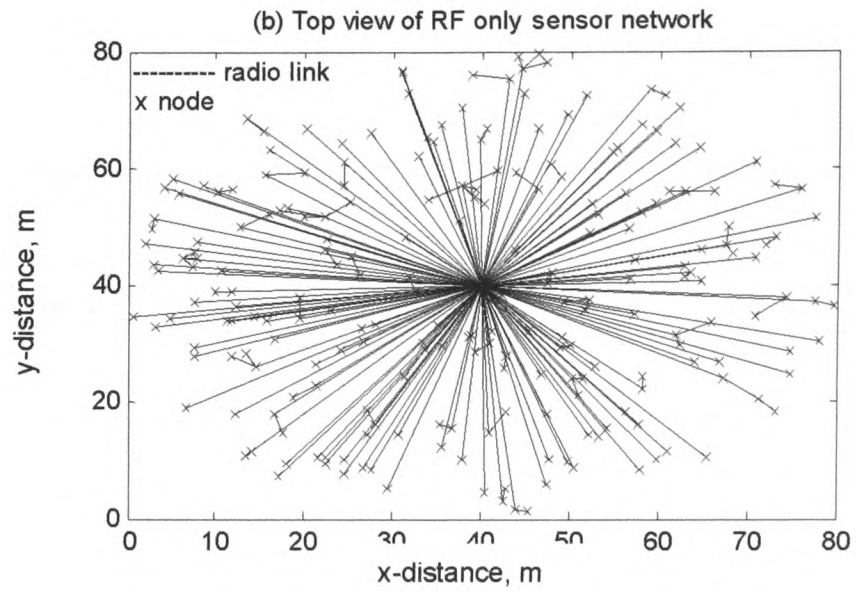

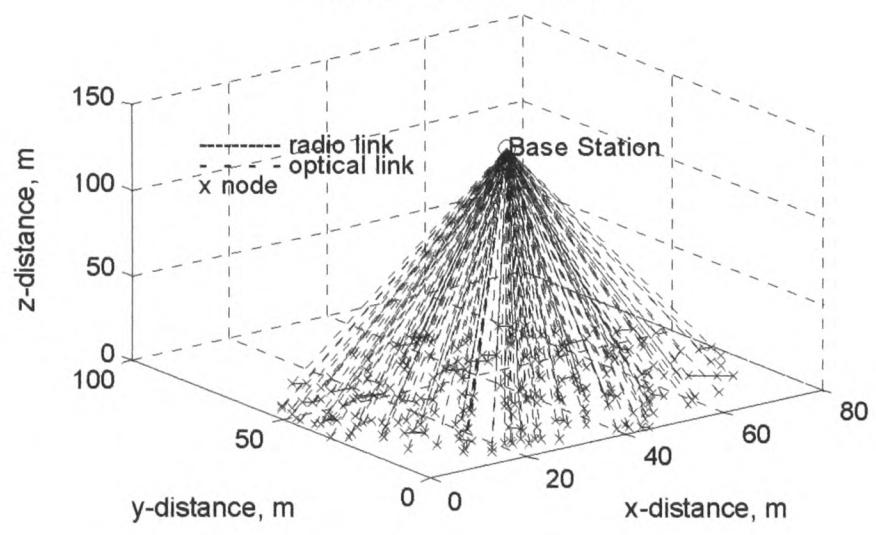

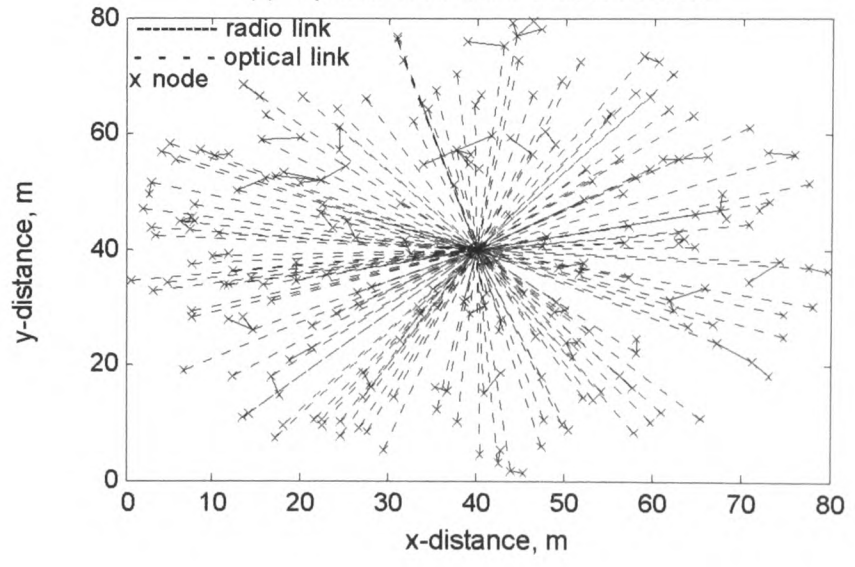

Figure 6.3: The WSNs for N=230, R=40m, h=140m, blocking factor=30%

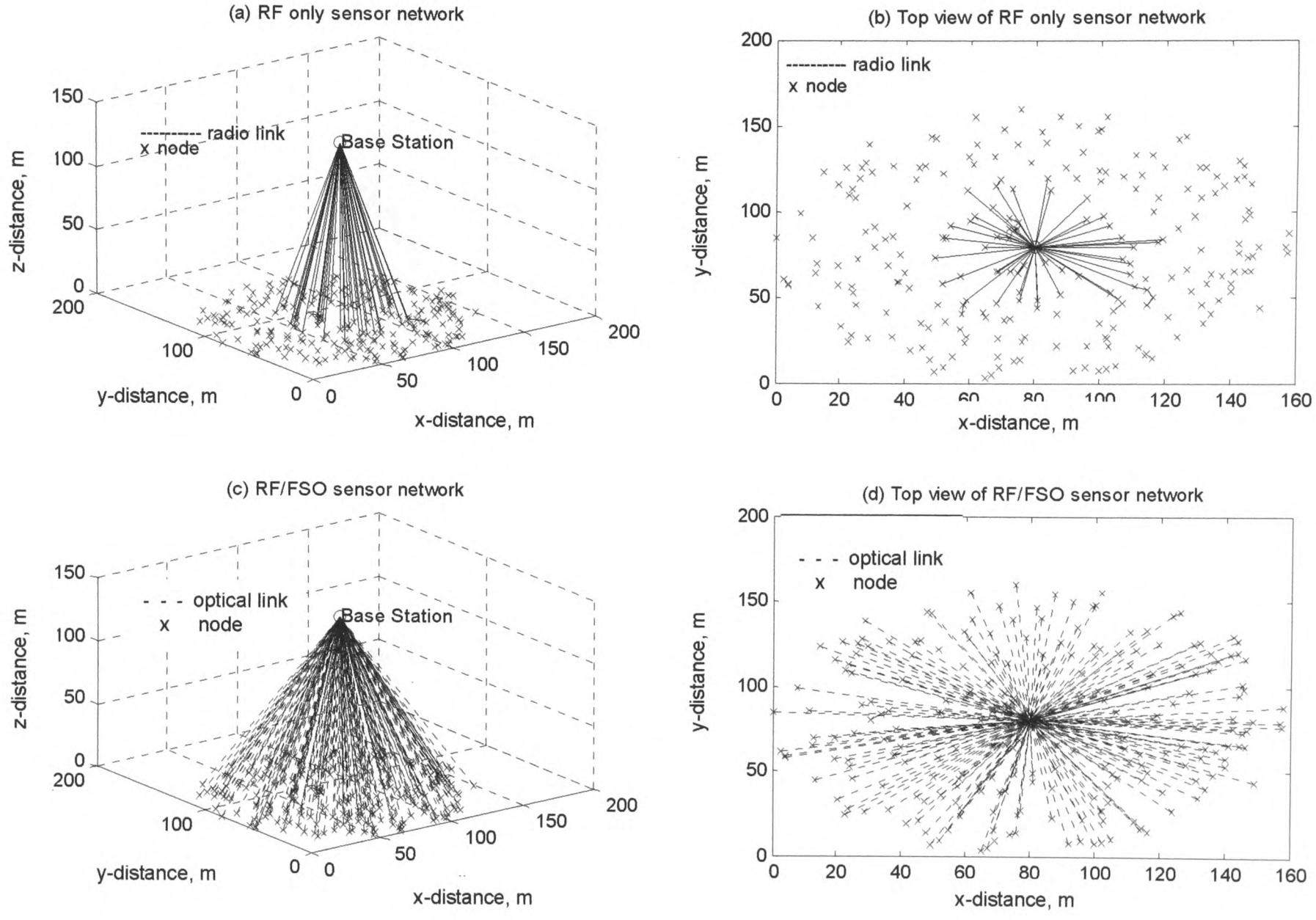

Figure 6.4: The WSNs for N=230, R=80m, h=140m, blocking factor=10%

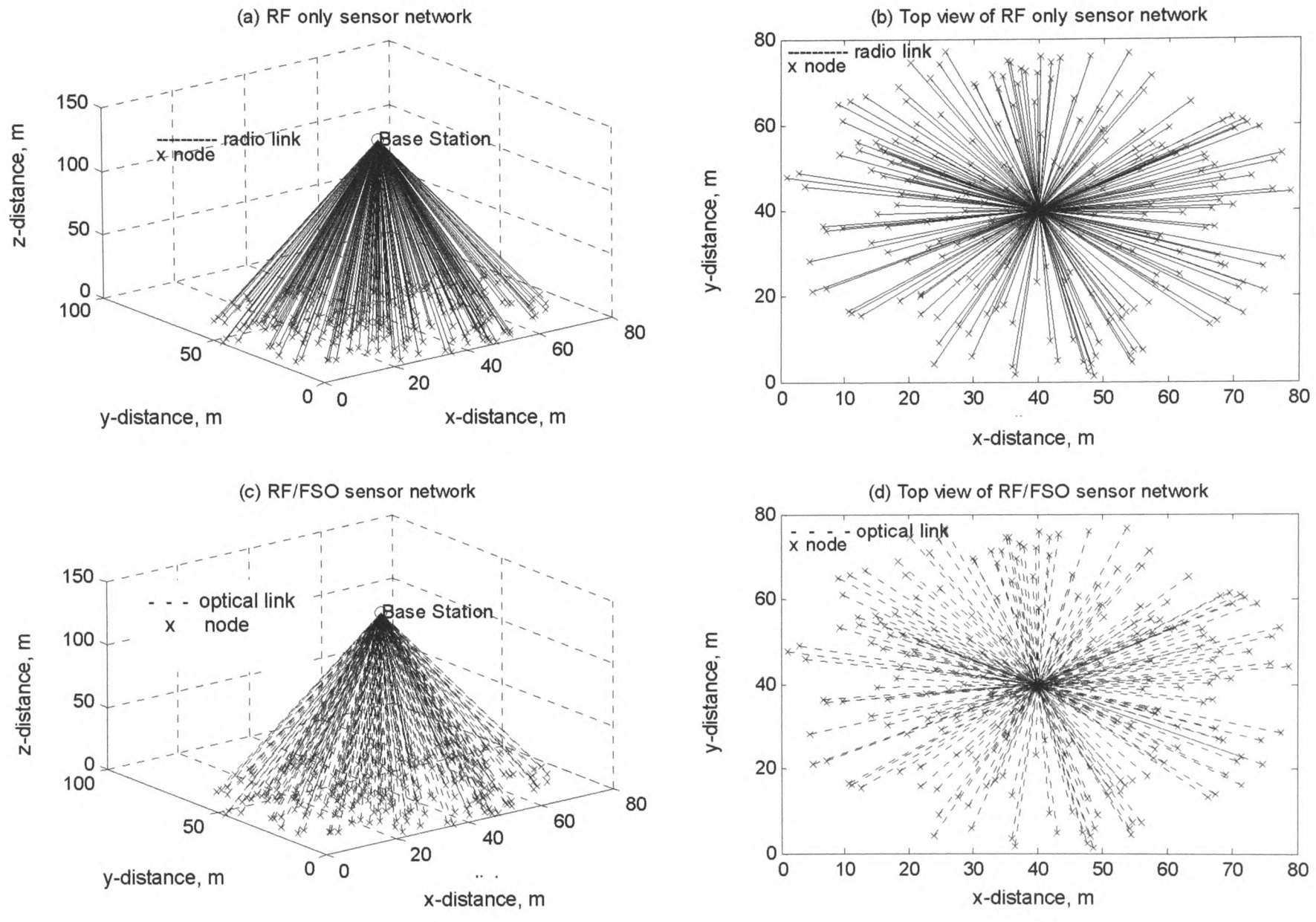

Figure 6.5: The WSNs for N=230, R=40m, h=140m, blocking factor=0%

Chapter 7

Network Lifetime and Coverage

In Chapter 6, several simulations of the network traffic for both the RF-only and RF/FSO WSN were presented. In this chapter, the RF/FSO WSN is studied in greater detail by considering several network parameters. These network parameters are used to study the network lifetime of the WSN and the average coverage area of the RF/FSO WSN.

Due to size restrictions, sensor nodes have a limited and irreplaceable source of power[19]. Sensor nodes are designed to be small, and their batteries need to be compact. Due to their small batteries, sensor nodes can expire quickly, and it is not always possible to replace the nodes that expire in a WSN. Therefore, in many cases, the deployed WSN is only expected to function for a single life-cycle. For example, to monitor areas of interest on Mars, NASA has plans to deploy sensor networks[44]. Replacing dead nodes in deployment scenarios like this may be difficult or impractical. The network lifetime is therefore an important design issue.

7.1. Definition of network lifetime and node failure

To study network lifetime, it is first necessary to define it, along with node failure. A node can be classified as being *alive* or *dead* based on the energy left in it[138]. Node failure occurs when a node is dead, or it can also happen when a node

is isolated. In Figure 7.1, node 23 is the cluster head for nodes 1, 5 and 12. As the cluster head is responsible for routing data in its cluster as well as sensing, it has a higher probability of dying faster. When node 23 dies, nodes 1, 5 and 12 become isolated from the network, as they are dependent on node 23 for communication with the base station. So, when node 23 dies, all four nodes: 1, 5, 12 and 23 face node failure.

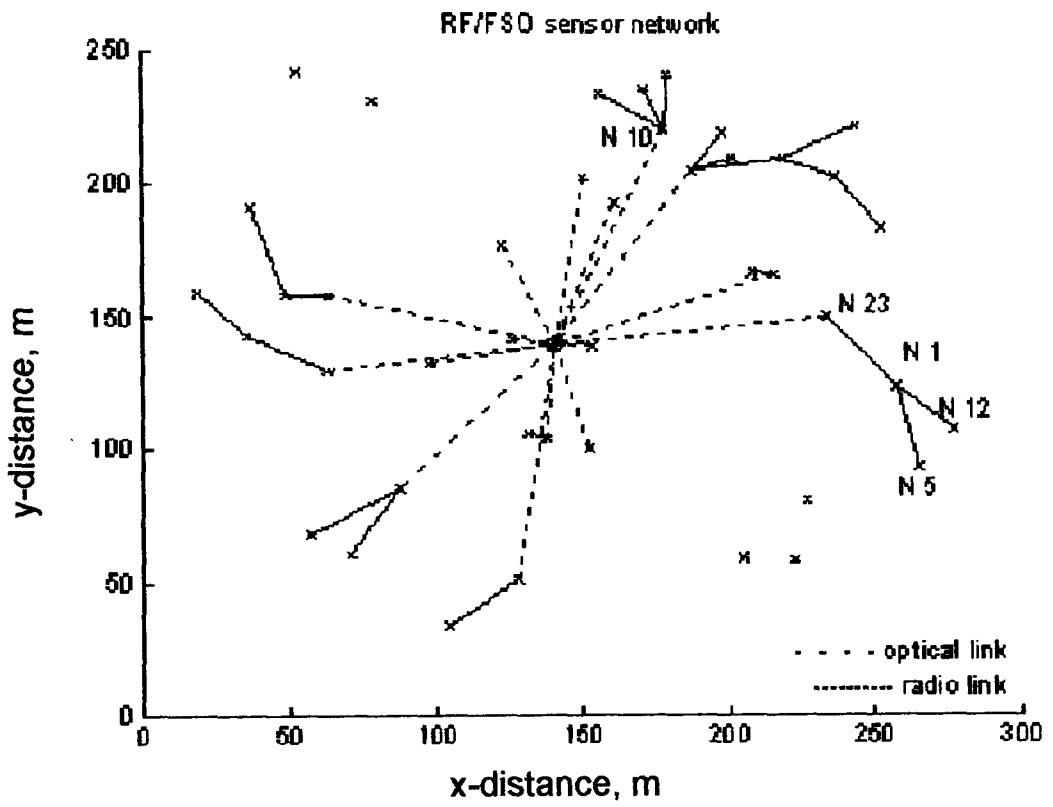

Figure 7.1: Aerial view of RF/FSO sensor field

There are several definitions available in the literature for WSN lifetime. One of the most common definitions for WSN lifetime is the time from when the network begins operation to the time of first node failure in the network[139]. Some of the more popular definitions of network lifetime are given in[44], and these are presented in Table 7.1. Table 7.2 lists the definitions adopted for the work in this report.

TABLE 7.1
Lifetime of Wireless Sensor Networks: Proposed Definitions

Reference(s)	Definition
[140-142]	Network lifetime is defined as the time until the first node failure. (Node failure can be due to the node dying after running out of energy, or being isolated due to the lack of a suitable cluster head to connect it to the base station.)
[78, 143-145]	Network lifetime is defined as the time until a percentage of initially deployed nodes have stopped operating due to node failure.
[138]	Network lifetime is defined in terms of the time when required network coverage is lost.
[146]	Network lifetime is defined as the mean expiration time of nodes.
[147]	Network lifetime is defined in terms of a fixed rate of packet of delivery. (In[147], the lifetime of the network is defined as the time until the packet delivery rate drops below 90%.)
[148]	Network lifetime is defined in terms of the number of flows still alive. (A flow represents *the long term rate of data transmission from source node to destination node*. The flow is zero for node pairs not communicating with each other[148].)

TABLE 7.2
Definitions adopted for work

Node Failure: Definition
Failure of the node to transmit and/or receive data due to the lack of energy resource (dead node) or the lack of a suitable cluster head to connect to the base station (isolated node).

Network Lifetime: Definition
Time from when the network begins sensing and transmitting data, until time when network coverage falls to 0% of total deployed area.

7.2. Network parameters

In this section, several network parameters are introduced to study the performance of the WSNs. The blocking factor, b_f, introduced in Chapter 4, is the percentage of deployed nodes without line of sight (LOS) to the base station. The base station optical hotspot was introduced in Chapter 6 (see Figure 6.1 in Chapter 6). The hotspot factor, δ, is defined as:

$$\delta = \frac{R}{r_{h,opt}} \tag{7.1}$$

where R is the deployment area radius and $r_{h,opt}$ is the optical hotspot radius. The deployment area is within the base station's optical hotspot if $\delta \leq 1$. The range ratio, β, is defined as:

$$\beta = \frac{d_{OPT}}{d_L} \tag{7.2}$$

where d_{OPT} is the maximum free space optical range and d_L is the maximum radio range for a node with LOS to the base station. The node density gives the number of nodes within the sensing range of a node[20]. Assuming that the sensing range is d_{PP}, the node density is defined as[20]:

$$\mu = \frac{N \cdot {d_{PP}}^2}{R^2} \tag{7.3}$$

where N is the number of deployed nodes.

7.3. Reconfiguring and non-reconfiguring networks

For the study presented in this work, two types of networks are considered: reconfiguring and non-reconfiguring networks. In non-reconfiguring networks, the links between the nodes do not change from the moment the network wakes up, until the network dies. Therefore, nodes depending on a cluster head become isolated when the cluster head dies. This is illustrated in Figure 7.2. Figure 7.2(a) shows the network when it first wakes up. Node 2 serves as a cluster head for nodes 4, 5 and 6. Figure 7.2(c) shows the network after node 2 dies. Although nodes 4, 5 and 6 are still alive (i.e. their batteries still have energy), they become isolated from the base station as the network does not reconfigure itself. (This is similar to the case discussed in Section 7.1, shown in Figure 7.1.)

In a reconfiguring network, if a cluster head dies, nodes that depended on it would route their data to new cluster heads. The isolated nodes connect themselves to the closest potential cluster head still alive, with a connection to the base station. It is possible that the isolated nodes will connect to different new cluster heads. This is shown in Figure 7.2(b). Upon the death of node 2, nodes 4 and 5 connect to node 1. Node 6 connects to node 3 (as node 3 is closer to node 6 than node 1). For the reconfiguring network, every node needs to keep information regarding a potential new cluster head in memory. This information will also need to be constantly updated as cluster heads die.

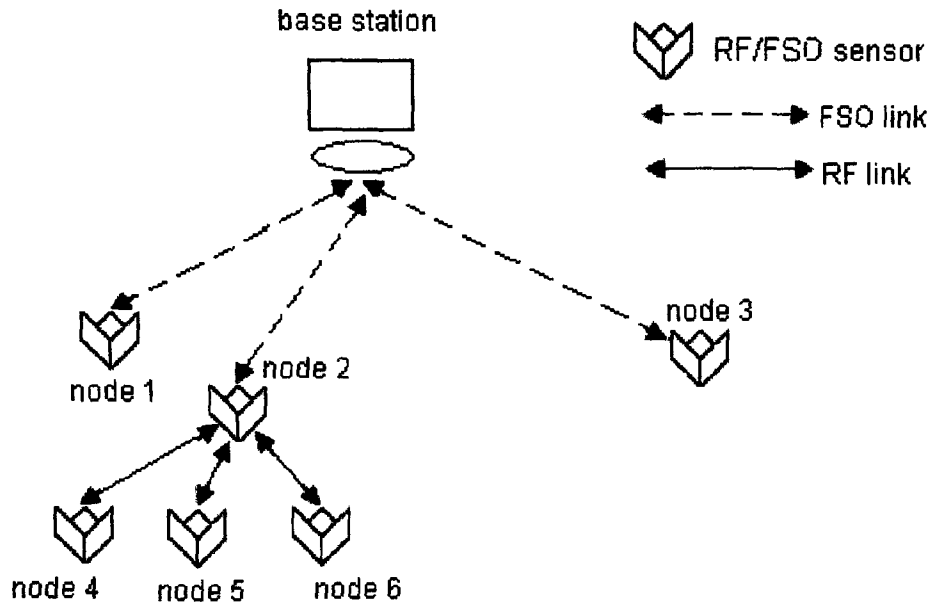

Figure 7.2(a)

Figure 7.2(a): RF/FSO WSN before node 2 dies

Figure 7.2(b): Reconfiguring RF/FSO WSN after node 2 dies

Figure 7.2(c): Non-reconfiguring RF/FSO WSN after node 2 dies

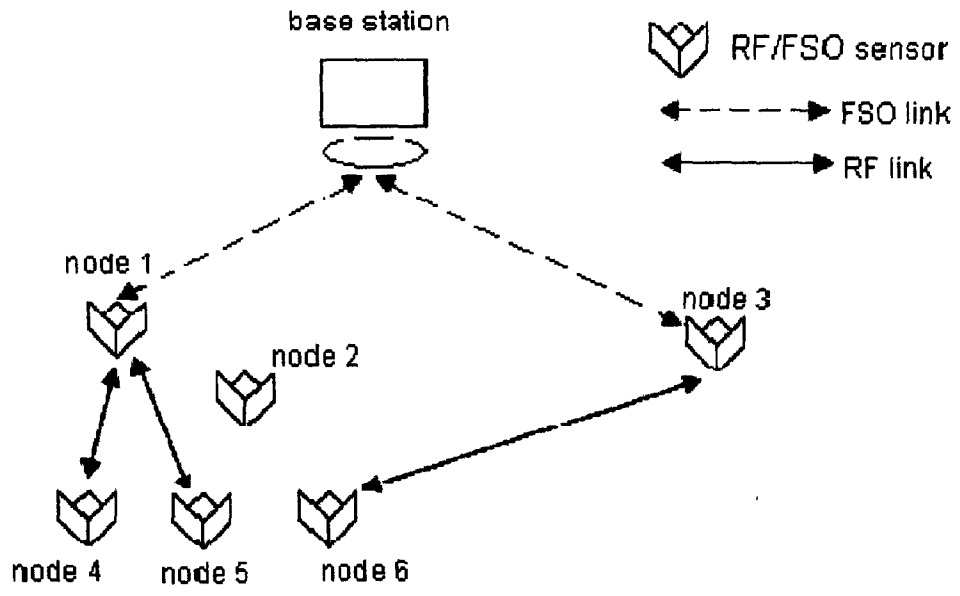

Figure 7.2(b)

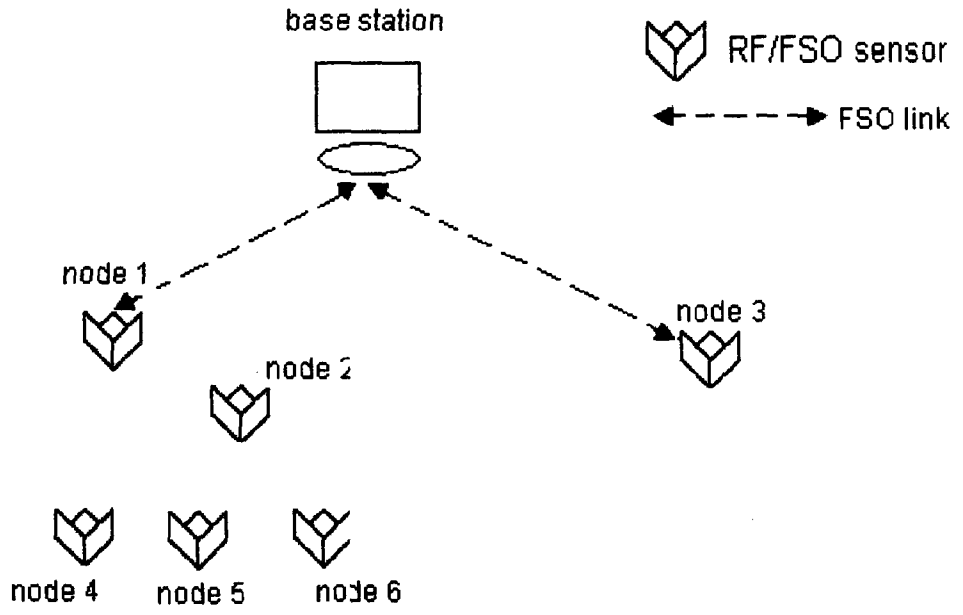

Figure 7.2(c)

7.4. Network lifetime performance parameters

7.4.1. Determining network coverage area

For the simulations, it is necessary to calculate the area still covered by the network throughout the lifetime of the network. This is because for the network lifetime definition in Table 7.2, the lifetime is determined based on the percentage of coverage area. To do this, a fixed-point template is used, as shown in Figure 7.3. The fixed point template is a circle with the deployment area radius, R, superimposed over a square with $2R$ x $2R$ points. The points are 1m horizontally and vertically apart from each other. This density of points was considered a good compromise between template resolution and code run time.

This template is placed over the deployment area of the network. The area coverage is determined as the percentage of template points within the sensing range of nodes. Figure 7.4 shows a template over a deployment area with 50% coverage, as half of all the template points falls within an area within node sensing range. The smaller shaded circles are the node sensing ranges.

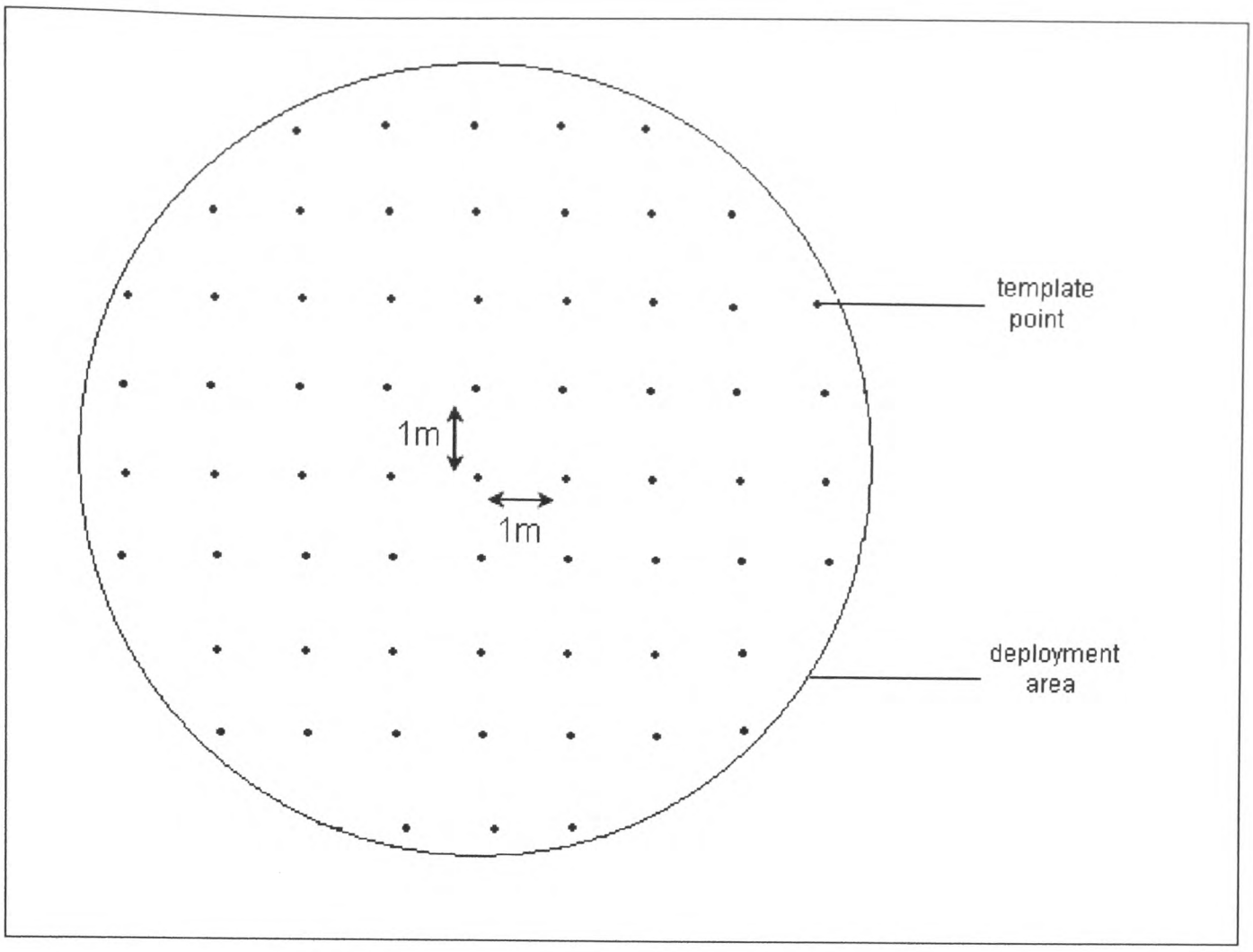

Figure 7.3: Fixed point template used to determine coverage area

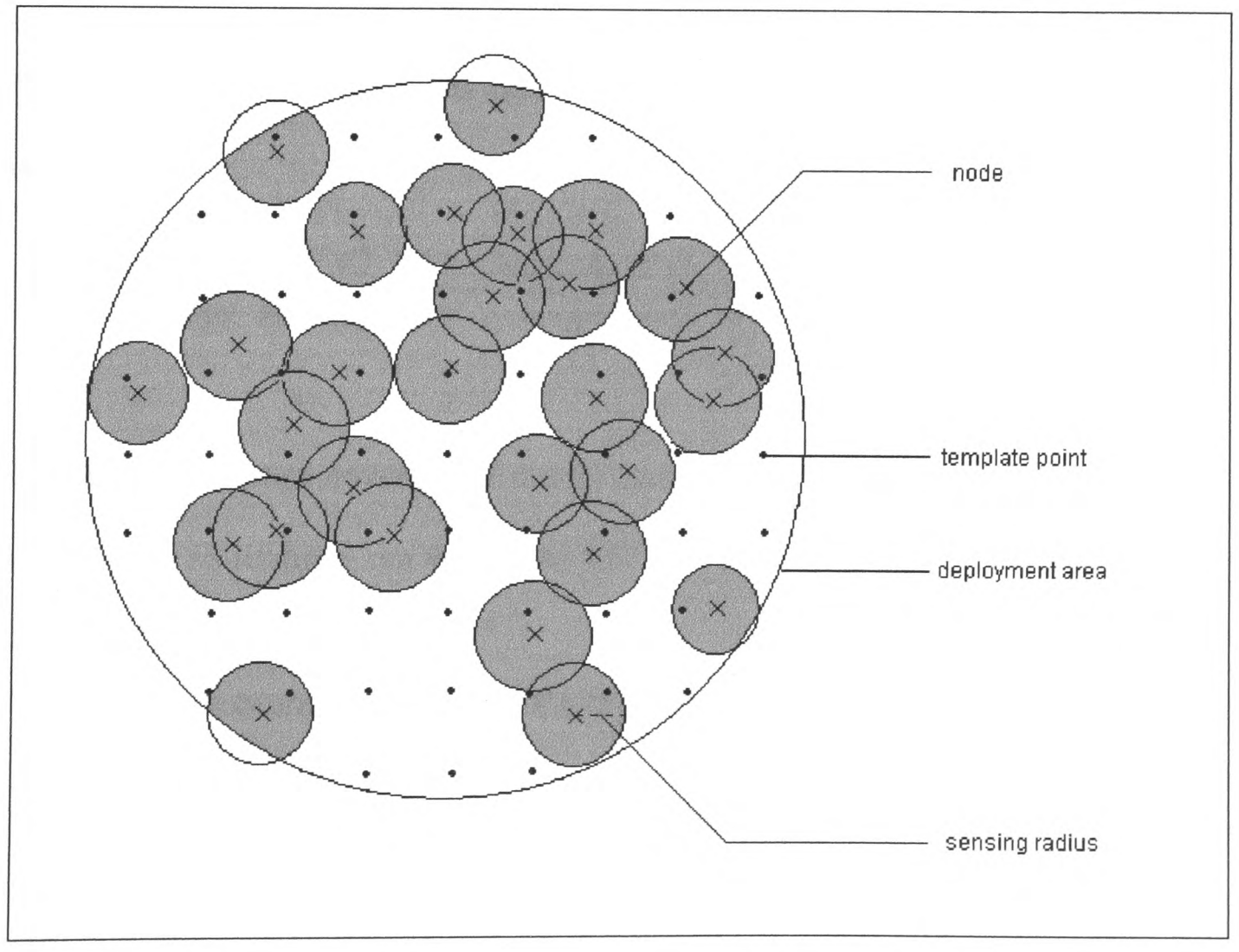

Figure 7.4: Fixed-point template over a deployment area with 50% coverage

7.4.2. Lifetime ratio, L_r

To study the relative lifetimes of the RF/FSO and the RF-only WSN, the network lifetime ratio, L_r, is introduced. It is defined as:

$$L_r = \left(\frac{RF\ /\ FSO\ WSN\ lifetime}{RF\ only\ WSN\ lifetime} \right) \tag{7.4}$$

7.4.3. Average coverage ratio, C_r

The RF/FSO WSN might outlast the RF-only WSN, but it is also interesting to investigate if it can at least provide a comparable level of coverage as the RF-only WSN over its lifetime. It would not be desirable to have a long lasting RF/FSO WSN which offered poor network coverage. The optimum aim is to have the RF/FSO WSN lasting longer than the RF-only WSN, whilst offering better, or equal, network coverage. To investigate this, the average coverage ratio, C_r, is determined. It is defined as:

$$C_r = \left(\frac{Average\ \ RF\ /\ FSO\ \ WSN\ \ coverage\ \ over\ \ RF\ /\ FSO\ \ WSN's\ \ lifetime}{Average\ \ RF\ only\ WSN\ \ coverage\ \ over\ \ RF\ only\ \ WSN's\ \ lifetime} \right) \tag{7.5}$$

(Note that the average coverage of the RF-only WSN in Equation 7.5 is the average coverage over *its* lifetime, not that of the RF/FSO WSN.)

7.4.4. Average coverage area of RF/FSO WSN

The third network performance parameter is the average coverage area of the RF/FSO WSN. This, more than the network lifetime, provides good insight into the performance of the RF/FSO WSN. Figures 7.5 and 7.6 illustrate this. Figures 7.5 and

7.6 show the lifetimes of the non-reconfiguring and reconfiguring networks respectively

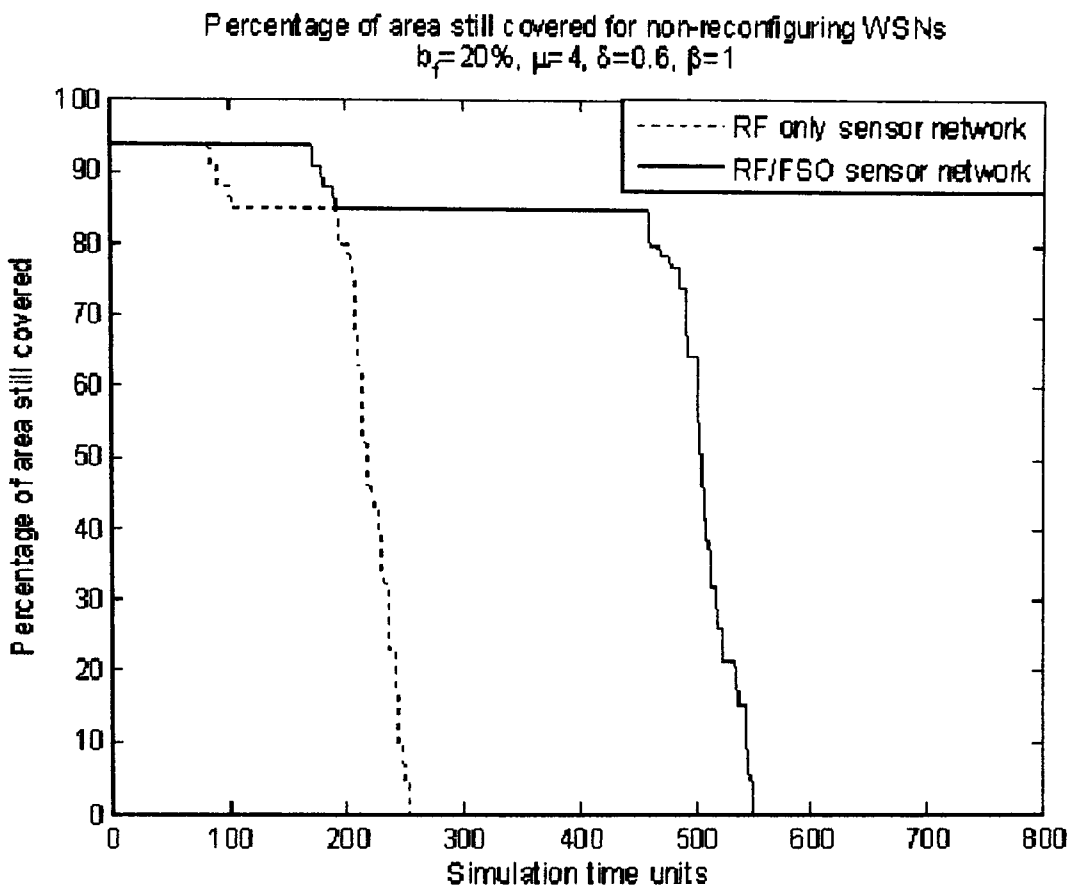

Figure 7.5: Percentage area still covered for non-reconfiguring WSNs

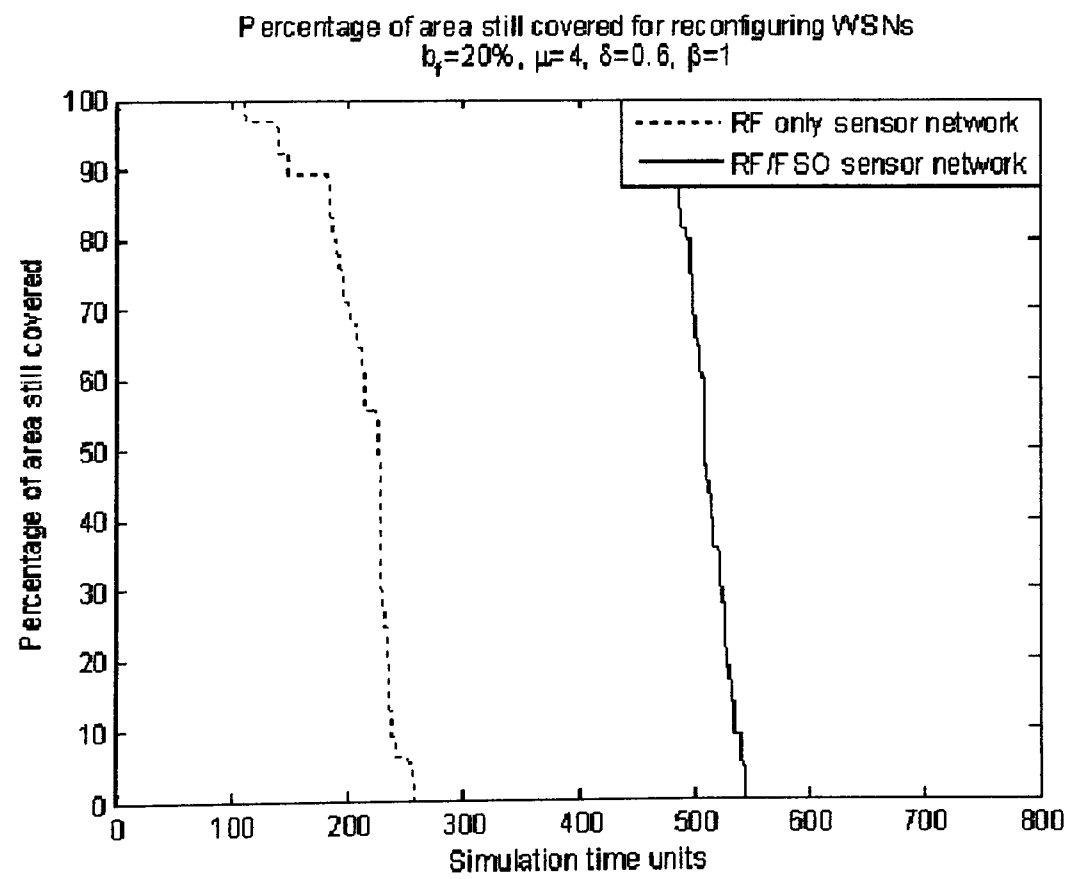

Figure 7.6: Percentage area still covered for reconfiguring WSNs

In Figures 7.5 and 7.6, both the reconfiguring and non-reconfiguring networks have the same network lifetimes (250 and 550 simulation time units). Based on the network lifetime alone, it would appear that reconfiguration does not improve network performance. Studying the average coverage area, however, shows the benefits of network reconfiguration. As shown in Figure 7.2, network reconfiguration ensures that nodes do not necessarily become isolated when their cluster head dies. This results in a larger average coverage area for the reconfiguring networks as shown in Figure 7.6. (The simulation parameters used are discussed in Section 7.5.)

There are steps in the curves shown in Figures 7.5 and 7.6. The steps are caused by cluster heads dying. When a cluster head dies, the nodes in its cluster may fail to find new cluster heads. The step is caused by a cluster head dying, and some or all of the nodes in the cluster becoming isolated. The steps in the curves in Figure 7.6 are less prominent as the network reconfigures itself upon the death of a cluster head, thus being able to better preserve network coverage.

7.5. Simulations and results

The parameters used for the simulations are given in Table 7.3. The maximum radio ranges, d_{PP}, d_L and d_{NL}, were discussed in Chapter 2. An energy budget of 1mJ is provided for each node, and the sensing radius is set to d_{PP}.

TABLE 7.3
Simulation Parameters

Parameter	Description	Value
h	base station height	140m
d_{PP}	maximum peer-to-peer radio range	5.6m
d_L	maximum node to base station radio range (with line of sight)	145.7m
d_{NL}	maximum node to base station radio range (without line of sight)	9.9m

From Equation 7.2, the maximum free space optical range, d_{OPT}, is

$$d_{OPT} = \beta \cdot d_L \tag{7.6}$$

From Equation 7.1, the deployment area radius, R, is

$$R = \delta \cdot \sqrt{{d_{OPT}}^2 - h^2} \tag{7.7}$$

From Equation 7.3, the number of nodes deployed, N, is

$$N = \mu \cdot \frac{R^2}{{d_{PP}}^2} \tag{7.8}$$

For every given set of parameters, the node coordinates are kept identical, when comparing configuring and non-reconfiguring networks. So, the network topologies for both the reconfiguring and non-reconfiguring networks are identical at the beginning of their lifetimes. For a number of cases (μ=2), the simulations were run three times with the average results being plotted. It was not feasible to do this for all the cases due to the long runtimes of the codes, especially for the larger deployment areas and node densities. To study δ, b_f and μ in Sections 7.5.1, 7.5.2, 7.5.3 respectively, β is set to 1. The optical links considered are highly directional, whereas the RF links are broadcast-based and omnidirectional. The maximum optical

range, d_{OPT} is thus always expected to be longer than the radio range, d_L. Therefore, β=1 (β being the ratio of d_{OPT} to d_L) represents a sufficiently pessimistic worst case to consider.

7.5.1. Hotspot factor, δ, results and discussion

In this section, the hotspot factor, δ, is studied. The lifetime ratio L_r, average coverage ratio C_r and the average RF/FSO WSN network coverage are studied for a selection of δ. This section aims to identify the range of δ which the RF/FSO WSN operates best in. Figures 7.7 – 7.11 show the lifetime ratio, L_r, for a range of hotspot factors and node densities.

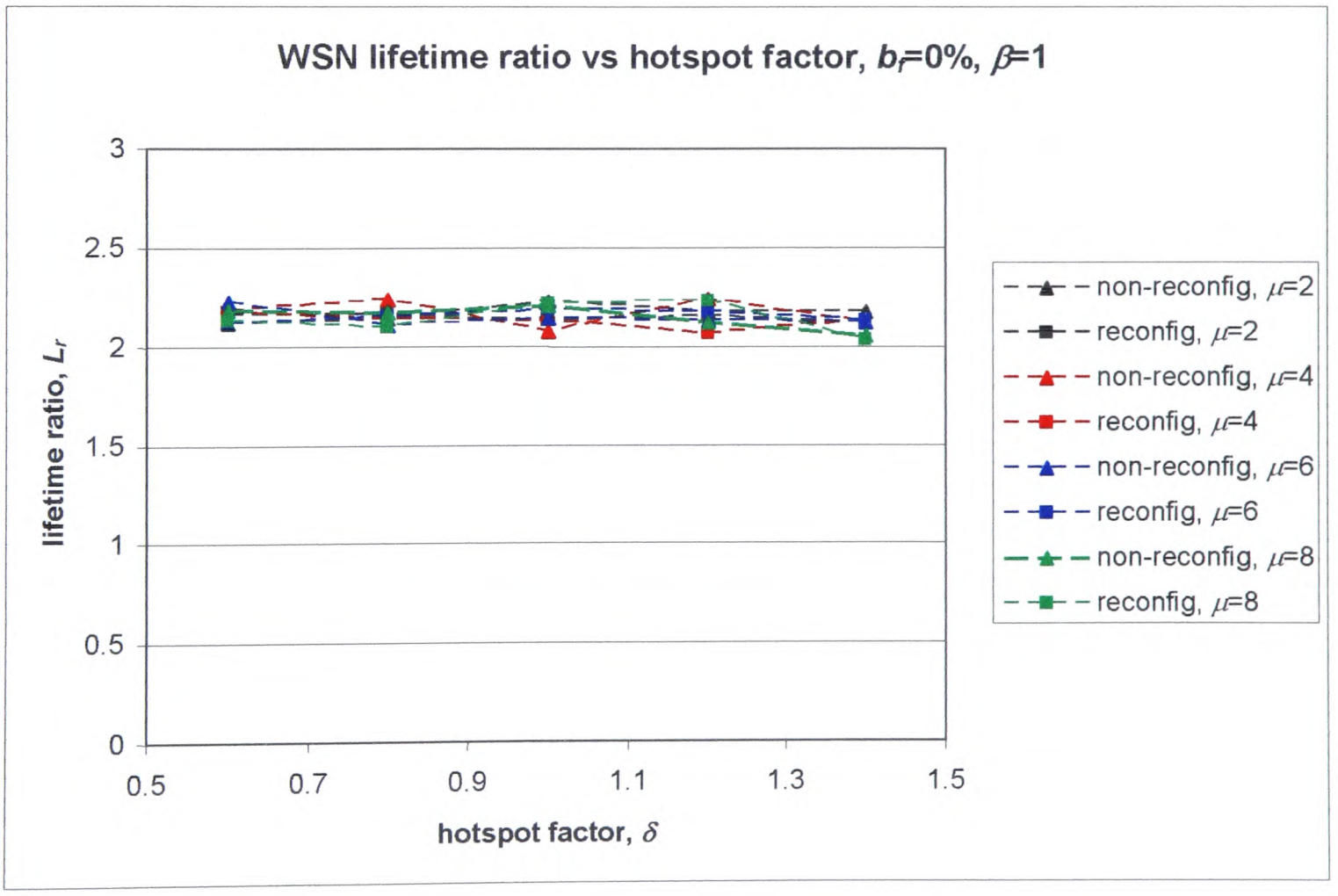

Figure 7.7: WSN lifetime ratio, L_r, vs hotspot factor δ, for blocking factor b_f=0%, range ratio β=1

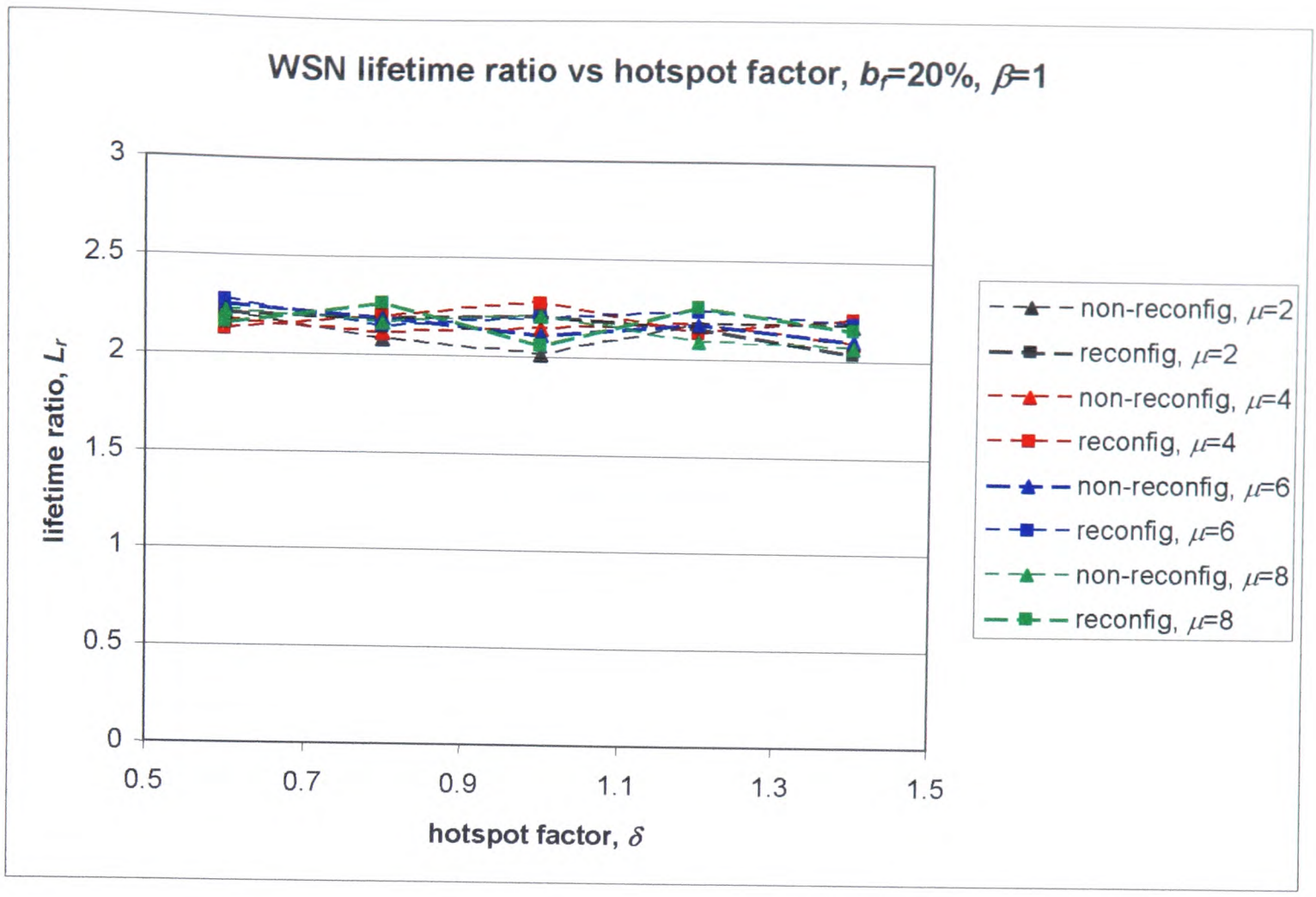

Figure 7.8: WSN lifetime ratio, L_r, vs hotspot factor, δ, for b_f=20%, β=1

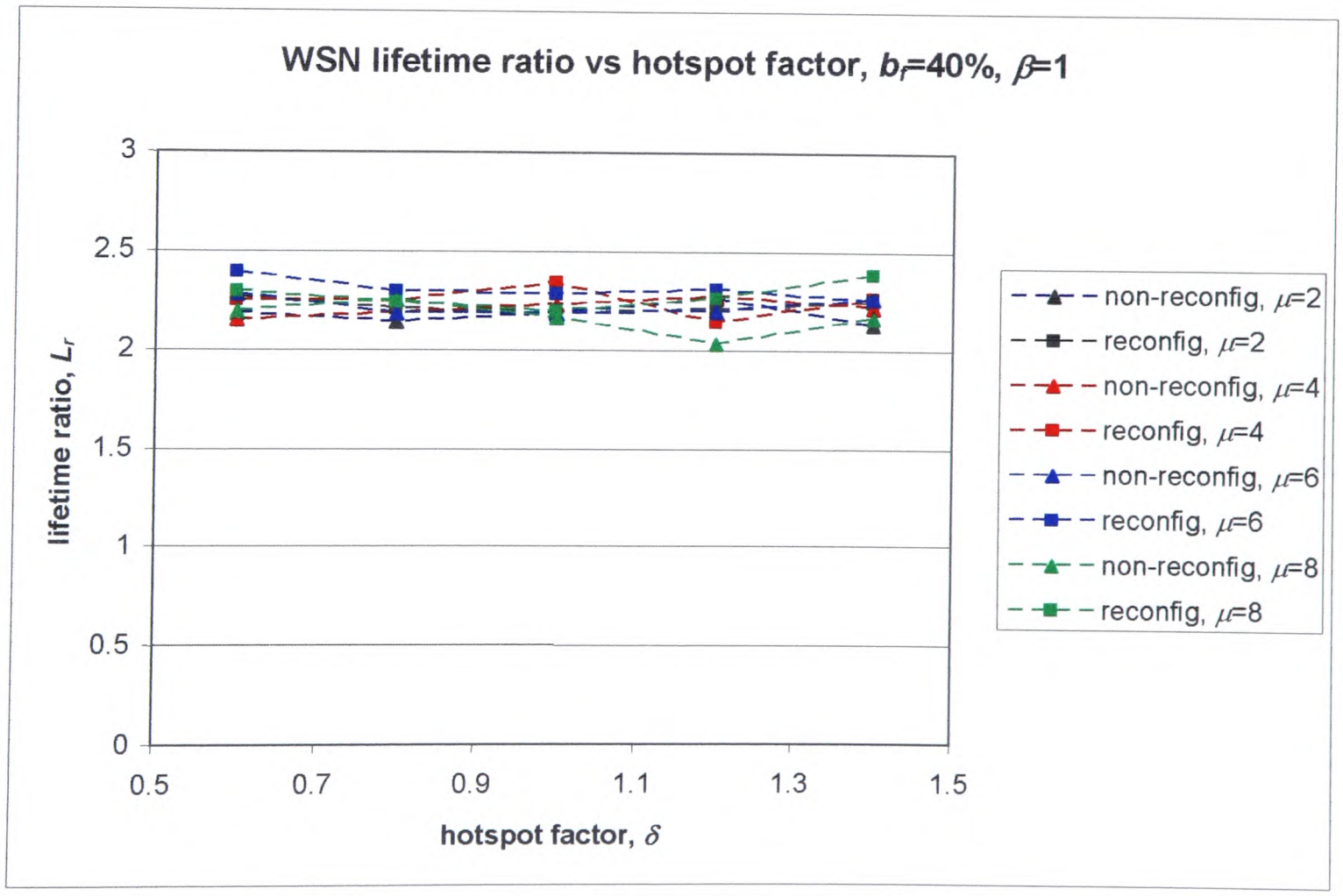

Figure 7.9: WSN lifetime ratio, L_r, vs hotspot factor, δ, for b_f=40%, β=1

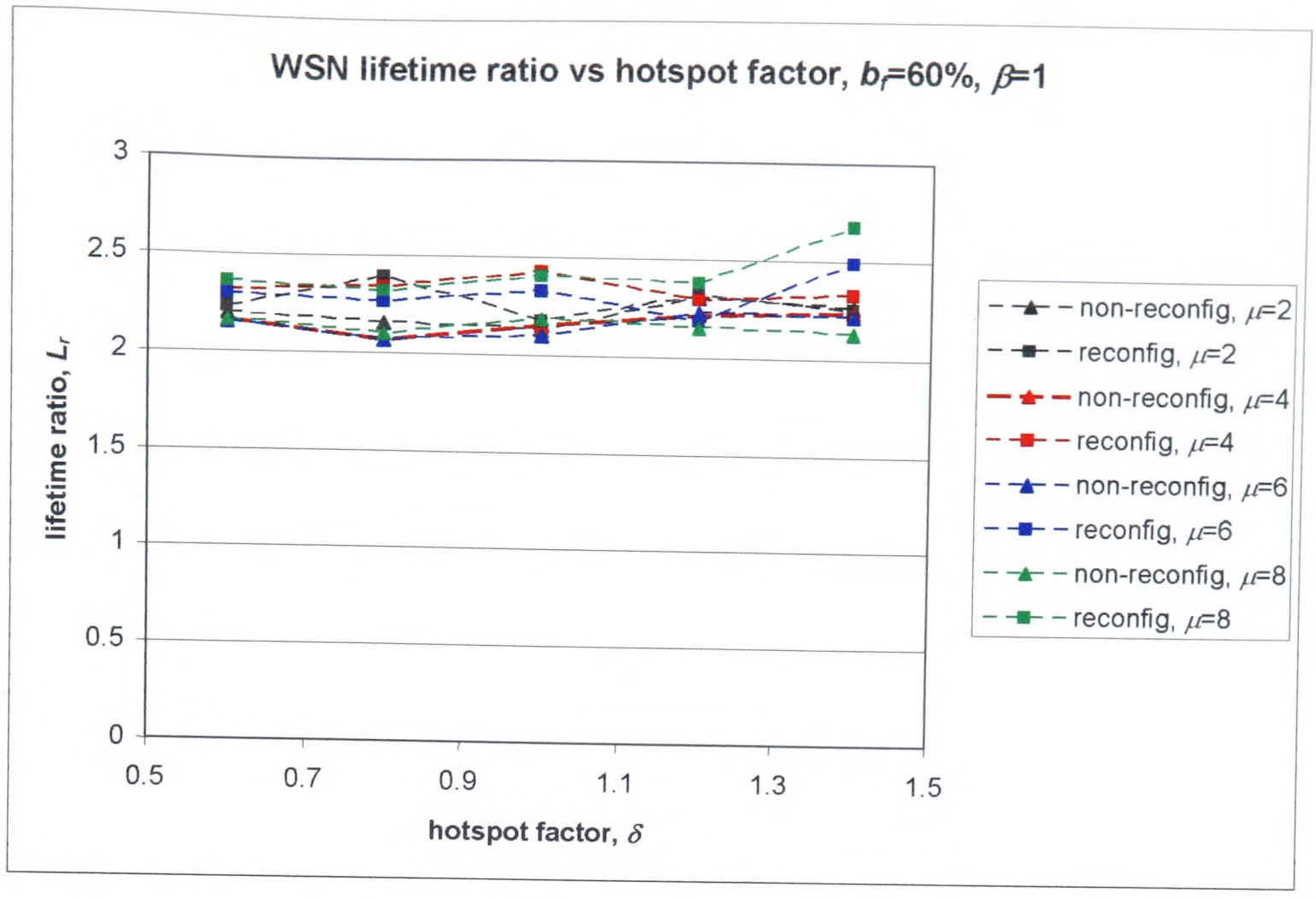

Figure 7.10: WSN lifetime ratio, L_r, vs hotspot factor, δ, for b_f=60%, β=1

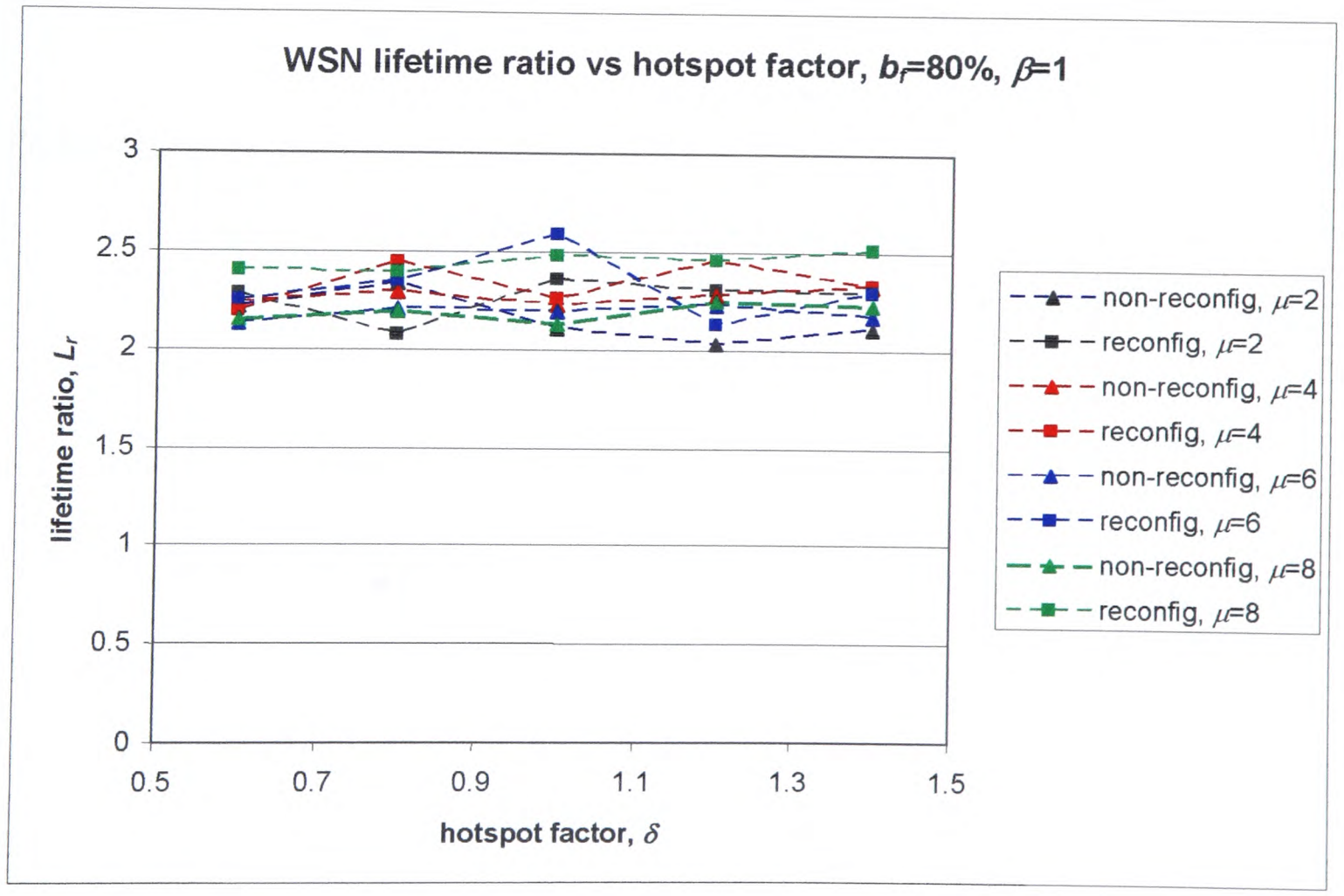

Figure 7.11: WSN lifetime ratio, L_r, vs hotspot factor, δ, for b_f=80%, β=1

The figures show that both the reconfiguring and non-reconfiguring RF/FSO WSNs last at least twice as long as their RF-only counterparts. The network lifetime is defined in Table 7.2 as the time when the network coverage area falls to zero. So, the network lifetime is determined by the last surviving node in the network. The last surviving node would have expended the least amount of energy over the duration of the network's lifetime. Therefore, it is most likely that this node did not serve as a cluster head and was directly connected to the base station. The energy expended by the last nodes in both the RF/FSO and RF-only WSNs is given in Table 7.4. (This is based on Table 5.1, in Chapter 5.)

TABLE 7.4
Energy expended by last nodes in RF/FSO and RF-only WSNs

Energy	**Last node in RF-only WSN**		**Last node in RF/FSO WSN**
Sensing	20 nJ/bit		20 nJ/bit
Processing sensed data	20 nJ/bit		20 nJ/bit
Communications	To drive transmitter electronics	50 nJ/bit	19 pJ/bit
	Transmitted RF energy	1 nJ/bit (max)	
Total	91 nJ/bit		40.019 nJ/bit

Therefore, on average, the ratio between the energies expended by the final node in the RF-only WSN to the final node in the RF/FSO WSN is 91/40.019=2.27. This explains the $2 \leq L_r \leq 2.5$ lifetime ratio range in Figures 7.7-7.11. The hotspot factor has no appreciable effect on the lifetime, as even if some nodes are outside the optical hotspot, the lifetime is dictated by a non cluster head node within the optical hotspot. Network reconfiguration also has little effect on the lifetime ratio for low

blocking factors ($0\% \leq b_f < 40\%$). This is because unless the blocking factor is extremely severe, there would be at least one non-cluster head node connected directly to the base station, which would remain a non-cluster head node until the network dies. For high blocking factors (60% and 80%), the lifetime ratio may exceed 2.5. This is discussed further in Section 7.5.2, where the blocking factor is studied in more detail.

The average coverage ratio, C_r, for different hotspot factors and node densities are shown in Figures 7.12 – 7.16.

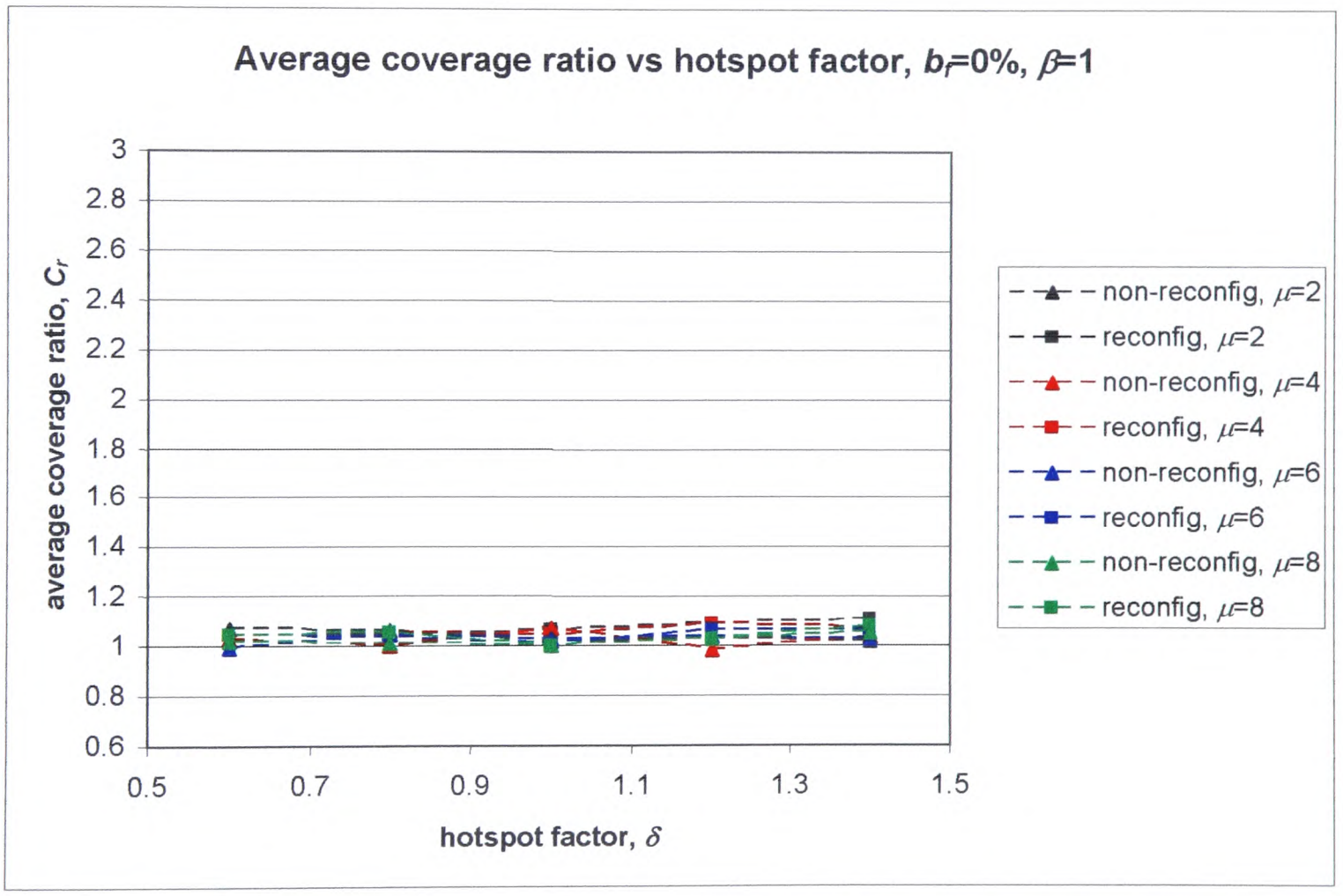

Figure 7.12: Average coverage ratio, C_r, vs hotspot factor δ, for blocking factor b_f=0%, range ratio β=1

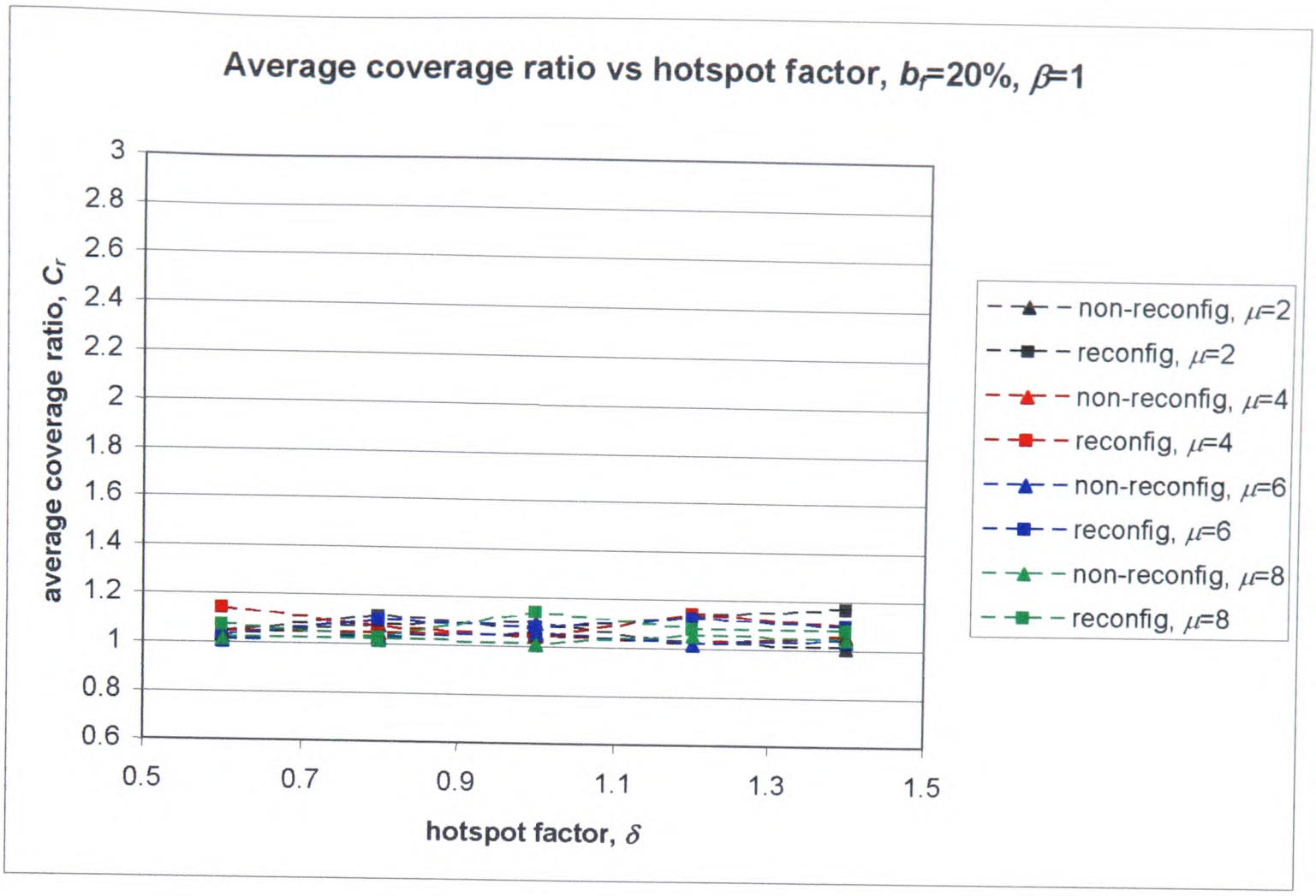

Figure 7.13: Average coverage ratio, C_r, vs hotspot factor, δ, for b_f=20%, β=1

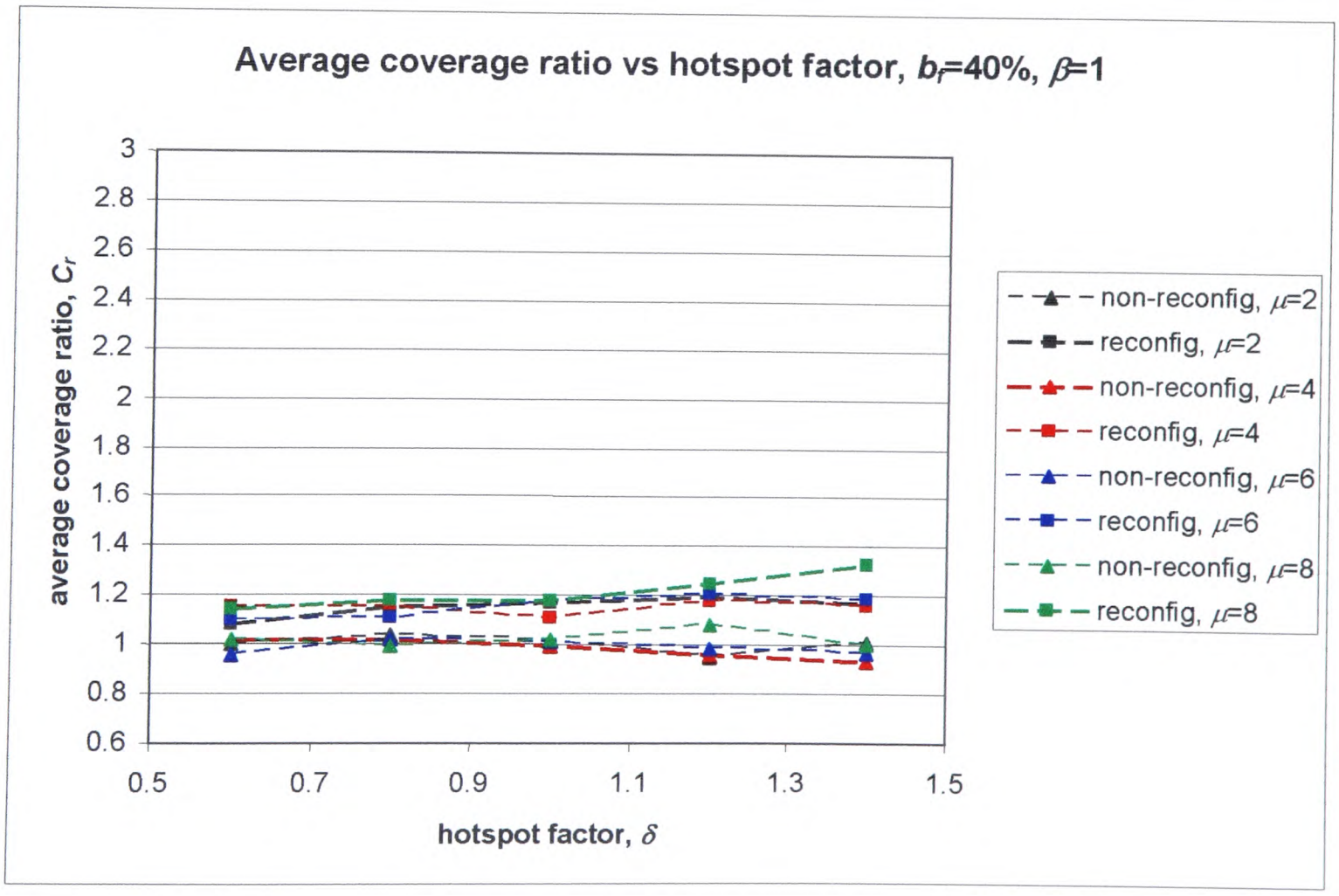

Figure 7.14: Average coverage ratio, C_r, vs hotspot factor, δ, for b_f=40%, β=1

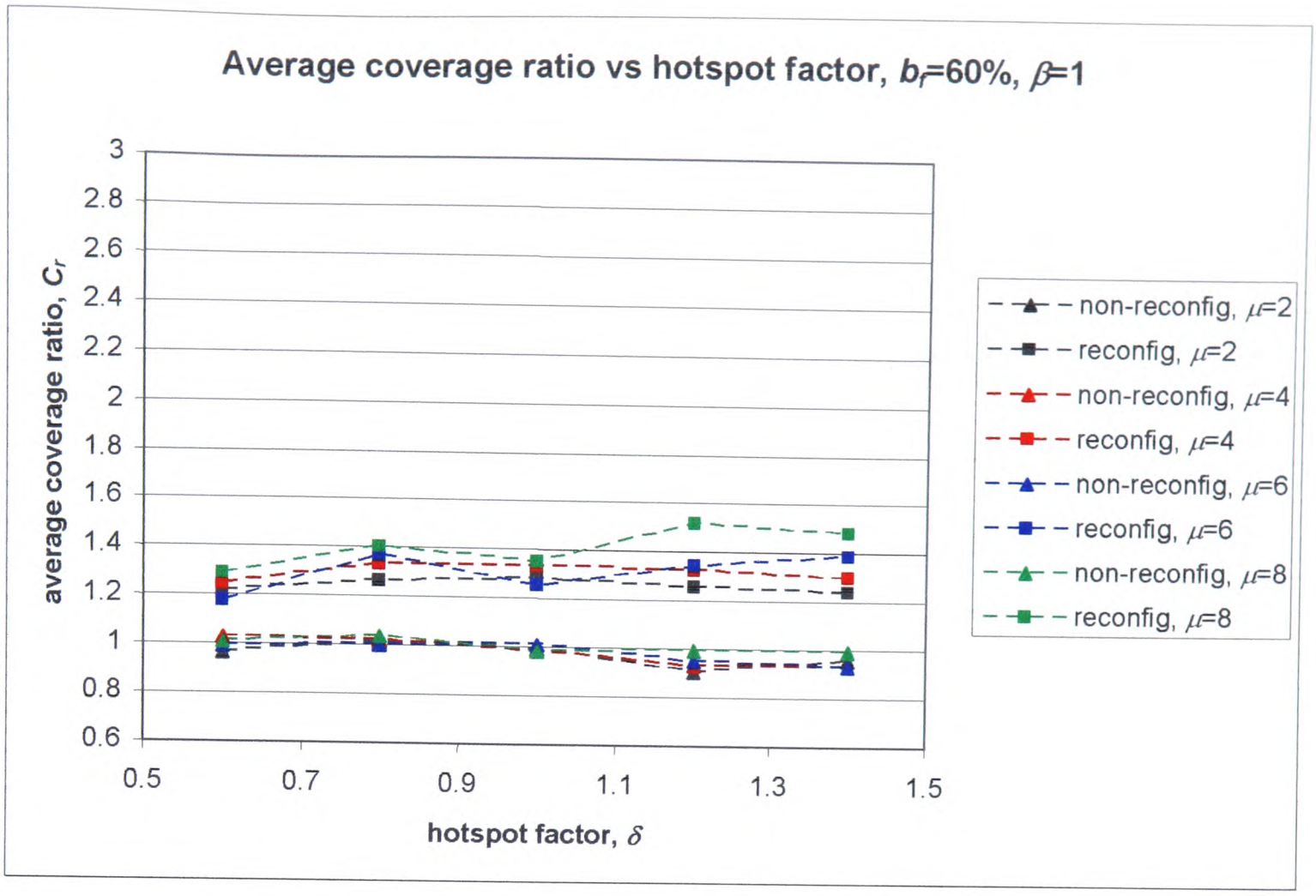

Figure 7.15: Average coverage ratio, C_r, vs hotspot factor, δ, for b_f=60%, β=1

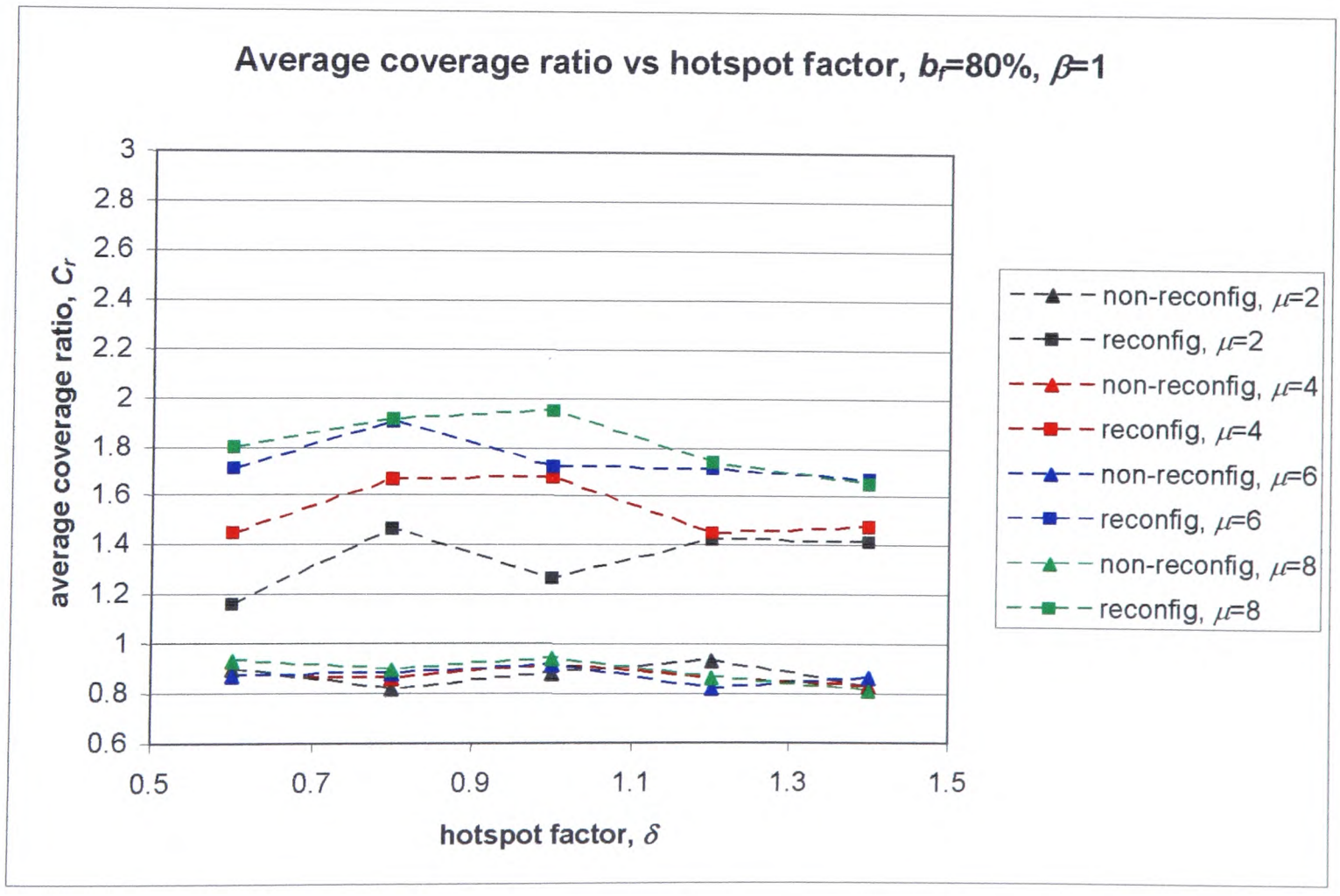

Figure 7.16: Average coverage ratio, C_r, vs hotspot factor, δ, for b_f=80%, β=1

For the higher blocking factors (b_f = 60% and b_f = 80% in Figures 7.15 and 7.16 respectively), reconfiguring networks result in higher C_r. This suggests that for higher blocking factors, there is an advantage in network reconfiguration. The simulations also suggest that the coverage offered by the non-reconfiguring RF/FSO WSN over its lifetime is not as good as that of the non-reconfiguring RF-only WSN over its lifetime for high blocking factors (b_f=40%, 60% and 80% in Figures 7.14, 7.15 and 7.16 respectively). The reconfiguring RF/FSO WSN however has a higher average coverage area than the reconfiguring RF-only WSN for the range of δ considered. The effect the blocking factor, b_f, has on the average coverage ratio, C_r, is discussed in Section 7.5.2, where the blocking factor is studied in more detail. The average coverage areas of the RF/FSO WSNs are shown in Figures 7.17 - 7.21.

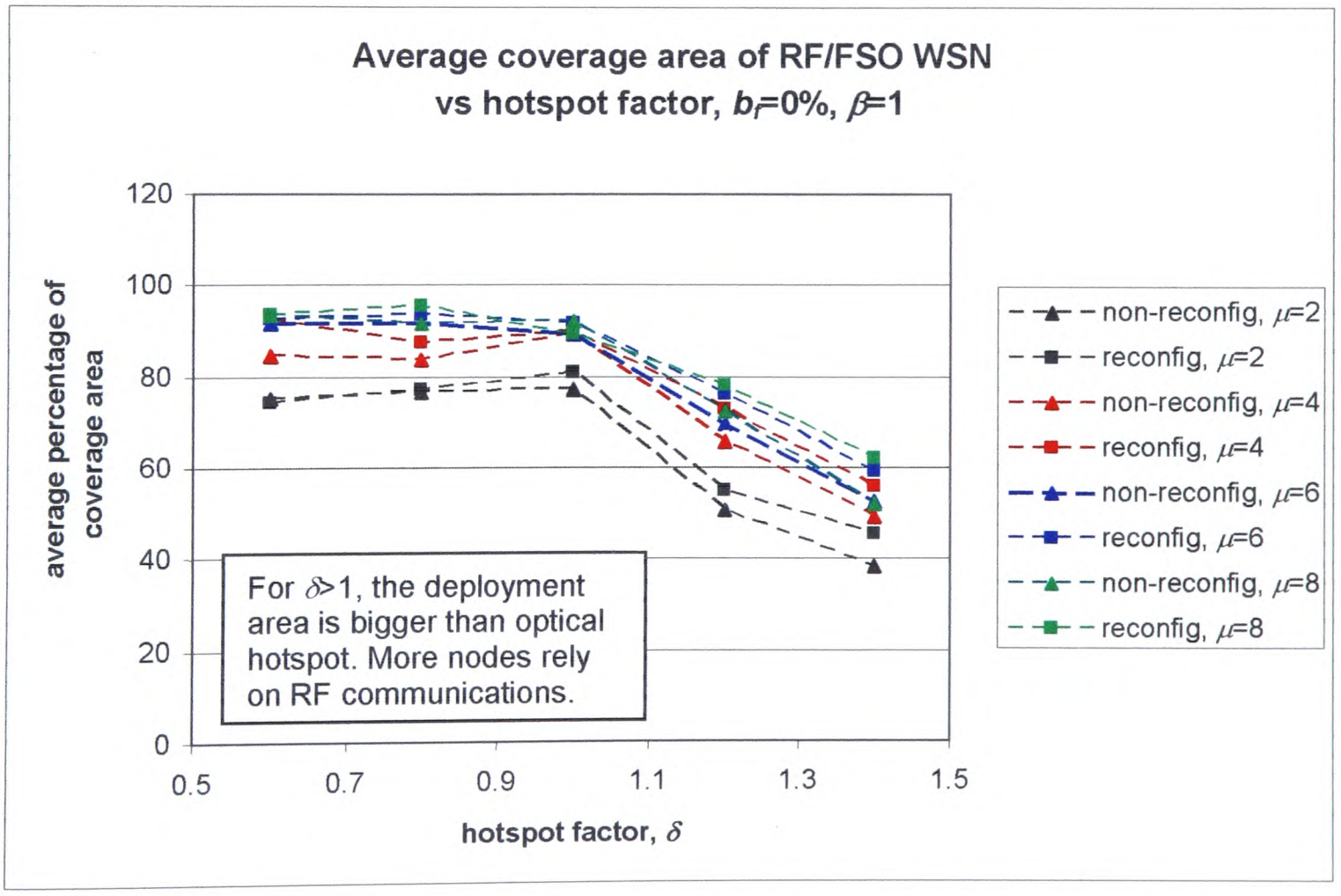

Figure 7.17: Average RF/FSO WSN coverage area vs hotspot factor, δ, for blocking factor b_f=0%, range ratio β=1

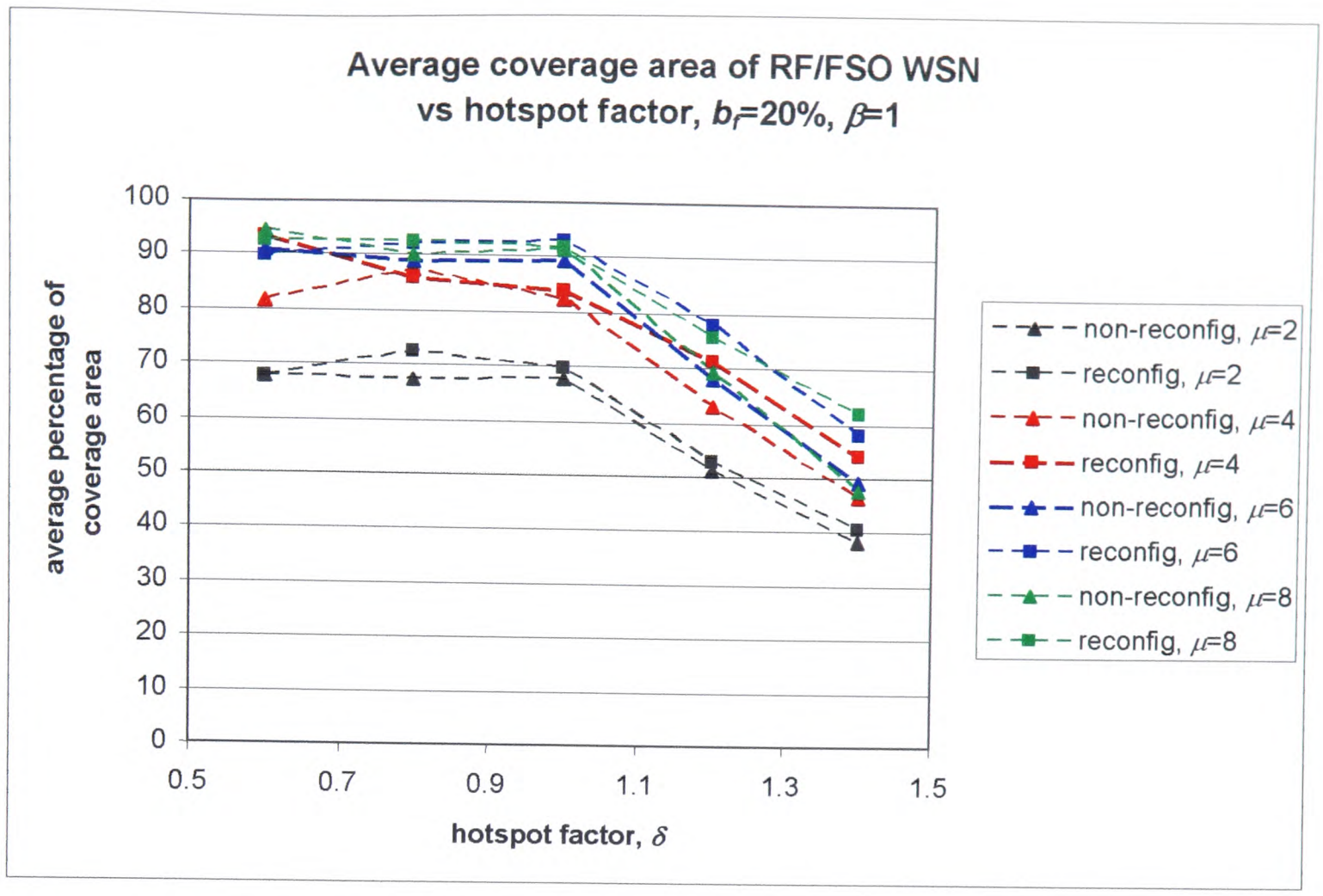

Figure 7.18: Average RF/FSO WSN coverage area vs hotspot factor, δ, for b_f=20%, β=1

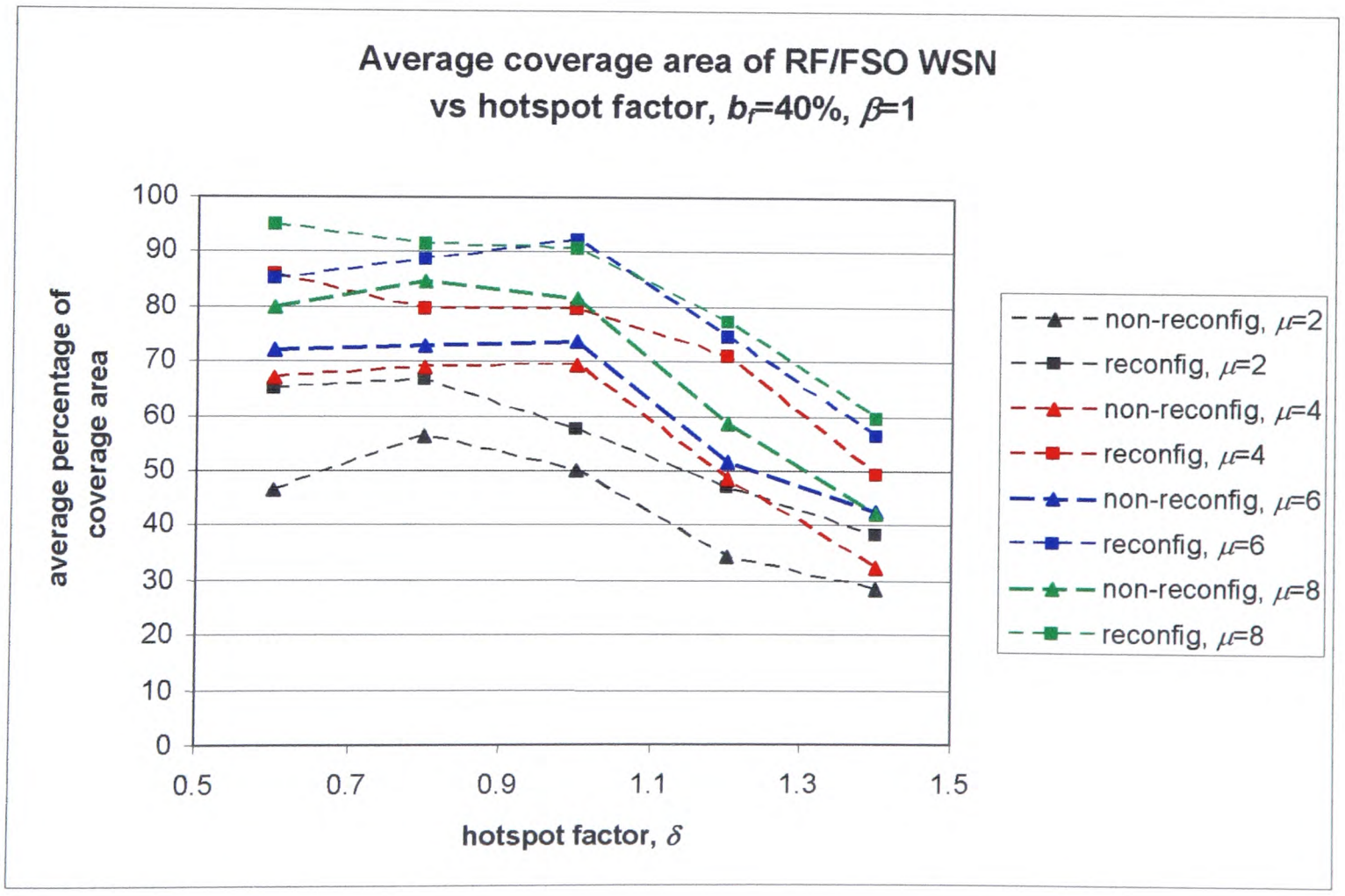

Figure 7.19: Average RF/FSO WSN coverage area vs hotspot factor, δ, for b_f=40%, β=1

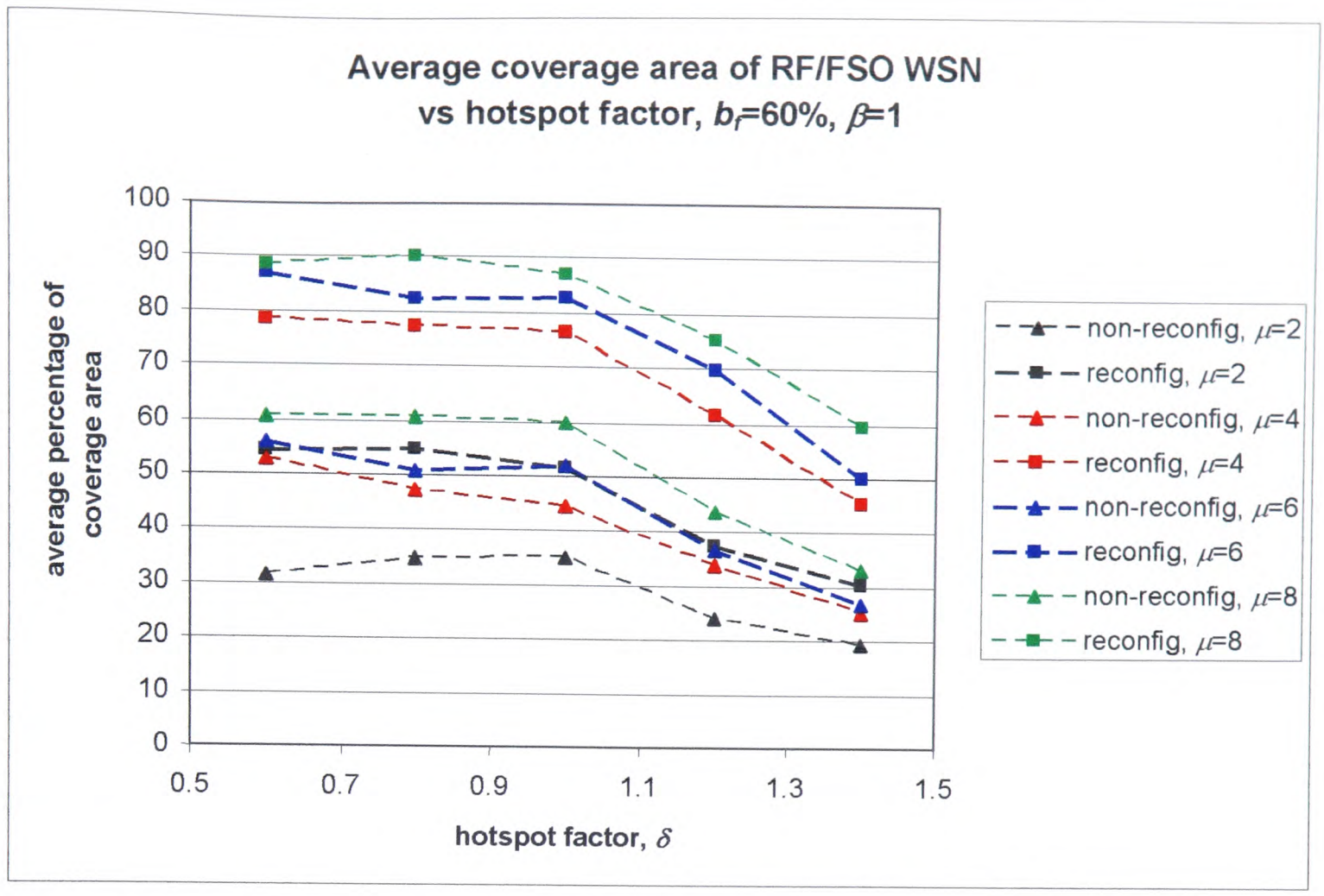

Figure 7.20: Average RF/FSO WSN coverage area vs hotspot factor, δ, for b_f=60%, β=1

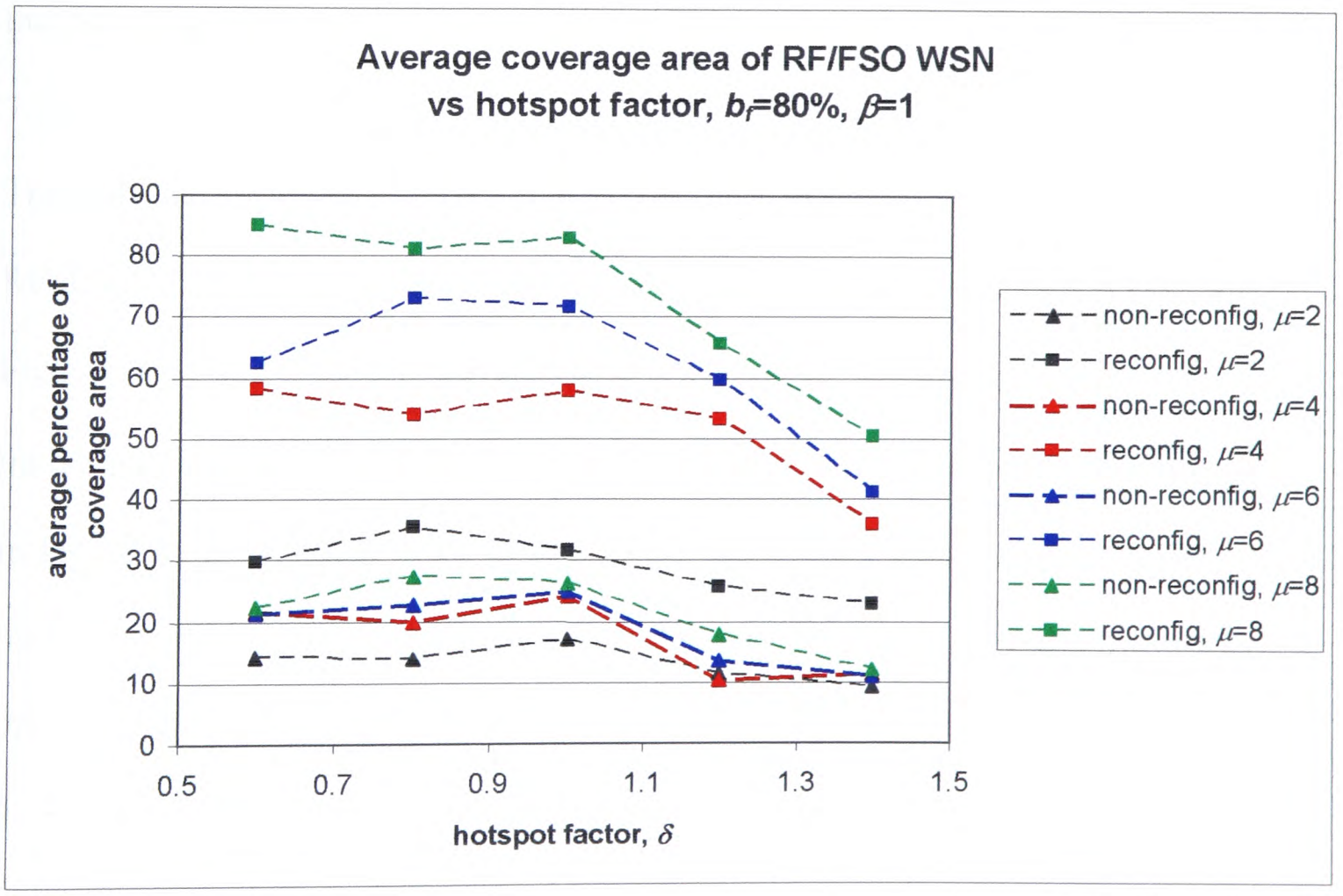

Figure 7.21: Average RF/FSO WSN coverage area vs hotspot factor, δ, for b_f=80%, β=1

As the blocking factor increases, the proportion of nodes required to serve as cluster heads increases, causing nodes to die more quickly. This, therefore, results in the decrease of the average coverage area per node as the blocking factor increases, which causes the increasing spread in the plots in Figures 7.17-7.21.

In Figures 7.17-7.21, the average coverage area falls off sharply after $\delta = 1$ for a wide range of node densities and blocking factors. This is because for $\delta > 1$, the RF/FSO WSN deployment area no longer falls within the optical hotspot of the base station. Outside the optical hotspot, more nodes rely on radio multihops to communicate with the base station, and this increases the energy required of individual nodes and cluster heads. This is illustrated in Figures 7.22-7.27. Figures 7.22-7.27 show the increase in RF multihop links required by the RF/FSO WSN as the deployment area becomes larger than the optical hotspot (δ>1). Figures 7.22 and 7.23 show aerial views of the RF/FSO WSN with $b_f = 0\%$ and 40% respectively. There are no RF links in the WSN in Figure 7.22, but some nodes require multihop RF links in Figure 7.23 WSN due to the blocking factor. Both the RF/FSO WSNs in Figures 7.22 and 7.23 are within the optical hotspot of the base station (δ=0.5), unlike the networks in Figures 7.24 and 7.25 (δ=1.5). Although b_f=0% for the WSN in Figure 7.24, the nodes in the fringes of the deployment area need to rely on radio multihops as they are too distant from the base station to communicate with it optically. The WSN in Figure 7.25 has more RF links than that in Figure 7.24, as b_f=40%.

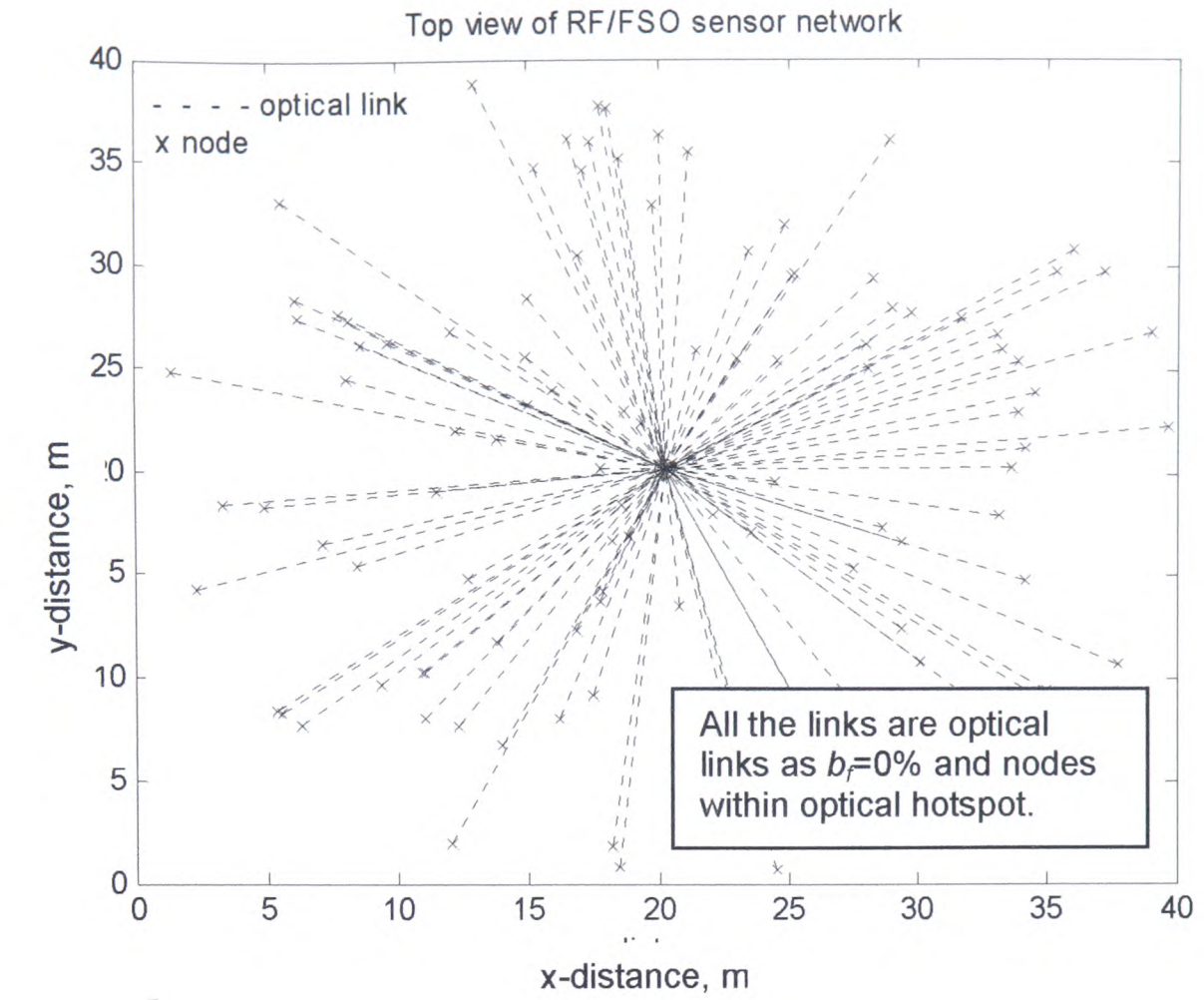

Figure 7.22: RF/FSO WSN top view, range ratio β=1, node density μ=8, hotspot factor δ=0.5, blocking factor b_f=0%

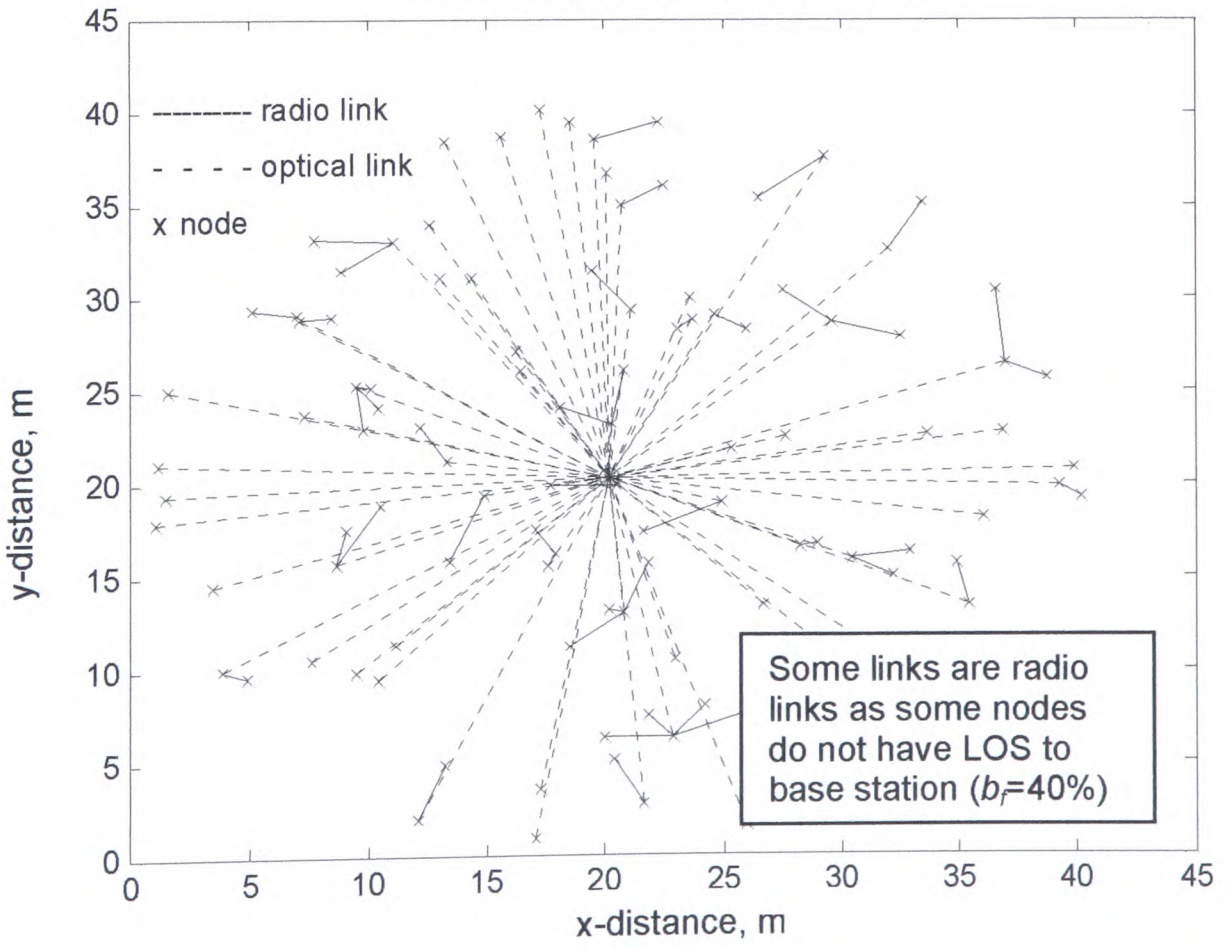

Figure 7.23: RF/FSO WSN top view, β=1, μ=8, δ=0.5, b_f=40%

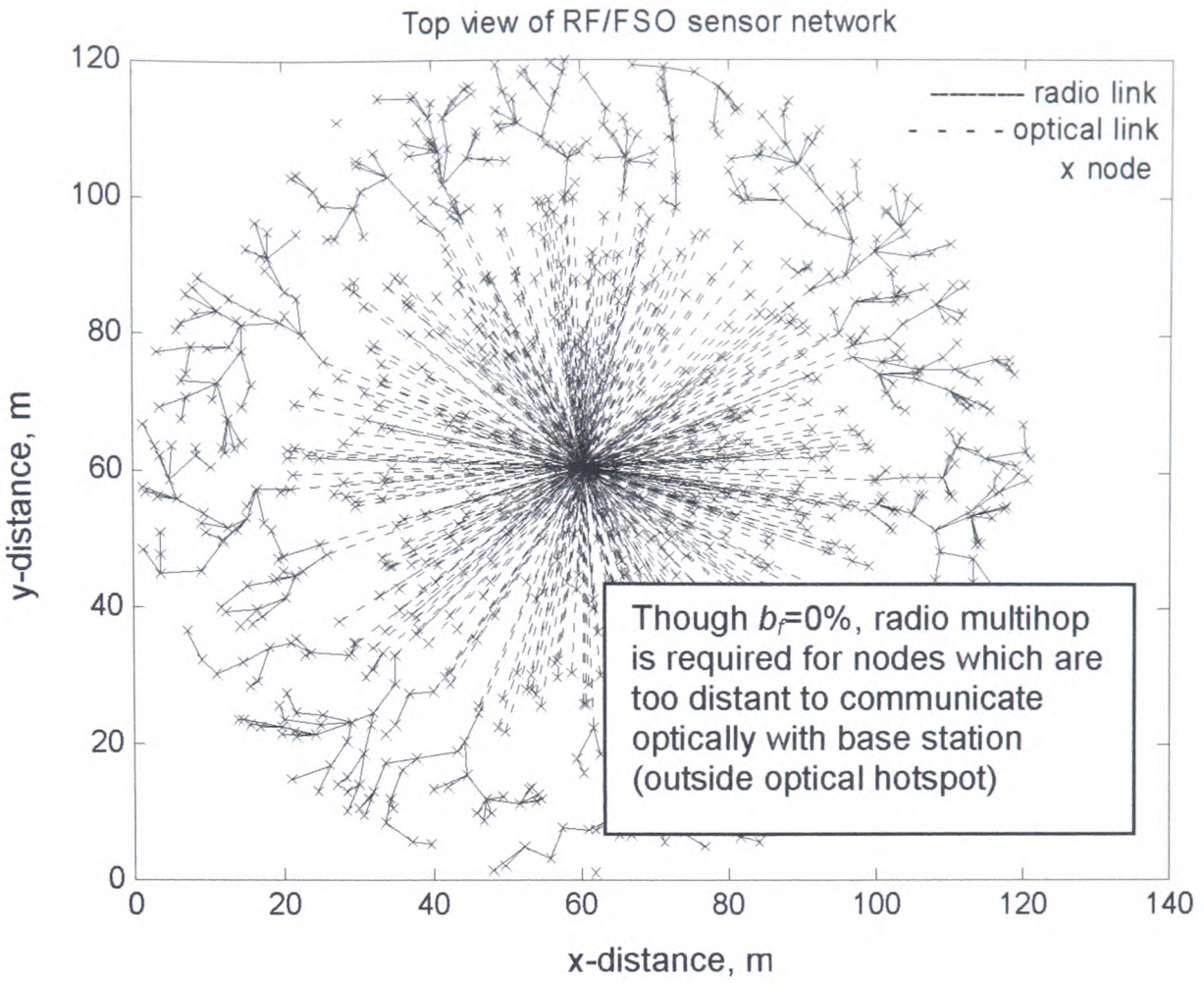

Figure 7.24: RF/FSO WSN top view, β=1, μ=8, δ=1.5, b_f=0%

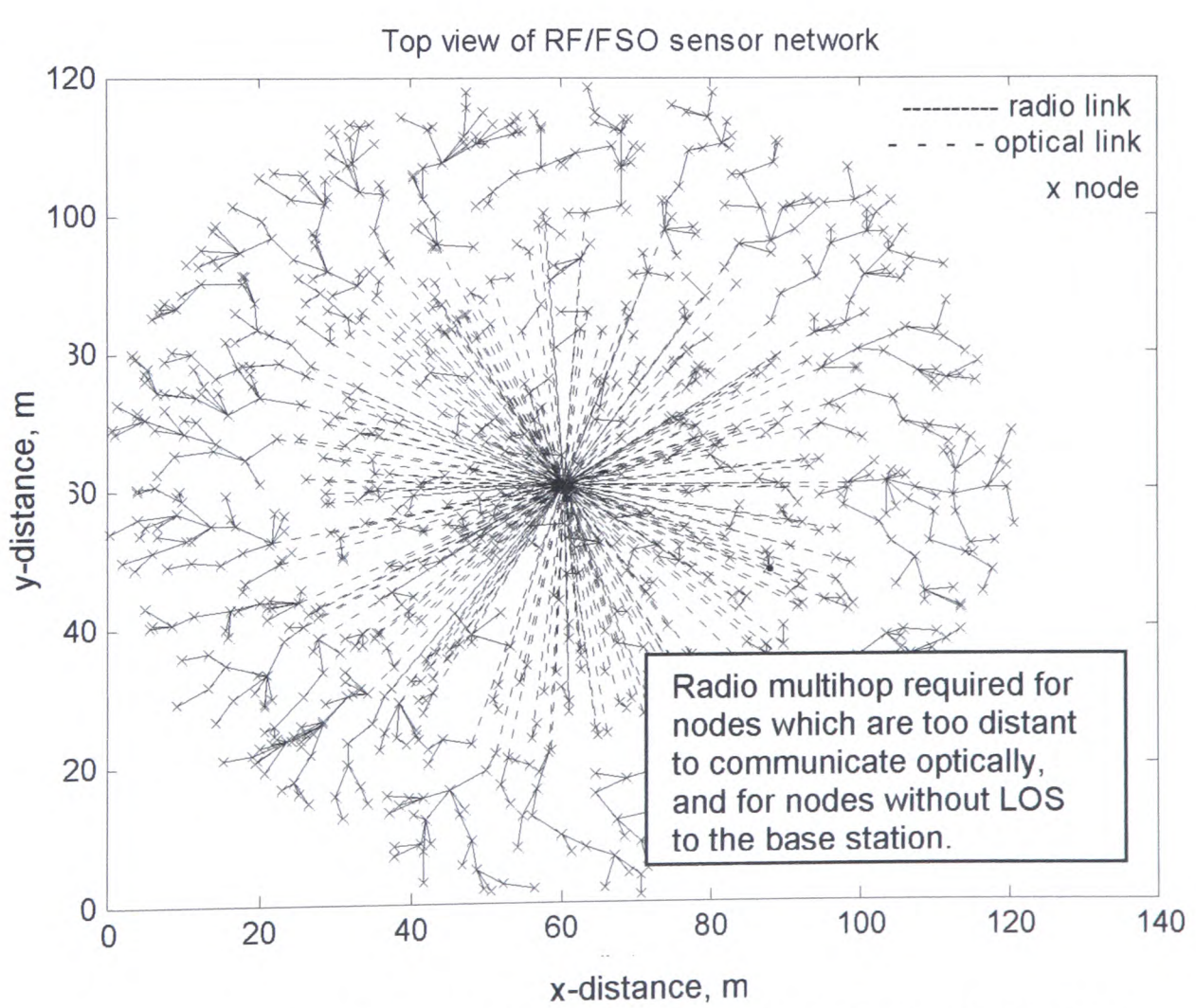

Figure 7.25: RF/FSO WSN top view, β=1, μ=8, δ=1.5, b_f=40%

Figure 7.26 shows an RF/FSO WSN which has its deployment area within the optical hotspot. The deployment area of the network in Figure 7.27 is larger than the optical hotspot. RF multihop communications requires more energy than FSO communications. This causes nodes to die more quickly for WSN deployment areas that lie outside the optical hotspot, which results in the loss of coverage area for $\delta>1$ shown in Figures 7.17-7.21. It is, therefore, best if the deployment area of the RF/FSO WSN is kept within the optical hotspot. For the remaining simulations, only $\delta \leq 1$ is considered. Figures 7.17-7.21 also show that network reconfiguration results in a higher average coverage area for the RF/FSO WSN, compared to the non-reconfiguring case.

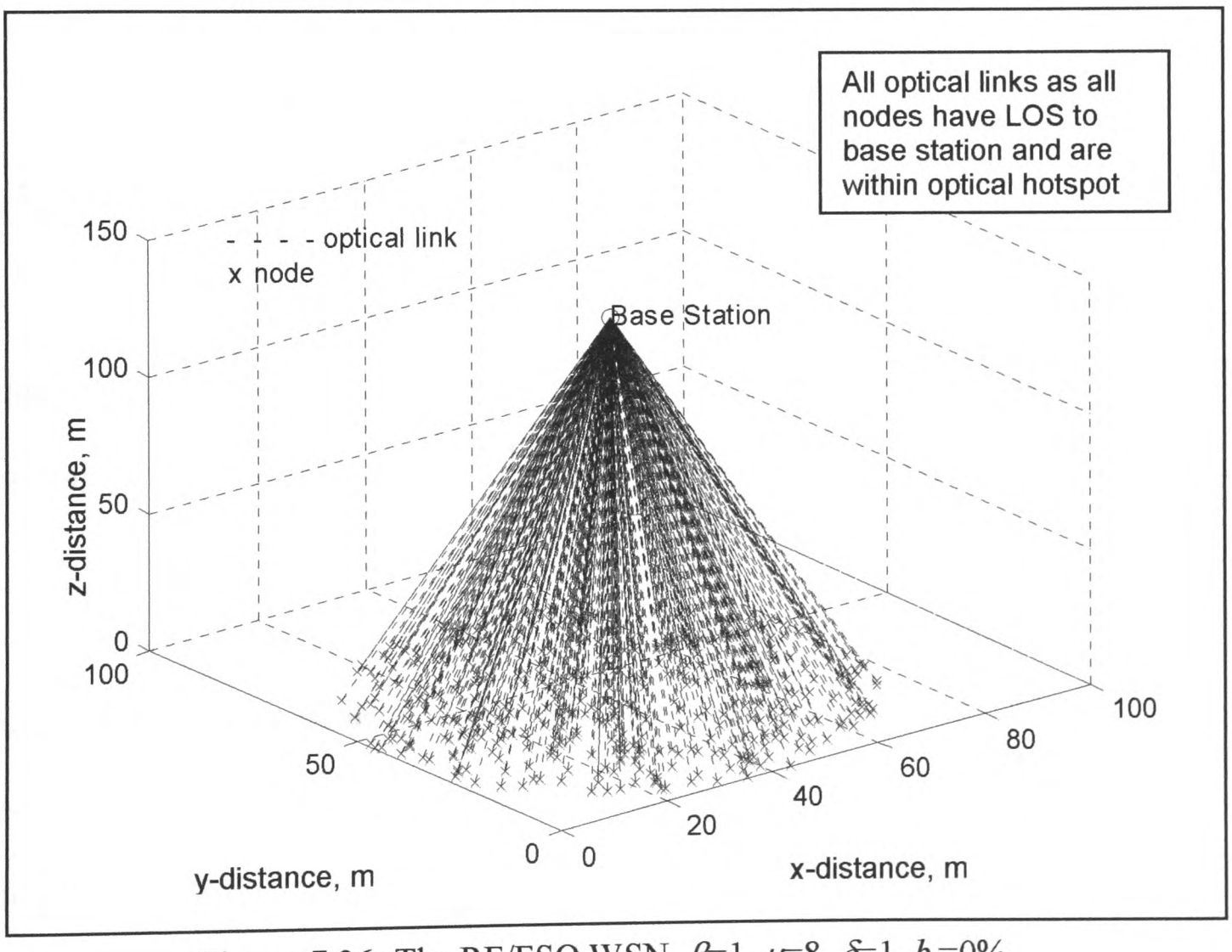

Figure 7.26: The RF/FSO WSN, β=1, μ=8, δ=1, b_f=0%

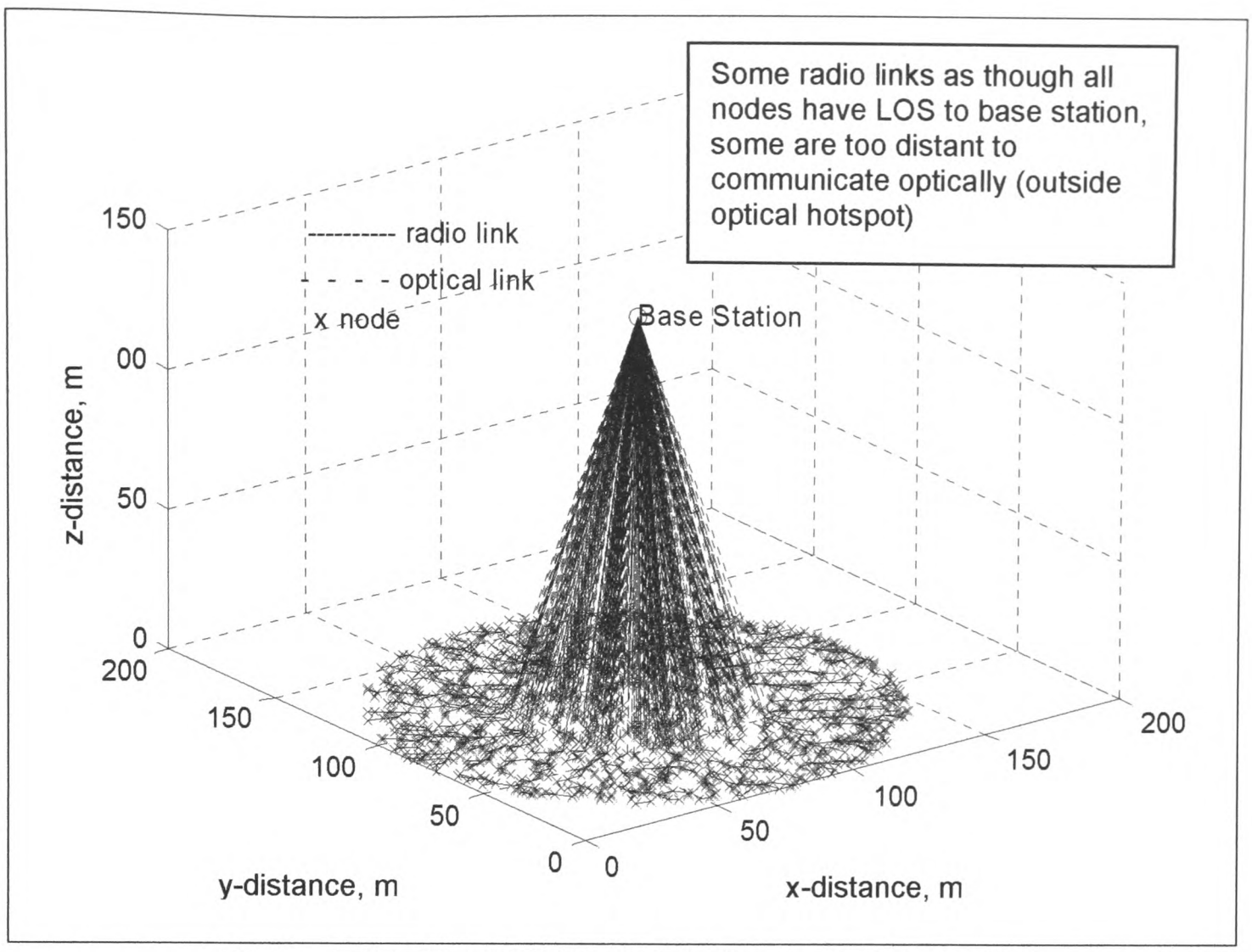

Figure 7.27: The RF/FSO WSN, β=1, μ=8, δ=2, b_f=0%

7.5.2. Blocking factor, b_f, results and discussion

The blocking factor, b_f, was discussed in Chapter 4. In this section, the lifetime ratio L_r, average coverage ratio C_r and the average RF/FSO WSN network coverage are studied for a selection of blocking factors in the range of $0\% \leq b_f \leq 80\%$.

Figures 7.28 -7.31 show the lifetime ratio plots for the range of blocking factors and node densities considered. The simulations show that for non-reconfiguring networks, the RF/FSO WSN lasts between 2 and 2.5 as long as the RF-only WSN. This is due to the relative energies expended by the last non-cluster head nodes in both networks, as was discussed in Section 7.5.1 (see Table 7.4).

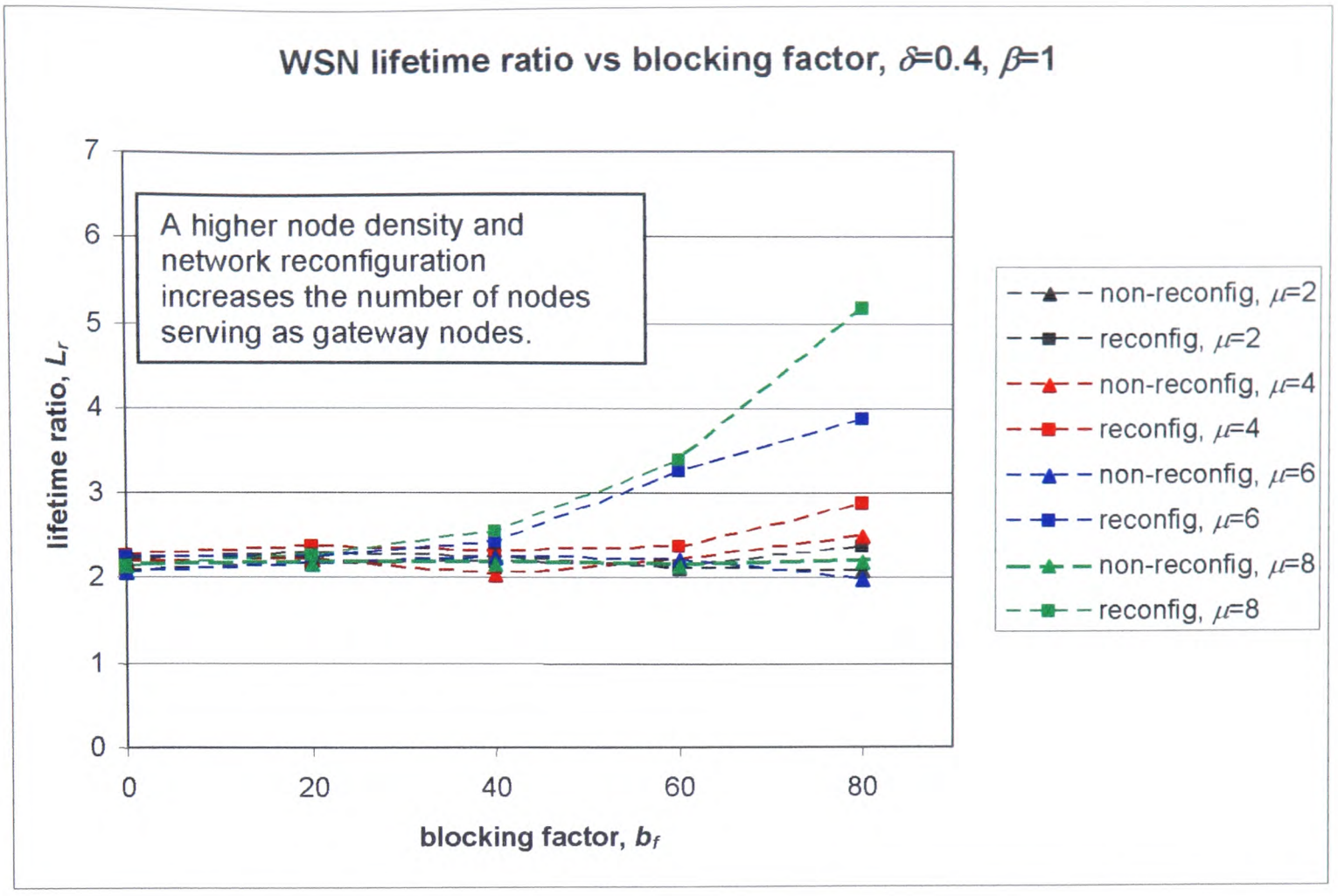

Figure 7.28: WSN lifetime ratio, L_r, vs blocking factor b_f, for hotspot factor δ=0.4, range ratio β=1

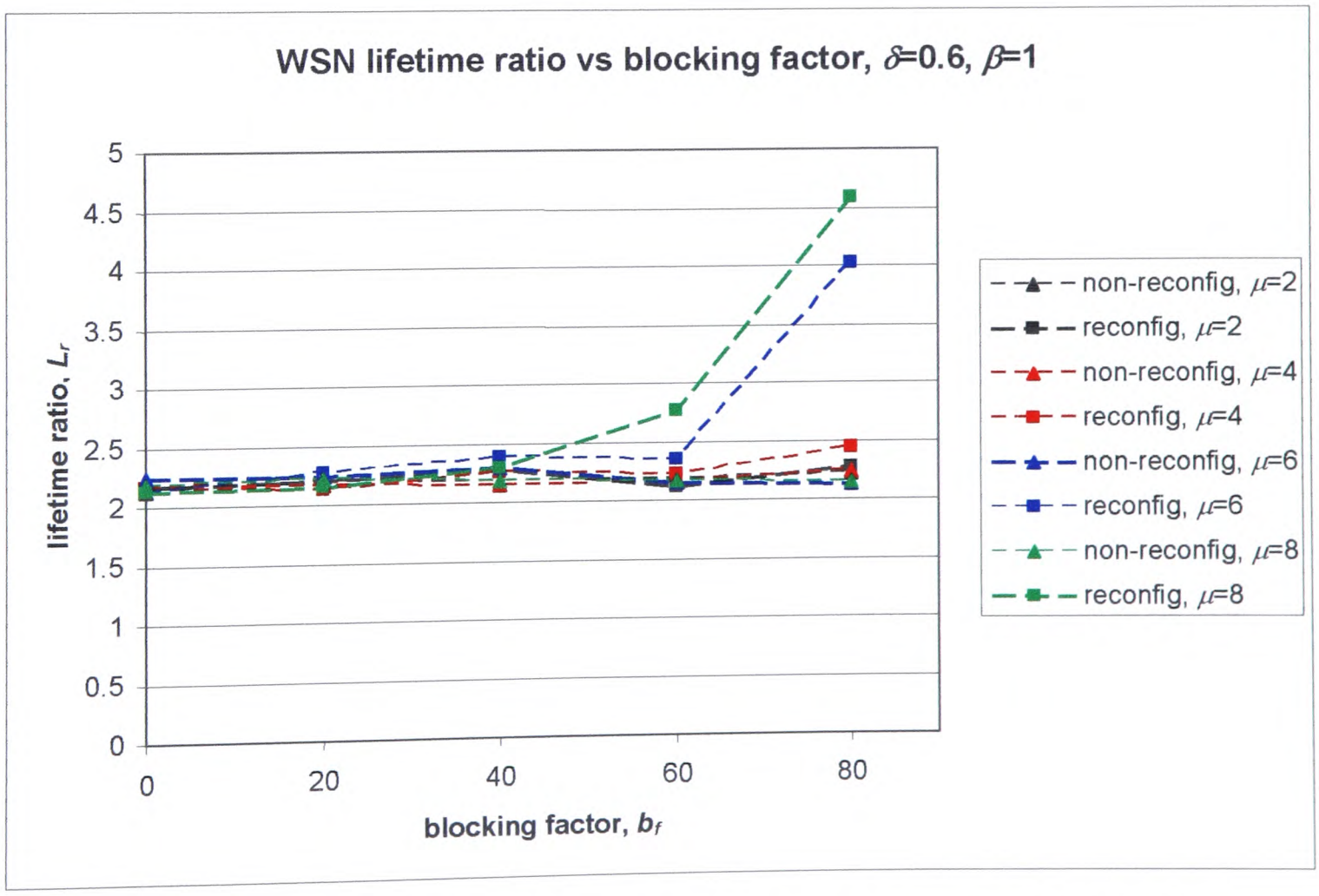

Figure 7.29: WSN lifetime ratio, L_r, vs blocking factor, b_f, for δ=0.6, β=1

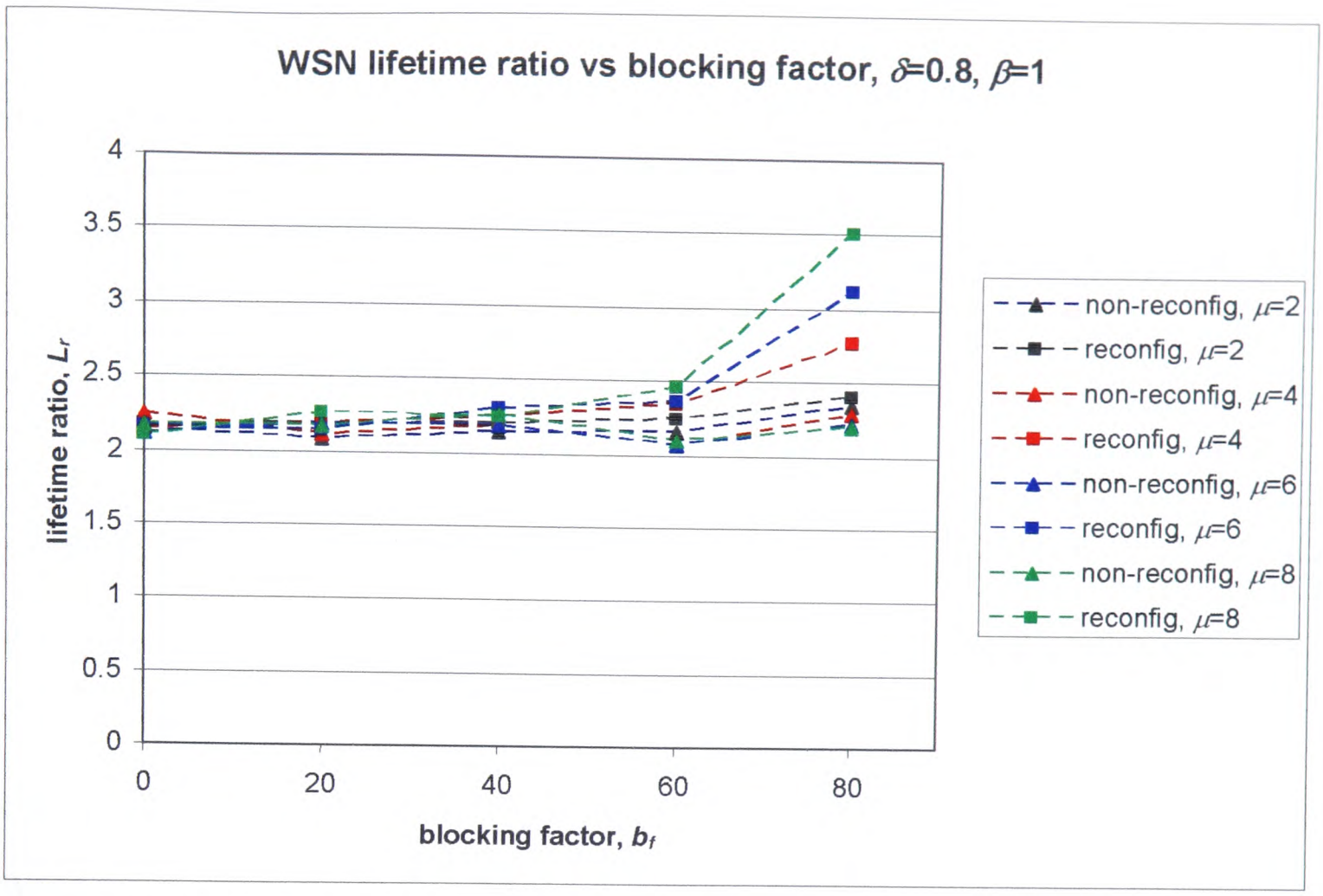

Figure 7.30: WSN lifetime ratio, L_r, vs blocking factor, b_f, for δ=0.8, β=1

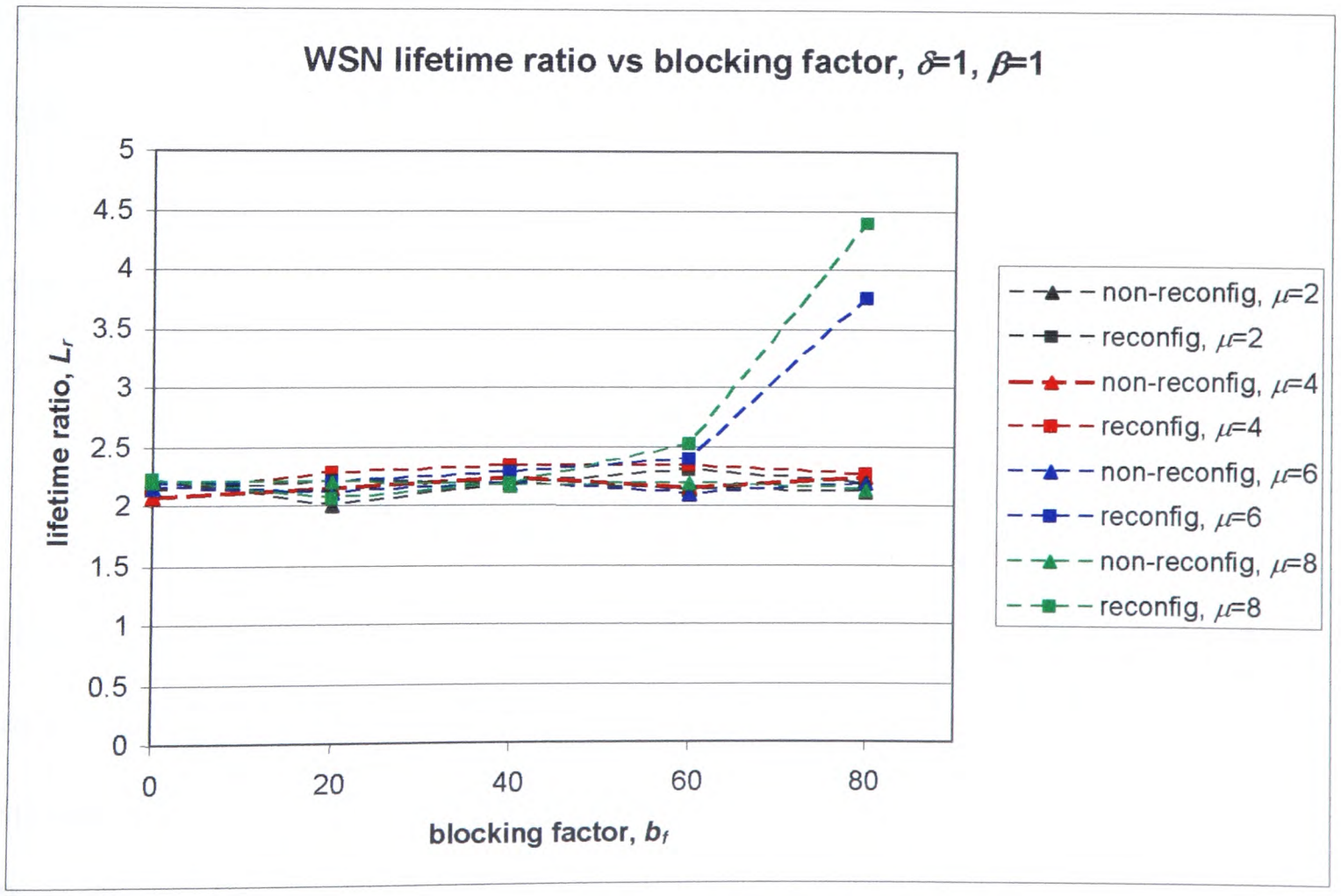

Figure 7.31: WSN lifetime ratio, L_r, vs blocking factor, b_f, for δ=1, β=1

However, for reconfiguring networks, the simulations results in Figures 7.28-7.31 show that the lifetime ratio, L_r, increases as the blocking factor and node densities increase. In a reconfiguring network, if the blocking factor is low (0%, 20% and 40%), a non-cluster head at the beginning of the network's lifetime may never be required to serve as a cluster head. In this case, the range of L_r will be $2 \leq L_r \leq 2.5$, as shown in Figures 7.28-7.31. However, for a high blocking factor, it is very likely that almost all nodes serve as cluster heads at some point in the lifetime of the reconfiguring network. In this case, the network's lifetime depends on the last gateway cluster head node still alive (as the nodes depending on it become isolated when it dies). The gateway nodes in the RF-only WSN expend more energy for communications to the base station, than those in the RF/FSO WSN. For the RF-only WSN, energy is expended by the gateway nodes for RF transmission, $E_{b,ta}$ and to drive the radio transmitter electronics, $E_{b,te}$ (see Figure 5.8 in Chapter 5). $E_{b,ta}$ is capped at 1nJ/bit, $E_{b,te}$=50nJ/bit (refer to Table 5.1). This is much higher than the energy required by RF/FSO gateway nodes to drive their passive optical transmitters, $E_{b,opt}$ (see Figure 5.7 in Chapter 5). $E_{b,opt}$=19pJ/bit (refer to Table 5.1). This causes the RF-only gateway nodes to die faster, resulting in $L_r \geq 2.5$ as shown in Figures 7.28 and 7.31.

When the blocking factor is very high (b_f=80%) in Figures 7.28-7.31, L_r remains within the range of $2 \leq L_r < 2.5$ at low node densities (μ=2, μ=4) for the reconfiguring networks. This is because in these cases, nodes are deployed so sparsely that at least one node will not have to serve as a cluster head as it is too far from other isolated nodes. So, the energy it expends can be summarised in Table 7.4.

The higher the node density, the larger the number of nodes attached to the last gateway node in the reconfiguring network. Thus, the speed at which the last node dies in the RF-only reconfiguring WSN (compared with the RF/FSO reconfiguring WSN) increases more rapidly with increasing node density. (The RF-only gateway node dies faster than its RF/FSO counterpart due to the higher energy it expends, as discussed earlier.) This causes L_r to be higher for μ=8 than μ=6 for the reconfiguring networks when b_f=80% in Figures 7.28-7.31.

Figures 7.32 – 7.35 show the average coverage ratios for the range of blocking factors and node densities considered. For non-reconfiguring networks, the average coverage ratio falls slightly, and is within the range of $0.8 \leq C_r \leq 1$ when the blocking factor is high (60%-80%). For high blocking factors, a large number of nodes in the RF/FSO WSN rely on multihop RF communications, which consumes more energy than FSO communications. The nodes expire more quickly and nodes depending on cluster heads become isolated when the cluster head dies (as the network is non-reconfiguring). For the reconfiguring networks though, the RF/FSO WSN network is able to match the coverage of the RF-only WSN. For high node densities or large blocking factors, the reconfiguring RF/FSO WSN is able to offer much better network coverage than the RF-only WSN. This is due to the comparatively lower energy expended by the RF/FSO WSN gateway nodes, when compared to the RF-only gateway nodes as was discussed earlier in this section.

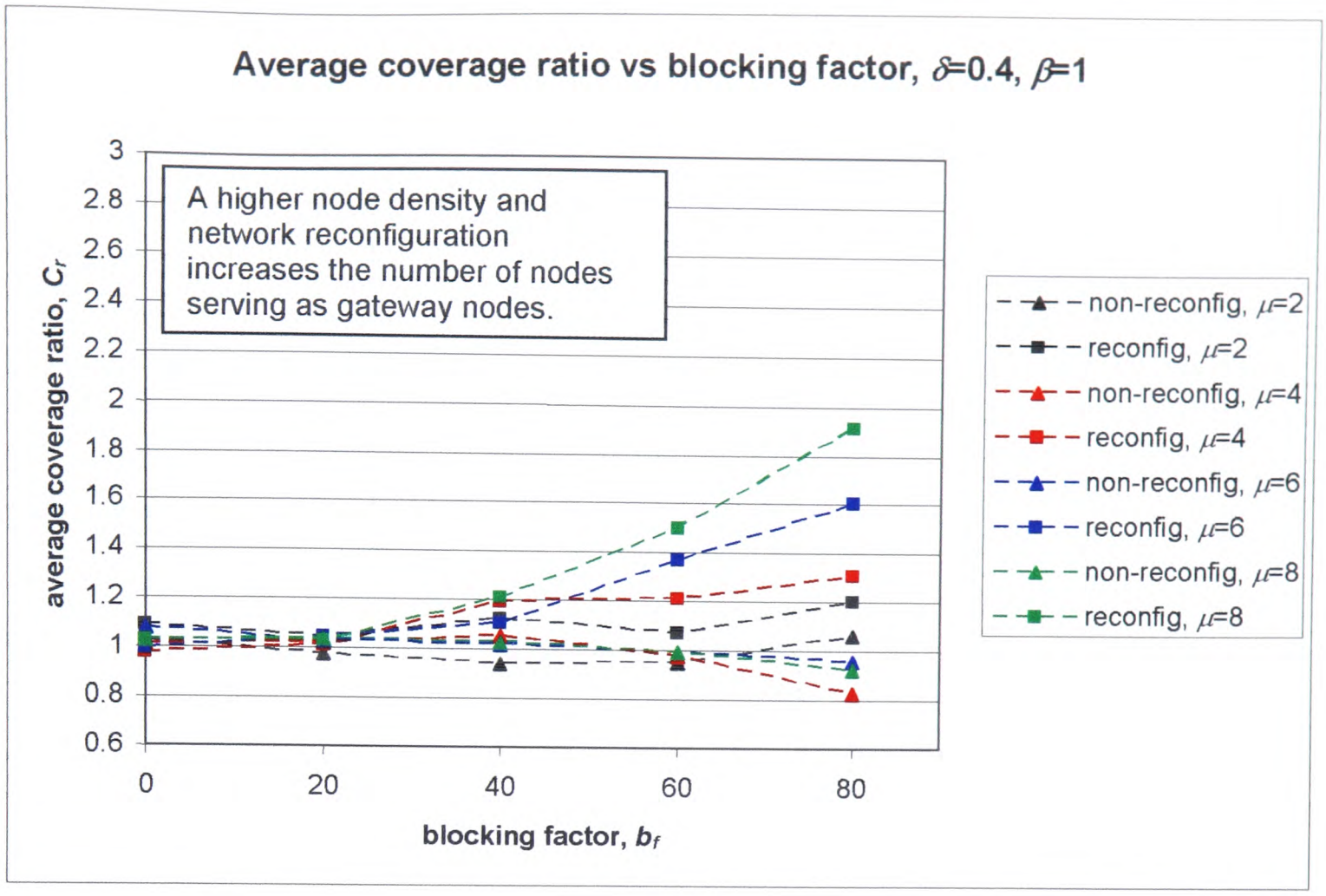

Figure 7.32: Average coverage ratio, C_r, vs blocking factor b_f, for hotspot factor δ=0.4, range ratio β=1

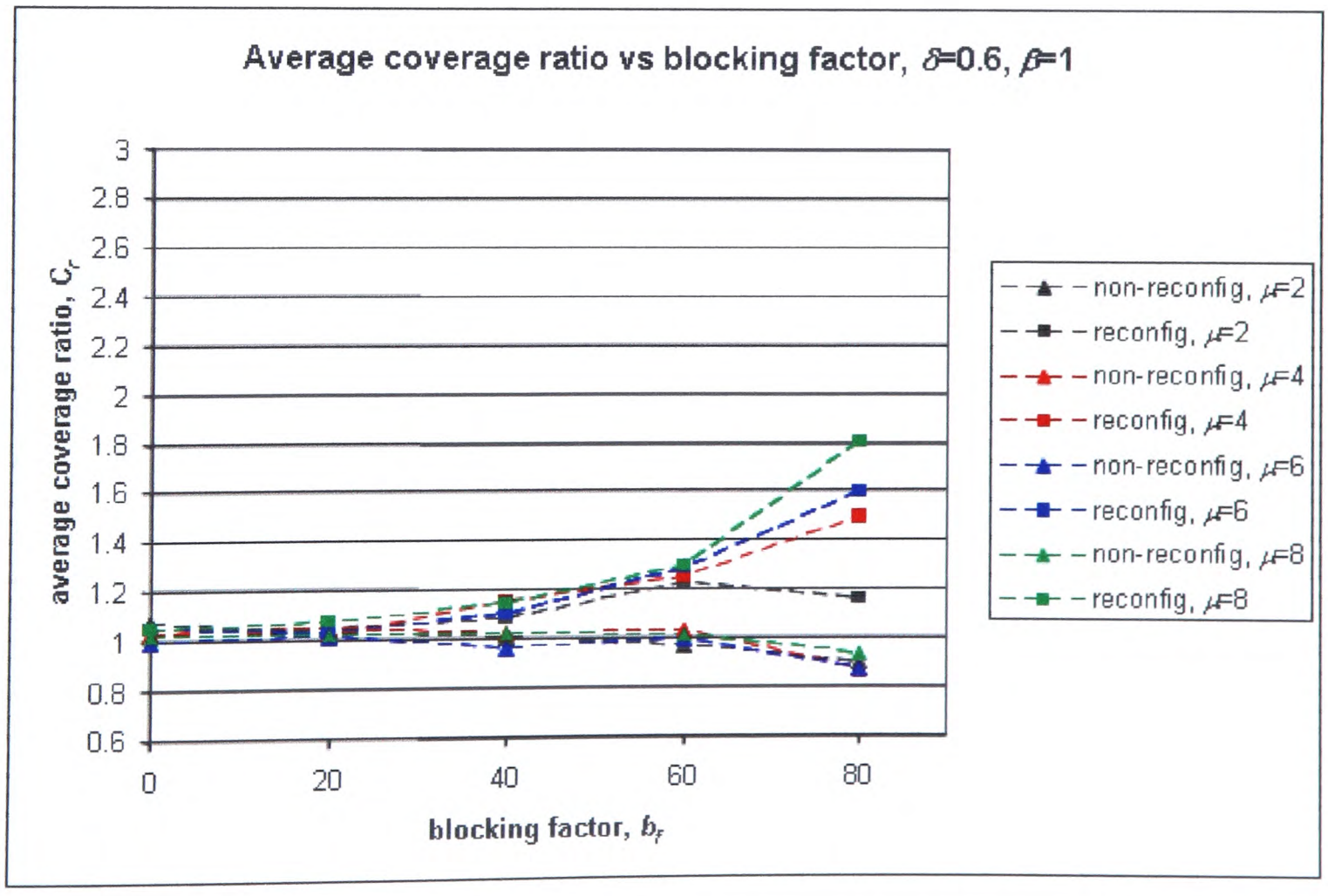

Figure 7.33: Average coverage ratio, C_r, vs blocking factor, b_f, for δ=0.6, β=1

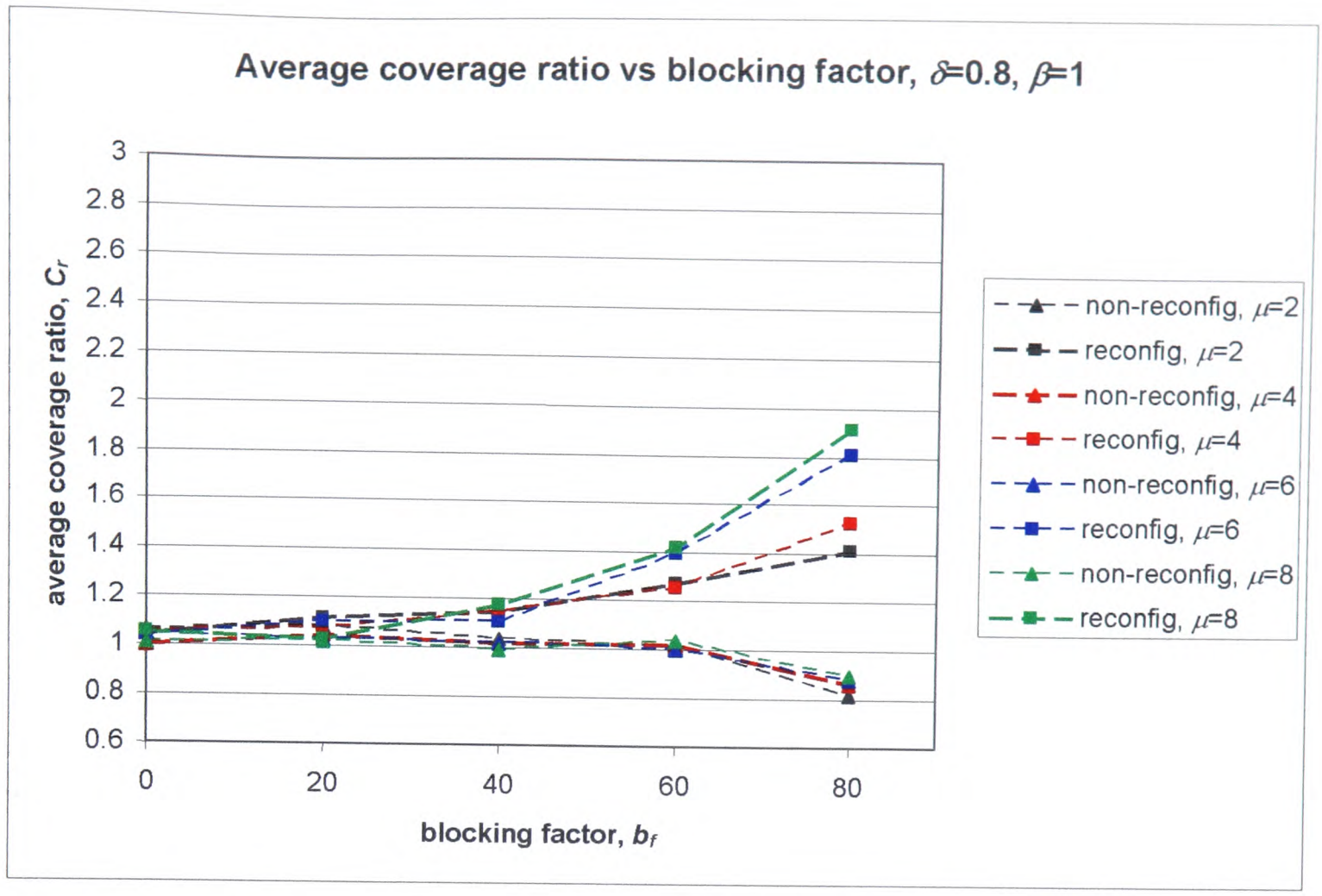

Figure 7.34: Average coverage ratio, C_r, vs blocking factor, b_f, for δ=0.8, β=1

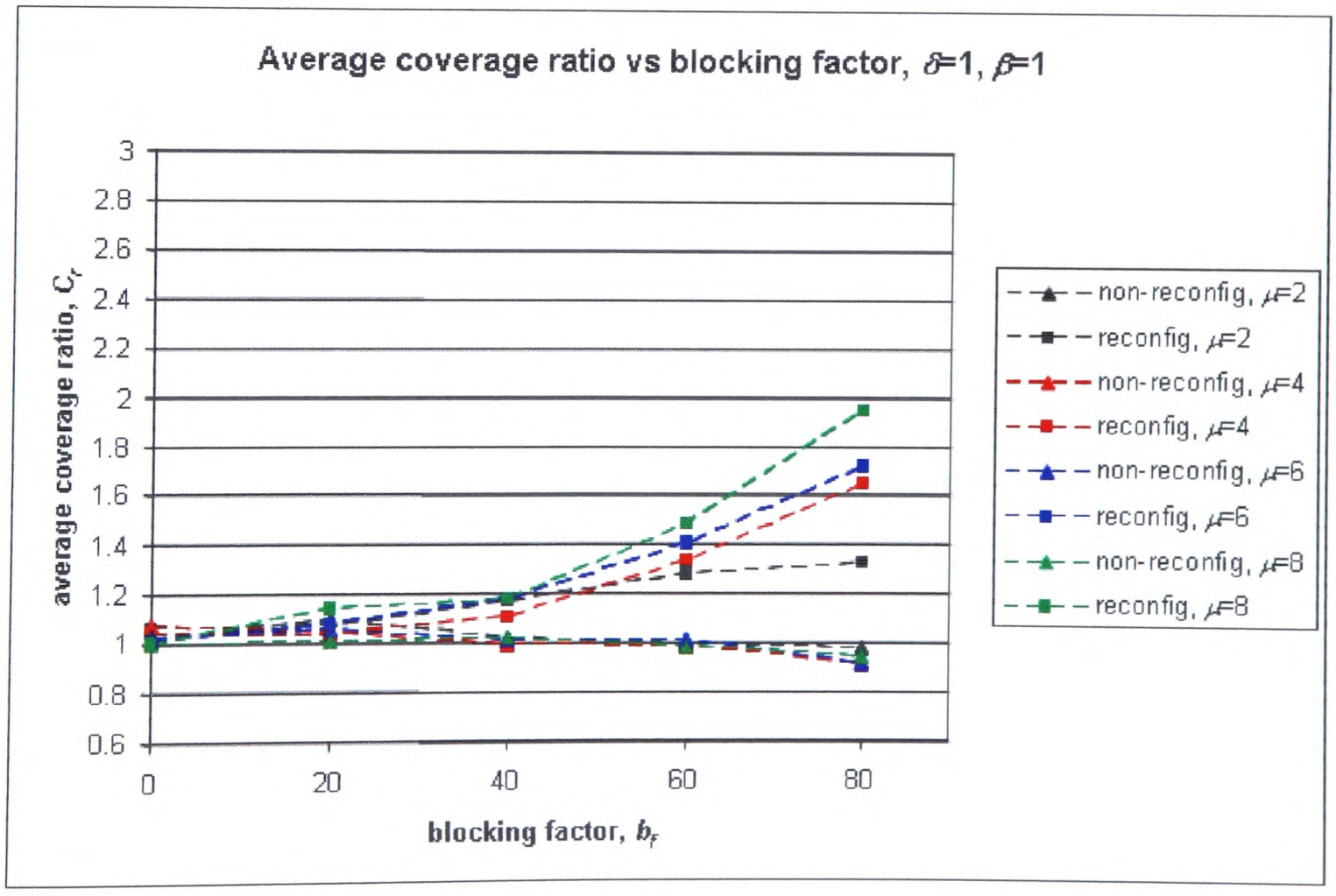

Figure 7.35: Average coverage ratio, C_r, vs blocking factor, b_f, for δ=1, β=1

Figures 7.36-7.39 show the average coverage area for the RF/FSO WSN for the range of blocking factors and node densities considered. The average coverage area is best when the blocking factor is low. This is because as the blocking factor increases, more nodes need to radio multihop to reach the base station. This increases the energy required per node, causing more nodes to die quickly which thus reduces the average coverage area. Figures 7.36-7.39 also suggest that network reconfiguration is less beneficial when the blocking factor is low, as fewer nodes require network reconfiguration to remain operational. The networks in Figures 7.36-7.39 are within the optical hotspot, as $\delta \leq 1$. In the optical hotspot, a low blocking factor means most nodes in the RF/FSO WSN are connected directly to the base station and do not require multihop radio communications.

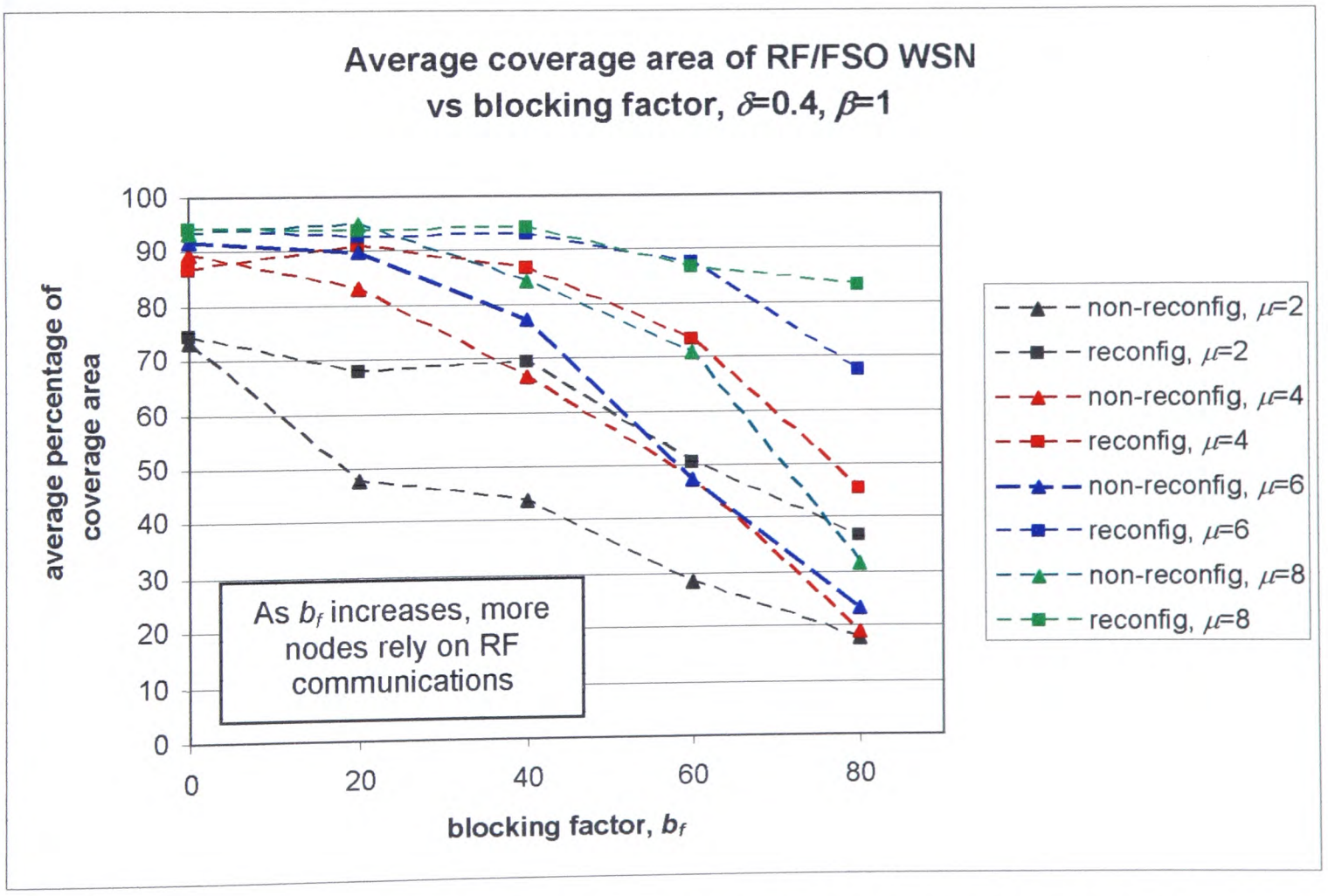

Figure 7.36: Average RF/FSO WSN coverage area vs blocking factor b_f, for hotspot factor δ=0.4, range ratio β=1

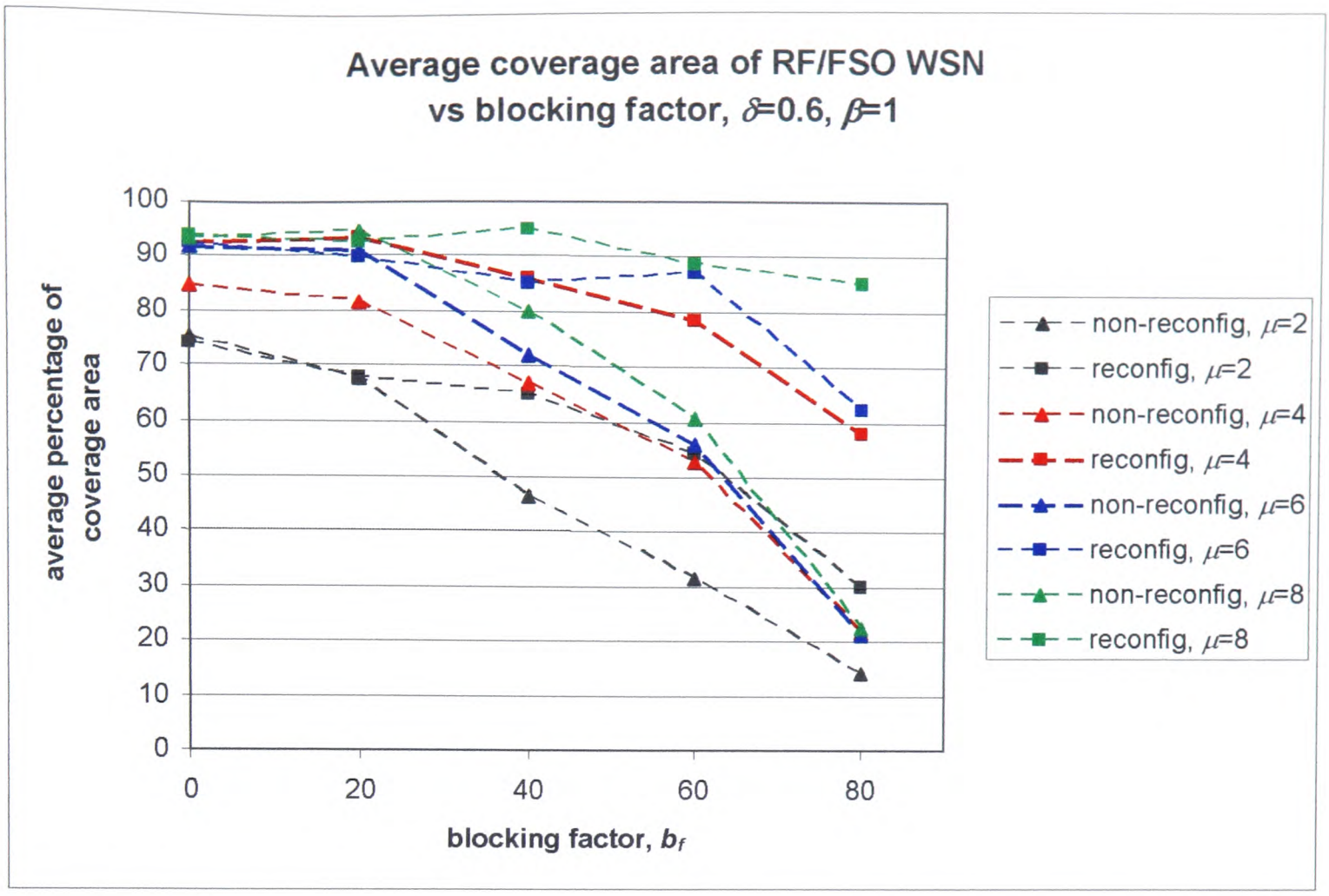

Figure 7.37: Average RF/FSO WSN coverage area vs blocking factor, b_f, for δ=0.6, β=1

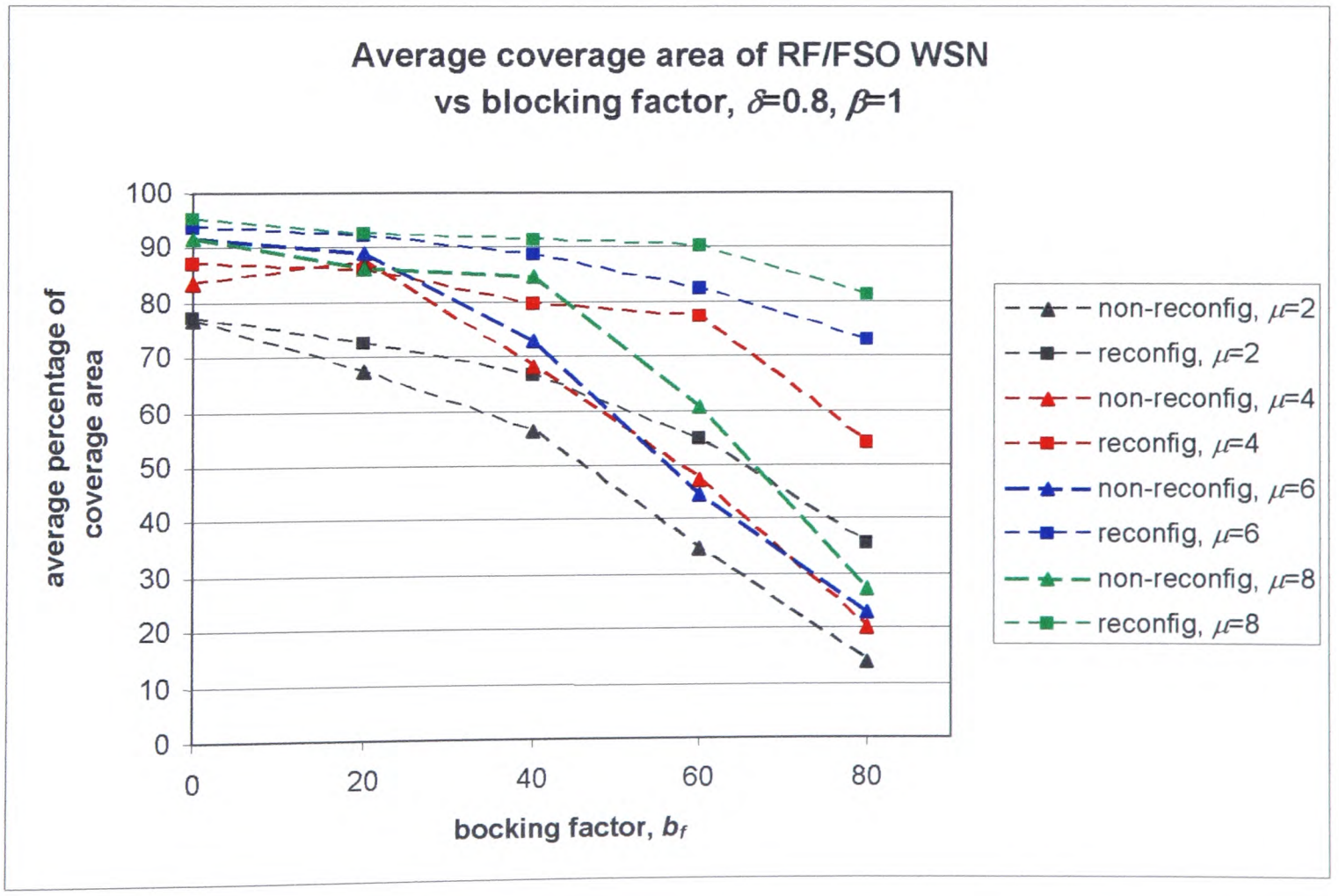

Figure 7.38: Average RF/FSO WSN coverage area vs blocking factor, b_f, for δ=0.8, β=1

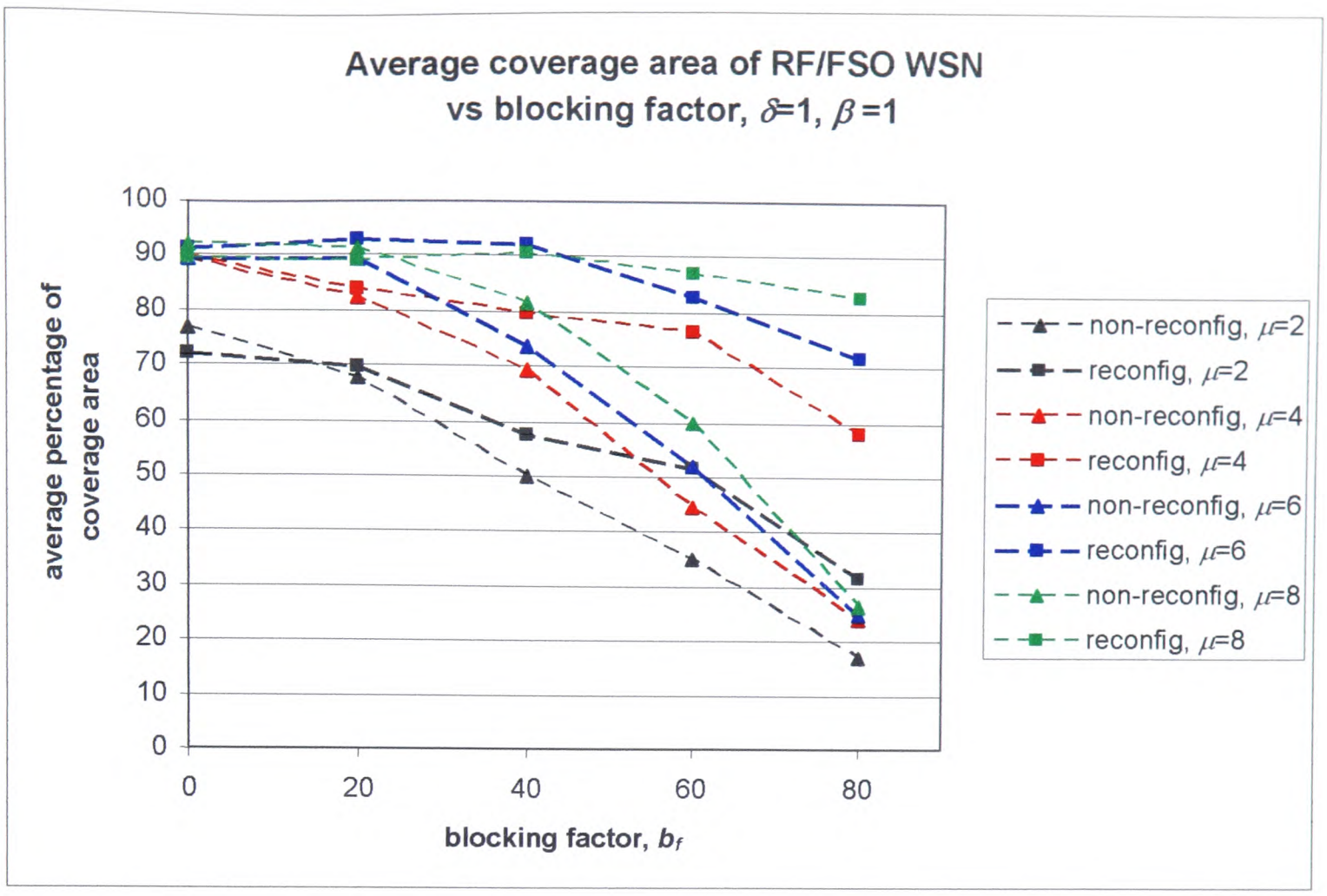

Figure 7.39: Average RF/FSO WSN coverage area vs blocking factor, b_f, for δ=1, β=1

7.5.3. Node density, μ, results and discussion

Node density was discussed in Section 1.4.2. In this section, the lifetime ratio L_r, average coverage ratio C_r and the average RF/FSO WSN network coverage are studied for a selection of node densities in the range of $2 \leq \mu \leq 10$. The plots of the lifetime ratios, L_r, for the range of node densities and hotspot factors considered are shown in Figures 7.40 – 7.44. For non-reconfiguring networks, L_r lies in the range of $2 \leq L_r \leq 2.5$. This was discussed in Section 7.5.1. When the blocking factor is high (60% and 80%), especially for high node densities ($6 \leq \mu < 10$), $L_r \geq 2.5$ as shown in Figures 7.43 and 7.44. This was discussed in Section 7.5.2.

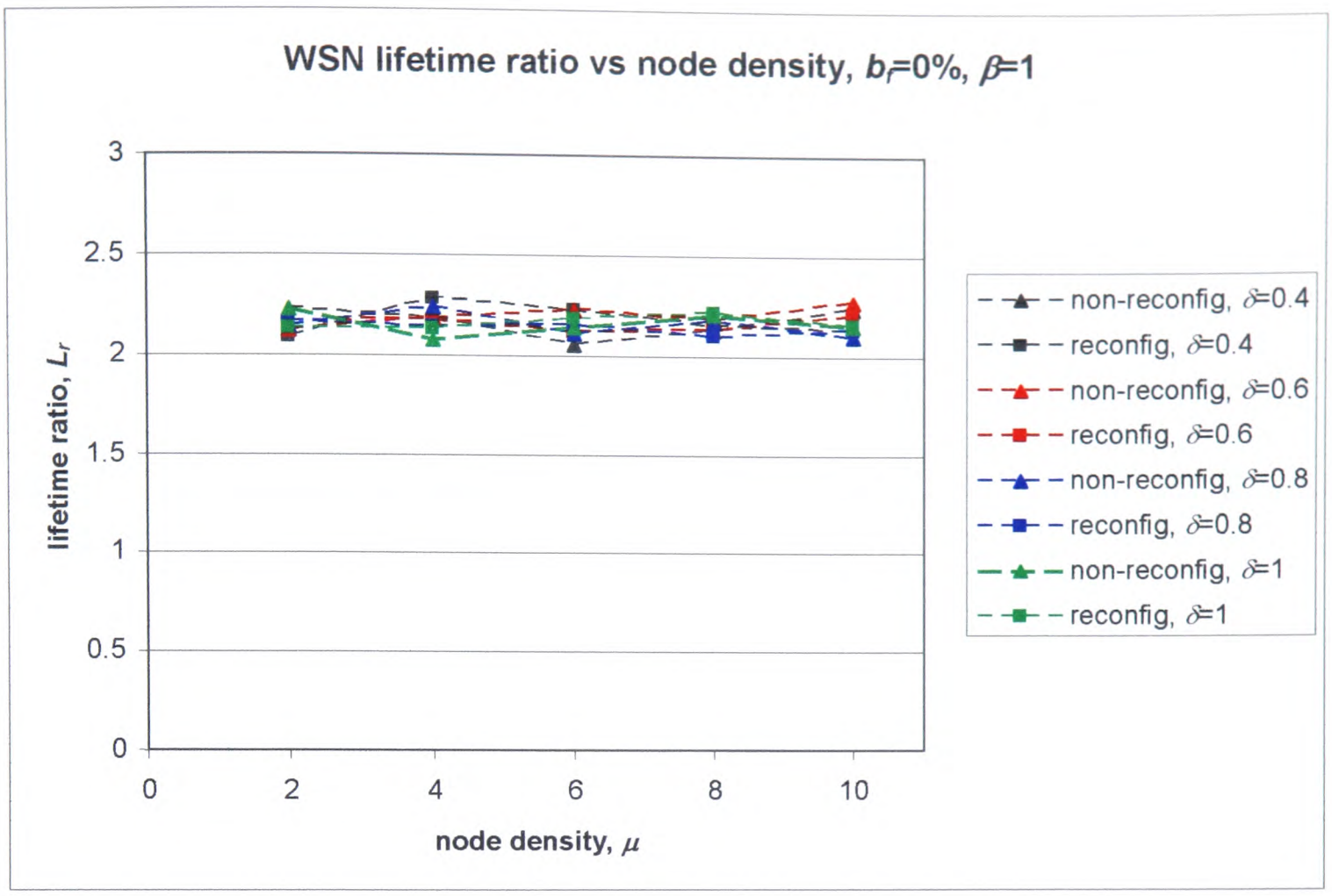

Figure 7.40: WSN lifetime ratio, L_r, vs node density μ, for blocking factor b_f=0%, range ratio β=1

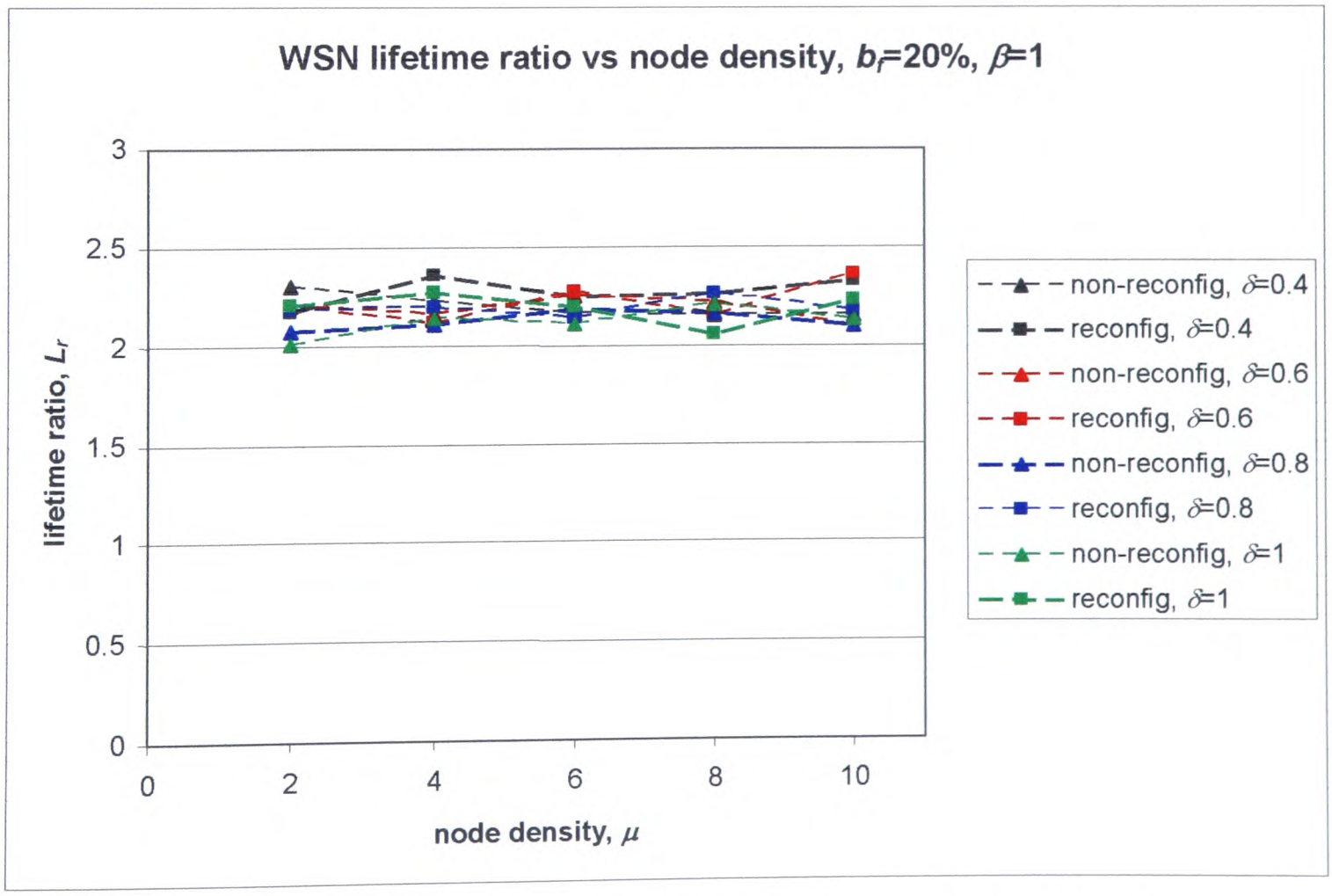

Figure 7.41: WSN lifetime ratio, L_r, vs node density, μ, for b_f=20%, β=1

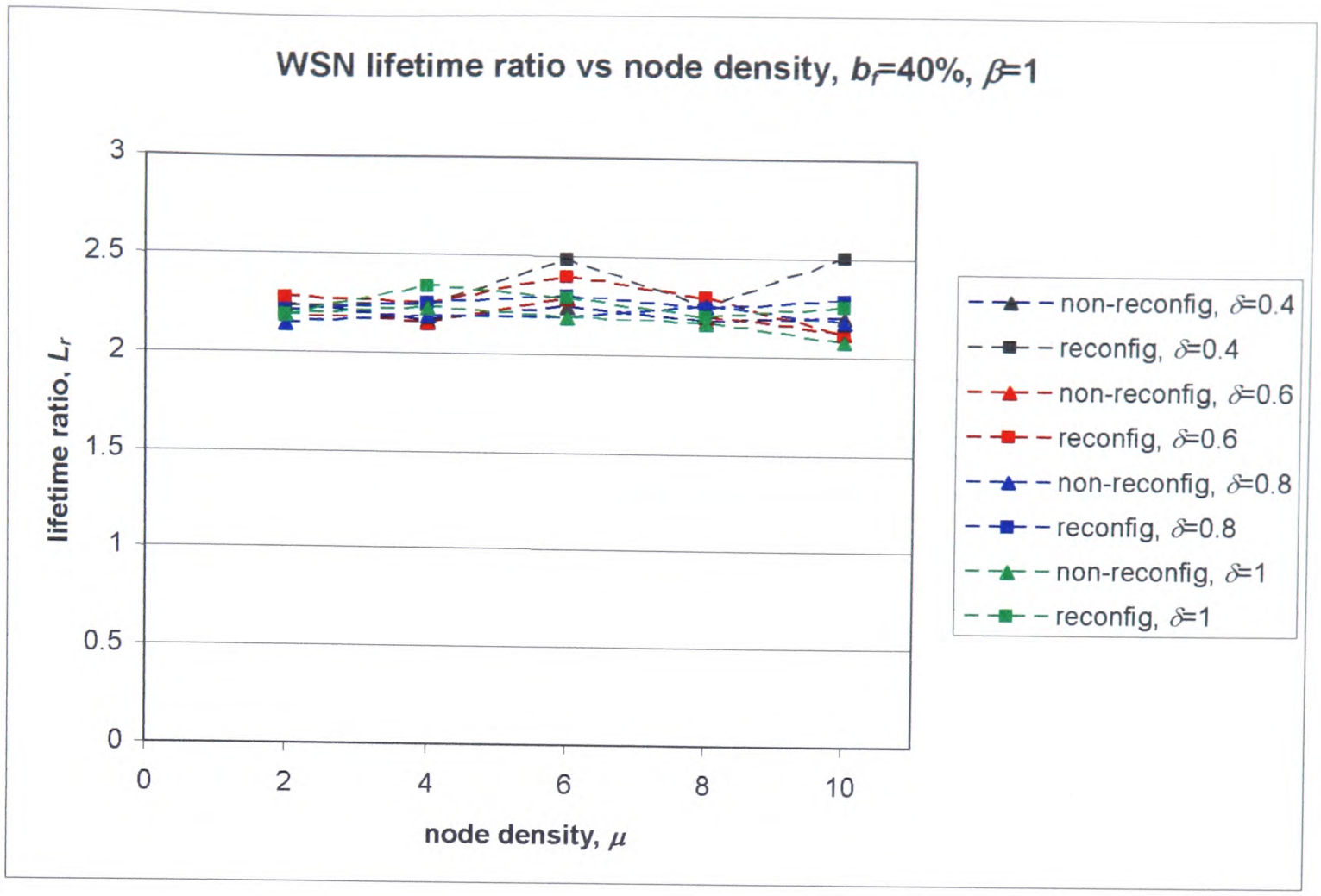

Figure 7.42: WSN lifetime ratio, L_r, vs node density, μ, for b_f=40%, β=1

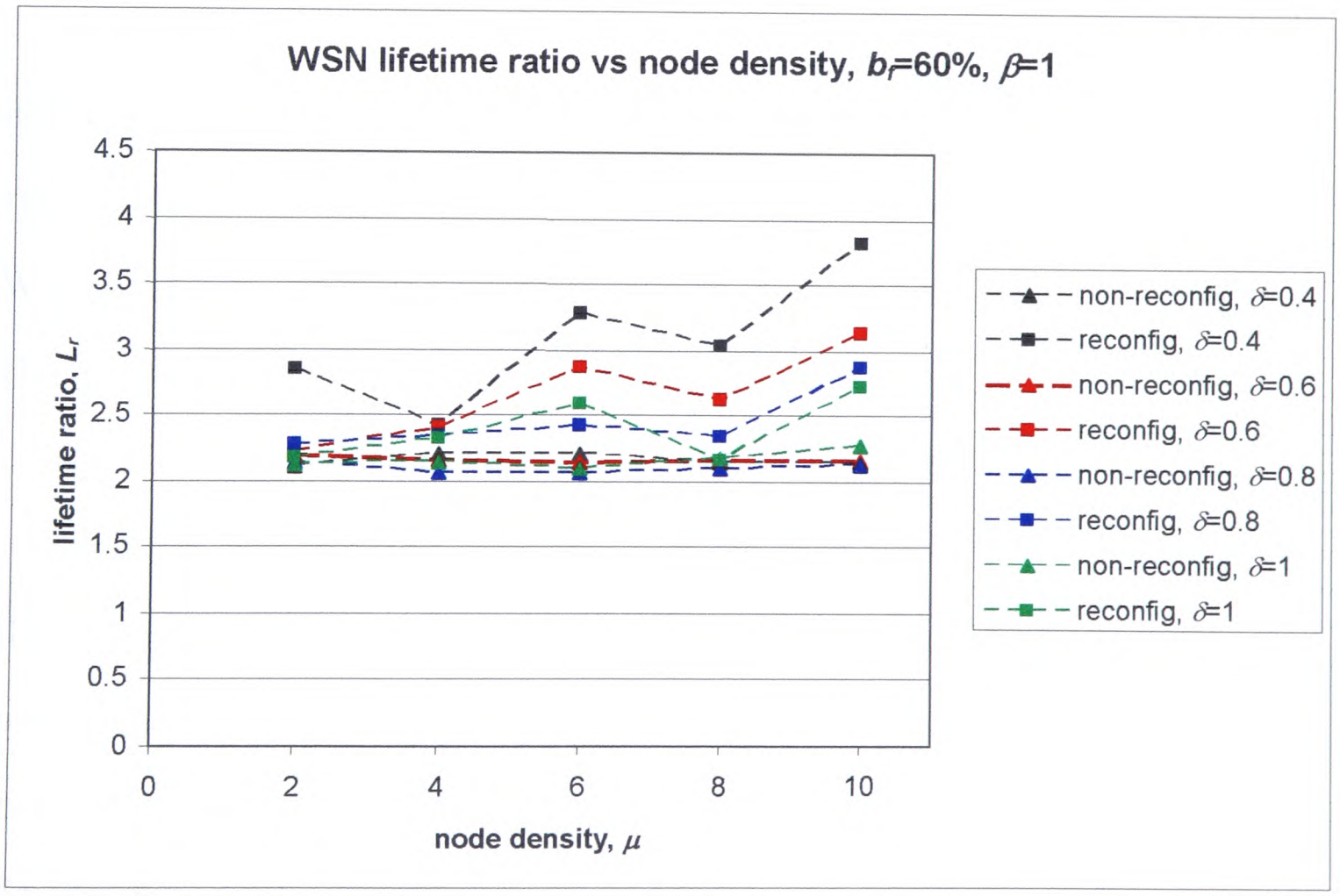

Figure 7.43: WSN lifetime ratio, L_r, vs node density, μ, for b_f=60%, β=1

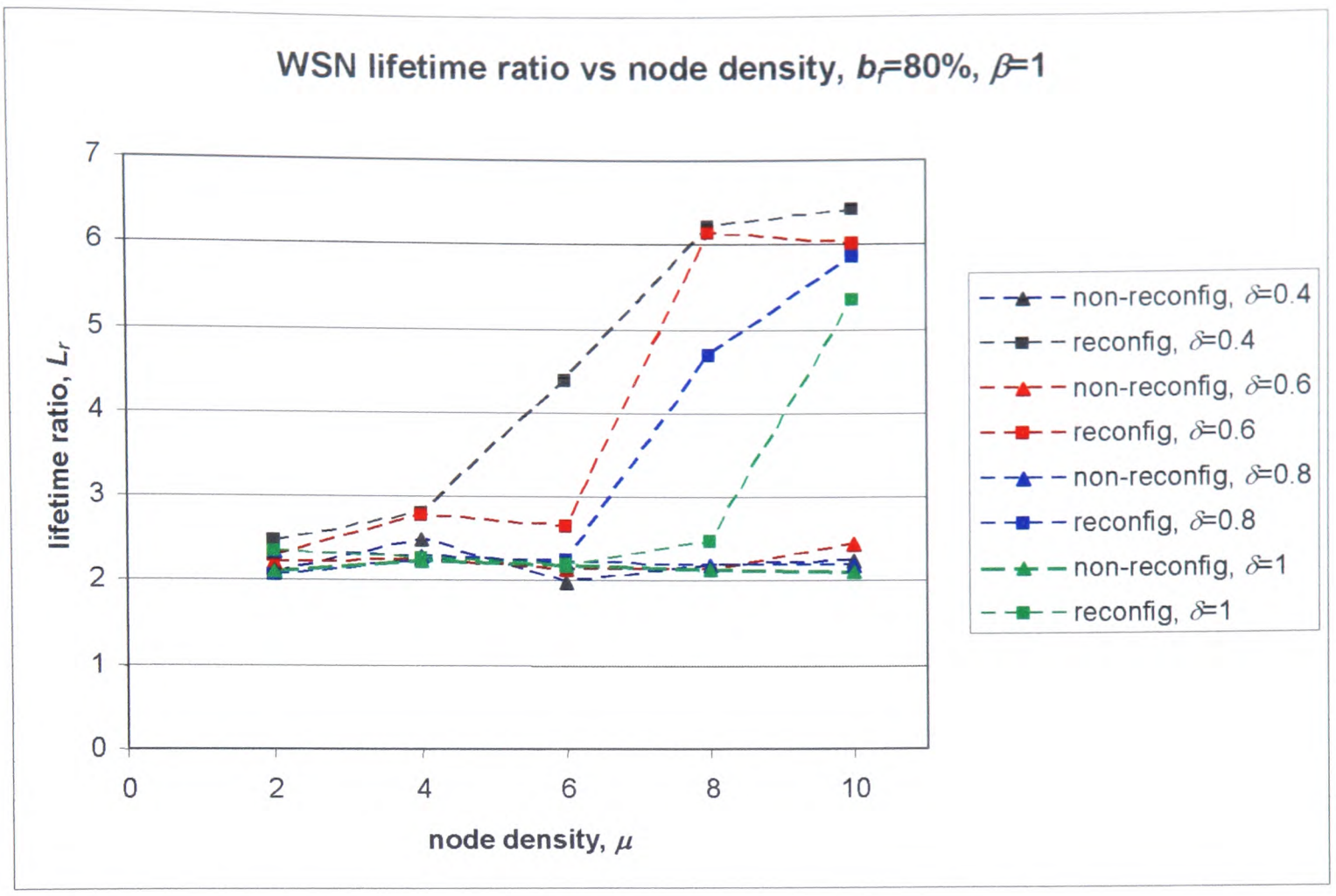

Figure 7.44: WSN lifetime ratio, L_r, vs node density, μ, for b_f=80%, β=1

Figures 7.45 – 7.49 show the average coverage ratios for the range of node densities and hotspot factors considered. The simulations show that for low blocking factors (0%, 20% and 40% in Figures 7.45, 7.46 and 7.47 respectively), the RF/FSO WSN is able to match the network coverage of the RF-only WSN. For higher blocking factors (60% and 80% in Figures 7.48 and 7.49 respectively), the average coverage ratio falls slightly, and is within the range of $0.8 \leq C_r \leq 1$ for non-reconfiguring networks. This is because when the blocking factor is high, nodes in the RF/FSO network depend on more RF multihops and expend more energy for communications. Nodes expire more quickly, and this reduces the network coverage. For high node densities and large blocking factors in Figures 7.48 and 7.49, the RF/FSO WSN is able to offer much better network coverage than the RF-only WSN. This is due to the comparatively lower energy expended by the RF/FSO WSN

gateway nodes, when compared to the RF-only gateway nodes which was discussed in Section 7.5.2.

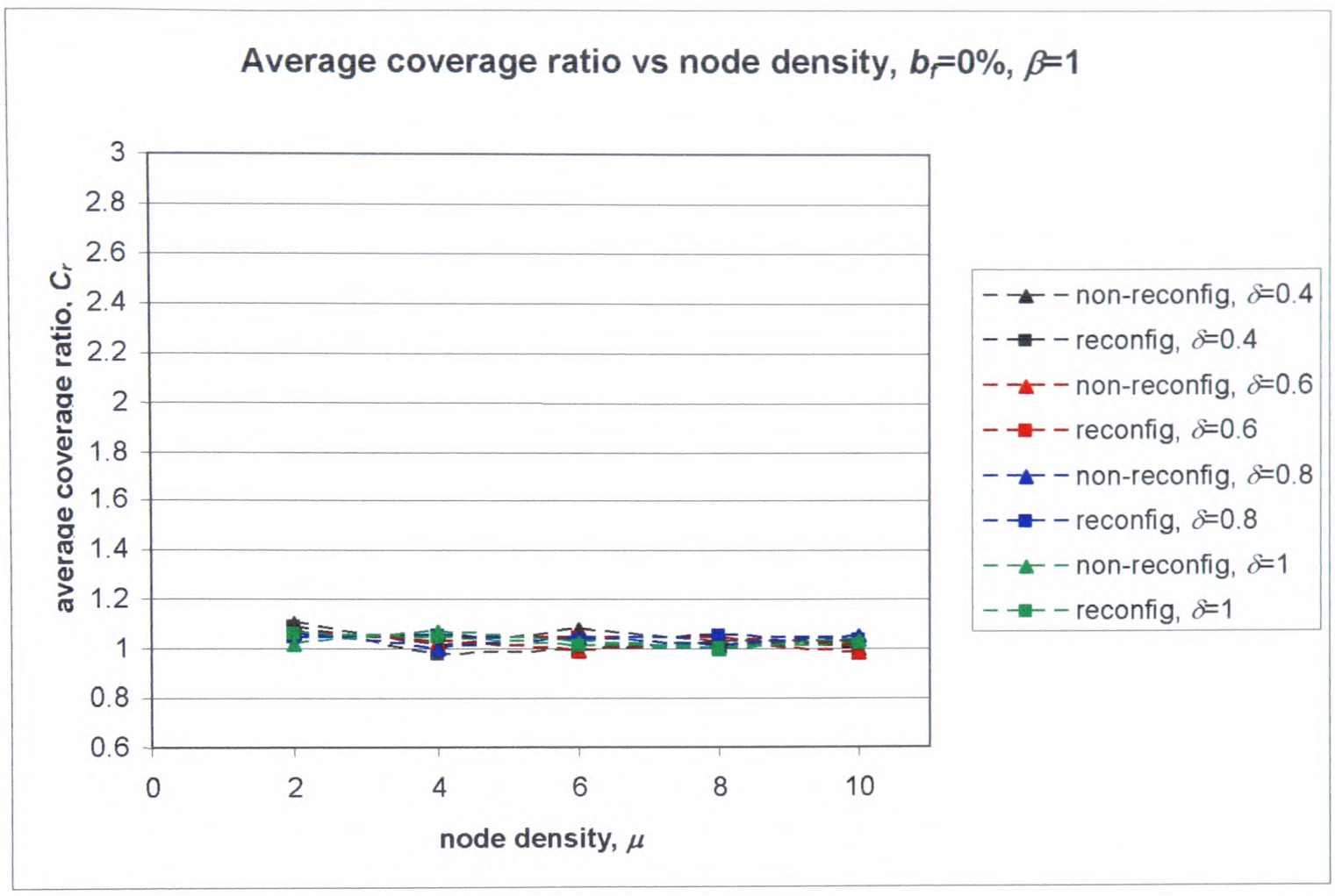

Figure 7.45: Average coverage ratio, C_r, vs node density μ, for blocking factor b_f=0%, range ratio β=1

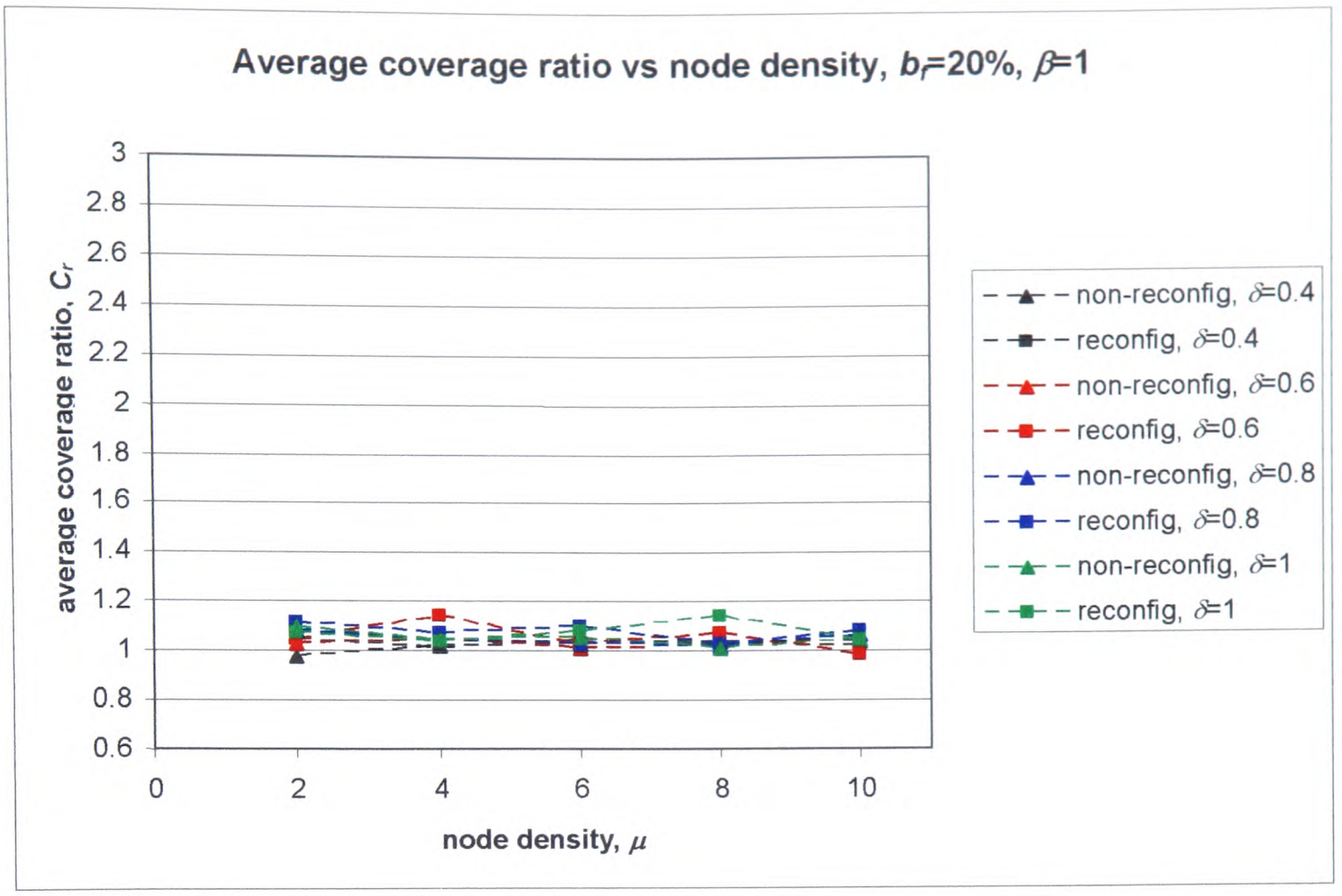

Figure 7.46: Average coverage ratio, C_r, vs node density, μ, for b_f=20%, β=1

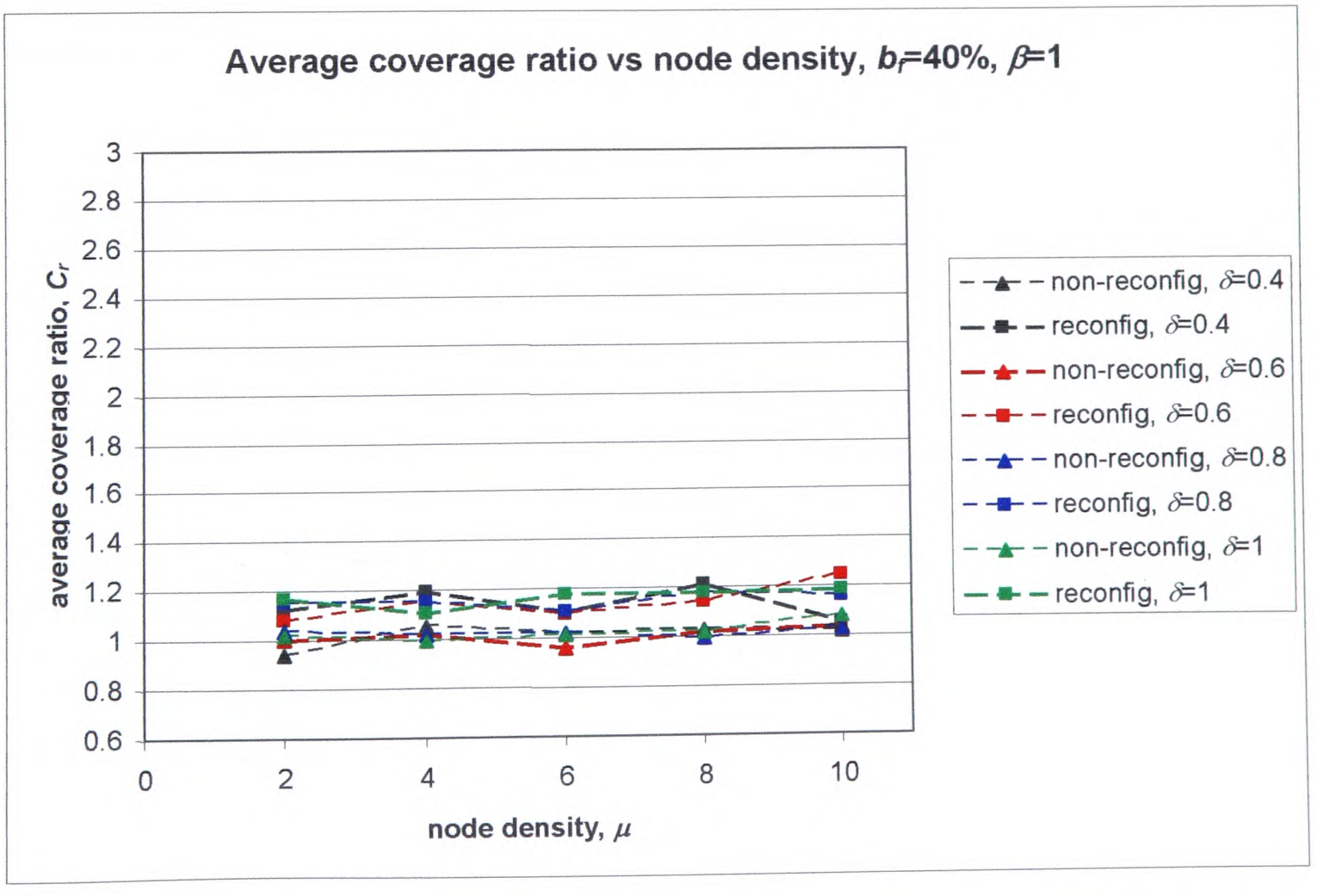

Figure 7.47: Average coverage ratio, C_r, vs node density, μ, for b_f=40%, β=1

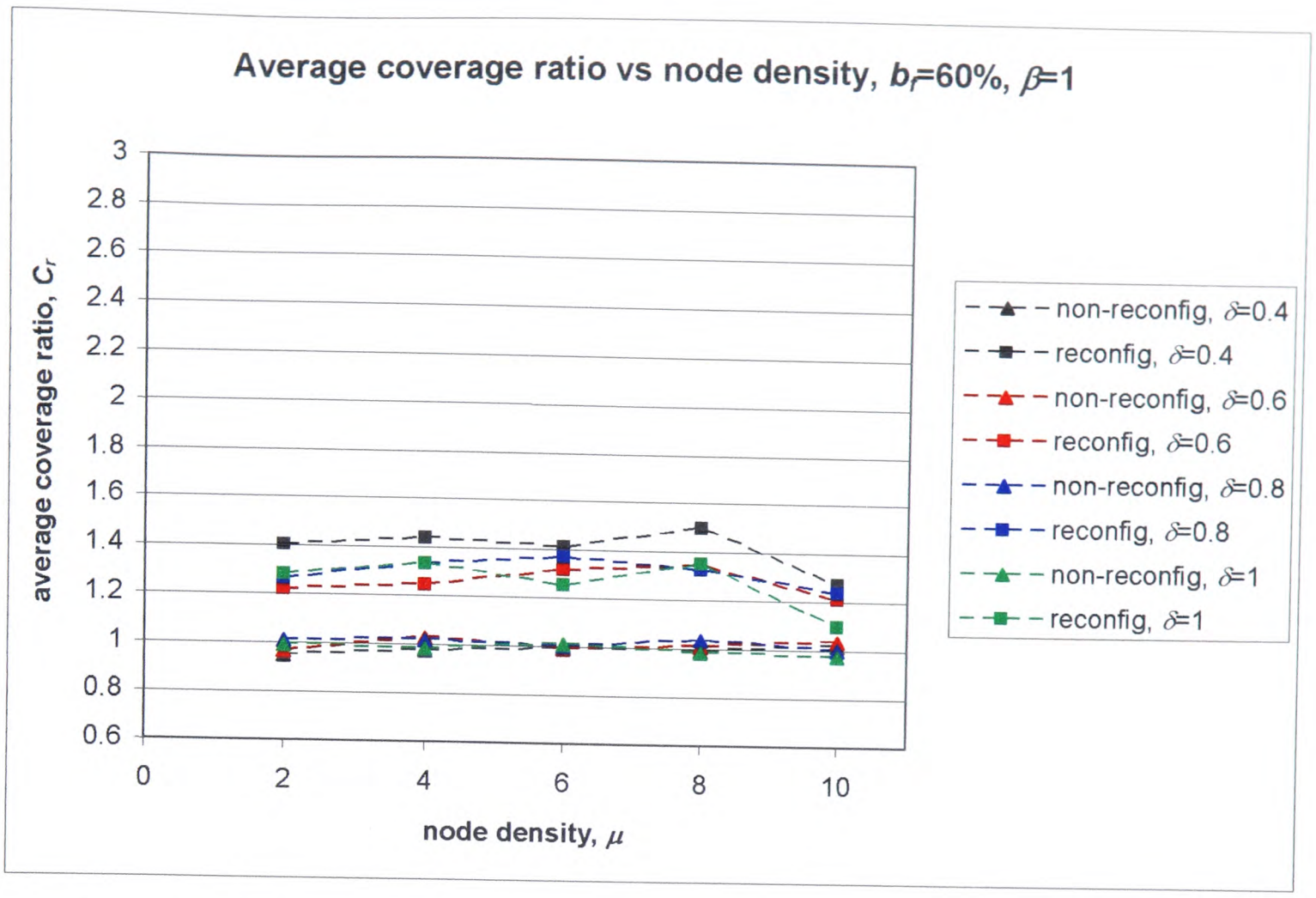

Figure 7.48: Average coverage ratio, C_r, vs node density, μ, for b_f=60%, β=1

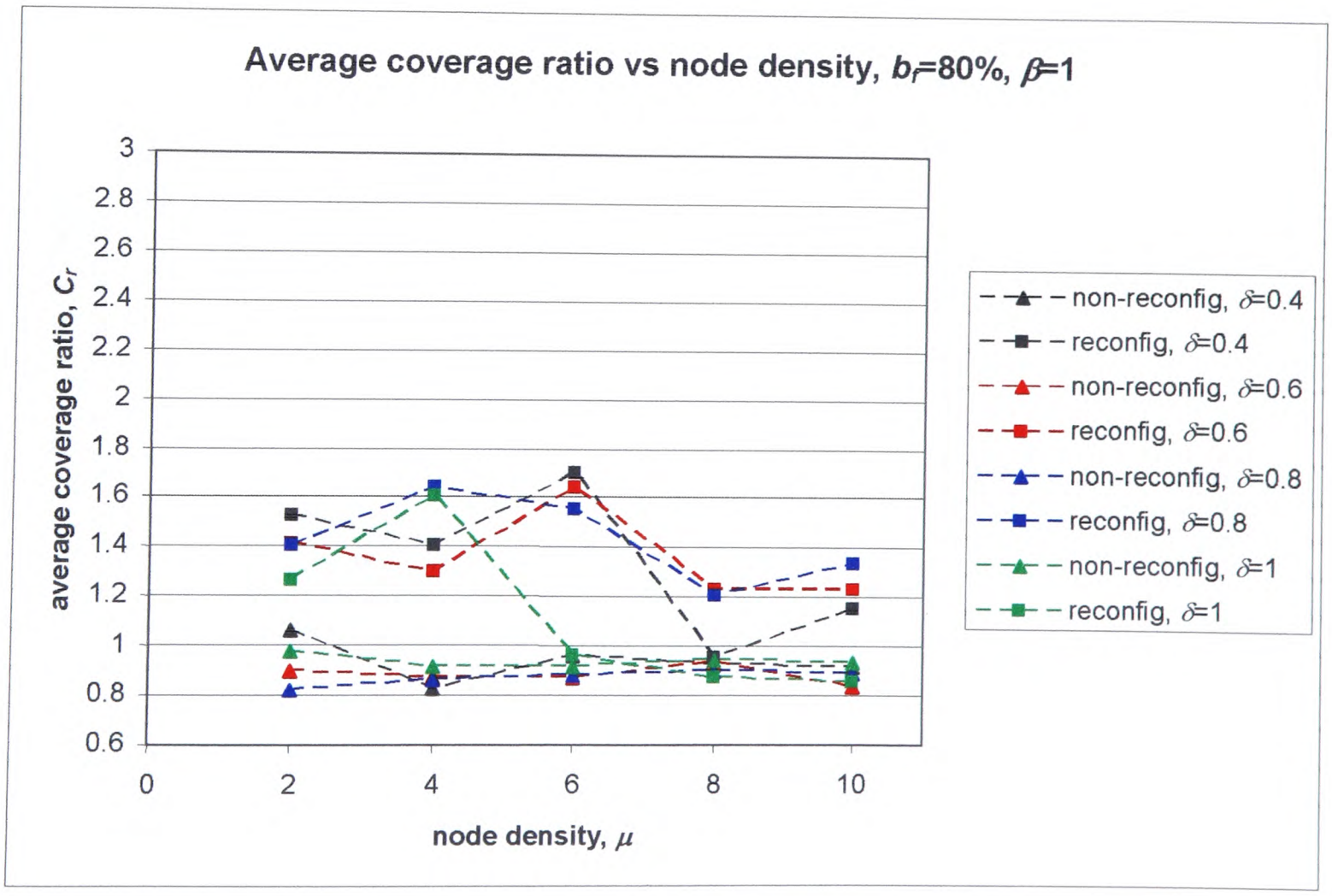

Figure 7.49: Average coverage ratio, C_r, vs node density, μ, for b_f=80%, β=1

Figures 7.50 – 7.54 show the average coverage area of the RF/FSO WSN for the range of node densities and hotspot factors considered. The average coverage area increases as the node density increases, as greater number of nodes lead to better network coverage. However, for low blocking factors (b_f=0%, 20%), simulations suggest that increasing the node density beyond μ=6, fails to further increase the average coverage area (see Figures 7.50 and 7.51). This agrees very well with the well-known paper by Kleinrock and Silvester[149], where they show that the optimum node density in multi-hop radio networks is six. The plots in Figures 7.50-7.54 again confirm that network reconfiguration is most beneficial when the blocking factor is high.

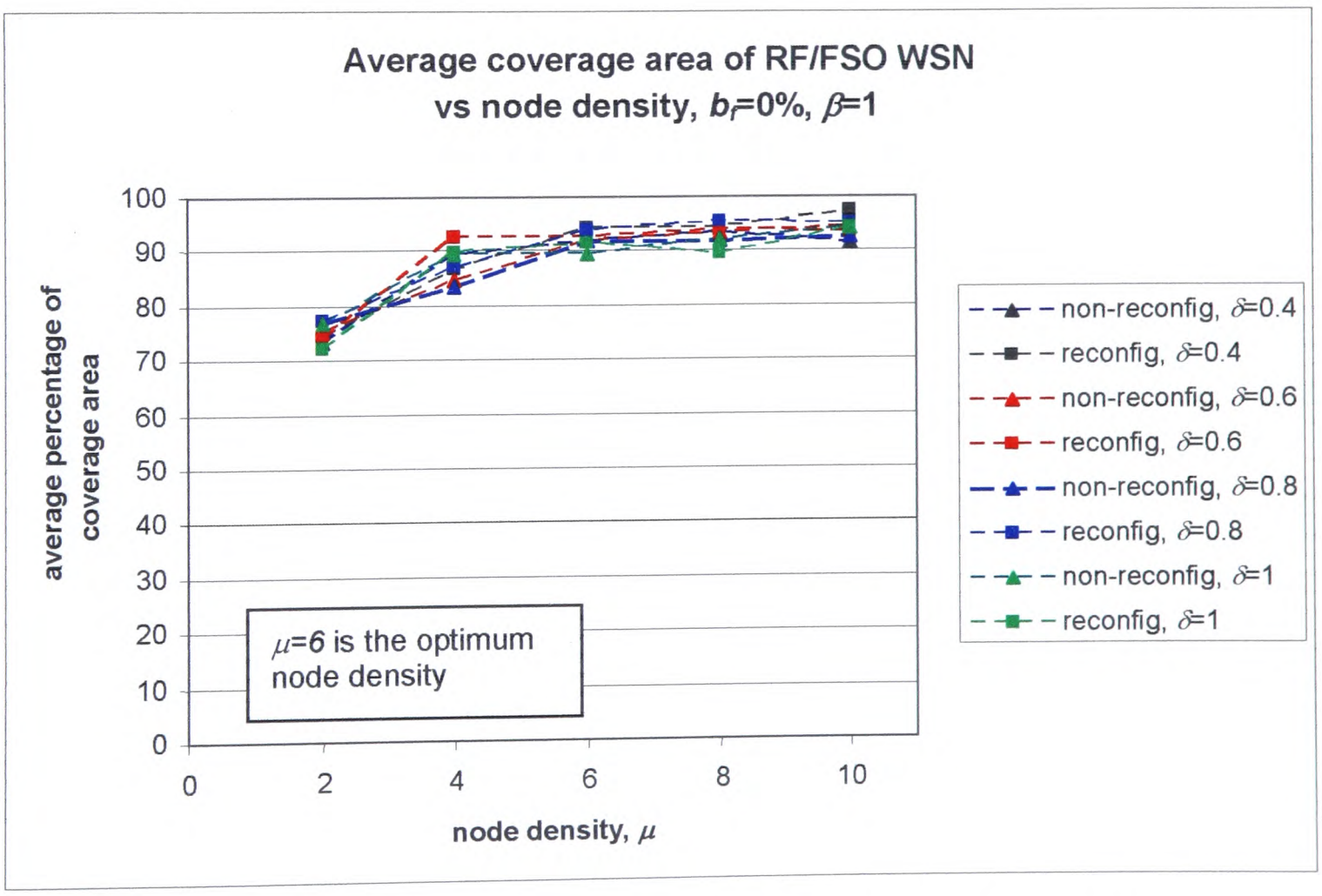

Figure 7.50: Average RF/FSO WSN coverage area vs node density μ, for blocking factor b_f=0%, range ratio β=1

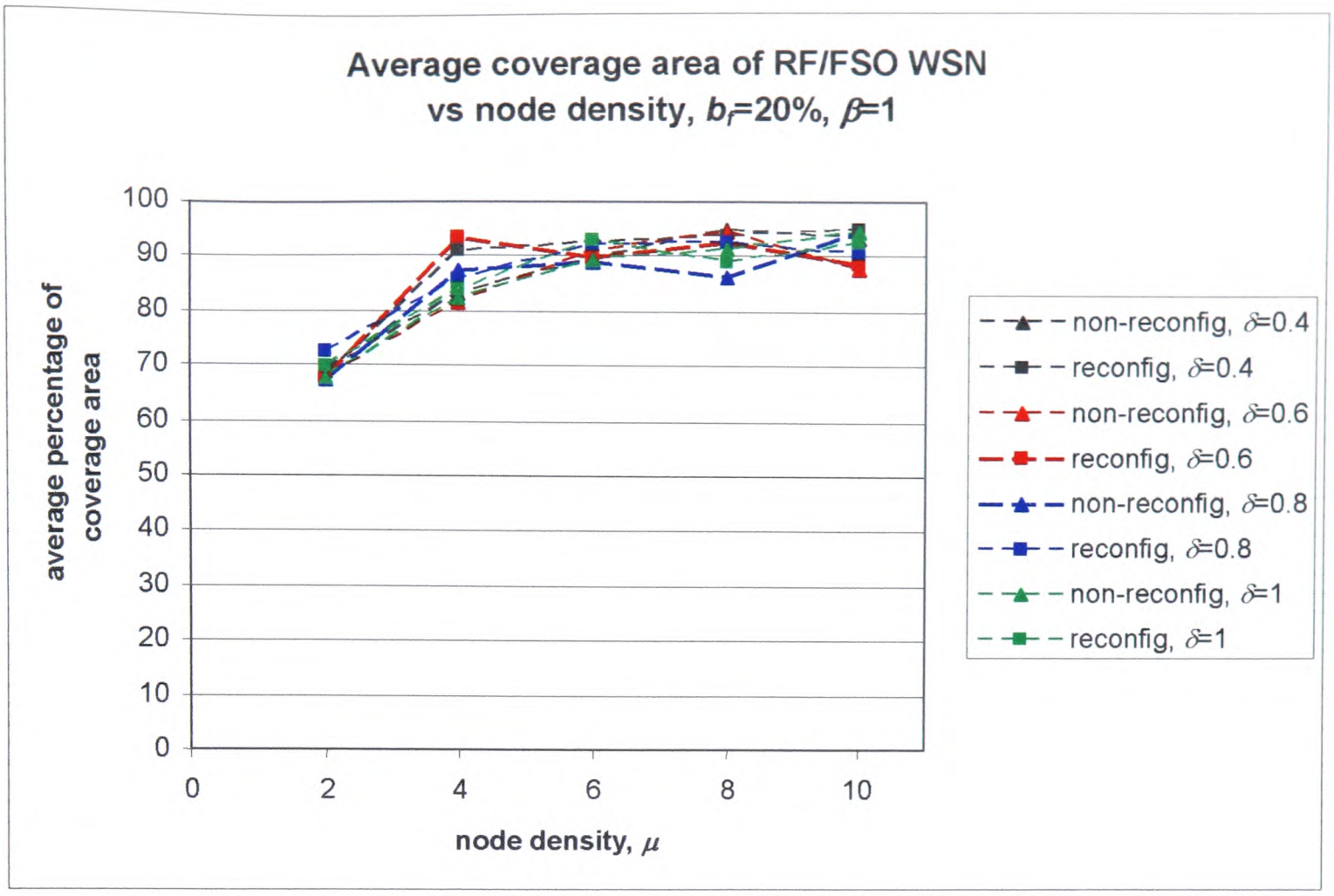

Figure 7.51: Average RF/FSO WSN coverage area vs node density, μ, for b_f=20%, β=1

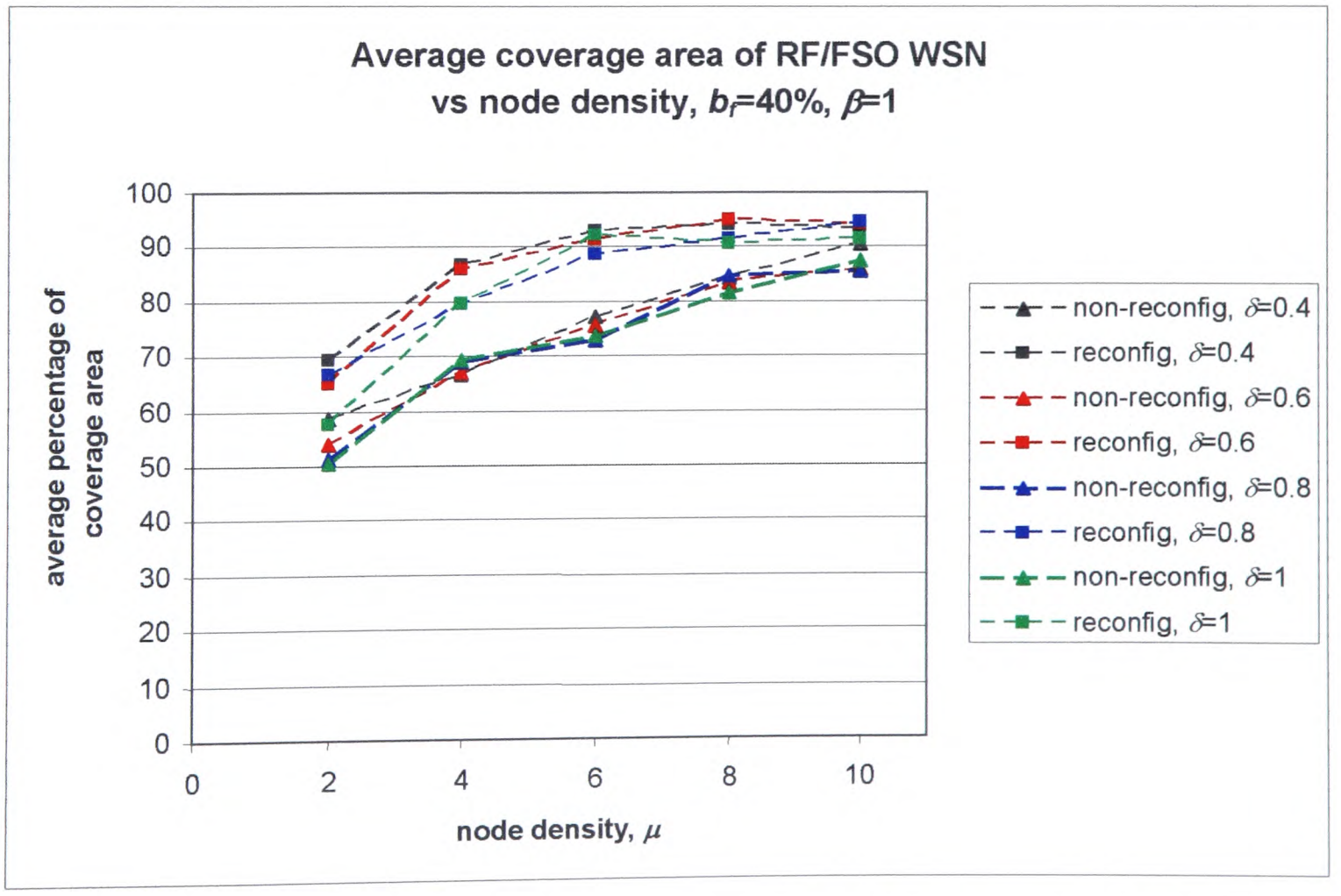

Figure 7.52: Average RF/FSO WSN coverage area vs node density, μ, for b_f=40%, β=1

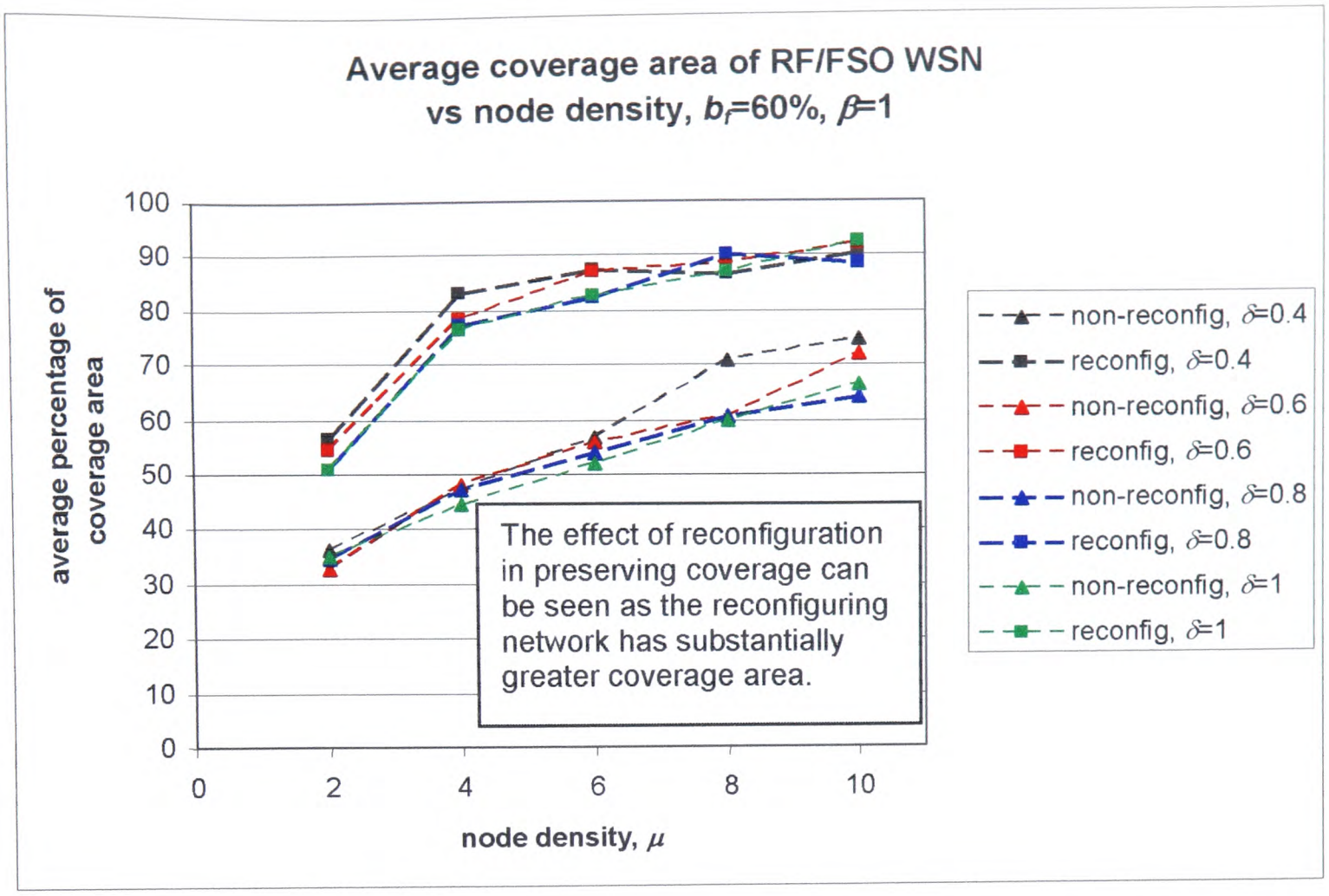

Figure 7.53: Average RF/FSO WSN coverage area vs node density, μ, for b_f=60%, β=1

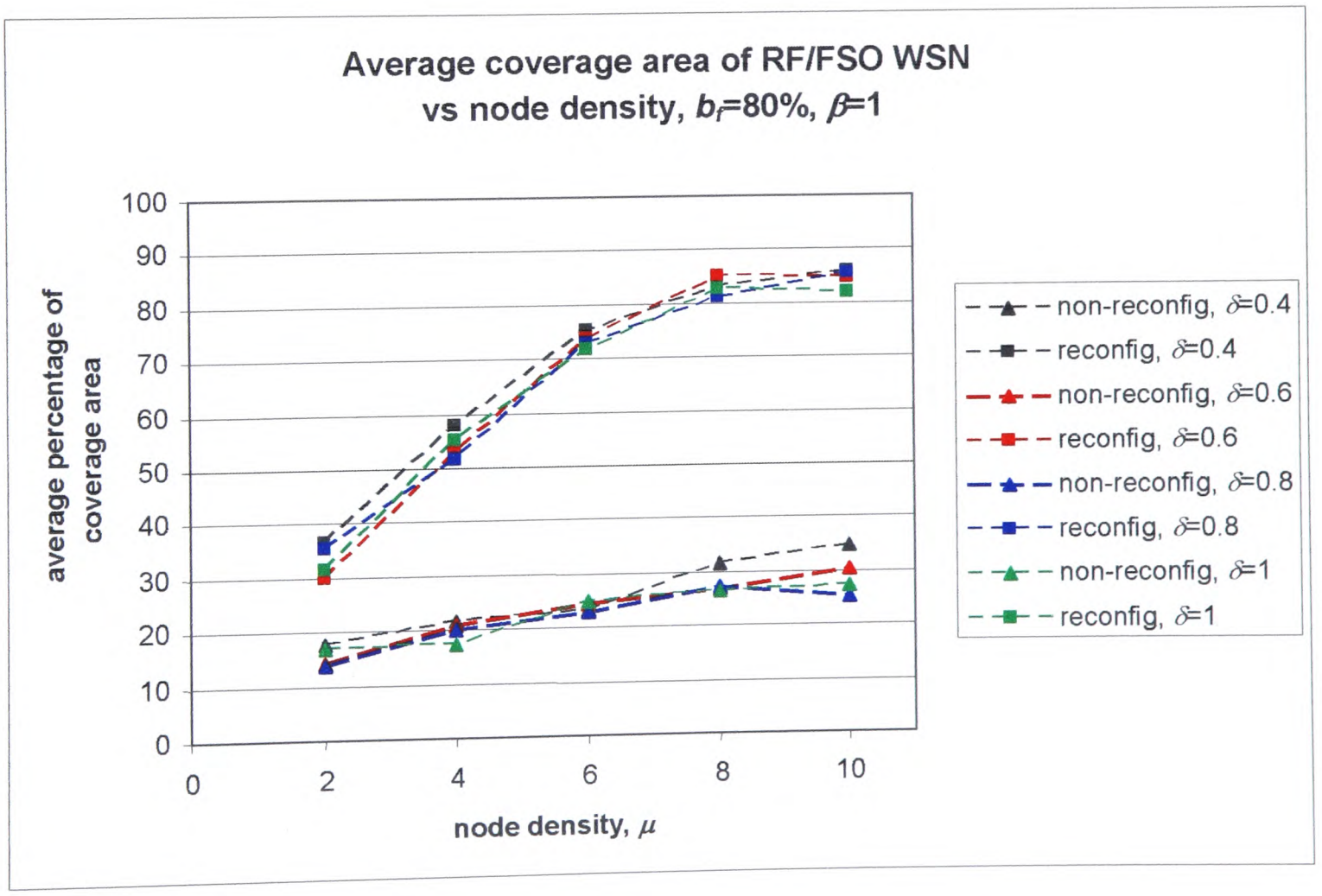

Figure 7.54: Average RF/FSO WSN coverage area vs node density, μ, for b_f=80%, β=1

7.5.4. Range ratio, β, results and discussion

For the simulations discussed in Sections 7.5.1 – 7.5.3, the range ratio, β, was set to one to represent the worst case scenario for d_{OPT}. However, in practice, d_{OPT} is likely to be greater than d_L, and having a longer communications range means that the RF/FSO network should be able to better support a larger network deployment area than the RF-only WSN.

In this section, the lifetime ratio L_r, average coverage ratio C_r and the average RF/FSO WSN network coverage are studied for a range of β. When $\beta=1$, d_{OPT} and d_L are equal. So the topologies of the RF/FSO and RF-only WSNs are similar. A typical value for d_{OPT} is 200m, as discussed in Section 3.4. As d_L is set to 145.7m for the simulations (see Table 7.3), d_{OPT}=200m corresponds to β=1.37. Therefore, for the simulations in this section, β is chosen to be in the range of $1 \leq \beta \leq 1.4$. As the value of β is increased, the deployment area becomes wider. The node density, μ, is set to three for the simulations in this section, and the number of nodes has to increase proportionately so the node density is kept constant. The network lifetimes were simulated using higher node densities for several cases, but they led to unacceptably long run times due to the number of nodes in the network.

The graphs in Figures 7.55 to 7.59 show that the RF/FSO WSN lasts at least twice as long as the RF-only WSN for the values of β and b_f considered. Despite the wide range of b_f considered, there is little spread in the lifetime ratio and little difference between reconfiguring and non-reconfiguring networks. The $2 \leq L_r \leq 2.5$

lifetime ratio range was discussed in Section 7.5.1, and it can be seen that the last node in the RF-only WSN expends about twice the energy of its RF/FSO counterpart. To analyze the simulation results of the average coverage ratio, C_r, the base station's radio hotspot is introduced next.

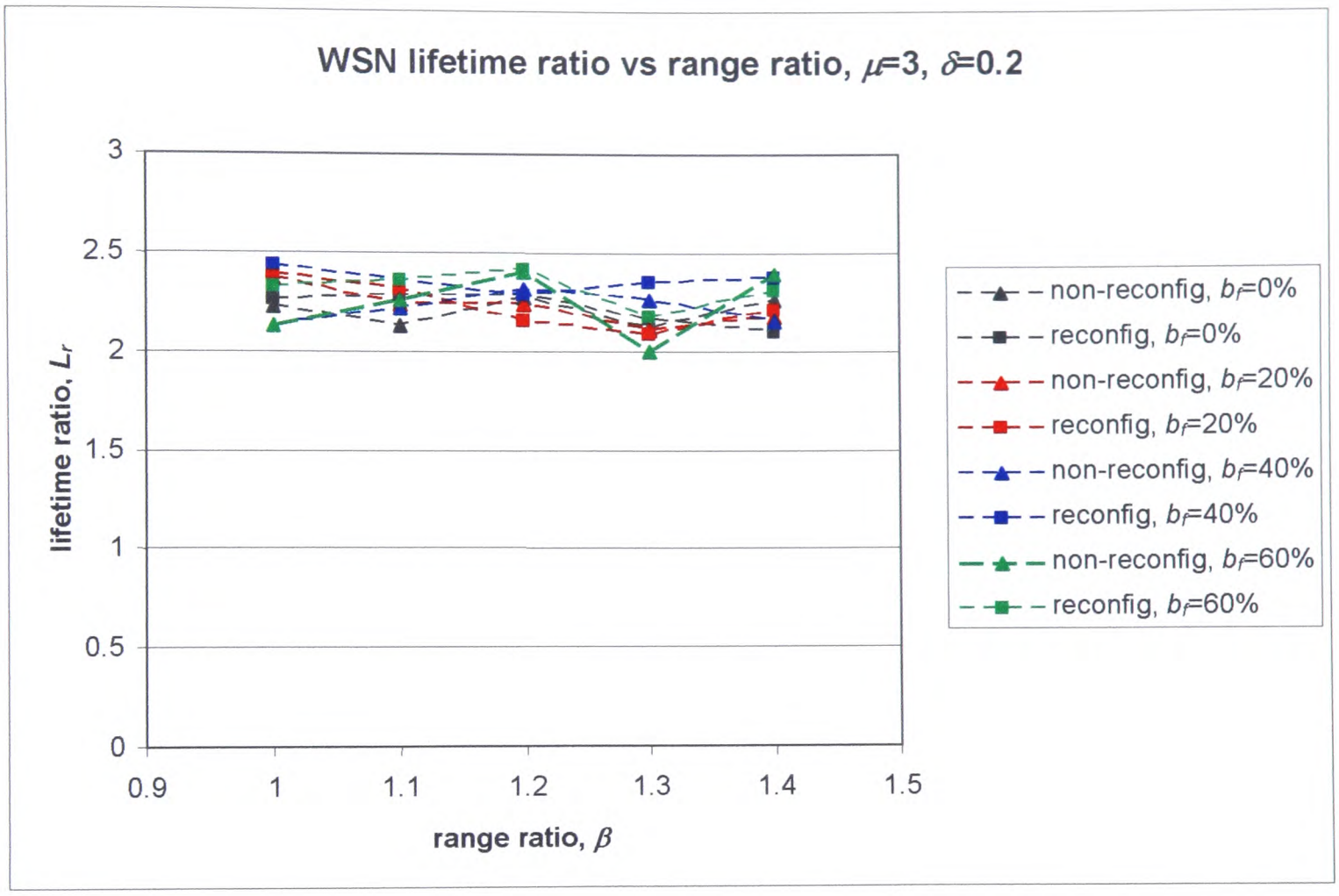

Figure 7.55: WSN lifetime ratio, L_r, vs range ratio β, for node density μ=3, hotspot factor δ=0.2

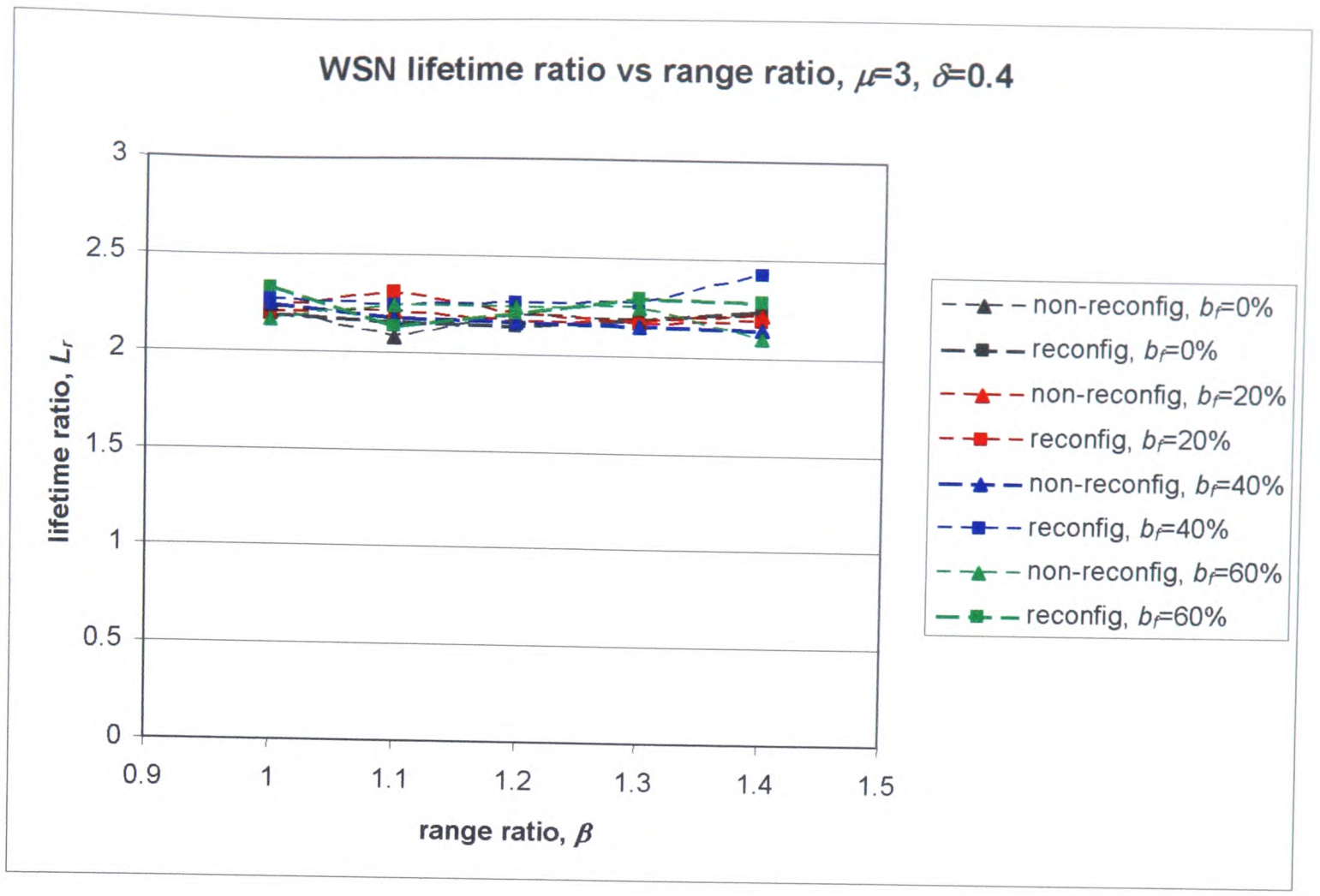

Figure 7.56: WSN lifetime ratio, L_r, vs range ratio, β, for μ=3, δ=0.4

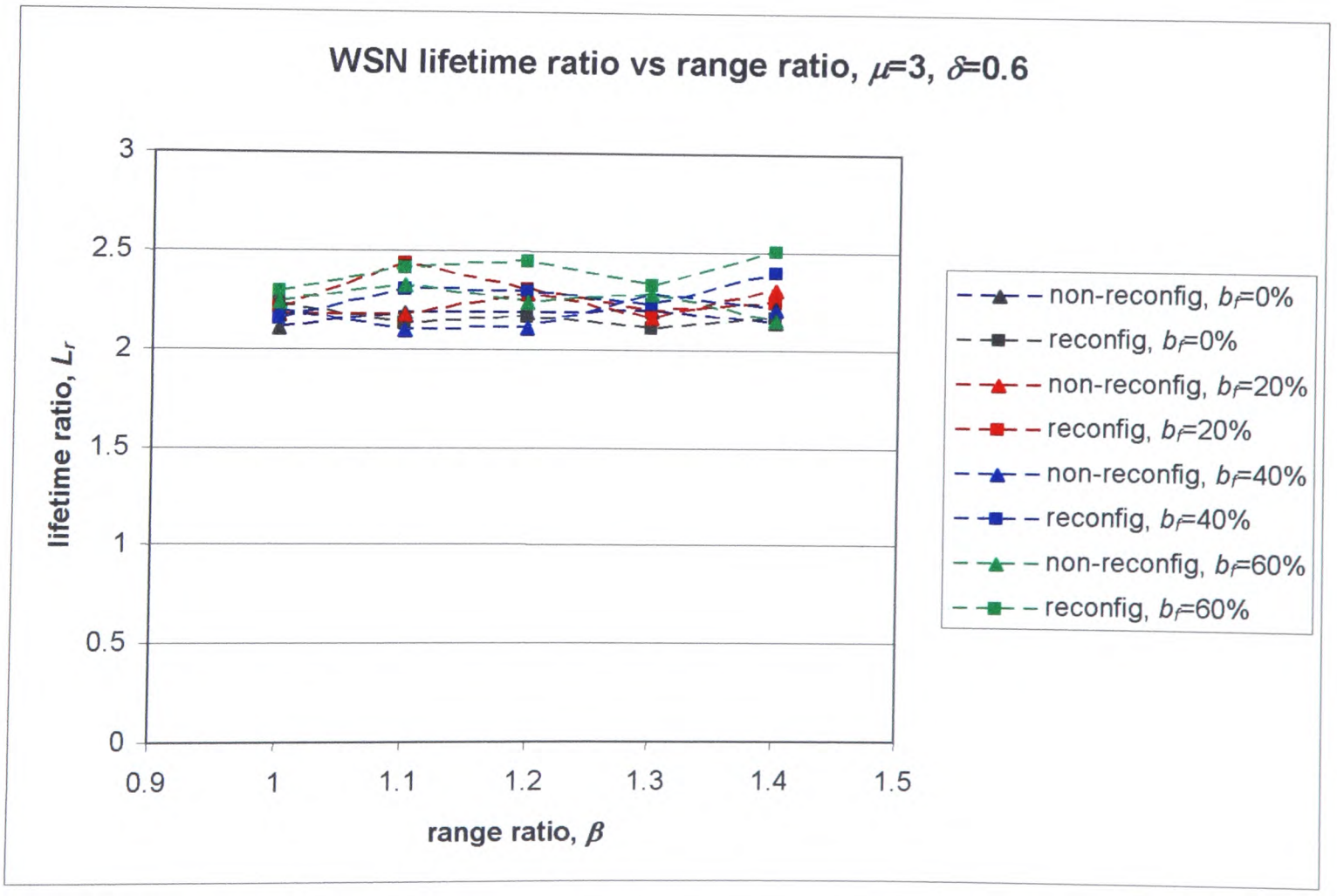

Figure 7.57: WSN lifetime ratio, L_r, vs range ratio, β, for μ=3, δ=0.6

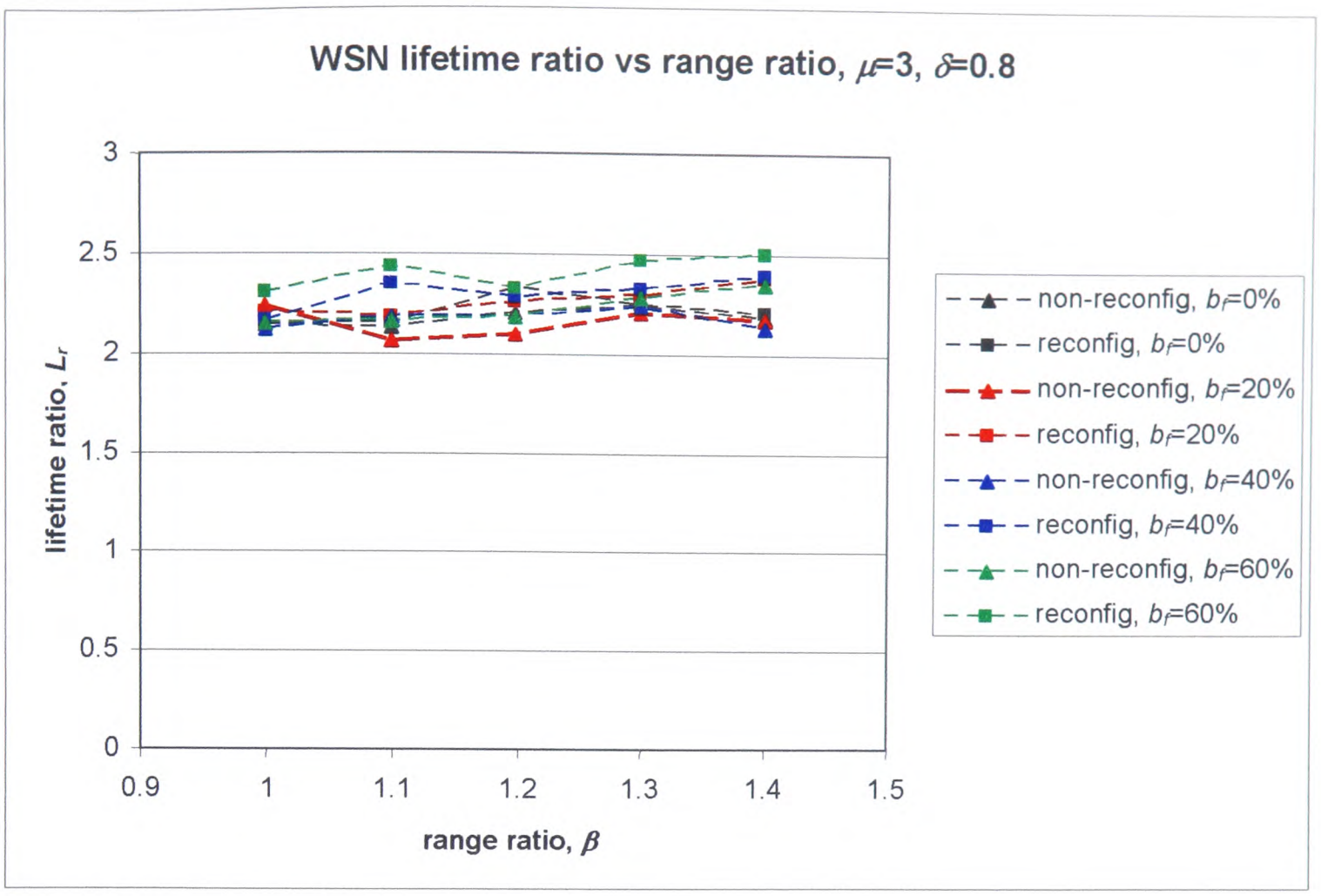

Figure 7.58: WSN lifetime ratio, L_r, vs range ratio, β, for μ=3, δ=0.8

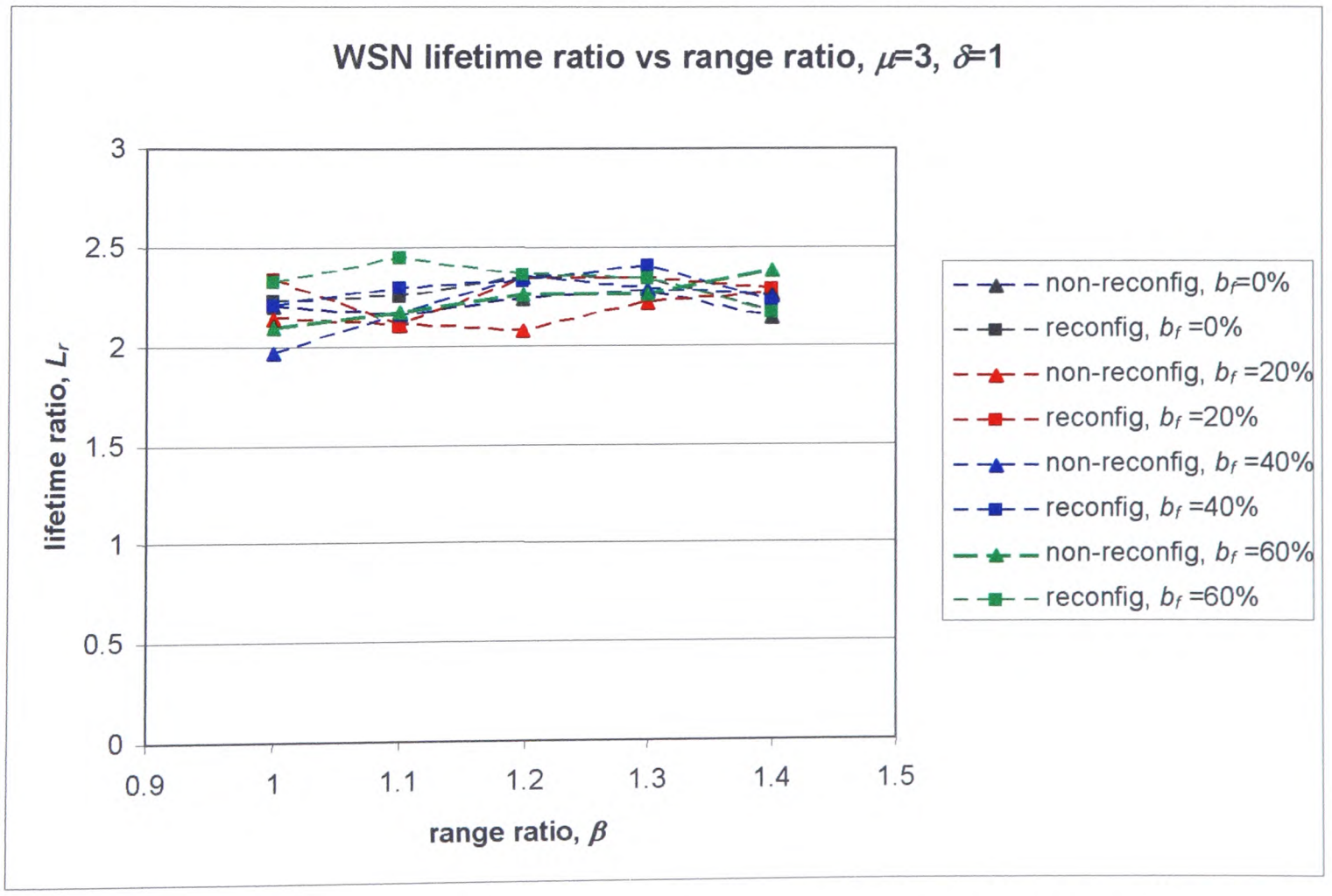

Figure 7.59: WSN lifetime ratio, L_r, vs range ratio, β, for μ=3, δ=1

The optical hotspot was discussed in Section 6.2. Figures 7.60 and 7.61 show the base station's optical and radio hotspots respectively. Within the radio hotspot, RF-only WSN nodes with LOS to the base station connect directly to the base station. In the RF/FSO WSN optical hotspot, nodes with LOS to the base station connect directly to the base station. In Figure 7.60 and 7.61, $r_{h,opt}$ and $r_{h,radio}$ are the optical and radio hotspot radii respectively, where:

$$r_{h,opt} = \sqrt{{d_{OPT}}^2 - h^2} \tag{7.9}$$

$$r_{h,radio} = \sqrt{{d_L}^2 - h^2} \tag{7.10}$$

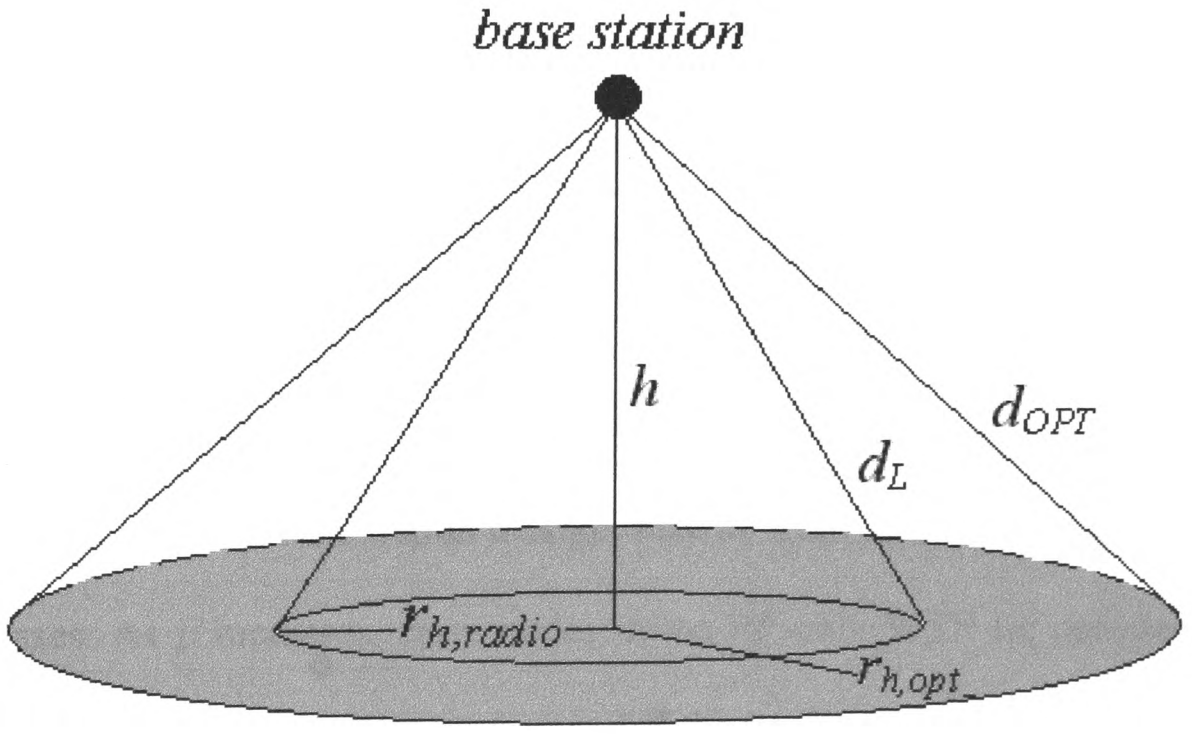

Figure 7.60: The base station's optical hotspot (shaded area)

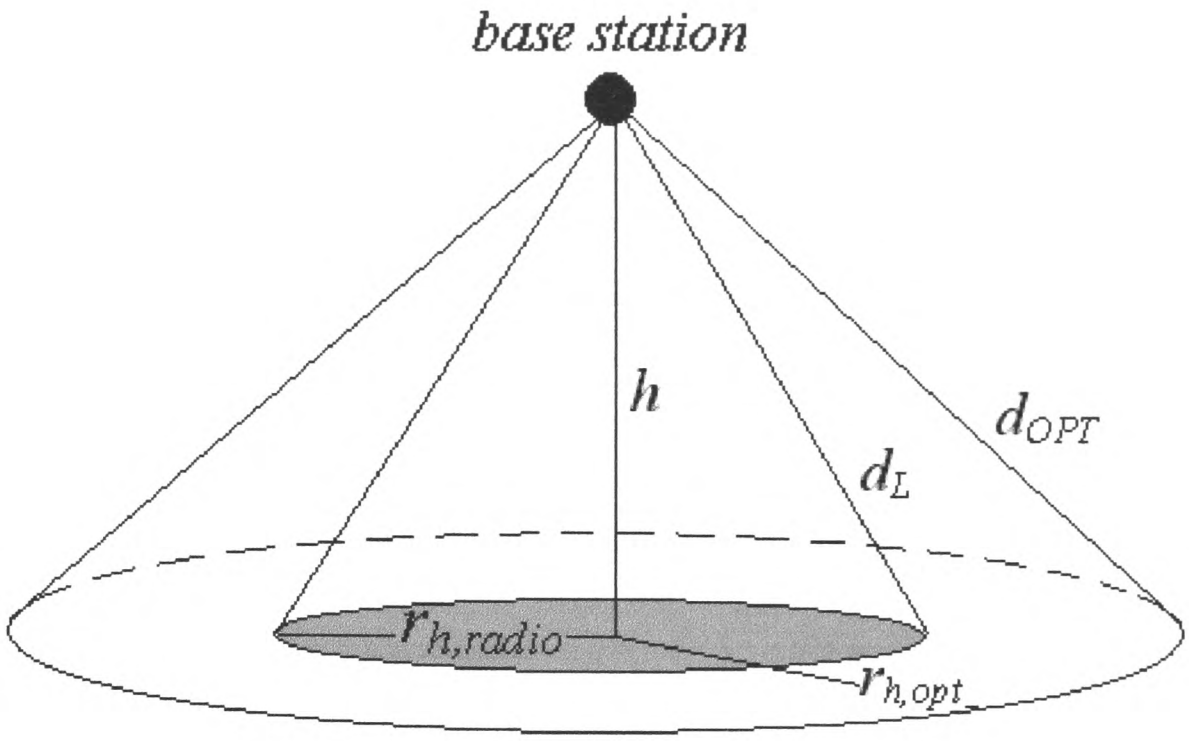

Figure 7.61: The base station's radio hotspot (shaded area)

Figures 7.62 – 7.66 show plots of the average coverage ratio, C_r, for the range of β and b_f considered. In Figure 7.62, the deployment area lies within both the base station's optical and radio hotspots. In Figure 7.63, $r_{h,radio}$ = 40.35m (From Equation 7.10. From Table 7.3, d_L=145.7m, h=140m.). The deployment area radius for β=1.2 and δ=0.4 in Figure 7.63 is 41.89m. This means that a small portion of nodes in the RF-only WSN will need to use multihops to reach the base station, as the distance between them and the base station is larger than d_L. This portion of nodes increases as β increases. As β increases, more nodes in the RF-only WSN lie outside the radio hotspot. Therefore, more energy is expended for multihop communications, causing nodes to expire more quickly. This reduces the RF-only WSN's network coverage and causes the average coverage ratio, C_r, to increase significantly with β as shown in Figures 7.63-7.66.

A typical value for d_{OPT}, calculated Section 3.6, is 200m. With d_L=145.7m, this corresponds to β=1.37. The longer optical range, d_{OPT} (compared to d_L), corresponds to β>1 and an optical hotspot which is larger than the radio hotspot. This means that the RF/FSO WSN is able to better support larger deployment areas.

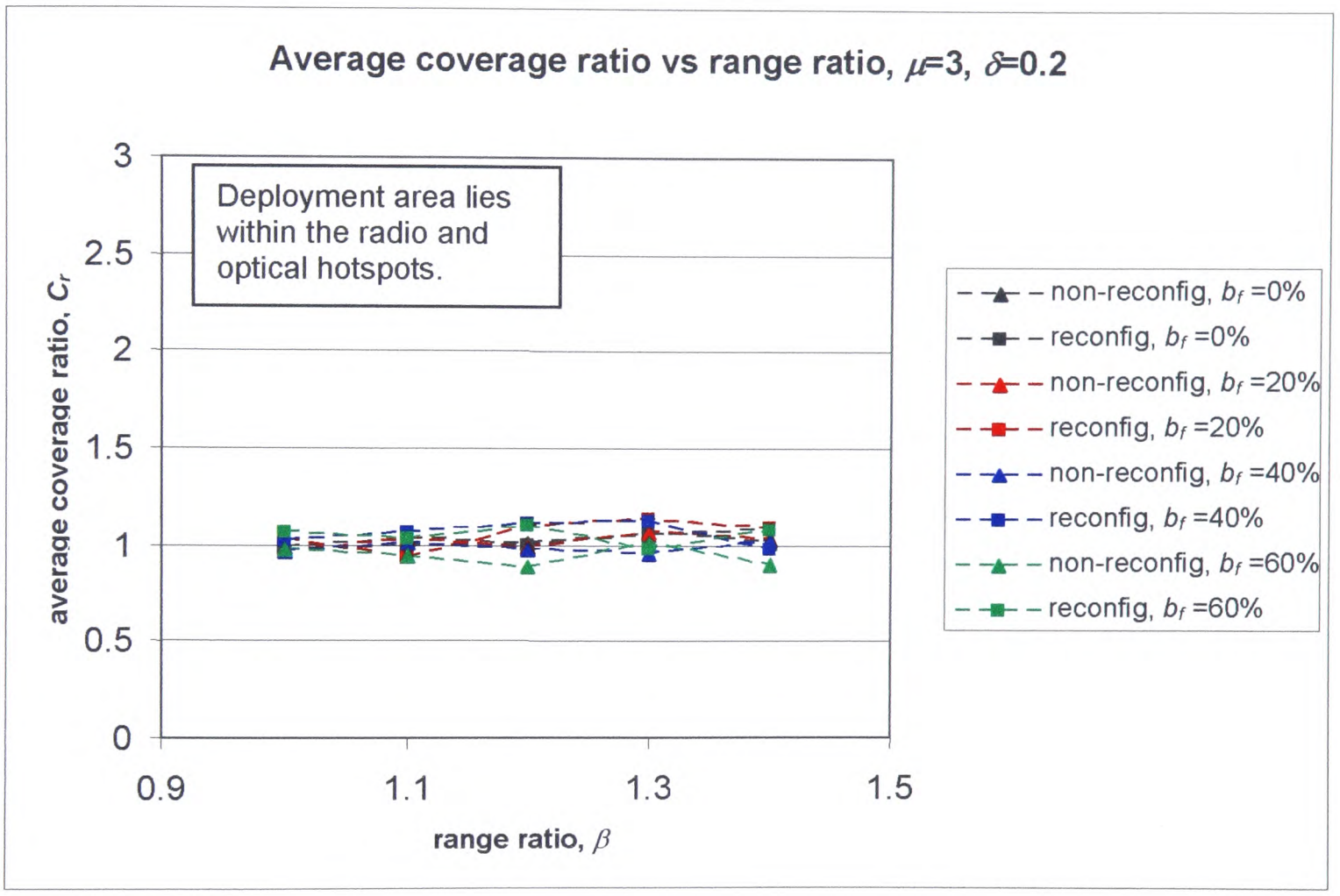

Figure 7.62: Average coverage ratio, C_r, vs range ratio β, for node density μ=3, hotspot factor δ=0.2

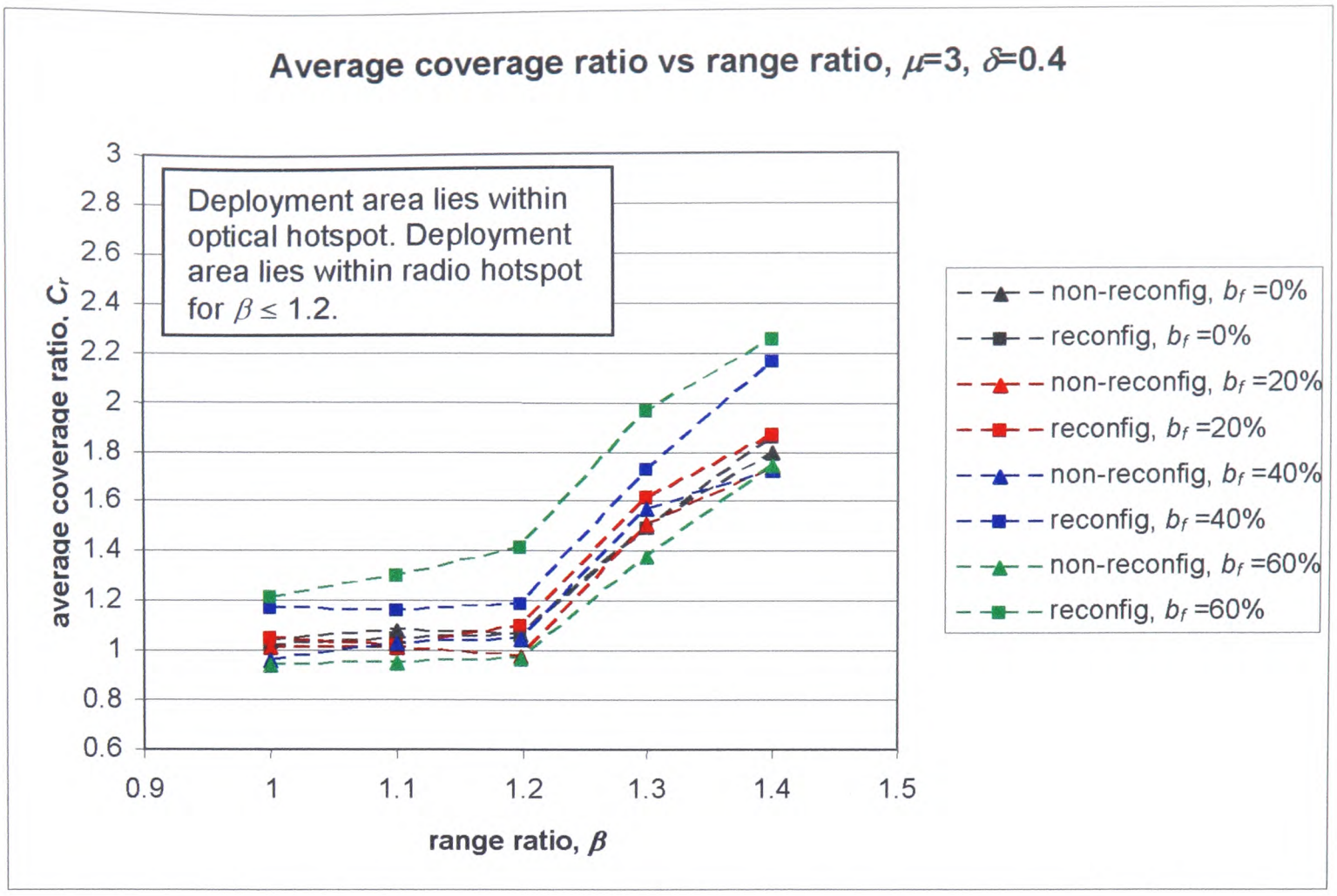

Figure 7.63: Average coverage ratio, C_r, vs range ratio, β, for μ=3, δ=0.4

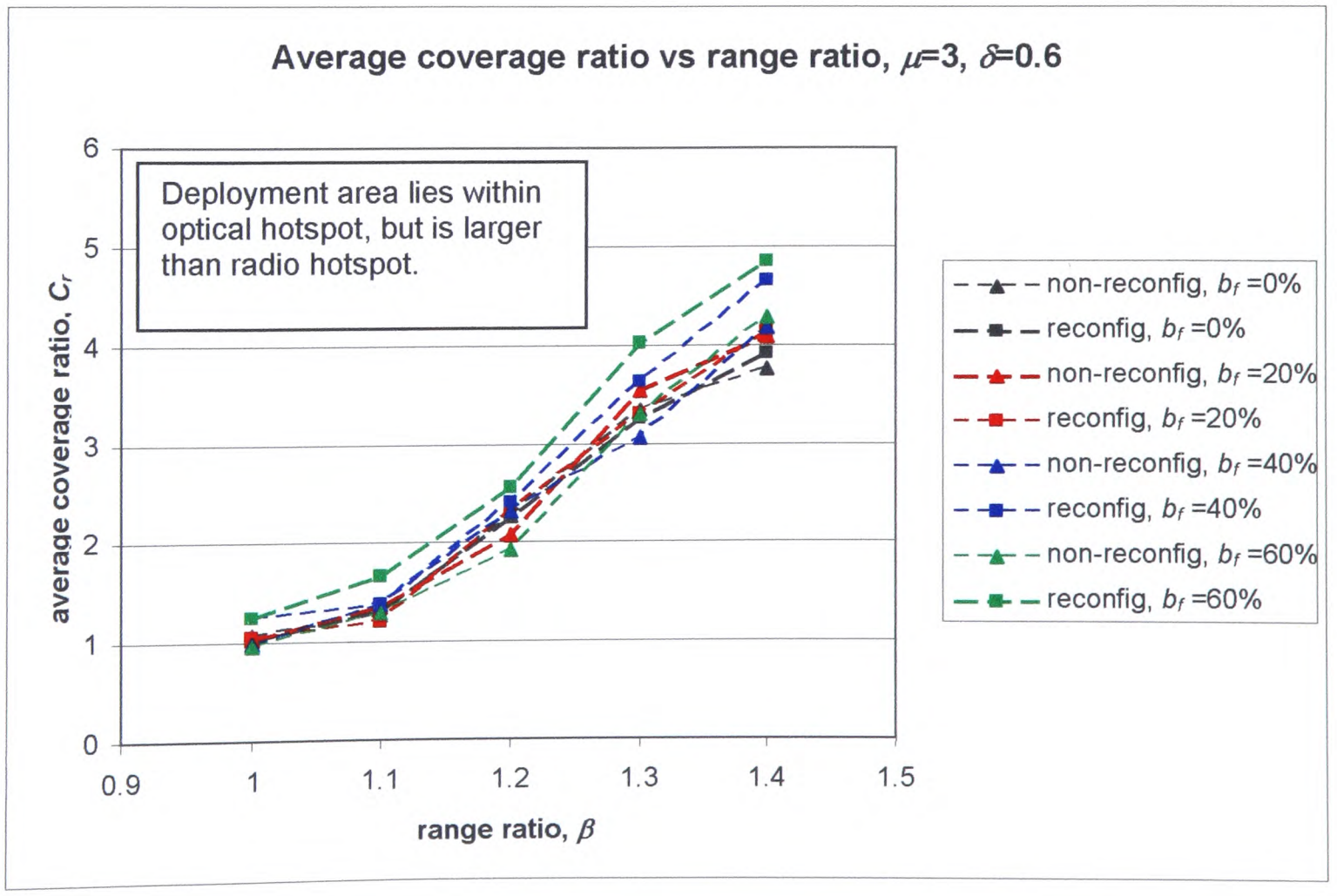

Figure 7.64: Average coverage ratio, C_r, vs range ratio, β, for μ=3, δ=0.6

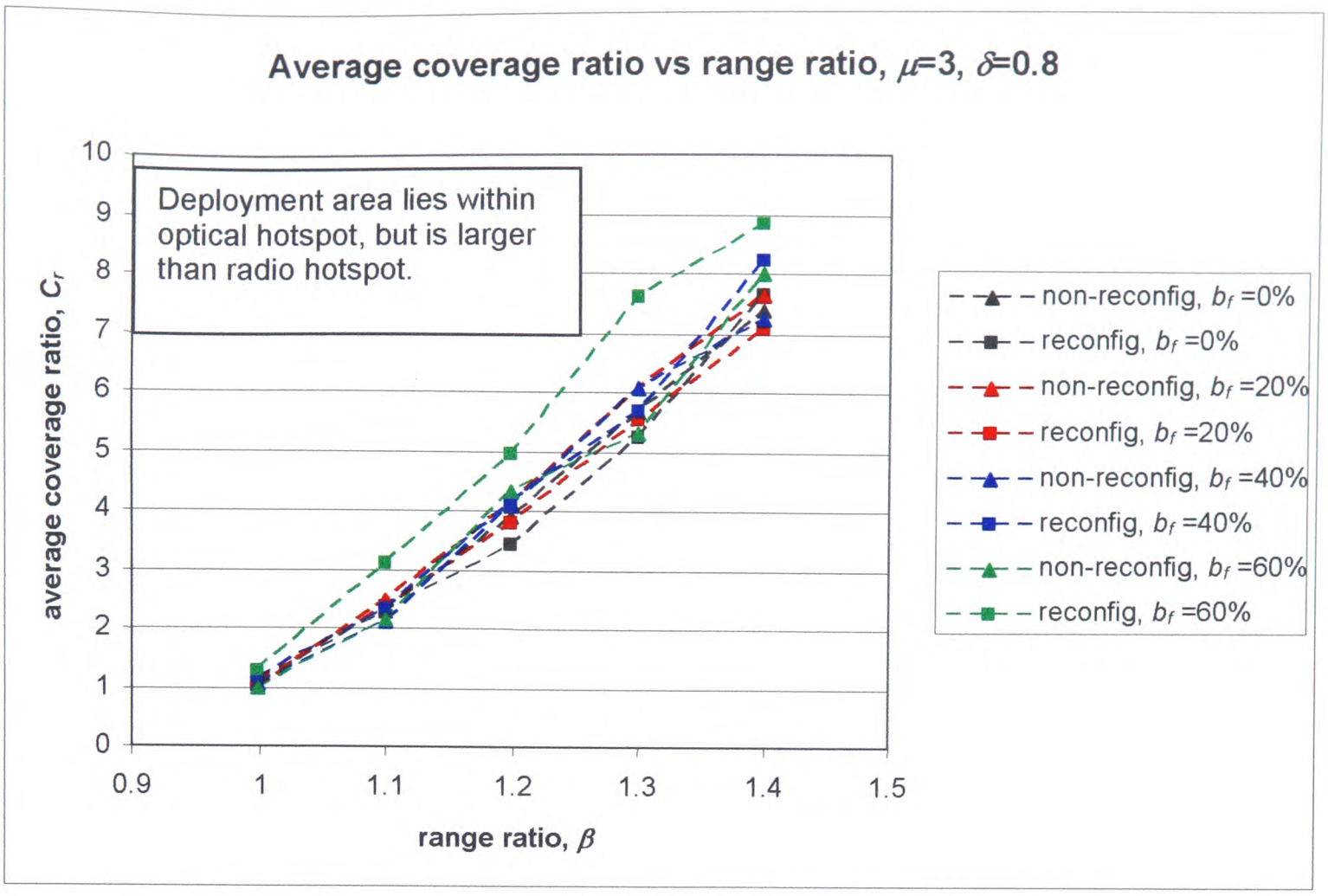

Figure 7.65: Average coverage ratio, C_r, vs range ratio, β, for μ=3, δ=0.8

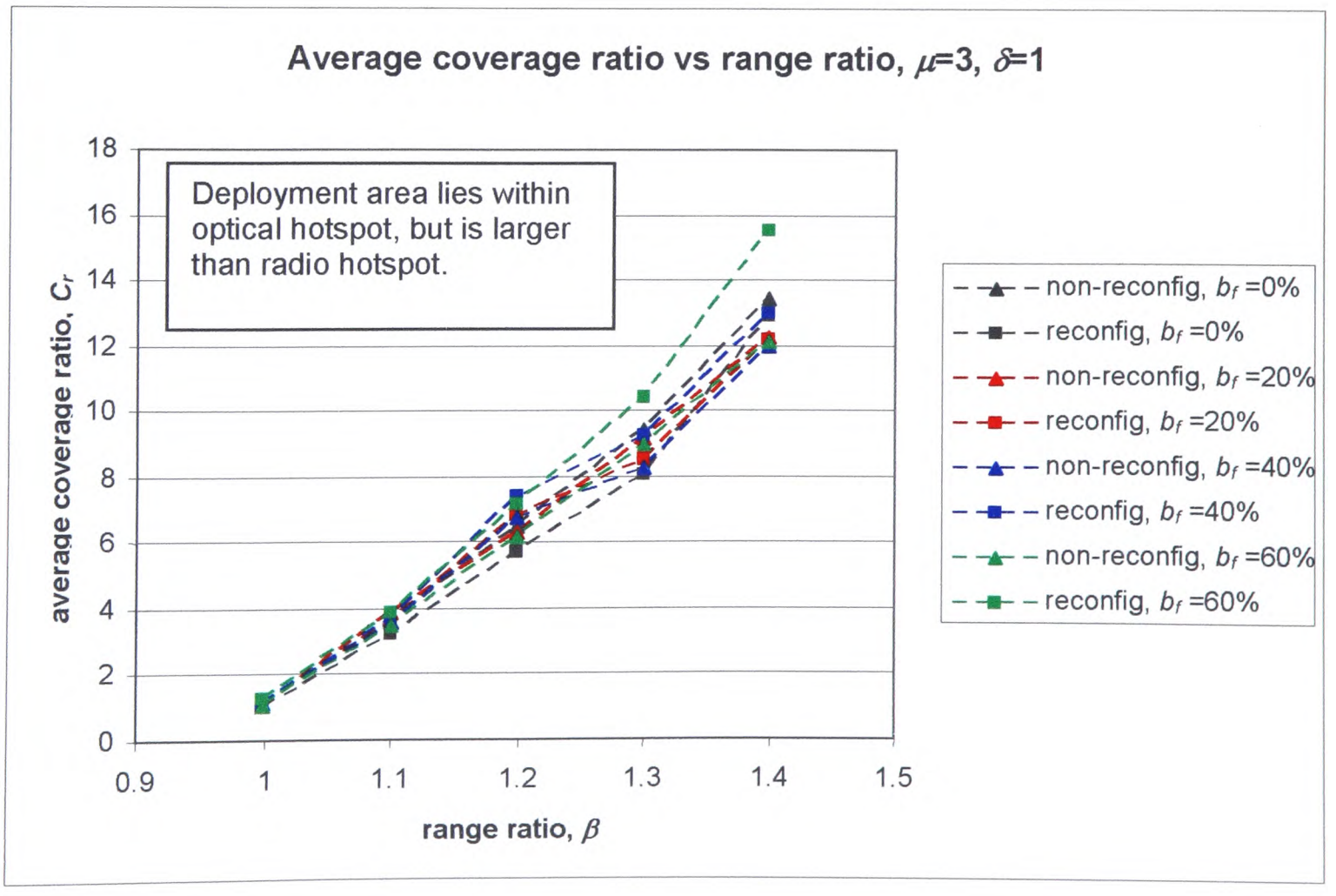

Figure 7.66: Average coverage ratio, C_r, vs range ratio, β, for μ=3, δ=1

Figures 7.67 – 7.71 show that the average coverage area of the RF/FSO WSN for the values of β and b_f considered. The graphs show that the average coverage area is almost constant for the different β considered. This is because as the deployment area increases with β, the number of nodes increases proportionately (as the node density, μ, is fixed at 3). So, similar network connectivity and coverage are maintained as β increases. In Figures 7.67 to 7.71, the average network area coverage decreases as the blocking factor increases and this was discussed in Section 7.5.2.

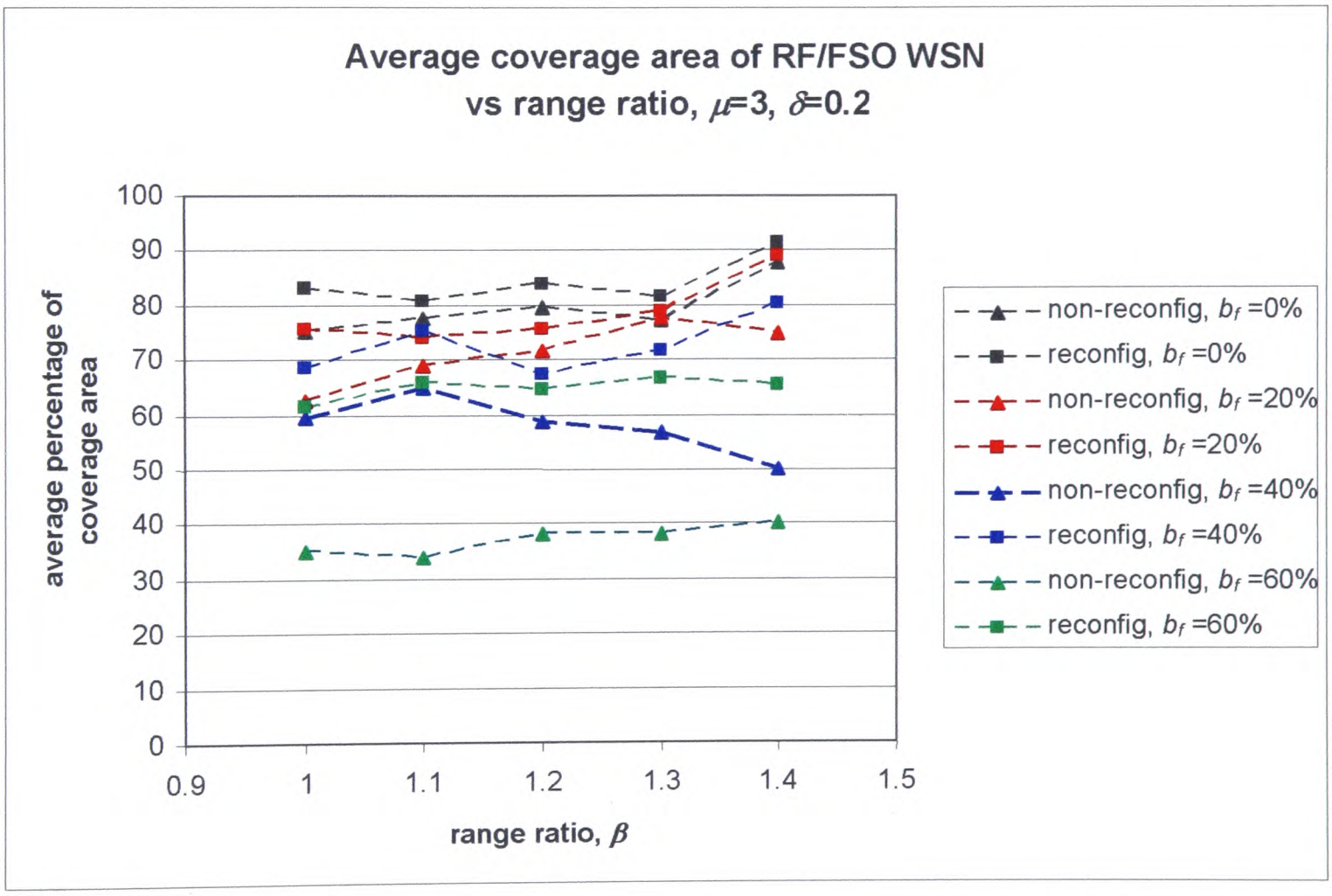

Figure 7.67: Average RF/FSO WSN coverage area vs range ratio β, for node density μ=3, hotspot factor δ=0.2

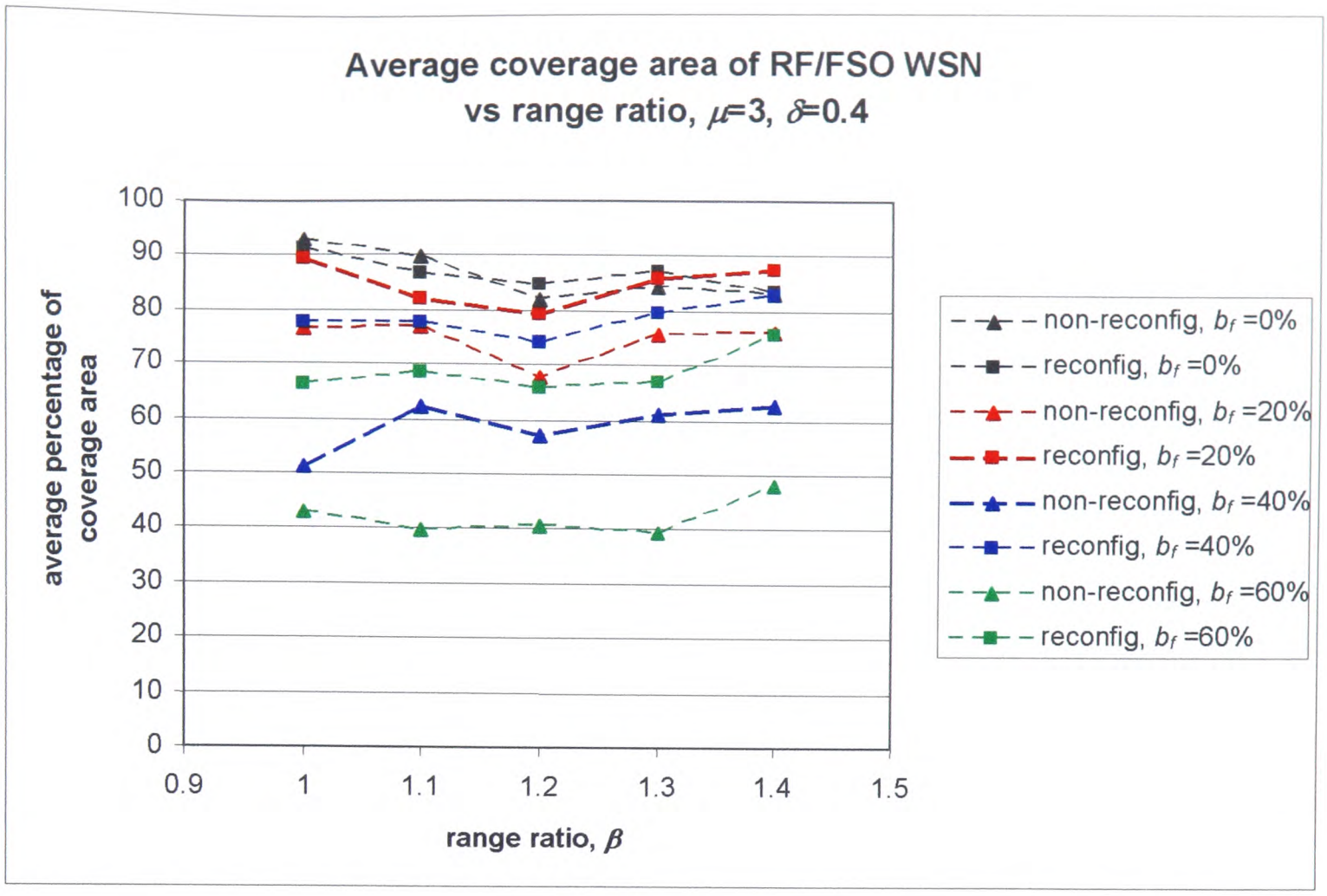

Figure 7.68: Average RF/FSO WSN coverage area vs range ratio, β, for μ=3, δ=0.4

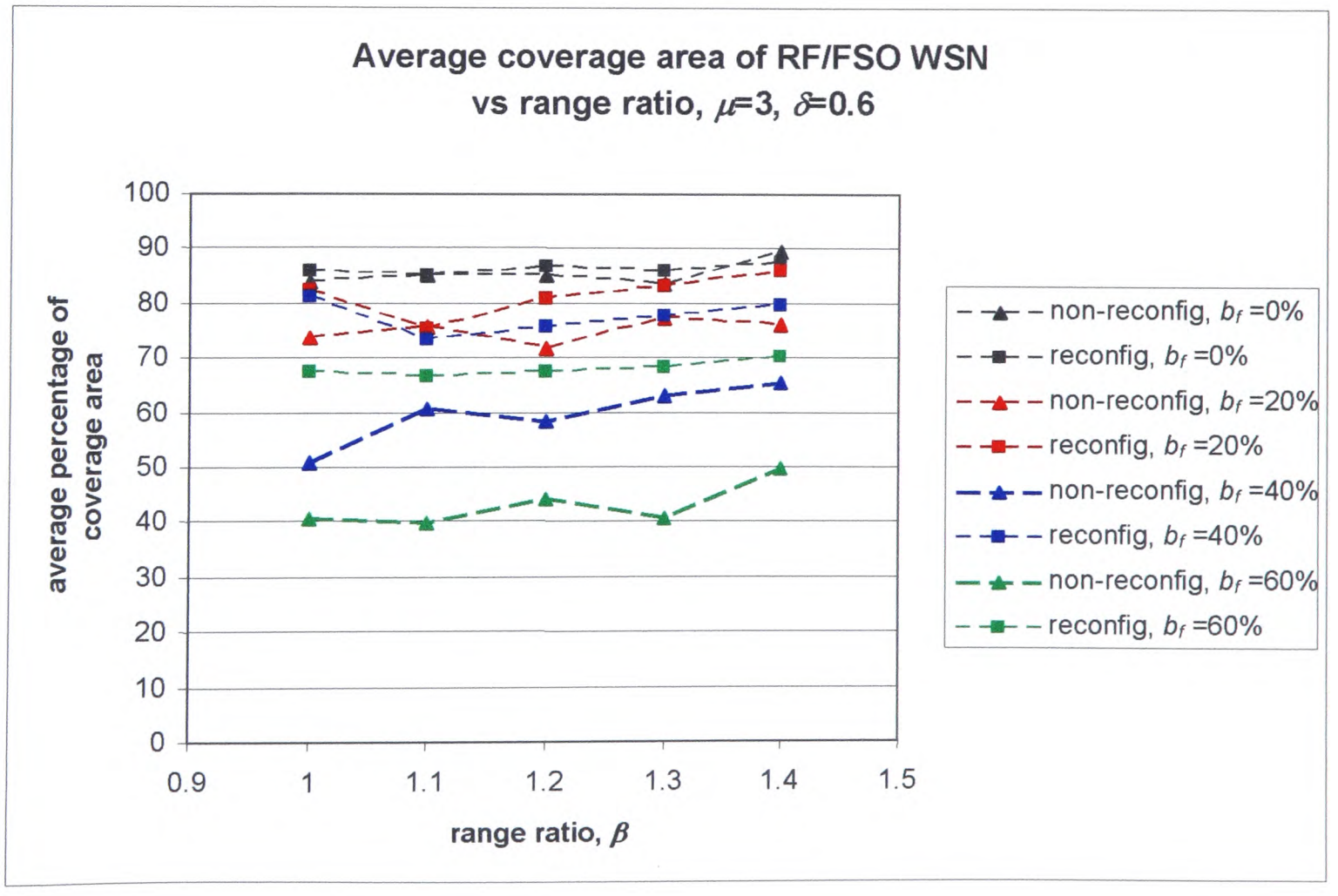

Figure 7.69: Average RF/FSO WSN coverage area vs range ratio, β, for μ=3, δ=0.6

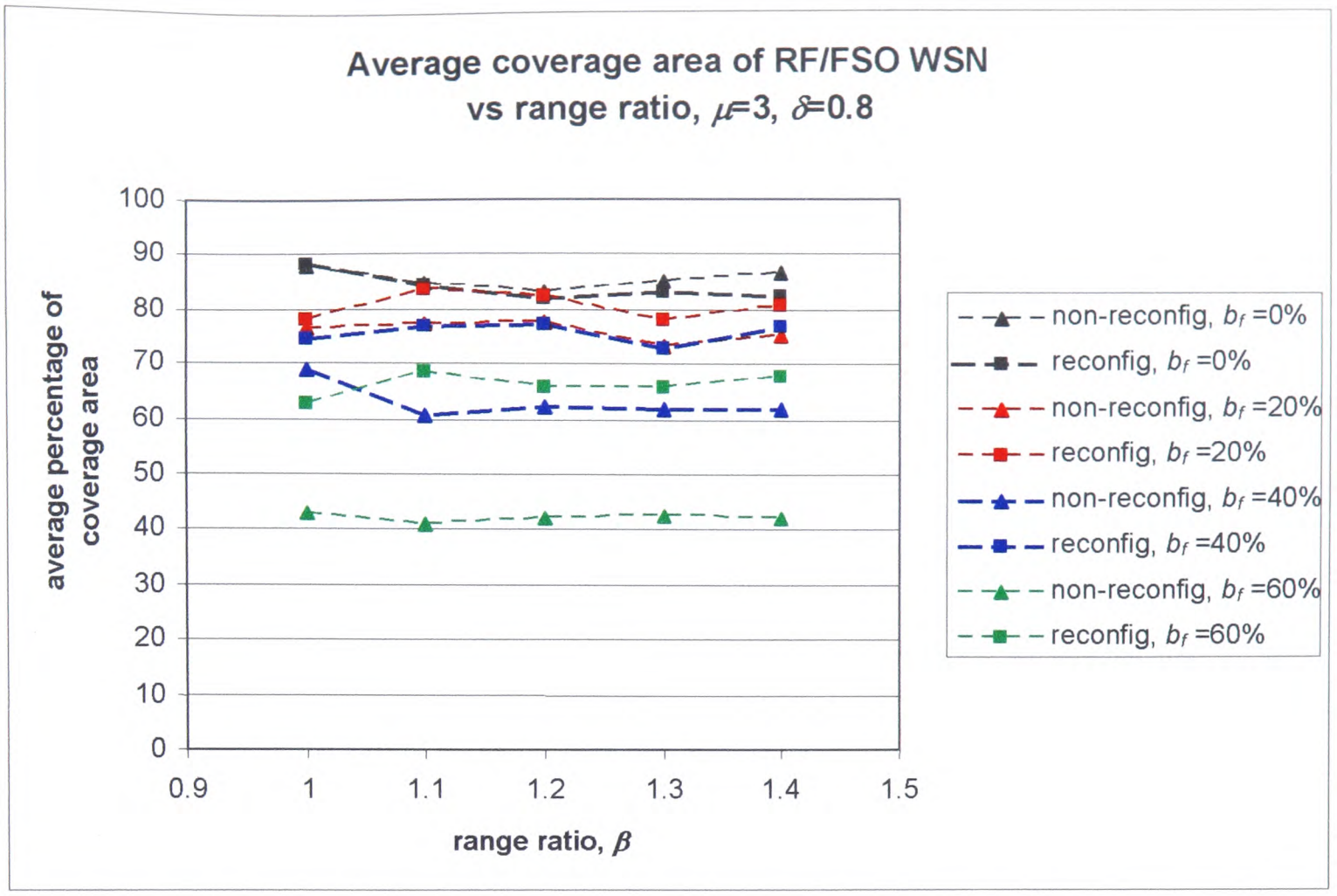

Figure 7.70: Average RF/FSO WSN coverage area vs range ratio, β, for μ=3, δ=0.8

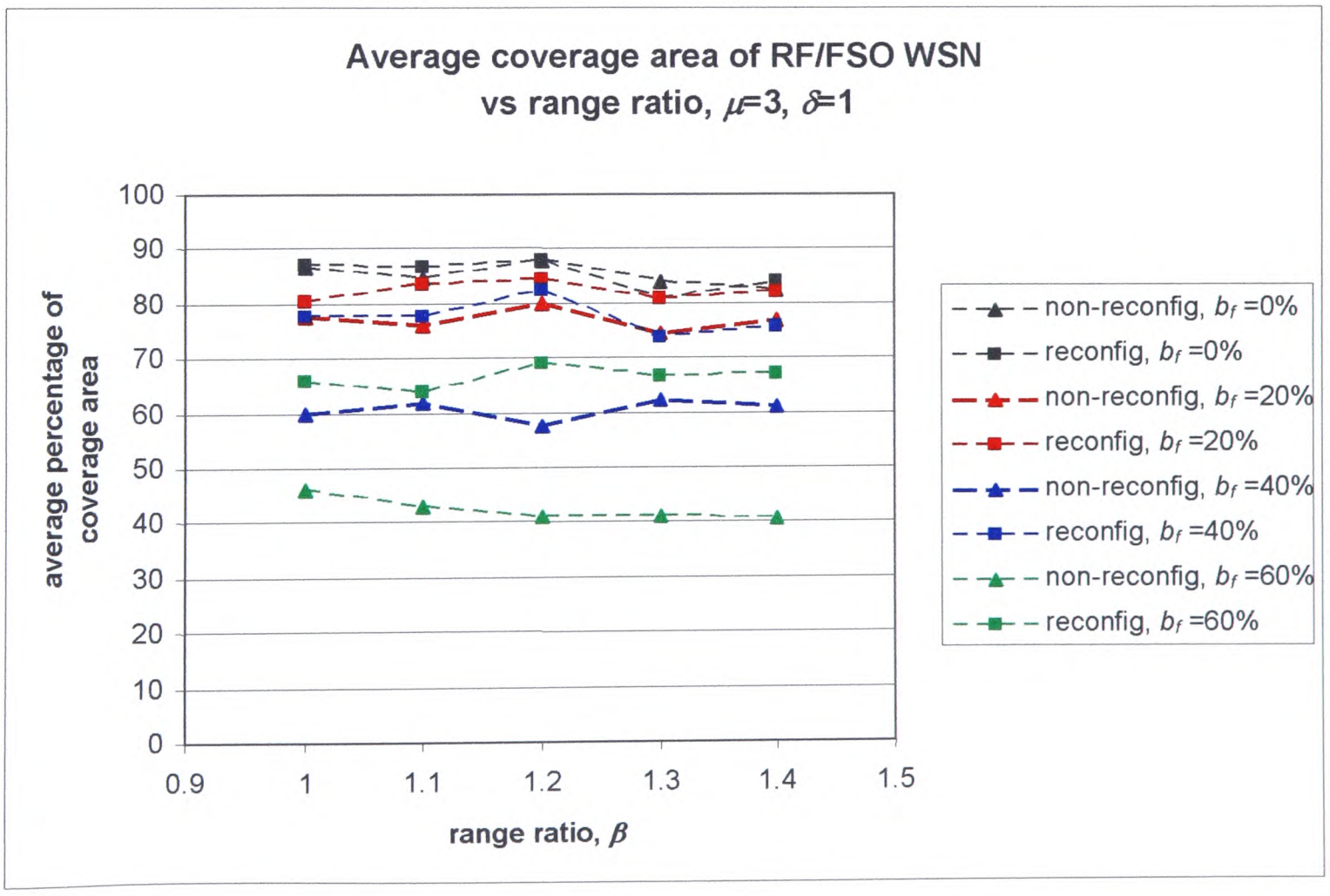

Figure 7.71: Average RF/FSO WSN coverage area vs range ratio, β, for μ=3, δ=1

7.6. A Case study: Comparison between the RF/FSO and LEACH WSNs

In this section, the reconfiguring RF/FSO WSN is compared against a well-known RF-only WSN proposed in the literature – the low-energy adapting clustering hierarchy (LEACH) WSN. The LEACH WSN is described in[22].

7.6.1. Comparing network characteristics

The characteristics of the proposed RF/FSO WSN are compared against a WSN using the LEACH protocol in this section. LEACH is an RF hierarchical-based WSN protocol[2]. It was chosen for comparison as the protocol most closely matched the RF/FSO WSN protocol described in this thesis. However, there are some differences between both the networks.

For the RF/FSO WSN, the cluster heads are selected at the beginning of the network's lifetime, and they continue to serve as cluster heads for their entire lives. Simulations show that when the deployment area is kept within the base station's optical hotspot, and the blocking factor is reasonably low (0%-20%), few nodes require RF multihops for communications. So, few nodes need to serve as cluster heads. When a cluster head dies, nodes in the cluster can find new cluster heads (in reconfiguring networks), so they don't become isolated.

The function of cluster head in the LEACH network is rotated among all nodes, so a cluster head does not die prematurely. For the LEACH protocol, the lifetime is divided into N/k rounds, where N is the number of nodes deployed, and k is the number of nodes elected as cluster heads during a round[22]. The pool of

possible cluster head shrinks, as nodes which have served as cluster heads in the previous set of N/k rounds, will not have to do so again until the next set of N/k rounds. All the nodes are expected to have served as cluster heads at least once after N/k rounds. So every node is eligible to be selected as a cluster head in the following round. The probability that the i-th node is chosen to become a cluster head during round r is given as[22]:

$$P_i = \begin{cases} \dfrac{k}{N - k * \left(r \bmod \dfrac{N}{k} \right)}; & C_i = 1 \\ 0 & ; C_i = 0 \end{cases} \tag{7.11}$$

where C_i is the indicator function used to determine if a node has served as a cluster head during the most recent (r mod (N/k)) rounds. C_i is one if a node has not served as a cluster head, and zero otherwise. Unlike the RF/FSO WSN, cluster heads in the LEACH network are not selected based on their proximity to the base station.

The LEACH protocol does not impose a limit on the RF energy expended for communications, like the RF/FSO protocol. In the LEACH network, nodes are assumed to be able to transmit with enough power if required[22]. In[22], the RF energy expended for transmission is also assumed to be proportional to d^n, with n=2 for $d<d_0$ and n=4 for $d \geq d_0$ as described in Table 2.2.

In[22], the authors attribute the good performance of the LEACH network to the rotation of cluster heads and data aggregation. Sensor nodes with overlapping sensor ranges can generate redundant data[21], and this can be aggregated using techniques like suppression, minima, maxima and averaging[2]. (Data aggregation

was discussed in Section 1.4.1.) A cluster head in the LEACH network performs data aggregation on all the signals it receives from the nodes in its cluster. The LEACH protocol assumes perfect data aggregation, so all signals that reach the cluster head can be aggregated into a single representative signal. This is a significant generalization, as it assumes that most of the data reaching the cluster head has a high degree of correlation and redundancy, and this was acknowledged by the authors in[22]. For the LEACH network, five percent of the nodes are selected to serve as cluster heads for each round. This was found to be the optimum percentage [22]. Therefore, on average, a 100 node network would have 19 nodes (and a cluster head) in each of its five clusters. Perfect data aggregation means that the cluster head aggregates the L-length packets it receives from the nodes in its cluster by a significant factor of 19 (data aggregation factor = 19), before transmitting an L-length representative packet to the base station. The RF-based LEACH network studied in this section is not exactly the same as the RF-only WSN that has been used for comparison throughout the thesis, especially since it employs data aggregation. The RF/FSO WSN presented in this thesis also does not employ data aggregation. A comparison of the characteristics of both the RF/FSO and LEACH wireless sensor networks is given in Table 7.5.

TABLE 7.5
RF/FSO and LEACH: Comparison of network characteristics

Characteristics	**RF/FSO WSN**	**LEACH WSN**
Communication links	Combination of RF and FSO links	RF links only
Base station	Must be elevated for FSO communications	Can be at same level with deployed nodes
Maximum transmitted RF energy	Imposed on RF links	Not imposed on RF links
Data aggregation	Not employed	Employed

Election of cluster heads	Cluster heads selected at start of network life, serve for life	Cluster heads rotated
Node power source	All nodes equipped with identical power sources	All nodes equipped with identical power sources

7.6.2. Network simulations

In this section, the network simulations of the LEACH and the RF/FSO WSNs are described. The reconfiguring RF/FSO WSN was shown to perform better than the non-reconfiguring network in earlier discussions in the chapter, and is therefore considered for the simulations in this section. The energy consumption model given in Table 6.1 is used for the simulations in this section. For the LEACH network, the base station does not have to be elevated, and is assumed to be at level with the deployed nodes[22]. Only the peer-to-peer communication from Table 6.1 is considered for the LEACH network. As the base station is on the ground, the node to base station RF model in the LEACH network is similar to the peer-to-peer RF model (described in Table 6.1). The energy expended for data aggregation is set to 5nJ/bit for every input signal to the cluster head as proposed in[22]. A data aggregation factor of 19 is assumed for the LEACH network simulation.

The data rate in sensor networks is quite low – several hundred bits per second per node[46]. For the simulations, the data rate is set to 200 bits per second. The data packet length is set to 200 bits. Every node is supplied with 1mJ of energy, as is the case in Section 7.5. The deployment area radius is set to 40m for both networks. The base station is 30m above the centre of the deployment area for the RF/FSO WSN. The blocking factor is set to 20%, to simulate a deployment area with

fairly good visibility of the base station. For the LEACH simulations, the base station is assumed to be in the middle of the deployment area. Each round in the LEACH network is set to last for 20 seconds, as suggested in[22]. The number of nodes is set to 100, with five cluster heads for each round. Both networks are simulated for 400 seconds. The definitions for node failure and network lifetime are defined in Table 7.2 and a summary of the network parameters used in this section is given in Table 7.6.

TABLE 7.6
Parameters for network simulation

Parameter	**Value**
number of deployed nodes, N	100
deployment area radius, R	40m
base station height, h (RF/FSO WSN)	30m
blocking factor, b_f (RF/FSO WSN)	20%
data rate	200 bps
packet length	200 bits
round duration (LEACH WSN)	20s
node energy supply	1mJ

Figures 7.72 and 7.73 show the network lifetimes of the reconfiguring RF/FSO and the LEACH WSNs respectively. For the LEACH network, five nodes are selected to serve as cluster heads during each round. As the network starts to die, each round may have fewer than five cluster heads functioning, as some may have run out of power[22]. This can be seen in Figure 7.73. At t=232s in Figure 7.73, almost all the nodes are dead. As the nodes elected to serve as cluster heads are dead, the network becomes isolated from the base station and network coverage is zero.

However, a few nodes are still alive and function very briefly at t=300s before also succumbing. This is shown as a short spike at about t=300s in Figure 7.73.

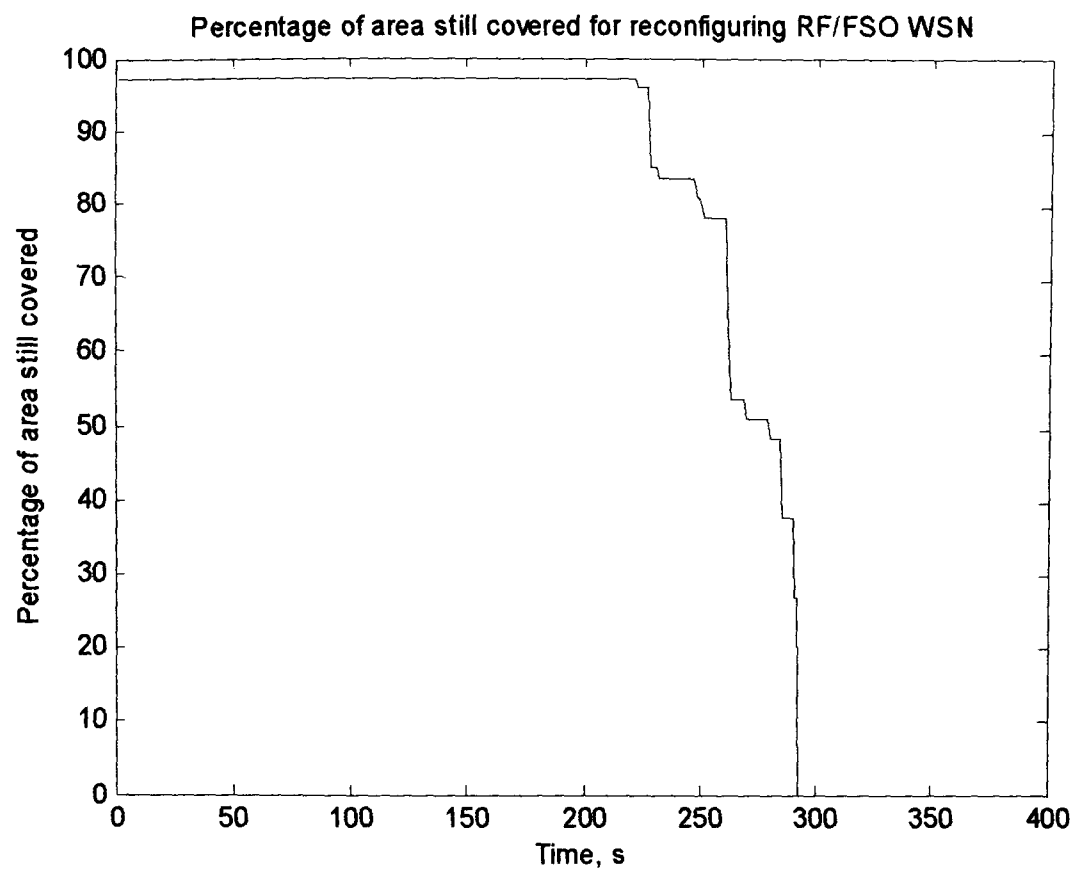

Figure 7.72: Lifetime of reconfiguring RF/FSO WSN

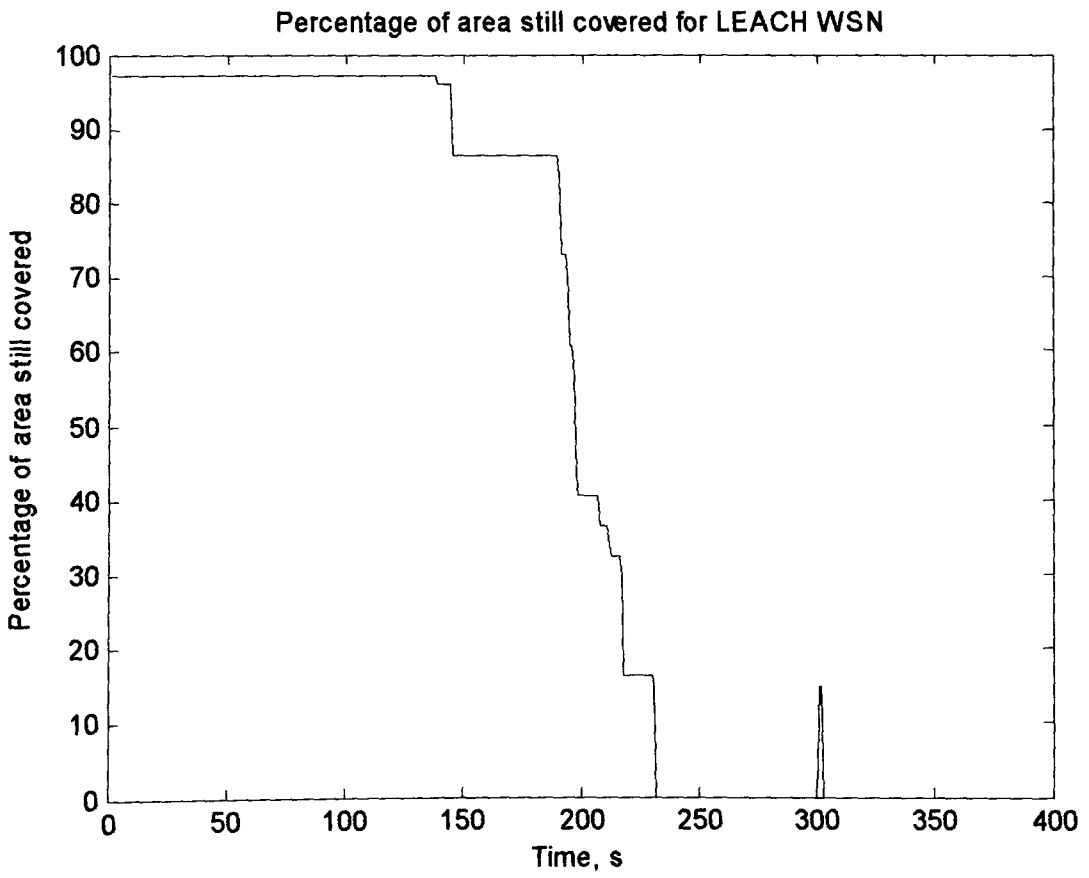

Figure 7.73: Lifetime of LEACH WSN

Table 7.7 summarizes the simulation results for both networks. The RF/FSO WSN lasts about 1.3 times as long as the LEACH network. The average lifetime network coverage of the RF/FSO WSN is also marginally better than that of the LEACH network.

TABLE 7.7
RF/FSO and LEACH: Network performance

Sensor network	**Lifetime**	**Average network coverage (over network lifetime)**
Reconfiguring RF/FSO WSN	293 s	90.0%
LEACH WSN	232 s	83.7%

Perfect data aggregation is assumed for the LEACH WSN, and this presumes that there is a high degree of redundancy in the signals that reach a cluster head. This may not always be the case in practical applications. However, despite not performing data aggregation, the reconfiguring RF/FSO WSN still lasts longer and has a better average coverage than the LEACH WSN. This analysis shows that the RF/FSO network has the potential to function better than existing high performance designs. Data aggregation could potentially increase the lifetime of the RF/FSO WSN, and this has been proposed as a future area of research in Chapter 8.

7.7. Conclusions

This chapter studied the lifetime and network coverage performance of the RF/FSO WSN. A wide range of network geometries was considered by varying the blocking factor b_f, node density μ, hotspot factor δ and range ratio β.

The simulations show that the RF/FSO WSN lasts at least twice as long as the RF-only WSN for the range of scenarios considered. Despite having a longer lifetime, the average network coverage area of the RF/FSO WSN is approximately equal or better than that of the RF-only WSN for the range of topologies considered. This shows the potential for WSNs with significantly longer lifetimes.

Simulations show that the best RF/FSO network coverage is achieved when the blocking factor is low and the node density is high. For low blocking factors, increasing the node density beyond six offers little improvement to network coverage. The deployment area of the RF/FSO WSN should be kept within the base station's optical hotspot. Simulations also show that as $\beta>1$ (due to the longer d_{OPT}), the RF/FSO WSN is better able to support larger deployment areas than the RF-only WSN. From the simulation results, network reconfiguration is most beneficial when the blocking factor is high.

A case study was performed to compare the reconfiguring RF/FSO WSN with the well-known RF-based LEACH WSN. Simulations showed that the reconfiguring RF/FSO WSN had a larger average coverage area and 26% longer lifetime than the LEACH network. The LEACH network performance calculated is very optimistic, as it considers perfect data aggregation by the cluster heads. This indicates that the RF/FSO WSN has the potential to significantly outperform realistic RF-based WSN networks.

In the next chapter, conclusions are drawn from the work, and possible further work is suggested.

Chapter 8

Conclusions and Further Work

8.1. Conclusions

This section provides a summary of the work presented in this thesis, which is followed by a discussion on the contributions of the thesis.

Chapter 1 provided an introduction to wireless sensor networks. The sensor node architecture and phases in the lifetime of the WSN were discussed. Several WSN design challenges were discussed and energy consumption was identified as an important consideration for WSNs. The chapter also introduced the RF/FSO WSN architecture as a means of potentially reducing the overall power consumption of the wireless sensor network. The various components of the network were then analysed.

Chapter 2 studied the RF links which were used in the network simulations. Three types of RF channels were introduced: the peer-to-peer channel between nodes on the ground and the node to base station channels – with and without line of sight. The RF channel propagation and fading models were discussed. The direct conversion receiver was assumed for simulations. The RF energy transmitted by the individual nodes was capped to encourage multihop routing. This meant that there was a maximum radio range over which the sensor node could transmit to fulfil

performance requirements. The maximum ranges for peer-to-peer RF communications and node to base station RF communications were derived for use in later simulations.

Chapter 3 studied the FSO link models which were used in the simulations. The modulating retroreflector (MMR) was introduced as a passive optical transmitter which would be used for the RF/FSO WSNs. Several MMR designs were discussed. The corner cube retroreflector was chosen as the MMR device for the WSN. The parameters used to simulate the FSO channel were introduced and the maximum FSO communications range was derived for network simulations.

Chapter 4 discussed how the RF/FSO WSN and the RF-only WSN configured themselves. It also described how the network configurations were simulated using MATLAB.

Chapter 5 discussed the sensor node energy models used for the simulations. It discussed the energy models used for communications, data processing and sensing. Models were determined for the non-cluster head WSN nodes, the RF-only WSN cluster head nodes and the RF/FSO WSN gateway nodes. Typical values of energy expended for node communications, data processing and sensing were then determined for simulations.

Chapter 6 discussed the simulation of network traffic and energy consumption of the RF/FSO and RF-only WSNs. The data reporting technique

adopted was discussed. The assumptions and methodology used to simulate network traffic was also discussed. To compare the energy consumption of both the RF/FSO and RF-only WSN, the mean ratio E_R was introduced. The simulation results show that the energy expended by the RF/FSO WSN is less than that of the RF-only WSN.

Chapters 2 - 6 discussed the models to be used for the network simulations. Chapter 7 discussed the results of the simulations. In Chapter 7 the lifetime and network coverage of the RF/FSO WSN was studied and compared against a traditional RF-based WSN. A number of network parameters was introduced to study the coverage and lifetime of the RF/FSO WSN: the blocking factor b_f, the hotspot factor δ, the range ratio β and node density μ. Two types of networks were considered: reconfiguring and non-reconfiguring networks.

The simulations show that for the wide range of scenarios considered, the proposed RF/FSO WSN reduces the overall energy consumption of the RF-only WSN. The lifetime of the RF/FSO WSN is at least twice as long as the RF-only WSN. When the blocking factor is not high, the RF/FSO WSN is able to match the lifetime network coverage of the RF-only WSN. Simulations also show that due to the longer optical communications range of the RF/FSO WSN, it is better able to support larger deployment areas than the RF-only WSN.

The selection of suitable network parameters for optimum RF/FSO WSN network performance was also studied. Simulations show that the best RF/FSO network coverage is achieved when the blocking factor is low and the node density is

high. However, when the blocking factor is low, simulations suggest that increasing the node density beyond six offers little improvement to network coverage. Better network coverage is also achieved when the deployment area is kept within the base station's optical hotspot. The simulation results suggest that network reconfiguration is most beneficial when the blocking factor is high. For reconfiguring networks, the RF/FSO WSN performs better than RF-only WSN for high blocking factors. A case study comparing the reconfiguring RF/FSO WSN and the LEACH WSN suggests that the reconfiguring RF/FSO WSN has a longer lifetime and larger average network coverage than the LEACH WSN.

The novel contributions of the thesis are as follows:

- A detailed study of a novel radio frequency and free space optical wireless sensor network (RF/FSO WSN), which could potentially reduce the total energy expended by current WSNs. To the best of the author's knowledge, a network of this type has not been studied previously.
- A comparison study between the performance of the RF/FSO WSN and an RF-only WSN, in terms of average energy consumption, network lifetime and network coverage.
- A comparison with an existing network in the literature, showing the advantages of the proposed RF/FSO WSN
- A guide to selecting suitable network parameters for optimum RF/FSO WSN network performance. This includes advice on selecting node densities and an appropriately-sized deployment area.

- A performance study, comparing the RF/FSO reconfiguring and non-reconfiguring network performance.

8.2. Further work

A possible area of further work would be to introduce data aggregation into the network. The results presented in this thesis show that increasing node density ensures a higher WSN network coverage for a longer time. However, this generates a lot of redundant data. Data processing consumes less energy than data communication[20]. If cluster heads aggregate data before sending it to the next cluster head or base station, the overall energy expended by the network could potentially be reduced.

To avoid redundant nodes, some nodes could also be forced to remain dormant until required. When the number of nodes alive drops below a certain threshold, these dormant nodes would wake up to replace dead nodes in the network, ensuring that network coverage disruption was kept to a minimum. This keeps data redundancy to a minimum whilst preserving network coverage.

The work in this thesis also assumed that a base station was available throughout the period of network operation. An area of potential research is to study how the network behaves when the base station communicates only intermittently with the sensor network. For example, the base station could be a light unmanned aircraft which visits the deployment area every few weeks to harvest data. For this, the network needs to be equipped with sufficient memory to store data before the

data can be relayed to the base station. The aircraft visits need to be sufficiently frequent so the limited memory resources of the nodes are not exhausted.

Preliminary investigations on commercial RF-based sensor nodes available were performed during the research, and controlling them proved to be challenging. Equipping a node with RF and FSO communication capabilities to show the benefits of an RF/FSO WSN may be difficult. However, the practical implementation of an RF/FSO node is an avenue for further research. Currently, researchers in the Communications Group at the University of Oxford are designing a WSN sensor node which will operate using optical links. This optical-based sensor node could be integrated with an RF-based sensor node, to assemble an RF/FSO WSN sensor node. There are a number of RF-based sensor nodes which are available commercially. An established commercial provider of radio sensor node platforms is Crossbow Technology [150] and a wide range of RF-based sensor nodes (or radio motes as the company markets them) is available. BTnode, developed by ETH Zurich, is a sensor node based on Bluetooth radio[151]. Sun SPOT, developed by Sun Microsystems Laboratories, is a sensor node operating in the 2.4GHz radio band[152]. Both BTnode and Sun SPOT are also available commercially.

References

[1] D. Estrin, R. Govindan, J. Heidemann, and S. Kumar, "Next century challenges: Scalable coordination in sensor networks," in *Proc. MobiCom*, 1999, pp. 263-270.

[2] J. N. Al-Karaki and A. E. Kamal, "Routing techniques in wireless sensor networks: a survey," *IEEE Wireless Communications*, vol. 11, pp. 6-28, 2004.

[3] A. Bogdanov, E. Maneva, and S. Riesenfeld, "Power-aware base station positioning for sensor networks," in *Proc. INFOCOM*, 2004, pp. 575-585.

[4] M. Wu, J. Xu, and X. Tang, "Processing Precision-Constrained Approximate Queries in Wireless Sensor Networks," in *Proc. 7th International Conference on Mobile Data Management*, 2006, Paper 31.

[5] K. Romer and F. Mattern, "The design space of wireless sensor networks," *IEEE Wireless Communications*, vol. 11, pp. 54-61, 2004.

[6] Yi Jen Lu and Tsang Ling Sheu, "An efficient routing scheme with optimal power control in wireless multi-hop sensor networks," *Computer Communications*, vol. 30, pp. 2735-2743, 2007.

[7] I. F. Akyildiz, Weilian Su, Y. Sankarasubramaniam, and E. Cayirci, "A survey on sensor networks," *IEEE Communications Magazine*, vol. 40, pp. 102-114, 2002.

[8] Qiangfeng Jiang and D. Manivannan, "Routing protocols for sensor networks," in *Proc. 1st IEEE Consumer Communications and Networking*

Conference, 2004, pp. 93-98.

[9] M. A. M. Vieira, C. N. Coelho, Jr., D. C. da-Silva, Jr., and J. M. da-Mata, "Survey on wireless sensor network devices," in *Proc. IEEE Conference on Emerging Technologies and Factory Automation*, 2003, vol. 1, pp. 537-544.

[10] C. Intanagonwiwat, R. Govindan, and D. Estrin, "Directed diffusion: A scalable and robust communication paradigm for sensor networks," in *Proc. MobiCom*, 2000, pp. 56-67.

[11] S. Vardhan, M. Wilczynski, G. J. Portie, and W. J. Kaiser, "Wireless integrated network sensors (WINS): distributed in situ sensing for mission and flight systems," in *Proc. IEEE Aerospace Conference*, 2000, vol. 7, pp.459-463.

[12] J. M. Rabaey, M. J. Ammer, J. L. da-Silva, Jr., D. Patel, and S. Roundy, "PicoRadio supports ad hoc ultra-low power wireless networking," *Computer*, vol. 33, pp. 42-48, 2000.

[13] A. Chandrakasan, R. Amirtharajah, Seonghwan Cho, J. Goodman, G. Konduri, J. Kulik, W. Rabiner, and A. Wang, "Design considerations for distributed microsensor systems," in *Proc. IEEE Custom Integrated Circuits Conference*, 1999, pp. 279-286.

[14] S. Roundy, P. K. Wright, and J. Rabaey, "A study of low level vibrations as a power source for wireless sensor nodes," *Computer Communications*, vol. 26, pp. 1131-1144, 2003.

[15] P. Bonnet, J. Gehrke, and P. Seshadri, "Querying the physical world," *IEEE Personal Communications*, vol. 7, pp. 10-15, 2000.

[16] L. Zhou, J. M. Kahn, and K. S. J. Pister, "Corner-cube retroreflectors based

on structure-assisted assembly for free-space optical communication," *Journal of Microelectromechanical Systems,* vol. 12, pp. 233-242, 2003.

[17] J. M. Kahn, R. H. Katz, and K. S. Pister, "Next century challenges: Mobile networking for smart dust," in *Proc. MobiCom,* 1999, pp. 271-278.

[18] X. Ji and H. Zha, "Robust sensor localization algorithm in wireless ad-hoc sensor networks," in *Proc. 12th International Conference on Computer Communications and Networks*, 2003, pp. 527-532.

[19] G. J. Pottie and W. J. Kaiser, "Wireless Integrated Network Sensors," *Communications of ACM*, vol. 43, pp. 551-558, 2000.

[20] I. F. Akyildiz, Weilian Su, Y. Sankarasubramaniam, and E. Cayirci, "Wireless sensor networks: a survey," *Computer Networks*, vol. 38, pp. 393-422, 2002.

[21] H. Cam, S. Ozdemir, P. Nair, D. Muthuavinashiappan, and H. Sanli, "Energy-efficient secure pattern based data aggregation for wireless sensor networks," *Computer Communications*, vol. 29, pp. 446-455, 2006.

[22] W. B. Heinzelman, A. P. Chandrakasan, and H. Balakrishnan, "An application-specific protocol architecture for wireless microsensor networks," *IEEE Transactions on Wireless Communications*, vol. 1, pp. 660-670, 2002.

[23] C. Intanagonwiwat, D. Estrin, R. Govindan, and J. Heidemann, "Impact of network density on data aggregation in wireless sensor networks," in *Proc. 22nd International Conference on Distributed Computing Systems*, 2002, pp. 457-458.

[24] E. M. Petriu, N. D. Georganas, D. C. Petriu, D. Makrakis, and V. Z. Groza, "Sensor-based information appliances," *IEEE Instrumentation and*

Measurement Magazine, vol. 3, pp. 31-35, 2000.

[25] Chien Chung Shen, C. Srisathapornphat, and C. Jaikaeo, "Sensor information networking architecture and applications," *IEEE Personal Communications*, vol. 8, pp. 52-59, 2001.

[26] D. Nadig, S. S. Iyengar, and D. N. Jayasimha, "A new architecture for distributed sensor integration," in *Proc. IEEE Southeastcon*, 1993, Paper 12.

[27] G. Hoblos, M. Staroswiecki, and A. Aitouche, "Optimal design of fault tolerant sensor networks," in *Proc. IEEE International Conference on Control Applications*, 2000, pp. 467-472.

[28] V. P. Mhatre, C. Rosenberg, D. Kofman, R. Mazumdar, and N. Shroff, "A minimum cost heterogeneous sensor network with a lifetime constraint," *IEEE Transactions on Mobile Computing*, vol. 4, pp. 4-15, 2005.

[29] D. Kedar and S. Arnon, "Non-line-of-sight optical wireless sensor network operating in multiscattering channel," *Applied Optics*, vol. 45, pp. 8454-8461, 2006.

[30] K. Akkaya and M. Younis, "A survey on routing protocols for wireless sensor networks," *Ad Hoc Networks*, vol. 3, pp. 325-349, 2005.

[31] W. R. Heinzelman, A. Chandrakasan, and H. Balakrishnan, "Energy-efficient communication protocol for wireless microsensor networks," in *Proc. Hawaii International Conference on System Sciences*, 2000, vol. 2: Mobile computing and wireless networks, Paper 1.

[32] S. Lindsey and C. S. Raghavendra, "PEGASIS: power-efficient gathering in sensor information systems," in *Proc. IEEE Aerospace Conference*, 2002, vol. 3, pp. 1125-1130.

[33] A. Manjeshwar and D. P. Agarwal, "APTEEN: A Hybrid Protocol for Efficient Routing and Comprehensive Information Retrieval in Wireless Sensor Networks," in *Proc. International Parallel and Distributed Processing Symposium*, 2002, pp. 195-202.

[34] A. Manjeshwar and D. P. Agarwal, "TEEN: A Routing Protocol for Enhanced Efficiency in Wireless Sensor Networks," in *Proc. 15th International Parallel and Distributed Processing Symposium*, 2001, pp. 2009-2015.

[35] V. Rodoplu and T.H. Meng, "Minimum energy mobile wireless networks," *IEEE Journal on Selected Areas in Communications*, vol. 17, pp. 1333-1344, 1999.

[36] F. Ye, H. Luo, J. Cheng, S. Lu, and L. Zhang, "A two-tier data dissemination model for large-scale wireless sensor networks," in *Proc. 8th Annual International conference on mobile computing and networking*, 2002, pp. 148-159.

[37] L. B. Ruiz, J. M. Nogueira, and A. A. F. Loureiro, "MANNA: a management architecture for wireless sensor networks," *IEEE Communications Magazine*, vol. 41, pp. 116-125, 2003.

[38] Sencun Zhu, S. Setia, S. Jajodia, and Peng Ning, "An interleaved hop-by-hop authentication scheme for filtering of injected false data in sensor networks," in *Proc. IEEE Symposium on Security and Privacy*, 2004, pp. 259-271.

[39] L. Subramanian and R. H. Katz, "An architecture for building self-configurable systems," in *Proc. First Annual Workshop on Mobile Ad Hoc Networking Computing*, 2000, pp. 63-73.

[40] S. De, Chunming Qiao, D. A. Pados, M. Chatterjee, and S. J. Philip, "An

integrated cross-layer study of wireless CDMA sensor networks," *IEEE Journal on Selected Areas in Communications*, vol. 22, pp. 1271-1285, 2004.

[41] J. N. Al-Karaki, R. Ul-Mustafa, and A. E. Kamal, "Data aggregation in wireless sensor networks - exact and approximate algorithms," in *Proc. IEEE Workshop on High Performance Switching and Routing*, 2004, pp. 241-245.

[42] http://www.intel.com/research/exploratory/heterogeneous.htm

[43] M. M. Iqbal, L. Gondal, and L. Dooley, "LACON: localized autonomic configuration in pervasive sensor networks," in *Proc. Intelligent Sensors, Sensor Networks and Information Processing Conference*, 2004, pp. 31-36.

[44] Q. Dong, "Maximizing system lifetime in wireless sensor networks," in *Proc. 4th Int. Symposium on Information Processing in Sensor Networks*, 2005, pp. 13-19.

[45] N. Noury, T. Herve, V. Rialle, G. Virone, E. Mercier, G. Morey, A. Moro, and T. Porcheron, "Monitoring behavior in home using a smart fall sensor and position sensors," in *Proc. 1st Annual International IEEE EMBS Special Topic Conference on Microtechnologies in Medicine and Biology*, 2000, pp. 607-610.

[46] R. C. Shah and J. M. Rabaey, "Energy aware routing for low energy ad hoc sensor networks," in *IEEE Wireless Communications and Networking Conference Record*, 2002, vol. 1, pp. 350-355.

[47] J. Carle and D. Simplot, "Energy-efficient area monitoring for sensor networks," *Computer*, vol. 37, pp. 40-46, 2004.

[48] I. I. Kim and E. Korevaar, "Availability of free space optics (FSO) and hybrid FSO/RF systems," in *Proc. SPIE Optical Wireless Communications IV*, 2001,

vol. 4530, pp. 84-95.

[49] J. Llorca, A. Desai, E. Baskaran, and S. Milner, "Optimizing performance of hybrid FSO/RF networks in realistic dynamic scenarios," in *Proc. SPIE Free-Space Laser Communications V*, 2005, vol. 5892, pp. 52-60.

[50] Tzung Hsien Ho, S. Trisno, A. Desai, J. Llorca, S. D. Milner, and C. C. Davis, "Performance and analysis of reconfigurable hybrid FSO/RF wireless networks," in *Proc. SPIE Free-Space Laser Communication Technologies XVII*, 2005, vol. 5712, pp. 119-130.

[51] J. Cartigny, D. Simplot-Ryl, and I. Stojmenovic, "An adaptive localized scheme for energy-efficient broadcasting in ad hoc networks with directional antennas," in *Proc. 9th International Conference on Personal Wireless Communications*, 2004, vol. 3260, pp. 399-413.

[52] W. S. Rabinovich, G. Gilbreath, P. G. Goetz, R. Mahon, D. Katzer, K. Ikossi-Anastasiou, S. C. Binari, T. J. Meehan, M. F. Stell, I. Sokolsky, J. A. Vasquez, and M. J. Vilcheck, "InGaAs multiple quantum well modulating retroreflector for free-space optical communications," in *Proc. SPIE Free-Space Laser Communication and Laser Imaging*, 2002, vol. 4489, pp. 190-201.

[53] H. Wu, B. Hamzeh, and M. Kavehrad, "Availability of airborne hybrid FSO/RF links," in *Proc. SPIE Digital Wireless Communications VII and Space Communication Technologies*, 2005, vol. 5819, pp. 89-100.

[54] P. Sharma, "Channel-state based scheduling in wireless sensor networks for reliable transmission," in *Proc. 19th IEEE Int. Parallel and Distributed Processing Symposium*, 2005, Paper 340.

[55] Tsung Hsien Lin, W. J., Kaiser, and G. J. Pottie, "Integrated low-power communication system design for wireless sensor networks," *IEEE Communications Magazine*, vol. 42, pp. 142-150, 2004.

[56] Ke Liu and A. M. Sayeed, "Asymptotically optimal decentralized type-based detection in wireless sensor networks," in *Proc. IEEE International Conference on Acoustics, Speech, and Signal Processing*, 2004, vol. 3, pp. 873-876.

[57] Xiaohua Li, "Blind channel estimation and equalization in wireless sensor networks based on correlations among sensors," *IEEE Transactions on Signal Processing*, vol. 53, pp. 1511-1519, 2005.

[58] Man Wah Chiang, Z. Zilic, K. Radecka, and J. S. Chenard, "Architectures of increased availability wireless sensor network nodes," in *Proc. IEEE Int. Test Conference*, 2004, pp. 1232-1241.

[59] E. Shih, S. Cho, N. Ickes, R. Min, A. Sinha, A. Wang, and A. Chandrakasan, "Physical layer driven protocol and algorithm design for energy-efficient wireless sensor networks," in *Proc. 7th annual Int. Conference on Mobile Computing and Networking*, 2001, pp. 272-287.

[60] T. S. Rappaport, *Wireless communications: principles and practice*, 2nd ed. Upper Saddle River, NJ: Prentice Hall, 2002.

[61] J. G. Proakis, *Digital communications*, 4th ed. New York, NY: McGraw-Hill, 2001.

[62] I. A. Glover and P. M. Grant, *Digital Communications*, 1st ed. Cornwall: Prentice Hall, 1998.

[63] M. K. Simon and M. S. Alouini, "A unified approach to the performance

analysis of digital communication over generalized fading channels," *Proceedings of the IEEE*, vol. 86, pp. 1860-1877, 1998.

[64] J. M. Molina-Garcia-Pardo, A. Martinez-Sala, M. V. Bueno-Delgado, E. Egea-Lopez, L. Juan-Llacer, and J. Garcia-Haro, "Channel Model at 868 MHz for Wireless Sensor Networks in Outdoor Scenarios," in *Proc. International Workshop on Wireless Ad-hoc Networks*, 2005, Paper 38.

[65] L. Noor and A. Anpalagan, "Direct conversion receiver for radio communication systems," *IEEE Potentials*, vol. 24, pp. 32-35, 2005.

[66] J. A. M. Jarvinen, J. Kaukovuori, J. Ryynanen, J. Jussila, K. Kivekas, M. Honkanen, and K. A. I. Halonen, "2.4-GHz receiver for sensor applications," *IEEE Journal of Solid State Circuits*, vol. 40, pp. 1426-1433, 2005.

[67] Nan Jin Oh, Sang Gug Lee, and Jinho Ko, "A CMOS 868/915 MHz direct conversion. ZigBee single-chip radio," *IEEE Communications Magazine*, vol. 43, pp. 100-109, 2005.

[68] J. G. Proakis and M. Salehi, *Communication Systems Engineering*, 2nd ed. New Jersey: Prentice-Hall, 2002.

[69] D. C. O' Brien and M. Katz, "Optical wireless communications within fourth-generation wireless systems [Invited]," *Journal of Optical Networking*, vol. 4, pp. 312-322, 2005.

[70] M. Younis, M. Youssef, and K. Arisha, "Energy-aware routing in cluster-based sensor networks," in *Proc. 10th IEEE Int. Symposium on Modelling, Analysis, and Simulation of Computer and Telecommunications Systems*, 2002, pp. 129-136.

[71] J. Zheng and M. J. Lee, "Will IEEE 802.15.4 make ubiquitous networking a

reality?: a discussion on a potential low power, low bit rate standard," *Communications Magazine, IEEE*, vol. 42, pp. 140-146, 2004.

[72] J. Yang and M. Rajan, "Microcell performance evaluation in IS-95 based CDMA networks," in *Proc. IEEE International Conference on Universal Personal Communications*, 1998, vol. 2, pp. 899-903.

[73] M. R. Souryal and N. Moayeri, "Channel-adaptive relaying in mobile ad hoc networks with fading," in *Proc. 2nd Annual IEEE Communications Society Conference on Sensor and Ad Hoc Communications and Networks*, 2005, pp. 142-152.

[74] M. Takai, J. Martin, and R. Bagrodia, "Effects of wireless physical layer modeling in mobile ad hoc networks," in *Proc. MobiHoc*, 2001, pp. 87-94.

[75] Q. Liang, "Fault-tolerant and energy efficient wireless sensor networks: a cross-layer approach," in *Proc. IEEE Military Communications Conference*, 2005, vol. 3, pp. 1862-1868.

[76] Q. Liang and L. Wang, "Fault-tolerant multipath transportation aided with channel coding and interleaver for wireless sensor networks," in *Proc. 15th IEEE International Symposium on Personal, Indoor and Mobile Radio Communications*, 2004, vol. 4, pp. 2679-2683.

[77] S. Jain and S. R. Das, "Exploiting path diversity in the link layer in wireless ad hoc networks," in *Proc. 6th IEEE Int. World of Wireless Mobile and Multimedia Networks Symposium*, 2005, pp. 22-30.

[78] A. Ephremides, "Energy concerns in wireless networks," *IEEE Wireless Communications*, vol. 9, pp. 48-59, 2002.

[79] C. C. Enz, A. El-Hoiydi, J. D. Decotignie, and V. Peiris, "WiseNET: an

ultralow-power wireless sensor network solution," *Computer*, vol. 37, pp. 62-70, 2004.

[80] A. Michail and A. Ephremides, "Energy-efficient routing for connection-oriented traffic in wireless ad-hoc networks," *Mobile Networks and Applications*, vol. 8, pp. 517-533, 2003.

[81] A. J. Goldsmith and S. B. Wicker, "Design challenges for energy-constrained ad hoc wireless networks," *IEEE Wireless Communications*, vol. 9, pp. 8-27, 2002.

[82] Jang Ping Sheu, Chen Wei Lai, and Chih Min Chao, "Power-aware routing for energy conserving and balance in ad hoc networks," in *Proc. IEEE Int. Conference on Networking, Sensing and Control*, 2004, vol. 1, pp. 468-473.

[83] S. Cheekiralla and D. W. Engels, "A functional taxonomy of wireless sensor network devices," in *Proc. 2nd International Conference on Broadband Networks*, 2005, vol. 2, pp. 949-956.

[84] R. Casas, H. J. Gracia, A. Marco, and J. L. Falco, "Synchronization in wireless sensor networks using Bluetooth," in *Proc. 3rd Int. Workshop on Intelligent Solutions In Embedded Systems*, 2005, pp. 79-88.

[85] X. Zhang and G. F. Riley, "Energy-aware on-demand scatternet formation and routing for Bluetooth-based wireless sensor networks," *Communications Magazine, IEEE*, vol. 43, pp. 126-133, 2005.

[86] J. Akella, Chang Liu, D. Partyka, M. Yuksel, S. Kalyanaraman, and P. Dutta, "Building blocks for mobile free-space-optical networks," in *Proc. International Conference on Wireless and Optical Communications Networks*, 2005, pp. 164-168.

[87] H. A. Willebrand and B. S. Ghuman, "Fiber optics without fiber," *IEEE Spectrum*, vol. 38, pp. 40-45, 2001.

[88] C. Jenkins, W. Johnstone, D. Uttamchandani, V. Handerek, and S. Radcliffe, "MEMS actuated spherical retroreflector for free-space optical communications," *Electronics Letters*, vol. 41, pp. 1278-1279, 2005.

[89] S. Junique, D. Agren, Qin-Wang, S. Almqvist, B. Noharet, and J. Y. Andersson, "A modulating retro-reflector for free-space optical communication," *IEEE Photonics Technology Letters*, vol. 18, pp. 85-87, 2006.

[90] W. S. Rabinovich, R. Mahon, P. G. Goetz, E. Waluschka, D. S. Katzer, S. C. Binari, and G. C. Gilbreath-, "A cat's eye multiple quantum-well modulating retro-reflector," *IEEE Photonics Technology Letters*, vol. 15, pp. 461-463, 2003.

[91] L. Yongbing, "An improved cat's-eye retroreflector used in a laser tracking interferometer system," *Measurement Science and Technology*, vol. 14, pp. 36-40, 2003.

[92] J. P. Oakley, "Whole-angle spherical retroreflector using concentric layers of homogeneous optical media," *Applied Optics*, vol. 47, pp. 1026-1031, 2007.

[93] R. B. Nilson and X. J. Lu, "Optimum design of spherical retroreflectors with refractive indices close to 2.0," *Transactions of the Institute of Measurements and Control*, vol. 18, pp. 212-215, 1996.

[94] B. A. Warneke, M. D. Scott, B. S. Leibowitz, Lixia Zhou, C. L. Bellew, J. A. Chediak, J. M. Kahn, B. E. Boser, and K. S. J. Pister, "An autonomous 16 mm/sup 3/ solar-powered node for distributed wireless sensor networks," in

Proc. IEEE SENSORS, 2002, vol. 2, pp. 1510-1515.

[95] Lixia Zhou, K. S. J. Pister, and J. M. Kahn, "Assembled corner-cube retroreflector quadruplet," in *Proc. IEEE Int. Conference on Micro Electro Mechanical Systems*, 2002, pp. 556-559.

[96] P. B. Chu, N. R. Lo, E. C. Berg, and K. S. J. Pister, "Optical communication using micro corner cube reflectors," in *Proc. 10th Annual IEEE Int. Workshop on Micro Electro Mechanical Systems*, 1997, pp. 350-355.

[97] Xiaoming Zhu, V. S. Hsu, and J. M. Kahn, "Optical modeling of MEMS corner cube retroreflectors with misalignment and nonflatness," *IEEE Journal of Selected Topics in Quantum Electronics*, vol. 8, pp. 26-32, 2002.

[98] G. C. Gilbreath, W. S. Rabinovich, T. J. Meehan, M. J. Vilcheck, R. Mahon, R. Burris, M. Ferraro, I. Sokolsky, J. A. Vasquez, C. S. Bovais, K. Cochrell, K. C. Goins, R. Barbehenn, D. S. Katzer, K. I. Anastasiou, and M .J. Montes, "Large-aperture multiple quantum well modulating retroreflector for free-space optical data transfer on unmanned aerial vehicles," *Optical Engineering*, vol. 40, pp. 1348-1356, 2001.

[99] C. M. Swenson, C. A. Steed, I. A. DeLaRue, and R. Q. Fugate, "Low power FLC-based retromodulator communications system," in *Proc. SPIE Free-Space Laser Communication Technologies IX,* 1997, vol. 2990, pp. 296-310.

[100] J. P. Drolet, J. S. Patel, K. G. Haritos, Weihua Xu, A. Scherer, and D. Psaltis, "Hybrid-aligned nematic liquid-crystal modulators fabricated on VLSI circuits," *Optics Letters*, vol. 20, pp. 2222-2224, 1995.

[101] D. C. O'Brien., J. J. Liu, W. W. Yuan, G. E. Faulkner, S. J. Elston, and S. Collins, "Optical wireless communications with low voltage self-powered

sensor motes," in *Proc. SPIE Free-Space Laser Communications VII*, 2007, vol. 6709, pp. 67090A1-67090A10.

[102] D. C. O'Brien, W. W. Yuan, J. J. Liu, G. E. Faulkner, S. J. Elston, S. Collins, and L. A. Parry-Jones, "Optical wireless communications for micro-machines," in *Proc. SPIE Free-Space Laser Communications VI*, 2006, vol. 6304, pp. 63041A1-63041A8.

[103] D. Sadot, A. Melamed, N. Dinur, and N. S. Kopeika, "Effects of aerosol forward scatter on the long- and short-exposure atmospheric coherence diameter," *Waves in Random Media*, vol. 4, pp. 487-498, 1994.

[104] D. Chadha, "Feasibility study of free space optical communication link through atmospheric turbulent channel," in *Proc. Conference on Optoelectronic and Microelectronic Materials and Devices*, 2004, pp. 311-314.

[105] Xiaoming Zhu and J. M. Kahn, "Free-space optical communication through atmospheric turbulence channels," *IEEE Transactions on Communications*, vol. 50, pp. 1293-1300, 2002.

[106] S. Arnon and N. S. Kopeika, "Effect of particulates on performance of optical communication in space and an adaptive method to minimize such effects," *Applied Optics*, vol. 33, pp. 4930-4937, 1994.

[107] A. M. Scott and K. D. Ridley, "Calculations of bit error rates for retro-reflective laser communications systems in the presence of atmospheric turbulence," in *Proc. SPIE Advanced Free-Space Optical Communications Techniques and Technologies*, 2004, vol. 5614, pp. 31-42.

[108] N. S. Kopeika, A. Zilberman, and Y. Sorani, "Measured profiles of aerosols

and turbulence for elevations of 2-20 km and consequences on widening of laser beams," in *Proc. SPIE Optical Pulse and Beam Propagation III*, 2001, vol. 4271, pp. 43-51.

[109] M. Born and E. Wolf, *Optics, principles of*, 6th ed. Canada: Pergamon, 1980.

[110] J. W. Goodman, *Statistical Optics*. New York: Wiley, 1985.

[111] A. Ishimaru, *Wave propagation and scattering in random media*, vol. 1-2. New York: Academic, 1978.

[112] S. Karp, R. Gagliardi, S. E. Moran, and L. B. Stotts, *Optical Channels*. New York: Plenum, 1988.

[113] A. Zilberman, N. S. Kopeika, and Y. Sorani, "Laser beam widening as a function of elevation in the atmosphere for horizontal propagation," in *Proc. SPIE Laser Weapons Technology II*, 2001, vol. 4376, pp. 177-188.

[114] L. C. Andrews and R. L. Phillips, *Laser Beam Propagation Through Random Media*: SPIE Optical Engineering Press, 1998.

[115] M. Uysal, Jing Li, and Meng Yu, "Error rate performance analysis of coded free-space optical links over gamma-gamma atmospheric turbulence channels," *IEEE Transactions on Wireless Communications*, vol. 5, pp. 1229-1233, 2006.

[116] L. C. Andrews, R. L. Phillips, and C. Y. Hopen, *Laser Beam Scintillation with Applications*: SPIE Press, 2001.

[117] T. H. Churnside and S. F. Clifford, "Log-normal Rician probability density function for optical scintillations in the turbulent atmosphere," *Journal of Optical Society America A.*, vol. 4, pp. 1923-1930, 1987.

[118] L. C. Andrews and R. L. Phillips, "Mathematical genesis of the I-K

distribution for random optical fields," *Journal of Optical Society America A.*, vol. 3, pp. 1912-1919, 1986.

[119] E. Jakeman and P. N. Pusey, "The significance of K-distributions in scattering experiments," *Physical Review Letters*, vol. 40, pp. 546-550, 1978.

[120] M. Abramowitz and I. A. Stegun, "Handbook of mathematical functions with formulas, graphs and mathematical tables," presented at NBS National Science Foundation Conference, Cambridge, MA, 1954.

[121] T. A. Tsiftsis, H. G. Sandalidis, G. K. Karagiannidis, and N. C. Sagias, "Multihop Free-Space Optical Communications Over Strong Turbulence Channels," in *Proc. ICC*, 2006, vol. 6, pp. 2755-2759.

[122] W. A. Crossland, M. J. Holmes, B. Robertson, and T. D. Wilkinson, "Liquid crystal polarization independent beam steering switches for operation at 1.5 microns," in *Proc. IEEE Lasers and Electro-Optics Society Annual Meeting*, 2000, vol. 1, pp. 46-47.

[123] M. Bhardwaj and A. P. Chandrakasan, "Bounding the lifetime of sensor networks via optimal role assignments," in *Proc. INFOCOM*, 2002, vol. 3, pp. 1587-1596.

[124] H. J. Zepernick and T. A. Wysocki, "Multipath channel parameters for the indoor radio at 2.4 GHz ISM band," in *Proc 49th. IEEE Vehicular Technology Conference*, 1999, vol. 1, pp. 190-193.

[125] Jin Zhu and S. Papavassiliou, "On the energy-efficient organization and the lifetime of multi-hop sensor networks," *IEEE Communications Letters*, vol. 7, pp. 537-539, 2003.

[126] M. N. Halgamuge, S. M. Guru, and A. Jennings, "Energy efficient cluster

formation in wireless sensor networks," in *Proc. 10th Int. Conference on Telecommunications*, 2003, vol. 2, pp. 1571-1576.

[127] Yufu Jia, Tianlin Dong, and Jian Shi, "Analysis on energy cost for wireless sensor networks," in *Proc. 2nd Int. Conference on Embedded Software and Systems*, 2005, pp. 144-151.

[128] A. Wang, W. B. Heinzelman, A. Sinha, and A. P. Chandrakasan, "Energy-scalable protocols for battery-operated microsensor networks," *Journal of VLSI Signal Processing Systems for Signal, Image, and Video Technology*, vol. 29, pp. 223-237, 2001.

[129] L. L. Dai and P. Basu, "Energy and Delivery Capacity of Wireless Sensor Networks with Random Duty-Cycles," in *Proc. ICC*, 2006, vol. 8, pp. 3505-3510.

[130] E. J. Duarte-Melo and M. Liu, "Analysis of energy consumption and lifetime of heterogeneous wireless sensor networks," in *Proc. GLOBECOM*, 2002, vol. 1, pp. 21-25.

[131] M. Younis, M. Youssef, and K. Arisha, "Energy-aware management for cluster-based sensor networks," *Computer Networks*, vol. 43, pp. 649-668, 2003.

[132] E. Ould-Ahmed-Vall, G. F. Riley, B. S. Heck, and D. Reddy, "Simulation of large-scale sensor networks using GTSNetS," in *Proc. 13th IEEE International Symposium on Modeling, Analysis, and Simulation of Computer and Telecommunication Systems*, 2005, pp. 211-218.

[133] R. Di-Prieto, L. V. Mancini, Yee Wei Law, S. Etalle, and P. Havinga, "LKHW: a directed diffusion-based secure multicast scheme for wireless

sensor networks," in *Proc. International Conference on Parallel Processing Workshops*, 2003, pp. 397-406.

[134] R. Mini, M. Machado, A. Loureiro, and B. Nath, "Prediction-based energy map for wireless sensor networks," *Ad Hoc Networks*, vol. 3, pp. 235-53, 2005.

[135] K. Sohrabi, J. Gao, V. Ailawadhi, and G. J. Pottie, "Protocols for self-organization of a wireless sensor network," *IEEE Personal Communications*, vol. 7, pp. 16-27, 2000.

[136] A. Woo and D. E. Culler, "A transmission control scheme for media access in sensor networks" in *Proc. 7th Annual International conference on mobile computing and networking*, 2001, pp. 221-235.

[137] S. Verma, Junfeng Xu, M. Hamada, and T. H. Lee, "A 17-mW 0.66-mm/sup 2/ direct-conversion receiver for 1-Mb/s cable replacement," *IEEE Journal of Solid State Circuits*, vol. 40, pp. 2547-2554, 2005.

[138] M. Bhardwaj, T. Garnett, and A P. Chandrakasan, "Upper bounds on the lifetime of sensor networks," in *Proc. ICC*, 2001, vol. 3, pp. 785-790.

[139] Yong Ma and J. H. Aylor, "System lifetime optimization for heterogeneous sensor networks with a hub-spoke technology," *IEEE Transactions on Mobile Computing*, vol. 3, pp. 286-294, 2004.

[140] P. Santi, D. M. Blough, and F. Vainstein, "A probabilistic analysis for the range assignment problem in ad hoc networks," in *Proc. MobiHoc*, 2001, pp. 212-220.

[141] Jae Hwan Chang and L. Tassiulas, "Energy conserving routing in wireless ad-hoc networks," in *Proc. INFOCOM*, 2000, vol. 1, pp. 22-31.

[142] S. Singh, M. Woo, and C. S. Raghavendra, "Power-aware routing in mobile and ad hoc networks," in *Proc. MOBICOM*, 1998, pp. 181-190.

[143] Y. Xu, J. S. Heidemann, and D. Estrin, "Geography-informed energy conservation for ad hoc routing," in *Proc. MOBICOM*, 2001, pp. 70-84.

[144] R. Wattenhofer, L. Li, P. Bahl, and Y. Wang, "Distributed topology control for power efficient operation in multihop wireless ad hoc networks," in *Proc. INFOCOM*, 2001, vol. 3, pp. 1388-1397.

[145] J. E. Wieselthier, G. D. Nguyen, and A. Ephremides, "Resource management in energy-limited, bandwidth-limited, transceiver-limited wireless networks for session-based multicasting," *Computer Networks*, vol. 39, no.2, pp. 113-131, 2002.

[146] C. K. Toh, "Maximum battery life routing to support ubiquitous mobile computing in wireless ad hoc networks," *IEEE Communications Magazine*, vol. 39, pp. 138-147, 2001.

[147] B. Chen, K. Jamieson, H. Balakrishnan, and R. Morris, "Span: An energy-efficient coordination algorithm for topology maintenance in ad hoc wireless networks," in *Proc. MOBICOM*, 2001, pp. 85-96.

[148] T. Brown, H. Gabow, and Q. Zhang, "Maximum flow-life curve for a wireless ad hoc network," in *Proc. MobiHoc*, 2001, pp. 128-136.

[149] L. Kleinrock and J. Silvester, "Optimum transmission radii for packet radio networks or why six is a magic number," in *Proc. IEEE National Telecommunications Conference*, 1978, pp. 4.3.1.-4.3.5.

[150] www.xbow.com

[151] http://www.btnode.ethz.ch

[152] http://www.sunspotworld.com/products/